

**3D SEISMIC INTERPRETATION OF
SOFT-SEDIMENT DEFORMATIONAL
PROCESSES OFFSHORE ISRAEL:
IMPLICATIONS FOR HYDROCARBON
PROSPECTIVITY**

JOSE FREY MARTINEZ

**Submitted in partial fulfilment of the requirements for the
degree of Ph.D.**

Cardiff University

March 2005

UMI Number: U584723

All rights reserved

INFORMATION TO ALL USERS

The quality of this reproduction is dependent upon the quality of the copy submitted.

In the unlikely event that the author did not send a complete manuscript and there are missing pages, these will be noted. Also, if material had to be removed, a note will indicate the deletion.



UMI U584723

Published by ProQuest LLC 2013. Copyright in the Dissertation held by the Author.
Microform Edition © ProQuest LLC.

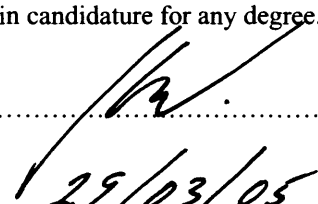
All rights reserved. This work is protected against
unauthorized copying under Title 17, United States Code.



ProQuest LLC
789 East Eisenhower Parkway
P.O. Box 1346
Ann Arbor, MI 48106-1346

DECLARATION

This work has not previously been accepted in substance for any degree and is not being concurrently submitted in candidature for any degree.

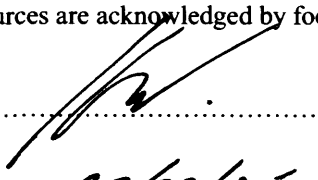
Signed..........(candidate)

Date.....29/03/05.....

STATEMENT 1

This thesis is the result of my own investigations, except where otherwise stated.

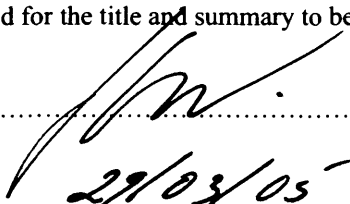
Other sources are acknowledged by footnotes giving explicit references. A bibliography is appended.

Signed..........(candidate)

Date.....29/03/05.....

STATEMENT 2

I hereby give consent for my thesis, if accepted, to be available for photocopying and for inter-library loan, and for the title and summary to be made available to outside organisations.

Signed..........(candidate)

Date.....29/03/05.....

This Thesis is dedicated in memory of my
Grandfather, José Martínez Cordero

“...pues es condición propia de los héroes resistir con tesón y ser inmortales...”

Don Quijote de la Mancha (Miguel de Cervantes)

SUMMARY

This thesis uses a combination of industry seismic (2D and 3D) and well data to investigate the typologies, genetics and mechanisms of soft-sediment deformational processes on the continental margin of Israel and their impact on the exploration and production of hydrocarbons. Research has been focused on the two major types of soft-sediment deformation in the region: clastic diapirism and submarine slope instability (i.e. submarine slumping). Such processes have occurred almost continuously throughout the post-Messinian history of the Israeli margin, and have played a critical role in its overall evolution and construction. Detailed analysis of the timing of occurrence, areal distribution and 3D appearance of the resultant structures has enabled an enhanced understanding of the causes, processes and results of soft-sediment deformational events to be obtained.

Clastic diapirism occurred during the first stages of refilling of the Mediterranean Sea after the Messinian Salinity Crisis, and was restricted to an area underlain by the Afiq Submarine Canyon (Oligocene in origin). The resultant bodies correspond to a series of four-way dip mounded features, and ridge-like structures that are mainly distributed along the axis and one of the flanks of the canyon, respectively. Seismicity and hydrocarbon generation have been proposed here as the main triggering mechanisms. Clastic diapirism plays a decisive role in the hydrocarbon prospectivity of the region as it largely modifies the reservoir properties and architectures of the largest accumulations of hydrocarbons discovered to date in Israel.

Submarine slope instability (i.e. submarine slumping) is the second dominant typology of soft-sediment deformation in the continental margin of Israel. Submarine slumping initiated during the Late Pliocene with the Israel Slump Complex (ISC), one of the biggest submarine slump deposits in the world described to date. Since then, slope failure has occurred almost continually up to the present day. Submarine failure in the area is linked to the dynamics of subsidence and deformation of the transform margin of the eastern Mediterranean. Seismicity and presence of gas in the sediments, together with localised oversteepening, have been proposed as the main triggering mechanisms.

The high spatial resolution provided by the 3D seismic data has enabled two principal types of submarine landslides to be distinguished according to their mechanism of frontal emplacement: *frontally confined* and *emergent*. In the first, the landslide undergoes a restricted downslope displacement and does not overrun the undeformed downslope strata. In the second significant downslope translation occurs since the landslide is able to abandon its original basal shear surface and translate freely over the seafloor. Such division is of critical importance as the formational mechanisms, and processes of translation and cessation are fundamentally different.

AUTHOR'S NOTE

Chapters Two, Three and Four of the present Thesis have been presented as papers for three different international publications. The present status of these publications are summarised as follows:

- **Chapter Two** has been published as: *Clastic intrusion of deepwater sands as a hydrocarbon trap-forming mechanism: examples from the Eastern Mediterranean*, Jose Frey-Martinez, Joe Cartwright, Ben Hall and Mads Huuse, AAPG Memoir, in press.
- **Chapter Three** has been published as: *3D seismic interpretation of slump complexes: examples from the continental margin of Israel*, Jose Frey-Martinez, Joe Cartwright and Ben Hall, Basin Research, 17, p. 83-108.
- **Chapter Four** has been submitted to Marine Geology as: *Compressional toe regions in major submarine landslides imaged with 3D seismic data: implications for slide mechanics*, Jose Frey-Martinez, Joe Cartwright and David James.

ACKNOWLEDGEMENTS

The words that I am about to write are certainly the most satisfying and looked-for of the last three years and a half of my life. These acknowledgements conclude a long time of work and dedication to this research project, and in them I would like to include all those people and organizations without whom this great adventure would have never been possible.

First of all, I would like to express my deep gratitude to my supervisors Joe Cartwright and Ben Hall for giving me the opportunity to undertake this project and for their continuous support. Joe, in particular, deserves all my appreciation and respect. His incessant guidance, encouragement and infinite patience have been decisive during all my research, and have definitely helped to improve the last result of my work. Joe also merits my gratitude for being able to pass on me part of his passion for geology, science and good presentations. I very much enjoyed our almost daily meetings and conversations, which were an incessant source of inspiration. It has definitely been a fortune to have been exposed to so many good advices and excellent ideas. I shall definitely take some of them with me. Ben is thanked for providing me with tonnes of data and reports, and for his input in many bureaucratic aspects of the research. Thanks also for showing me some of the hidden sides of a PhD.

BG-Group is thanked for sponsoring the project and for providing all the data and allowing their use in publications. I am also grateful to many people in BG-Group for sharing their vast knowledge of the geology of Israel and for helping me to dig into piles of reports and well composite logs. Jason Canning and Iain Campbell are especially thanked for this. I am also truly indebted to Steve Maddox for his continuous advice, motivation and help throughout my PhD. Thanks also to the reviewers of the different papers included in this thesis (Zvi Garfunkel, Paul Spencer, Lorna Strachan, Al Fraser and Steve Adiletta). Their comments definitely helped to improve the last result of the publications.

The people of the 3D Lab at Cardiff University are very much thanked for their companionship and assistance during all these years. In particular, Richard Davies deserves my gratitude not only for patiently reading large parts of my work, but also for his valuable advice with other more mundane matters. Mads Huuse is thanked for reading many of my wordy manuscripts and for providing me with good papers and

better coffee. David James provided excellent advice and assistance with many of the manuscripts, and from here I would like to transmit my gratitude to him. His knowledge and understanding of countless geological aspects have been an excellent source of inspiration. Thanks also to all the managers of the 3D Lab and, in particular, to Neil Ferguson who kept on dealing with the huge amounts of data that I constantly tried to squeeze into the system.

Andy Robinson deserves to be thanked for an infinite list of things, really. Above all, for his help and support from the very first day of my arrival in Cardiff, for teaching me so many tricks of seismic interpretation, and for his friendship. He is also greatly admired for his vast understanding of Spanish football. My officemates, Valente and Mike, are greatly thanked for making the last hectic and hardest months of my PhD much more enjoyable, and for keep on providing me with massive amounts of coffee and excellent comradeship. I really enjoyed our nonsense and endless conversations about geology, international politics, history and cars. If *they* let us, we could easily fix the world in just one morning.

Thanks also to Julie and David for making me feel so welcomed to this wet island and for always having a fire and a glass of good wine ready. Julie, in especial, deserves all my gratitude for her permanent support, for always being there when I needed her and for her impartiality. David is thanked for so many excellent moments talking about bridges, British customs, and for sharing my passion for good Spanish food. My old friends back in Spain (Enric, Javi, Pacheco, Carlos and Jose) are thanked for turning quiet afternoons into sleepless nights and for keep on reminding me where my real place is. I am very grateful to Jose for accepting to come along in many of those never-ending walks in the mountains, and for pretending to be interested in my conversations about geology, slumps and petroleum systems. Carlos is thanked for many great moments talking and talking without saying much.

My parents, Manuel and Pilar, and my sister Pilar are greatly thanked for their incessant help and moral support. My sister, in particular, has repeatedly demonstrated her love, compassion and care, and I am very grateful to her for that. I would probably not be writing this now without her constant support. Finally and obviously: Claudia. My greatest inspiration, my continuous support and my best friend. Her love, infinite patience and great sense of humour have not only made my PhD much easier but my life far more enjoyable.

TABLE OF CONTENTS

Summary	i
Author's note	ii
Acknowledgements	iii
Table of Contents	v
List of Figures	viii
List of Tables	xiv
List of Appendices and Enclosures	xv
List of Acronyms	xvi

CHAPTER ONE

1. Introduction	1 - 1
1.1 Rationale	1 - 1
1.2 Aims of study	1 - 3
1.3 Location and geological setting	1 - 4
1.4 History of hydrocarbon exploration in Israel	1 - 7
1.5 Database	1 - 10
1.6 Methodology	1 - 13
1.7 Terminology for slope instability processes	1 - 14
1.8 Thesis layout	1 - 17

CHAPTER TWO

2. Clastic intrusion of deepwater sands	2 - 1
2.1 Abstract	2 - 1
2.2 Introduction	2 - 2
2.3 Geological setting	2 - 3
2.4 Database and methodology	2 - 8
2.5 Stratigraphic context of the mounded structures	2 - 11
2.5.1 Unit 1 (Canyon fill)	2 - 11
2.5.2 Unit 2 (Messinian deposits)	2 - 12
2.5.3 Unit 3 (Lower Yafo Formation)	2 - 12
2.6 General appearance of the mounded structures	2 - 13
2.6.1 Overburden	2 - 19
2.6.2 Marginal depressions	2 - 20
2.7 Detailed description of the mounded structures	2 - 23
2.7.1 Nir Mound Complex	2 - 23
2.7.1.1 Seismic character of the NMC	2 - 24
2.7.1.2 Well-log calibration of the NMC lithology	2 - 26
2.7.1.3 Allochthonous material within the NMC	2 - 28
2.7.2 Mairi Mound Complex	2 - 29
2.7.2.1 Seismic character of the MMC	2 - 30
2.7.2.2 Seismic calibration of the MMC lithology	2 - 34
2.7.3 Alpha Mound	2 - 35
2.7.2.1 Seismic character of the AM	2 - 36
2.8 Timing of the mounded structures	2 - 38
2.9 Canyon margin ridge structures	2 - 40

2.10 Discussion	2 - 44
2.10.1 Origin of the canyon axis mounded structures	2 - 46
2.10.2 Genetic model and evolution	2 - 50
2.10.3 Implication for hydrocarbon exploration and production	2 - 54
2.11 Conclusions	2 - 57

CHAPTER THREE

3. 3D seismic interpretation of slump complexes	3 - 1
3.1 Abstract	3 - 1
3.2 Introduction	3 - 2
3.3 Regional tectono-stratigraphic context	3 - 3
3.4 Data and methodology	3 - 8
3.5 Recognition of slump deposits on 3D seismic data	3 - 9
3.6 Stratigraphic context of slump deposits in the study area	3 - 11
3.6.1 Unit T30	3 - 12
3.6.2 Unit T20	3 - 15
3.6.2 Unit T10	3 - 16
3.7 Detailed 3D mapping of slump deposits	3 - 16
3.7.1 The Israel Slump Complex	3 - 18
3.7.1.1 Seismic character of the Israel Slump Complex	3 - 18
3.7.2 The Gaza Slump Complex	3 - 29
3.7.2.1 Seismic character of the Gaza Slump Complex	3 - 31
3.8 Proto-slumps	3 - 36
3.9 Discussion	3 - 38
3.10 Conclusions	3 - 45

CHAPTER FOUR

4. Compressional toe regions in submarine landslides	4 - 1
4.1 Abstract	4 - 1
4.2 Introduction	4 - 2
4.3 Geological setting	4 - 5
4.4 Data and methodology	4 - 9
4.5 Seismic stratigraphic framework	4 - 10
4.6 The Israel Slump Complex	4 - 12
4.6.1 General characteristics	4 - 12
4.6.2 Internal seismic character of the toe region	4 - 18
4.6.2.1 Dimensions of the thrust structures	4 - 24
4.7 The T20 Slump	4 - 30
4.7.1 General characteristics	4 - 30
4.7.2 Internal seismic character of the toe region	4 - 36
4.7.2.1 Dimensions of the thrust structures	4 - 38
4.8 Discussion	4 - 39
4.9 Mechanics	4 - 43
4.10 Conclusions	4 - 47

CHAPTER FIVE

5. Summary and discussion	5 - 1
5.1 Introduction.....	5 - 1
5.2 Summary of results	5 - 2
5.2.1 Results from the analysis of clastic diapirism (Chapter 2)	5 - 2
5.2.2 Results from the 3D seismic analysis of slump complexes (Chapter 3).....	5 - 3
5.2.3 Results from the analysis of compressional toe regions (Chapter 4).....	5 - 4
5.3 Time-space reconstruction of soft-sediment deformational processes offshore Israel.....	5 - 6
5.4 Implications for hydrocarbon prospectivity.....	5 - 9
5.4.1 Implications of clastic diapirism.....	5 - 10
5.4.2 Implications of submarine slope failure.....	5 - 11
5.5 Worldwide analogues.....	5 - 14
5.5.1 Analogues for clastic diapirism	5 - 14
5.5.2 Analogues for submarine slope instability.....	5 - 16
5.6 Limitations and future research	5 - 20

CHAPTER SIX

6. Conclusions	6 - 1
6.1 General conclusions	6 - 1
6.2 Clastic diapirism	6 - 2
6.3 Submarine slope instability.....	6 - 3
6.4 Compressional toe regions in submarine landslides	6 - 4
6.5 Implications for hydrocarbon prospectivity.....	6 - 5
6.5.1 Implications of clastic diapirism.....	6 - 5
6.5.2 Implications of submarine slope failure	6 - 5
7. References	7 - 1

Appendices

- **1.** (CD-1): Summary table of exploration and production wells in Israel and collection of support maps.
- **2.** (CD-2): Thesis in digital format.
- Publications.

LIST OF FIGURES

Chapter One: Introduction

Figure No.	Figure Caption	Page No.
1.1	General geographical map of part of the Eastern Mediterranean showing its main regional structural elements.	1-5
1.2	Southeast-northwest seismic cross section through onshore and offshore Israel (see Figure 1.1 for location) showing the main structural elements.	1-6
1.3	Map of Israel showing the location of the most significant oil and gas fields discovered until 2005. The location of the study area is also indicated.	1-9
1.4	Location map of the study area showing the full extent of the 2D and 3D seismic surveys and the position of the exploration wells used in this study.	1-11
1.5	(a) Seismic section across the seabed showing the waveform response of a single wavelet. (b) Same seismic section as a colour density display.	1-12

Chapter Two: Clastic diapirism

Figure No.	Figure Caption	Page No.
2.1	Geological sketch of part of the Eastern Mediterranean showing the main structural elements, tectonic plates and study area. Modified from Garfunkel (1998).	2-4
2.2	Generalized chrono-stratigraphic and lithological scheme of the post-Eocene continental margin of Israel. The lithological column is based on unpublished well reports. The time-scale is non-linear.	2-5
2.3	Map showing the areal distribution of the Yafo Sand Member offshore Israel. The gross of the Yafo Sand Member was supplied from the southern Levant hinterland via the Afiq and el-Arish Submarine Canyons, and deposited in deepwater as base-of-slope submarine fans. The mounded structures (marked M) are distributed along the Afiq Submarine Canyon in the Med Ashdod 3D area.	2-6
2.4	Regional dip seismic section through the continental margin of Israel (see Figure 3 for location). This seismic profile illustrates the post-Cretaceous configuration of the study area. Note the presence of an extensive unconformity and a thick deposit of evaporites resulting from the Messinian Salinity Crisis. Several large-scale slump deposits and shore parallel growth faults appear within the post-Messinian continental margin. Note the presence of a series of mounded structures at the base of the Pliocene-Quaternary interval.	2-7
2.5	Seismic profile across the Afiq Submarine Canyon (see Figure 3 for location) showing the three main seismic units defined in this paper (Units 1-3). Unit 1 are composed of sub-horizontal, continuous and aggradational seismic reflections that onlap the margins of the canyon. Unit 2 is an uneven veneer of discontinuous to transparent seismic reflections that pinch out against the flanks of the canyon. Unit 3 consists of continuous, high-amplitude seismic reflections onlapping and downlapping the flanks of the canyon. Further discussion on unit architecture is given in the text. The colors used for the seismic unit boundaries are consistent throughout this paper.	2-9
2.6	3D visualization of two representative mounded structures in the study area. Mounded structures are delimited by a relatively concordant, continuous and flat-lying lower boundary and by a convex-upward and discontinuous upper boundary. The lower and upper boundaries correspond to the base and top of the Yafo Sand Member respectively. The internal parts of the mounded structures show chaotic seismic reflections in the cores (enclosed by dashed black lines) and more continuous seismic reflections in the flanks and crests (marked X). Note the presence of flat-spots crosscutting the flanks and "pull-up" features underlying the cores of the structures.	2-15
2.7	Structural map in two-way time of the top of the Yafo Sand Member in the Med Ashdod 3D area (TWT, 2000 ms--1700 m). The mounded structures appear as circular to elongated culminations flanked by marginal depressions. The mounds form both isolated and complex features. The majority of the structures are aligned in a NW-SE trend along the axis of the Afiq Submarine Canyon. Note the presence of ridge-like shale diapirs parallel to the northern rim of the Afiq Submarine Canyon.	2-16
2.8	Seismic section along the axis of the Afiq Submarine Canyon in the Med Ashdod 3D area (see Figure 7 for location). There are ten mounded structures confined to the Yafo Sand Member (YSM)	2-18

	and the Yafo Mudstone Member. They all form dome-like features delimited by the base and top of the Yafo Sand Member (lower and upper boundaries respectively). Note the presence of “pull up” features underlying the cores of the mounded structures. The overburden is significantly deformed above the structures. Further discussion of the geometrical relationships of the mounded structures to the overburden is given in the text.	
2.9	(a) Structurally flattened horizontal coherence-slice across the overburden of the mounded structures in part of the Med Ashdod 3D area (see Figure 7 for location). Note the presence of radial and concentric faults within the overburden of the mounded structures. The faults surround the crests and flanks of the largest mounded structures in the area (outlined by white dashed lines). (b) Schematic depiction illustrating the plan view of the fault systems around the mounded structures.	2-21
2.10	Seismic profile across the Afiq Submarine Canyon (see Figure 7 for location). The NMC-1 appears in its central parts. There are marginal topographic depressions (marked D) on both sides of the mounded structure. Note the presence of a small-scale diapiric structure in the northern flank of the Afiq Submarine Canyon. There are “pull up” features below the NMC-1. The overburden is clearly folded towards the flanks and crest of the NMC-1 and shows significant thickness variations towards the structure.	2-22
2.11	Catalogue of seismic sections through the NMC illustrating the seismic appearance of its internal parts (see Figure 8 for location). The internal seismic reflections within the Yafo Sand Member (marked YSM) are truncated and bent-up toward the cores of the NMC. Note the presence of several fractures underlying the mounds. (a) Seismic section across the NMC-1. The flanks and crest of this mound contain many resolvable block-like seismic events (marked X) that can be traced up to the preserved parts of the YSM. The core consists of chaotic seismic facies (marked C). There are several “soft” seismic events corresponding mainly to the block-like seismic events (X) along the flanks and crest. (b) Seismic section across the NMC-2 showing an internal appearance that is highly equivalent to that of the NMC-1.	2-25
2.12	Log of exploration well Nir-1, showing depth of the NMC-1. Note the presence of box-shaped gamma log motifs suggesting presence of clean sandstones within the structure. Dip and azimuth indicate highly disturbed sediments especially towards the core of the mound. Note the presence of allochthonous microfaunal and nannofossil taxa within the structure. A gas-water contact (marked GWC) has been penetrated at 1951.6 m.	2-27
2.13	Seismic profile across the Afiq Submarine Canyon (see Figure 7 for location). The MMC-1 appears in its central parts. Note the presence of marginal topographic depressions (marked D) on both sides of the mounded structure. There are small-scale diapiric structures towards the northern flank of the canyon. There are clear “pull up” features below the MMC-1. The overburden is folded towards the flanks and crest of the MMC-1 and shows substantial thickness variations towards the structure.	2-31
2.14	(a) Structurally flattened horizontal coherence-slice across the MMC (see Figure 7 for location). The internal parts of the MMC consist of concentric and continuous seismic events in the flanks (marked X) that surround three chaotic cores (one for each component mounded structure, marked C). (b) Schematic depiction illustrating the internal parts of the MMC in plan view.	2-32
2.15	Catalogue of seismic sections through the MMC illustrating the seismic appearance of its internal parts (see Figure 14 for location). Note that the internal seismic reflections within the Yafo Sand Member (marked YSM) are truncated and bent-up toward the cores of the MMC. (a) Seismic section across the MMC-1. The flanks and crest of this component mound show many resolvable seismic events (marked X) that can be traced up to the preserved parts of the YSM. The core consists of chaotic seismic facies (marked C). There are two clear flat-spots restricted to the flanks of the structure. These represent gas-water contacts (marked GWC). (b) Seismic section across the MMC-2 showing an internal appearance that is highly equivalent to that of the MMC-1. (c) Seismic section across the MMC-3. Note the presence of continuous seismic reflections in the flanks and crest of the mound (X). The internal seismic reflections within the YSM are truncated against the basal central parts of the structure. There is a clear gas-water contact (GWC) continuously traceable across the crest of the mound.	2-33
2.16	Seismic examples of the internal geometries of the BMS. Note the bulbous morphology and highly organized internal structure of this mound. (a) Seismic profile across the BMS (see Figure 8 for location). Note the presence of continuous seismic reflections (marked X) along the flanks and crest of the structure. These correspond to the Yafo Sand Member (marked YSM) which is deflected up toward the chaotic centre of the mound (marked C). (c) Seismic profile across the BMS perpendicular to Figure 16A. There are continuously traceable seismic reflections (X) across the crest of the mound from the YSM. (d) Time slice through the BMS. Note the presence of concentric and continuous seismic reflections (X) enclosing a core of chaotic seismic facies (marked C).	2-37
2.17	(a) Close up on the northeastern flank of the Afiq Submarine Canyon (see Figure 10 for location) showing the internal appearance of the marginal ridges. They form steep-sided domed features (marginal flank dips of up to 15°). Note that the internal seismic character is dominated by chaotic seismic reflections most likely derived from the canyon infill. Note the presence of velocity pushdown effects beneath the structure. (b) Schematic depiction illustrating the marginal ridges and the internal parts of the Afiq Submarine Canyon. Dashed arrows indicate interpreted pathways for fluidized sediment flowage.	2-42

2.18	Schematic cross-sectional evolution summarizing the key stages in development of the mounded structures, and explaining geometrical relationships of the mounds to the overburden (see text for detailed discussion).	2-55
------	---	------

Chapter Three: 3D seismic interpretation of slump complexes

Figure No.	Figure Caption	Page No.
3.1	(a) Geological sketch of part of the Eastern Mediterranean showing the main structural elements. The box marks the approximate location of the study area. Modified from Garfunkel (1998). (b) Location map for the study area showing the 2D and 3D seismic database used in the study and locations of key exploration wells (A and B mark the location of the Gaza Marine-1 and the Or-South-1S wells respectively).	3-4
3.2	Regional dip seismic section through the continental margin of Israel (see Figure 3.1 for location). This seismic profile illustrates the post-Cretaceous configuration of the study area. Note the presence of an extensive unconformity and a thick deposit of evaporites resulting from the Messinian Salinity Crisis. Listric shore parallel growth faults are related to gravity-driven deformation of the Pliocene-Holocene continental margin and to salt tectonics.	3-6
3.3	Generalised chrono-stratigraphic and lithological scheme of the post-Eocene continental margin of Israel. The lithological column is based on unpublished well reports.	3-7
3.4	3D visualization of representative slump deposits in the study area. Slump masses form intervals of disrupted and chaotic seismic facies enclosed by the basal shear and the top surfaces. White arrows mark the main downslope direction of movement. (a) 3D seismic block showing the upslope parts of a slump deposit. Note the listric character of the basal shear surface towards the headscarp and the irregular morphology of the top surface. Presence of downlap from the overlying strata. (b) 3D seismic volume showing the downslope parts of a slump deposit. Note the presence of other older slump deposits being intersected. The basal shear and the top surfaces mark the limits between the chaotic seismic facies within the slump deposits and the continuous reflections of the outer undeformed strata. Note the presence of a frontal ramp towards the toe of the slump mass.	3-10
3.5	Seismic section (a) crossing the central parts of the Levant 3D area (see Figure 3.1b for location) and (b) interpretation showing the stratigraphic context of slump deposits in the study area. Shaded areas correspond mainly to simple slump deposits. Note that there is a concentration of slump deposits in the locations overlying pre-Messinian canyons. Slumps increase in number and decrease in size upwards (see text for discussion).	3-13
3.6	Maps showing the areal distribution of slump deposits within the 3D seismic surveys in the three seismic-stratigraphic units defined in the text. Arrows indicate the interpreted directions of movement. Dashed lines represent the flanks of the Afiq and el-Arish canyons. (a) Areal distribution of a major slump complex within Unit T30. (b) Areal distribution of slump deposits within Unit T20. Note the concentration of slump deposits in the areas underlain by the Arish and el-Arish canyons. (c) Areal distribution of slump deposits within Unit T10.	3-14
3.7	3D perspective view of the present day seabed in the Levant 3D area. Note the presence of several slump complexes covering the slope region. These form arrays of elongated slump deposits extending from the shelf to the base of slope areas. Note the presence of headscarps and secondary crown-cracks. Inset shows the Gaza Slump Complex (marked by GSC).	3-17
3.8	Map of the ISC showing its areal extension. Note its enormous areal extent (c. 4800 km ²). The dashed line (parallel to the coastline) marks the general trend of large tectonic structures from the Syrian Arc system. Arrows indicate the gross transport direction of the slump mass. Seismic sections (indicated with thick dashed lines) are used to illustrate the regional seismic appearance of the ISC (Figures 3.9-3.11). The area where detailed 3D seismic interpretation has been undertaken is indicated by the shaded box (Figure 3.12).	3-19
3.9	(a) Dip geo-seismic section through the continental margin of Israel (see Figure 3.8 for location). The profile images the ISC as a package of chaotic seismic facies within the Lower Pliocene slope system. Reflections within the ISC exhibit local rotation away from the headscarp. The toe region forms an abrupt change from chaotic facies (ISC) to continuous facies (base of slope units). Note the presence of salt-detachment growth faults deforming the ISC. (b) Strike geo-seismic section through the continental margin of Israel (see Figure 3.8 for location). The profile images the ISC as a continuous body extending from the southern to the northern parts of the margin. The lateral margins of the ISC appear as limits to the chaotic facies within the slump mass. Note the presence of discordances in the basal shear surface and faults deforming the slump mass.	3-20
3.10	Seismic profiles along the ISC. (a) 2D seismic profile in the upslope parts of the ISC (see Figure 3.8 for location). The headscarp forms a steeply dipping interface forming the updip boundary between the chaotic seismic facies within the slump body and the continuous reflections of the upper slope. Clear onlap of the headscarp by post-slump sediments is observed. (b) 3D seismic profile through	3-22

	the toe region of the ISC (see Figure 3.8 for location). The toe region appears as the downslope boundary between chaotic seismic facies of the ISC and the continuous reflections of the base of slope. Note the presence of a clear frontal ramp and the slump mass being buttressed against the downslope strata. Older slump deposits appear affected by the ISC.	
3.11	3D seismic profile across the ISC (see Figure 3.8 for location). Note the intensively chaotic seismic facies of the internal parts of the ISC bounded above and below by the top and basal shear surface respectively. A lateral flank of the ISC forms a highly steep ramp separating chaotic for continuous seismic facies. Note the presence of a ramp indenting the basal shear surface and a block of undisturbed reflections within the ISC (see text for discussion). A horizontal coherence-slice (Figure 3.12) and three seismic profiles (Figure 3.13) are used to further illustrate the internal geometry of the ISC.	3-24
3.12	Structurally flattened horizontal coherence-slice across the Levant 3D area (see Figure 3.8 for location). The internal geometry of the lower region of the ISC is clearly observable. Sharp lateral ramps mark the limits of the slump mass. Note the contrast between the slumped and the undisturbed sediment and the presence of concentric arcs of ridge-like structures due to downslope compressional stress. <i>In situ</i> blocks of undisturbed sediments are observed. Arrows indicate the interpreted direction of transport of the slump mass.	3-25
3.13	Seismic examples of the internal geometries of the ISC (see Figure 3.12 for location). The direction of movement is northeast-southwest. (a) Dip seismic section showing imbricated series of closely spaced thrusts. (b) Enlargement of the section across a group of thrusts. Note that thrusts ramp up from the basal shear surface (see text for discussion). (c) Dip seismic section showing a large-scale ramp in the basal shear surface. Note the presence of imbricated thrusts propagating in the direction of movement and an onlapped depression.	3-26
3.14	Schematic depiction of part of the ISC. The upslope parts of the slump mass correspond to the depletion zone. This is characterized by extensional deformational structures and thinning of the slump mass. Note the presence of listric faults forming a series of rotational blocks that are tilted downslope. The downslope part of the slump body corresponds to the accumulation zone. This is characterized by compressional structures and thickening of the slump mass. The slump mass is buttressed against the downslope strata in the toe region. Note the presence of individual “ <i>in situ</i> ” blocks, which have been interpreted as indicators of a limited downslope displacement.	3-30
3.15	Dip maps extracted from the present day seabed in the Levant 3D area. (a) Dip map showing the present-day shelf and slope. The dashed line represents the shelf-break. Four main arrays of slumps (marked by arrows) are observable. Note the marked headscarps located close to the shelf break. Slump deposits create elongated bodies extending downslope. The box outlines the position of the GSC. (b) Enlargement of the GSC. Note the presence of three clear headscarps suggesting a complex history of instability. The strike-parallel lineaments upslope of the headscarps GSC-1 and GSC-2 are interpreted as crown-cracks. Note the presence of two elongated bodies interpreted as proto-slumps (PS-1 and PS-2). The continuous straight lines indicate the position of seismic profiles used to illustrate the internal appearance of the GSC and the PS-1 (Figures 3.16 and 3.18 respectively).	3-32
3.16	Catalogue of seismic sections through the GSC illustrating the seismic appearance of its internal parts (see Figure 3.15b for location). The dashed line marks the basal shear surface. (a) Seismic section parallel to the direction of transport illustrating the GSC-1 and the GSC-3. The headscarps and toe regions for both slump deposits are shown. Note the close relationship between the headscarp of the GSC-1 and minor faults updip suggesting retrogressive failure. (b) Seismic section perpendicular to the direction of transport through the headscarp of the GSC-1. Note the two clear lateral margins creating a negative topography and the presence of a block-like feature. (c) Seismic section perpendicular to the direction of transport through the toe region (see Figure 3.15b for location). The lateral margins form a positive topographic relief. The seabed appears crenulated.	3-33
3.17	Schematic depiction of part of the GSC. The slump body is divided into two main parts: the depletion zone and the accumulation zone. The depletion zone shows a spoon-shaped depression suggesting reduction of the sediment column. Note the presence of a clear headscarp and evidences of retrogressive failure in the upslope parts. The accumulation zone is characterized by compressional structures and gain of material. In the toe region the slumped material over runs the previous seabed. Inspired by O’Leary (1991).	3-37
3.18	Seismic profile through the PS-1(see Figure 3.15b for location). Note the small topographic depressions on the seabed interpreted as crown-cracks. These correspond to faults and fractures that are rooted in an interval of discontinuous seismic reflections interpreted here as an incompetent layer.	3-39

Chapter Four: Compressional toe regions in submarine landslides

Figure No.	Figure Caption	Page No.
4.1	Schematic depiction of the two main types of submarine landslides according to their frontal emplacement. (a) Frontally emergent landslide. Note that the material ramps out the basal shear surface onto the seabed and is free to travel considerable distances over the undeformed slope position. (b) Frontally confined landslide. The mass is buttressed against the frontal ramp and does not abandon the original basal shear surface.	4-4
4.2	(a) Geological sketch of part of the Eastern Mediterranean showing the main structural elements. The box marks the approximate location of the study area. Modified from Garfunkel (1998). (b) Location map for the study area showing the 3D seismic database used in the study and locations of key exploration wells.	4-6
4.3	Generalised chrono-stratigraphic and lithological scheme of the post-Eocene continental margin of Israel. The lithological column is based on unpublished well reports.	4-7
4.4	Regional dip seismic section through the continental margin of Israel (see Figure 4.2 for location). This seismic profile illustrates the post-Cretaceous configuration of the study area. Note the presence of an extensive unconformity and a thick deposit of evaporites resulting from the Messinian Salinity Crisis. Listric shore parallel growth faults are related to gravity-driven deformation of the Pliocene-Holocene continental margin and to salt tectonics.	4-8
4.5	Seismic section (a) crossing the central parts of the Levant 3D area (see Figure 4.2b for location) and (b) interpretation showing the stratigraphic context of slump deposits in the study area. Shaded areas correspond mainly to simple slump deposits. Note that there is a concentration of slump deposits in the locations overlying pre-Messinian canyons. Slumps increase in number and decrease in size upwards.	4-11
4.6	Map of the ISC showing its areal extension. Note its enormous areal extent (c. 4800 km ²). The dashed line (parallel to the coastline) marks the general trend of large tectonic structures from the Syrian Arc system. Arrows indicate the gross transport direction of the slump mass. Seismic sections (indicated with thick dashed lines) are used to illustrate the regional seismic appearance of the ISC (Figures 4.7-4.8).	4-13
4.7	Seismic profiles along the ISC. (a) 2D seismic profile in the upslope parts of the ISC (see Figure 4.6 for location). The headscarp forms a steeply dipping interface forming the updip boundary between the chaotic seismic facies within the slump body and the continuous reflections of the upper slope. Clear onlap of the headscarp by post-slump sediments is observed. (b) 3D seismic profile through the toe region of the ISC (see Figure 4.6 for location). The toe region appears as the downslope boundary between chaotic seismic facies of the ISC and the continuous reflections of the base of slope. Note the presence of a clear frontal ramp and the slump mass being buttressed against the downslope strata. Older slump deposits appear affected by the ISC.	4-14
4.8	3D seismic profile across the ISC (see Figure 4.6 for location). Note the intensively chaotic seismic facies of the internal parts of the ISC bounded above and below by the top and basal shear surface respectively. A lateral flank of the ISC forms a highly steep ramp separating chaotic for continuous seismic facies. Note the presence of a ramp indenting the basal shear surface and a block of undisturbed reflections within the ISC. A three seismic profiles (Figure 4.9) are used to further illustrate the internal geometry of the ISC.	4-16
4.9	Seismic profile in the dip direction along the ISC. Note the presence of resolvable seismic reflections within the slump deposit (marked S). These are significantly similar to the surrounding strata. The basal shear surface follows the strata of the underlying contourite drift deposits.	4-17
4.10	(a) Seismic profile in the dip direction along a segment of the ISC (see Figure 4.6 for location). The internal parts of the slump deposit are composed of upslope dipping tilted seismic reflections. These reflections are offset and create locally developed listric geometries (marked Y). (b) Interpretation showing five markers that have been used to accurate correlation across the ISC. Thrust structures ramping up to the top of the slump deposit are interpreted. Minor extensional structures are also interpreted.	4-19
4.11	(a) Structurally flattened horizontal coherence-slice across part of the toe region of the ISC (see Figure 4.6 for location). Note the presence of arc-like concentric structures (marked C). These are interpreted as thrust fault planes. There are also coherent parts of the slump deposit interpreted as "in situ" blocks. It is important to note the presence of planes of dislocation within the slump mass (marked D). A marks a seismic artefact. (b) Interpretation. The black arrows indicate the inferred direction of displacement of the slump mass. T-5 and T-10 correspond to two fault planes studied in detailed.	4-23
4.12	Displacement vs distance graphs of tow representative thrust structures within the toe region of the T20 slump deposit.	4-26
4.13	Representation of the displacement along a representative thrust structure (T-5). Note that the maximum displacement is in the centre of the structure suggesting higher levels of displacement in the central parts of the slump mass.	4-27

4.14	Isochron of the T20 slump deposit. The headscarp forms an arcuate feature adjacent to thin deposits of sediment. The toe region is characterised by a considerable increase in the thickness of material.	4-31
4.15	Seismic profile across the headscarp of the T20 slump. The slump mass appears significantly depressed in relation to the surrounding strata. There is clear evidence of onlap. The internal parts of the slump deposit are dominated by deformational extensional and compressional structures.	4-32
4.16	Seismic profile across the toe region of the T20 slump deposit. The slump mass overrides the coeval seafloor and thins significantly towards its distal parts.	4-34
4.17	Seismic profile across the toe region of the T20 slump in the strike direction. The slump mass overrides the coeval seafloor. The lateral flanks are concordant with the overlying and underlying strata and thin gradually towards the distal parts. The internal parts of the T20 slump deposit are dominated by thrust structures. C marks the position of a possible outrunner block. The direction of translation of the slump mass is approximately perpendicular to the seismic section.	4-35
4.18	(a) Maximum amplitude seismic extraction within the toe region of the T20 slump deposit. Note the presence of high amplitudes in the core of the toe. These correspond to areas dominated by thrust structures. Towards the lateral and frontal parts the amplitudes diminish. The core and the outermost parts are separated by a clear limit between high and low amplitudes. In the frontal parts, the slump material shows clear concentric arc-like structures, which correspond to thrust planes. (b) Schematic depiction of the interpretation of the internal parts of the toes region of the T20 slump.	4-37
4.19	Schematic depiction of the suggested mechanism for downslope translation of frontally confined submarine landslides. The material does not override the frontal part but translated downslope but deforming and integrating the foreland into the frontal parts of the slump.	4-45

Chapter Five: Summary and discussion

Figure No.	Figure Caption	Page No.
5.1	Schematic depiction of the different stages and basinal distribution of soft-sediment deformation offshore Israel. The red dotted line marks the position of the continental shelf break.	5-7
5.2	Worldwide distribution of possible analogues of the soft-sediment deformational structures presented in this research project.	5-17

LIST OF TABLES

Chapter Four: Compressional toe regions in submarine landslides

Table No.	Table Caption	Page No.
4.1	Measurements undertaken at fifteen different thrust structures within the toe region of the T20 slump deposit.	4-28

Chapter Five: Summary and discussion

Table No.	Table Caption	Page No.
Table 5.1	List of possible analogues for the submarine landslides presented in this research project. Their location, slope angle, volume and process are listed	5-19

APPENDICES

CD-1

Folder No.	Content
1.1	List of all the exploration and production wells in Israel.
1.2	Collection of maps (TWT and attributes), and time and coherence-slices undertaken during this research project as support to the analysis presented in the thesis.

CD-2

Folder No.	Content
2.1	Digital copy of the thesis.

ENCLOSURE

Published paper:

Frey-Martinez, J., J. Cartwright, and B. Hall, 2005, 3D seismic interpretation of slump complexes: examples from the continental margin of Israel. *Basin Research*, v. 17, p. 83-108.

ACRONYMS

Acronym	
AM	Alpha Mound
DHI	Direct Hydrocarbon Indicator
GSC	Gaza Slump Complex
GSC-1	Gaza Slump Complex-1
GSC-2	Gaza Slump Complex-2
GSC-3	Gaza Slump Complex-3
GWC	Gas Water Contact
ISC	Israel Slump Complex
ISC-1	Israel Slump Complex-1
ISC-2	Israel Slump Complex-2
ISC-3	Israel Slump Complex-3
YSM	Yafo Sand Member
MMC	Mairi Mound Complex
MMC-1	Mairi Mound Complex-1
MMC-2	Mairi Mound Complex-2
MMC-3	Mairi Mound Complex-3
NMC	Nir Mound Complex
NMC-1	Nir Mound Complex-1
NMC-2	Nir Mound Complex-2
NMC-3	Nir Mound Complex-3
T-5	Thrust-5
T-10	Thrust-10

Chapter One: Introduction

1.1. Rationale

Soft-sediment deformation is a common phenomenon to many geological settings worldwide. Numerous stratigraphical, sedimentological and scaled physical studies have demonstrated that underconsolidated sediments can become non-tectonically deformed, affecting many of their physical properties at various scales and bearing great importance to the configuration of sedimentary basins (e.g. Diller; 1889; Anketell et al., 1970; Allen, 1984; Cartwright, 1994; Nichols et al., 1994; Dixon, 1995; Davies, 2003). At small scales, soft-sediment deformation can modify the grain size distribution, clast orientation, porosity and permeability of siliciclastic sediments (e.g. Lowe, 1975). At larger scales, it may alter primary sedimentary structures, bed contacts, and even the overall geometries of entire sedimentary bodies (e.g. Davies, 2003). It is clear from field evidence, and consistent with experiment and theory, that soft-sediment deformation is associated in time with the earliest stages of sediment consolidation, when the deposit is weakest and pore fluid is being expelled most rapidly (Allen, 1984). The resultant structures form peculiar and intriguing geological features, ranging from polygonal fault systems (e.g. Cartwright, 1994) to sand injectites (e.g. Hurst and Cronin, 2001), mud diapirs (e.g. Van Rensbergen and Morley, 2003), and slope failures (e.g. Lewis, 1975; Prior and Coleman, 1978) amongst others. Soft-sediment deformation can have a critical impact on the hydrocarbon prospectivity of sedimentary basins as it has the potential to generate traps, influence migration pathways, and alter the original architecture of reservoirs. In addition, it plays a significant role in the slope stability of continental margins since it may control the redistribution of vast amounts of sediment from shallow to deepwater settings.

Research on soft-sediment deformation dates back to the 19th century to the pioneering work of Diller (1889), who first recognised sand injectites within sedimentary successions. Since this original work, the ever-increasing resolution of subsurface data has yielded many new insights into soft-sediment deformation, not only from regions clearly prone to sediment remobilisation, such as active tectonic settings or regions with exceptionally large sediment supply, but also from tectonically quiescent areas. However,

despite the advances in knowledge throughout more than a century of research, soft-sediment deformation still remains one of the most interesting and enigmatic sedimentary phenomena in the geologic record. Indeed, many questions regarding its triggering mechanisms, genetics, resultant structures and significance for the exploration and production of hydrocarbons are still unanswered. This is mainly due to the lack of 3D data, which has been a persistent obstacle to the identification and detailed analysis of the structures resulting from soft-sediment deformation, their areal extent and geological context.

The present PhD project uses commercial seismic (2D and 3D) and well data to analyse the characteristics, formation and significance for hydrocarbon prospectivity of two types of soft-sediment deformation on the continental margin of Israel: clastic diapirism and submarine slope instability (i.e. submarine slumping). This area is ideal for such an analysis because it contains many well-preserved examples of both deeply buried and shallow soft-sediment deformational structures. The combination of seismic and borehole data provides an excellent coverage of the margin and enables these structures to be analysed to a high degree of accuracy that could not be attained by any other combination of methods. By using the Israeli continental margin as a natural laboratory, this research project provides new valuable insights into the typologies, triggers, formational processes and resultant structures of soft-sediment deformation, and its impact on the exploration and production of hydrocarbons. Although the examples illustrated in this thesis are specific to the study area, the results and ideas presented should find applicability in other continental margins worldwide.

The present chapter commences by providing a list of the principal aims of this PhD research project. Subsequently, a concise overview of the location and geological setting of the study area, the data and methodology used, and an account of the history of hydrocarbon exploration in Israel are presented. The chapter ends with the thesis layout. More detailed background to the geological setting of the study area, the datasets and methodologies employed throughout this research, and a review of the previous literature are provided in subsequent chapters.

1.2. Aims of study

This thesis has a number of aims, the majority of which are related to improve current understanding of clastic diapirism and slope instability processes in general. However, because this research is a Joint Industry Project (Cardiff University-BG Group), a series of resultant aims are to recognise how these processes may control the hydrocarbon prospectivity of the continental margin of Israel. The two groups of objectives are tackled by systematically addressing a number of key aims within the case-study area. These are stated thus:

- Account for the geometries and internal fabrics of clastic diapirs in 3D.
- Explore means for dating clastic diapirism combining 3D seismic and well data.
- Develop means for recognising lithological compositions of clastic diapirs using 3D data.
- Investigate the spatial distribution of the effects of clastic diapirism in the sedimentary cover sequence.
- Explore the genetics and triggering mechanisms for clastic diapirism.
- Produce criteria for identifying submarine slumps and distinguishing them from other features on seismic data.
- Account for the distribution of submarine slump deposits within the study area.
- Constrain the relative timing of key slope failures by using 3D data.
- Describe the geometries and internal appearance of key slump deposits in 3D.
- Measure and analyse in detail the geological structures within slump deposits.
- Develop means for identifying the propagation direction of slumps.
- Analyse the kinematics and dynamics of submarine slumps.
- Highlight areas of high potential for future slope instability in the study area.
- Assess the implications of clastic diapirism and submarine slumping in relation to hydrocarbon exploration and production on the continental margin of Israel.

1.3. Location and geological setting

The continental margin of Israel is located in the south-eastern Mediterranean Sea, situated some 150 km east of the Nile River delta (Figure 1.1). Extending from the south of the Gaza Strip to Haifa city, the studied portion of the continental margin covers c. 23,000 km² in a SW-NE direction and forms part of the Levant Basin.

The Israeli continental margin is situated in an active tectonic setting at the zone of interaction between the African and the Arabian plates, and close to the Dead Sea Transform in the east and the Cyprian Arc in the northwest (Figure 1.1). Its early development is related to a sequence of rifting events from the Early Permian to the Middle Jurassic (Garfunkel, 1998). Throughout this period, opening of the Tethys Ocean caused rifting to the north of the African plate and resulted in break-up of the extensive shallow-water carbonate platform that had dominated the paleogeography of the region (Figure 1.2). The subsequent continental break-up that led to the initiation of spreading in the eastern Mediterranean resulted in the formation of a passive continental margin from the end of the Middle Jurassic (Garfunkel and Derin, 1984). During this period, shallow-water carbonate platforms bordered by deepwater basins developed until the Late Cretaceous (Garfunkel, 1998).

In the Late Cretaceous, a change in the relative motion of the African plate with respect to the Eurasian plate led to a compressive stress regime and the formation of the Syrian Arc system (Figure 1.1; Ben-Avraham, 1989; Tibor & Ben-Avraham, 1992; Eyal, 1996). Since the beginning of the Tertiary, active subduction and collision activity has been occurring to the north leading to the formation of the Zagros and Taurus mountain chains (Tibor and Ben-Avraham, 1992). Rifting and opening of the Red Sea, together with the initiation of the Dead Sea Transform, commenced in the Miocene. As a consequence, the shelf area experienced localised tectonic uplift and became intermittently emergent. Conversely, the slope and basin areas continued to subside (Buchbinder and Zilberman, 1997). At the end of the Miocene, the evolution of the margin was greatly influenced by the desiccation of the Mediterranean Sea during the Messinian Salinity Crisis (Tibor & Ben-Avraham, 1992). An extensive sub-aerial

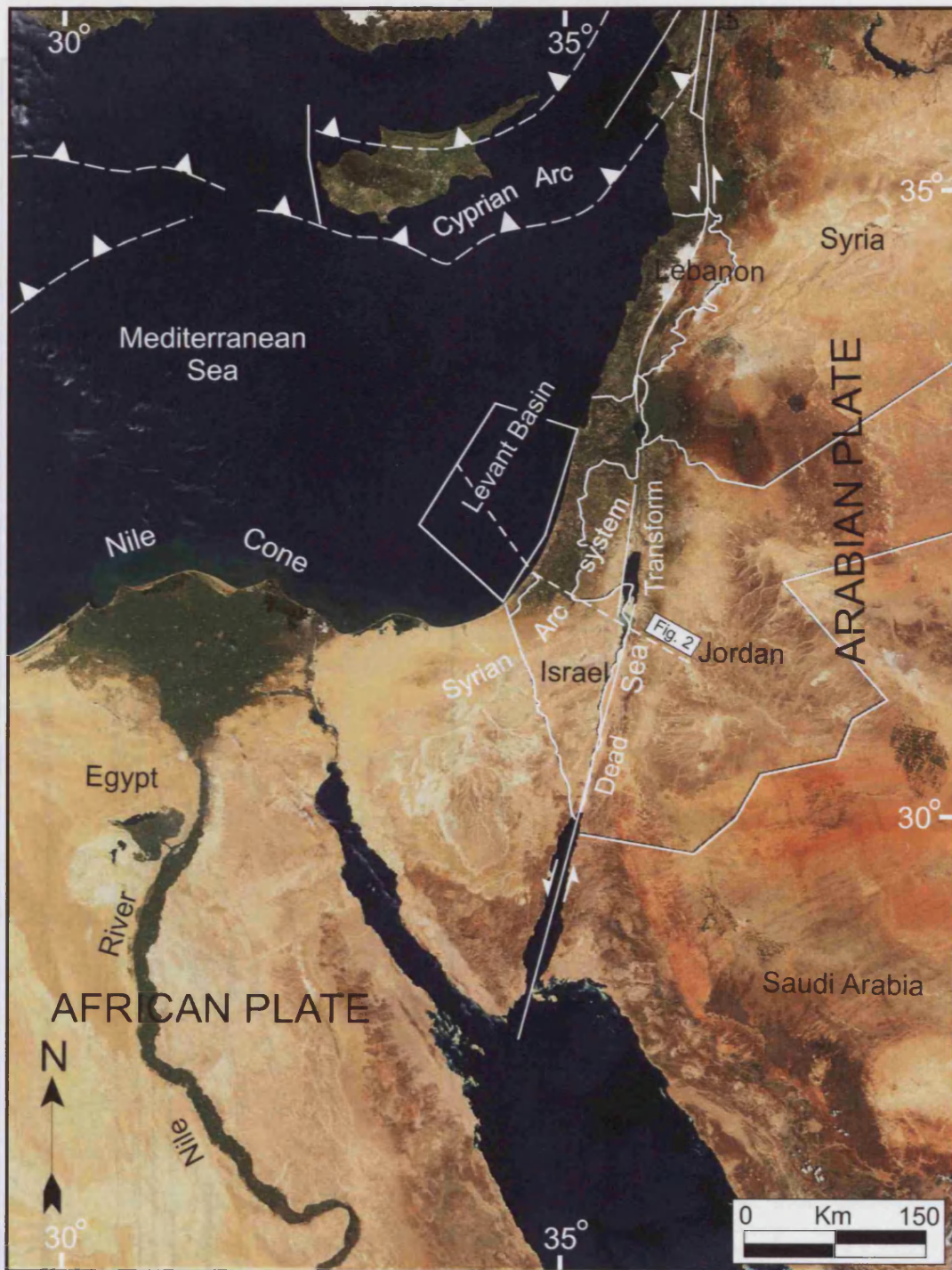
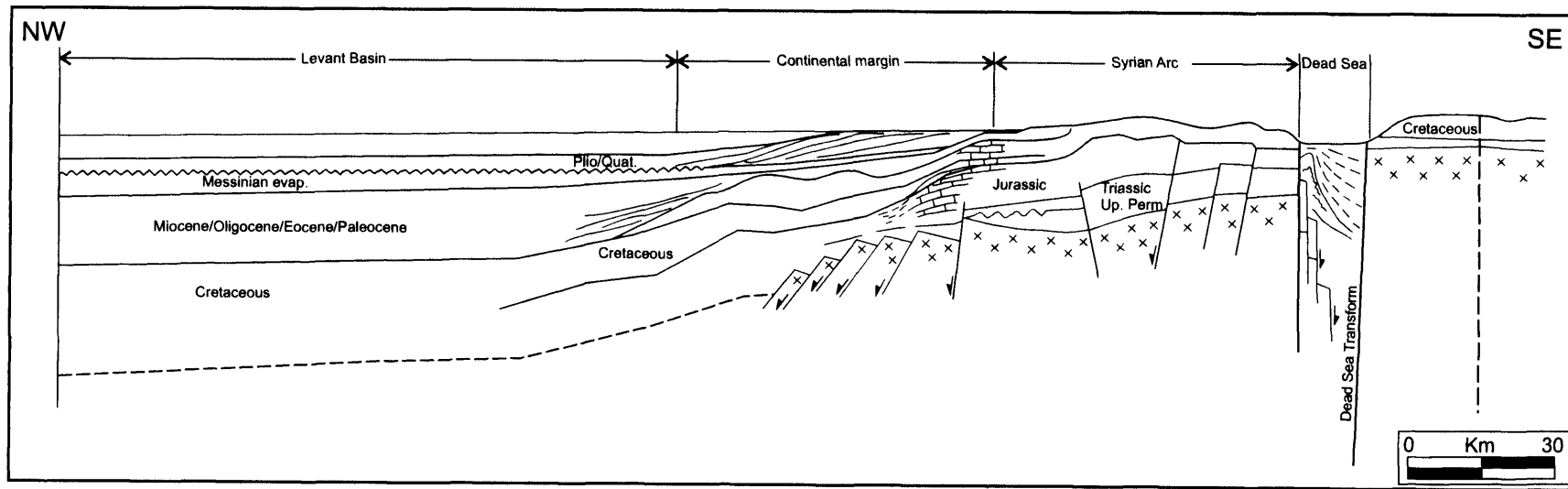


Figure 1.1 General geographical map of part of the Eastern Mediterranean showing its main regional structural elements. The solid-line box marks the approximate position of the study area. The dashed lines indicate the trend of the main thrust systems. Solid lines mark the main fault systems. Note the location of Figure 1.2. Structural elements after Vidal et al. (2000). Satellite image from www.nasa.org.



1-6 **Figure 1.2** Schematic cross-section through onshore and offshore Israel (see Figure 1.1 for location) showing the main structural elements. Modified from Garfunkel (1998).

unconformity formed along basin margins whilst thick evaporitic deposits were laid down over the former basin floor (Hsü et al., 1978; Montadert et al., 1978; Figure 1.2).

During the Pliocene, the vertical tectonic movement reached its peak (Almagor, 1993) and a major transgression submerged the exposed Upper Miocene shelf (Buchbinder and Zilberman, 1997). Large volumes of Nile-derived siliciclastic sediments were deposited on the continental margin. Simultaneously, subsidence along the margin increased significantly, possibly as a result of the large volumes of siliciclastic sediment being deposited from the Nile River, or to a change in motion along the Dead Sea Transform (Tibor et al., 1992). During this period, the gross configuration of the margin constituted a strongly aggradational system, with sigmoidal clinofolds linking shelf to slope (Figure 1.2). Simultaneously, several episodes of large-scale soft-sediment deformation and gravitational tectonics occurred (e.g. Almagor, 1980, 1984 and 1986; Garfunkel, 1984; Garfunkel & Almagor, 1985 and 1987). This scenario has persisted until the present day.

1.4. History of hydrocarbon exploration in Israel

Hydrocarbon exploration in Israel (including the West Bank and Gaza) commenced in the 1940's, with the first exploration well being drilled in 1947 in the Heletz area south of Ashkelon (Figure 1.3; Israeli Ministry of National Infrastructures, 2001). Since then, approximately 470 wells have been drilled, of which 120 are appraisal and development wells (Fleischer, 2000; **Appendix 1**). Most of the early exploration efforts were focused on shallow stratigraphic intervals along the Mediterranean coastal plain, and the Negev and Dead Sea regions (Figure 1.3). In 1955, the first commercial discovery (Heletz oil field) was made in Cretaceous formations. Since then, exploration focused on similar intervals and Upper to Middle Jurassic structures in the Negev region. This resulted in the discovery of the first gas fields (Zohar, Kidod and Hakanaim near Arad) and a further oil discovery in Kokhav, near Heletz. There was also a non-commercial oil discovery at Gurim, near Arad (Figure 1.3; Israeli Ministry of National Infrastructures, 2001).

During the 1960's, exploration was primarily centred in the areas around the Heletz and Zohar gas fields. Simultaneously, an American consortium lead by Esso (now ExxonMobil) drilled six offshore wells along the Mediterranean coast targeting Jurassic

antiform structures from the Syrian Arc system. However, no commercial discovery was made (Israeli Ministry of National Infrastructures, 2001). From 1967, exploration decreased within the areas of earlier interest, and efforts were focused on shallow structures in the Gulf of Suez. This strategy, however, was abandoned during the oil price crisis of 1973, and exploration efforts were then shifted to large structures in deeper and unexplored intervals of the Sinai and Gulf of Suez. This new approach resulted in the discovery of the Sadot gas field (Figure 1.3). Simultaneously, exploration continued on the Mediterranean coastal plain which resulted in the discovery of the Shiqma gas field and the Ashdod oil field (Figure 1.3). During the 1980's substantial drilling was carried out to test Triassic and Permian plays in the Negev region without success (e.g. Fleischer, 2000).

During the early 1990's, exploration was focused offshore the Mediterranean coast of Israel (Maddox, pers. comm. 2003). Three exploration wells were drilled on the continental margin by Isramco, the Israeli national oil company, of which two tested oil from Jurassic structures of the Syrian Arc system (i.e. Yam-1 and Yam-2). Between 1999 and 2001, a British-Israeli-American consortium lead by BG-Group discovered significant hydrocarbon accumulations in Early Pliocene formations (Yafo Sand Member) offshore the Gaza Strip and southern Israel (Or, Gaza, Mari, Noa and Nir fields; Figure 1.3). These accumulations are the biggest hydrocarbon discovery ever made in Israel, and one of the most significant reservoirs in the south-eastern Mediterranean (initial estimates of 3.5 Tcf of proved biogenic gas). However, since the discovery of these plays, appraisal and production have had mixed success. Although several relatively major gas accumulations have been appraised within the Yafo Sand Member, a major uncertainty remains 3D prediction of reservoir architecture, with many appraisal wells failing to find good reservoir intervals (Hall, pers. comm. 2002). During the course of appraisal of two of the gas fields (Mari and Nir), it became obvious that some post-depositional process had affected the original architecture of some of the reservoirs, and that an inclusive understanding of such process was required in order to successfully pursue the plays. This problem forms the core of one of the main research topics of the present thesis (clastic diapirism), and will be examined and discussed in detail in **Chapter 2**.



Figure 1.3 Map of Israel showing the location of the most significant oil and gas fields discovered until 2005. The location of the study area is also indicated. Modified from Israeli Ministry of National Infrastructures (2001).

1.5. Database

The database employed in this research project consists of industry seismic (2D and 3D) and well data. All the data were obtained through BG-Group under a three-year confidentiality agreement. No potential field data were available for this study, although published gravity and magnetic maps were used in the interpretation of regional tectonics. The location of the data is shown in Figure 1.4.

Approximately 6000 km of regional high-resolution seismic profiles comprise the 2D seismic data. These correspond to over 60 profiles acquired during the 1980's covering the entire Israeli continental margin in a 10 km by 10 km grid (Figure 1.4). All the profiles are oriented orthogonally and parallel to the Israeli Mediterranean coast. The quality and resolution of individual 2D seismic profiles varies considerably. Generally, those in the northern parts of the continental margin are of poorer quality than those in the central and southern parts as they were acquired during the early 1980's before advances in the fields of data acquisition and processing were made.

Two 3D seismic surveys (Levant and Med Ashdod), acquired by Geco-Prakla in 2000, comprise the 3D seismic data used in this study (Figure 1.4). The total coverage of these two datasets amounts to 2500 km², extending from shelf to deepwater offshore the Gaza Strip. The Levant and Med Ashdod surveys were acquired with an in-line trace interval of 6.25 m and a line spacing of 25 m. The final data for these two surveys were defined on a 12.5 by 12.5 m grid with 6400 bin cells per sq km after processing by Geco-Prakla (BG-Group Report SA9029, 2000). All the data are offset pre-stack time migrated and near zero phase with SEG normal polarity, meaning that an increase in acoustic impedance is represented by a positive amplitude. The zero phase nature of the data was determined from examination of the seismic response of the seabed (Figure 1.5). Such response consists of a peak flanked by two side lobes, which is interpreted to be due to an increase in acoustic impedance at the transition between seawater (low velocity) and the sediment (high velocity). The dominant frequency of the seismic data varies with depth as P and S wave velocity tends to increase with depth due to compaction and diagenesis (e.g. Brown, 2003). Nevertheless, the acquisition and processing parameters of both 3D

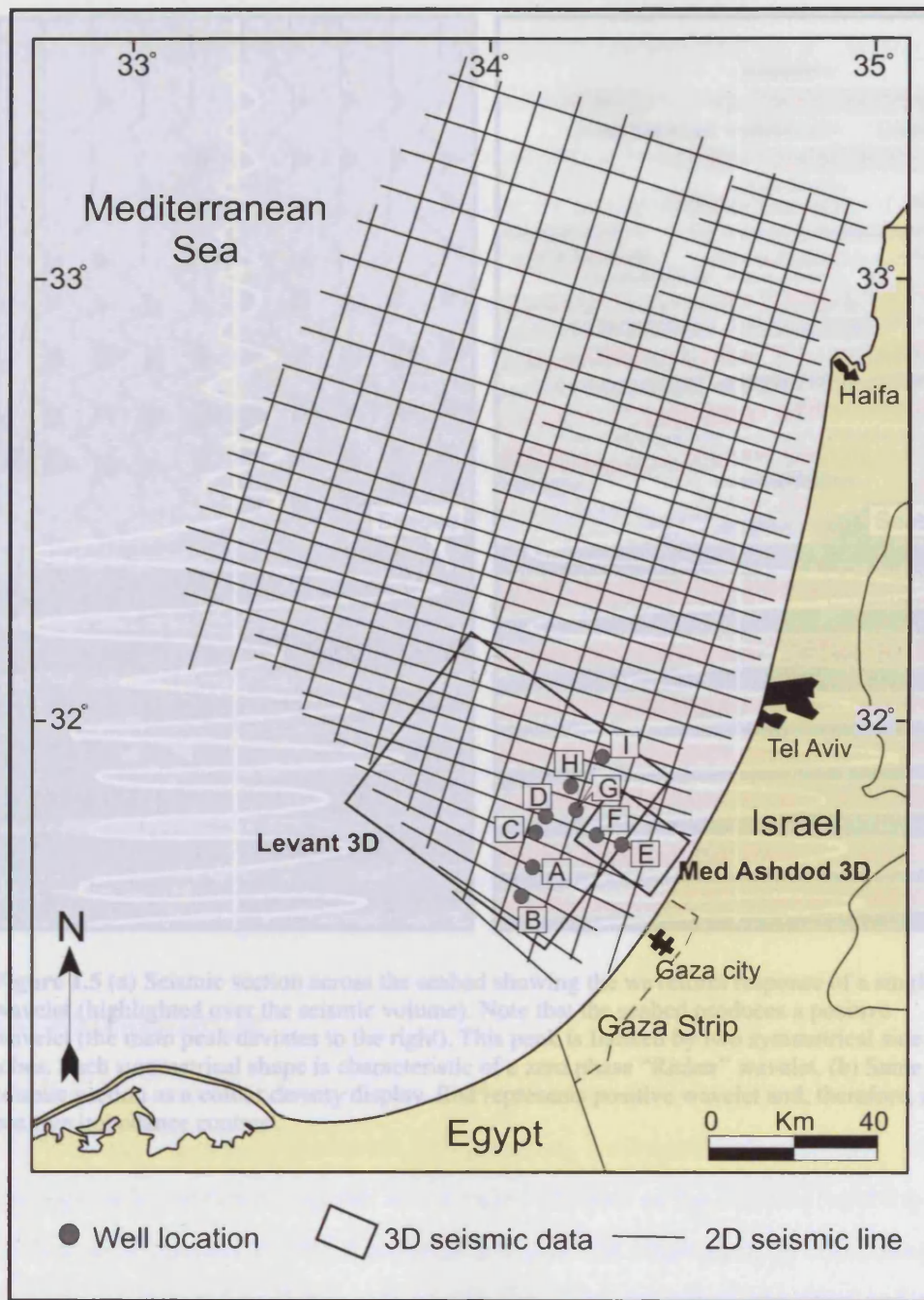


Figure 1.4 Location map of the study area showing the full extent of the 2D and 3D seismic surveys and the position of the exploration well used in this study. Nomenclature for the exploration wells is: A= Gaza Marine-1, B= Gaza Marine-2, C= Noa-1 South, D= Noa-1, E= Nir-1, F= Or South-1, G= Or-1, H= Yam West-2, I=Yam West-1.

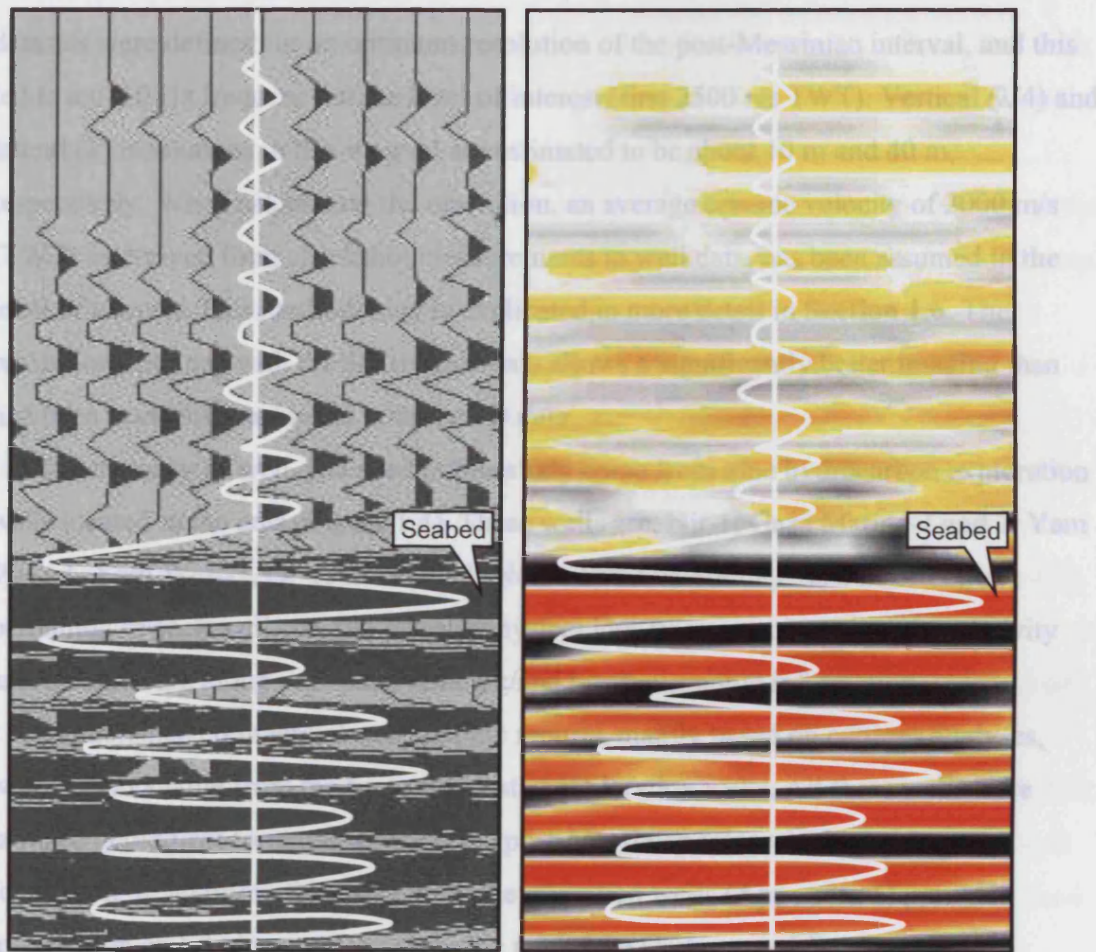


Figure 1.5 (a) Seismic section across the seabed showing the waveform response of a single wavelet (highlighted over the seismic volume). Note that the seabed produces a positive wavelet (the main peak deviates to the right). This peak is flanked by two symmetrical side lobes. Such symmetrical shape is characteristic of a zero phase "Ricker" wavelet. (b) Same seismic section as a colour density display. Red represents positive wavelet and, therefore, a positive impedance contrast.

comprehensive approach of seismic interpretation, calibrated with well data, was used. This approach combined regional and detailed analysis of the features resulting from soft-sediment deformation. Firstly, a regional analysis was undertaken by combining all the available seismic and well data. Major structural elements were identified and regional stratigraphic correlation was undertaken. Subsequently, a refined seismic-stratigraphic framework was established for the continental margin offshore the Gaza Strip by tying the 3D seismic data with litho- and biostratigraphic information from the wells. The borehole information was employed also to undertake basic depth conversions within the levels of interest in this part of the margin. Precise constraint of the velocity distribution

datasets were defined for an optimum resolution of the post-Messinian interval, and this led to a c. 50 Hz frequency at the level of interest (first 2500 ms TWT). Vertical ($\lambda/4$) and lateral (λ) resolutions in this interval are estimated to be about 10 m and 40 m, respectively. When calculating the resolution, an average seismic velocity of 2000 m/s (TWT) as derived from checkshot measurements in well data, has been assumed in the level of interest. This methodology is explicated in more detail in **Section 1.6**. The resolution obtained with the 3D seismic data allows a significantly better imaging than had been previously achieved with the 2D data.

The majority of well data used in this study come from nine hydrocarbon exploration wells located in the area (Figure 1.4). These wells are: Nir-1, Gaza Marine-1 and 2, Yam West-1, Yam West-2, Or-1, Or South-1, Noa-1 and Noa South-1. The information pertaining to each well consists of petrophysical logs (γ -ray, sonic, velocity, resistivity and checkshots), along with paleontologic and biostratigraphic information.

Unpublished commercial stratigraphic reports, mainly based on cuttings analyses, were also available from the first seven listed exploration wells. All these wells have targeted geological formations within the post-Messinian interval which this study focuses on. In addition, thirty-one deeper exploration wells (**Appendix 1**) provided information on lithology and stratigraphic age of the Cretaceous-Miocene intervals.

1.6. Methodology

In order to understand the processes of soft-sediment deformation in the study area, a comprehensive approach of seismic interpretation, calibrated with well data, was used. This approach combined regional and detailed analysis of the features resulting from soft-sediment deformation. Firstly, a regional analysis was undertaken by combining all the available seismic and well data. Major structural elements were identified and regional stratigraphic correlation was undertaken. Subsequently, a refined seismic-stratigraphic framework was established for the continental margin offshore the Gaza Strip by tying the 3D seismic data with litho- and biostratigraphic information from the wells. The borehole information was employed also to undertake basic depth conversions within the levels of interest in this part of the margin. Precise constraint of the velocity distribution

within the post-Messinian interval was attempted by calibrating the 3D seismic data with checkshot-derived velocities from six of the exploration wells. However, no consistent or even comparable response for any of the six velocity/depth curves was obtained.

Consequently, an alternative approach was to correlate key stratigraphic markers from the completion logs throughout the 3D seismic data. This was done in order to define a series of intervals within the post-Messinian sequences in which depth conversion could be undertaken individually. However, the stratigraphic markers were too erratically and sparsely located to be of any use in defining any accurate division. In view of these limitations, an averaged value of 2000 m/s (TWT), as obtained from the checkshot of the Gaza Marine-1 exploration well, was considered for the entire post-Messinian interval. The Gaza Marine-1 well was selected based on the continuous petrophysical logs (γ -ray, sonic, velocity, resistivity and checkshots) it provided for the entire post-Messinian interval. An maximum error of 7-12% is estimated for the depth conversions based on this well.

Finally, accurate 3D mapping and seismic attribute analysis, calibrated with well data, was employed to investigate the basinal distribution, seismic geometry, dimensions and lithology of a series of representative examples of soft-sediment deformational structures in the study area. The portion of the margin offshore the Gaza Strip was selected for detailed analysis of these structures because of their higher occurrence in this region, their intriguing geometries, and the superior resolution provided by the 3D seismic data. Indeed, these seismic data offered the fundamental advantage of analysing soft-sediment deformational structures in three dimensions, with a maximum resolution in the scale of meters that could be correlated over thousands of sq km. It also allowed accurate investigation into the external and internal geometries of the structures, and into their timing and relationship with the surrounding strata.

1.7. Terminology for slope instability processes

Previous research on slope instability processes around the world has been clouded by a variable and imprecise use of terminology referring to their formational mechanisms and resultant structures. As a result, a number of terms (i.e. slump, slide) and misleading

definitions that relate to identical processes are currently in use. This overlapping in terminology may be partly due to the different groups of earth scientists studying slope instability processes and to their varying analytical methods. Engineering geologists, for example, typically analyse subaerial bodies with total areas of less than 10 km² from scar to deposit (Varnes, 1978). Conversely, sedimentologists and structural geologists often study ancient submarine examples with unknown areas that may exceed 60,000 km² (Bugge, 1983). Engineering geologists may therefore appreciate if a backward rotation of sediment has occurred (in which case the process is termed slumping) or if collapse has been due to a non-rotational downslope movement (then termed sliding). Structural geologists and sedimentologists on the other hand cannot state with certainty that an element of backward rotation has occurred since analysis is typically focused on a small portion of each resulting body. In this case, the internal appearance of the resultant bodies (e.g. deformational structures) is typically used to distinguish between slides and slumps.

Slumps and slides, along with debris flows and turbidity currents, are considered part of the continuum of gravity-driven transport sediment processes (Stow, 1986; Figure 1.6). Each transport type is characterised by mass of sediment that moves above a basal shear surface. However, the behaviour of the ensuing flow and hence resultant depositional mechanism may be significantly different. Slumps, for example, involve a limited downslope movement of a more or less coherent block of material, usually on a rotational glide plane, with some but limited internal deformation (e.g. Varnes, 1978). Slumps may evolve into slides, in which the slump body undergoes significant translational movement, usually on a glide plane which is approximately slope parallel. Slide blocks tend to disintegrate as they move downslope, giving another gradational boundary to debris flow. Debris flows are characterised by uniformly dispersed grain flow behaviours in which an almost total internal disaggregation occurs. In many cases, discerning between the different types of these formational processes may be significantly complicated as most large submarine failures are complex and can often involve all three processes. In this thesis, the majority of analysed slope instability processes are considered to be slumps based on the definition by Stow (1986). According to Stow (1986), a slump is *a laterally displaced sediment mass bounded by a basal shear surface*

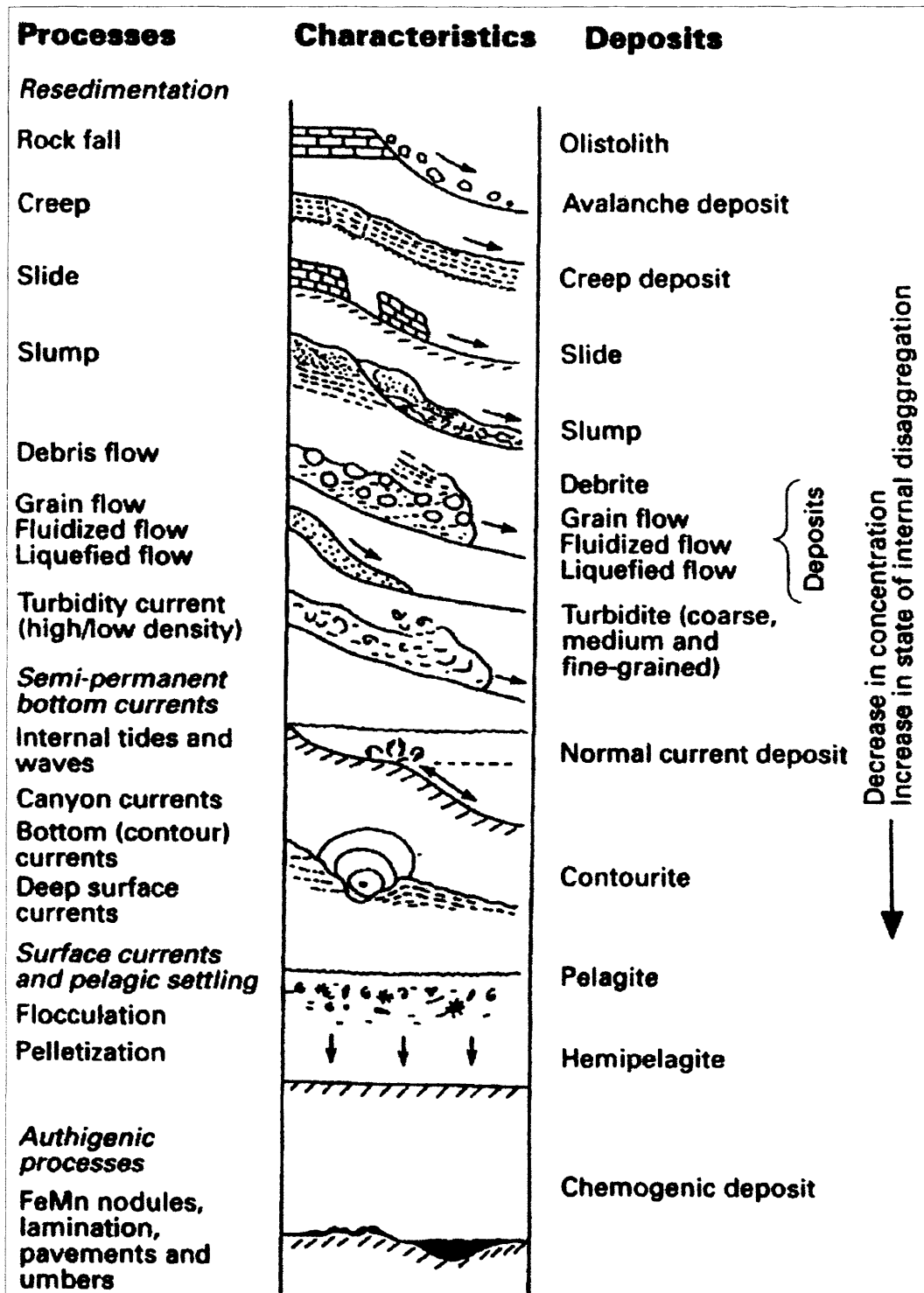


Figure 1.6 The range of deep-water resedimentation processes and their products. From Stow (1986).

and with evident contortion and rotation of the contained strata. This definition has been followed in this thesis based on the geometrical aspect of the internal parts of the studied bodies as seen on 2D and 3D seismic data. It should be taken into account, however, that slides and debris flows most likely also occurred in the study area although they are considered as minor processes compared to slumping.

1.8. Thesis layout

The core of this thesis is structured into three submitted papers (**Chapters 2, 3 and 4**) addressing the two main topics analysed during this research project (i.e. clastic diapirism and submarine slope instability). The last two chapters (**Chapters 4 and 5**) discuss and conclude, respectively, the main scientific results of this investigation. The thesis is thus divided as follows:

- **Chapter 2** addresses the topic of clastic diapirism in the study area and its impact on hydrocarbon prospectivity. An overview of the geological setting and a description of the stratigraphic context of clastic diapirism initiate the chapter. Subsequently, detailed seismic and lithological analysis focuses on the stratigraphic interval affected by clastic intrusion. A comprehensive analysis of four case studies is then undertaken. A model for the origin and evolution of clastic diapirism in the area, and its implications for hydrocarbon prospectivity conclude this chapter.
- **Chapter 3** introduces and addresses the topic of submarine slope instability on the continental margin of Israel. The chapter commences with an overview of the terminology and criteria used to identify and describe submarine slump deposits on 3D seismic data. Subsequently, a description of the stratigraphic context of the submarine slump deposits in the southern parts of the study area is undertaken. A detailed 3D analysis of two representative case studies, together with the description of a series of diagnostic structures for potential failures, is also presented. The chapter concludes by discussing the possible triggering mechanisms for submarine failure offshore Israel and the advantages of 3D seismic data to analyse submarine failure processes and results.

- **Chapter 4** addresses the core of another important line of investigation within the topic of submarine slope instability: the formation of compressional toe regions and the frontal propagation of submarine landslides. 3D seismic data are used to discuss the development of large-scale compressional structures in the toe regions of two major submarine landslides. The chapter concludes by analysing the possible causes for the different forms of frontal propagation of submarine landslides, and by proposing a geomechanical model for their occurrence.
- **Chapter 5** draws together the key scientific results of the research which are detailed in the discussion points of **Chapters 2, 3 and 4**, and provides insights into their significance for the exploration and production of hydrocarbons. A review of possible worldwide analogues for the structures studied in this thesis is also undertaken, demonstrating their global implications and applicability. A brief overview of the limitations and uncertainties associated with the study and proposals for future work conclude the chapter.
- **Chapter 6** lists the main conclusions of this research project.

Chapter Two: Clastic intrusion of deepwater sands¹

2.1 Abstract

Three-dimensional (3D) seismic data from the continental margin offshore Israel (Eastern Mediterranean) show a number of large-scale mounded structures interpreted to be clastic intrusions. These features are confined to the Lower and Middle Pliocene and restricted in an area of 40 by 20 km along the Afiq Submarine Canyon, a former depositional fairway of Oligocene age. The mounded structures are circular to oval in plan view, range from 0.5 to 2 km in diameter at their base and are flanked by kilometre-scale depressions interpreted as regions of sediment depletion. In cross-section, the mounds are up to 400 m in height and have flank dips of up to 20°-25°. The largest mounded structures may reach up to c. 0.75 km³ in volume and represent economic hydrocarbon reservoirs.

Well data and direct hydrocarbon indicators show that the mounded structures are predominantly composed of gas-saturated sandstones along their flanks and crests while their centres are heterolithic. Petrophysical interpretation indicates the presence of chaotic and remobilised sediments within the mounded structures. The relationships of the mound-like structures to the overburden exhibit both depositional and deformational geometries (e.g., onlap, forced folding). The proposed model for the formation of these mound-like features is hydraulic “jacking up” of the overburden by forceful vertical and lateral intrusion of clastic sediment during shallow burial. Several episodes of intrusion alternated with deposition of fine-grained clastic sediments during the Early and Middle Pliocene to create the complex structures presented in this chapter. The suggested model has implications for the understanding of the trapping mechanism and reservoir properties of these structures and needs to be incorporated in exploration and development planning.

¹Published as:

Clastic intrusion of deepwater sands as a hydrocarbon trap-forming mechanism: examples from the Eastern Mediterranean, AAPG Memoir, in press.

2.2 Introduction

In recent years, three-dimensional (3D) seismic data have revealed many examples of clastic sediment remobilisation reconfiguring deepwater sands into a complex variety of intrusive and mounded geometries (e.g., Jenssen et al., 1993; Brooke, 1995; Dixon et al., 1995; Nichols, 1995; Lonergan and Cartwright, 1999; Cole et al., 2000; Lonergan et al., 2000; Duranti et al., 2002; Molyneux et al., 2002; Davies, 2003; Hurst et al., 2003; Huuse et al., 2003; Løseth et al., 2003). The dominant processes invoked in this remobilisation are the liquefaction, fluidisation and intrusion of the coarse grained reservoir facies. Understanding the processes and products of large-scale remobilisation is critical for the exploration and production of hydrocarbons because remobilisation exerts significant control on the geometry (Dixon et al., 1995; Lonergan et al., 2000), properties (Duranti et al., 2002) and intra-field connectivity (Guargena et al., 2002) of reservoir sands.

In this chapter, we describe a series of kilometre scale steep-sided convex upwards mound-like features from offshore Israel, which we argue are related to clastic sediment intrusion during shallow burial. These structures consist of a complex arrangement of isolated features and compound arrays that form a sinuous trail above the axis of the Afiq Submarine Canyon (Oligocene in origin). In many cases, the mounded features are sufficiently large to form economic hydrocarbon reservoirs hosting some of the largest gas fields discovered to date offshore Israel. A number of these structures have been targeted by exploration drilling, proving in many cases the presence of tens of metres thick sandstones with excellent reservoir quality (30% porosity, up to 12 Darcy permeability and 81% average net to gross). These reservoirs, however, represent a challenge to the effective recovery of hydrocarbons due to their extreme geometric variability, lithologic heterogeneity and intricate reservoir compartmentalisation.

The aim of this chapter is to describe and unravel the genesis of the mounded features with special emphasis on their implications for hydrocarbon exploration and production. The chapter commences with an overview of the geological setting and a description of the stratigraphic context of the Afiq Submarine Canyon. The main arguments of the chapter are subsequently developed through detailed seismic and lithological analysis focused on the interval of the reservoir affected by clastic intrusion. Exceptional seismic

imaging provided by the 3D seismic data and good calibration with borehole data allows an accurate external and internal geometrical analysis of the mounded structures. We conclude the study by presenting a model for the origin and evolution of these mounds, taking into account a variety of possible origins and their implications for hydrocarbon prospectivity. With substantial accumulations of proven recoverable natural gas remaining to be produced and the potential for new gas discoveries offshore Israel, an in depth understanding of the mechanisms forming the mounded structures and their impact on reservoir quality and architecture will be critical to an efficient assessment of future exploration and production in the region. Although the examples illustrated in this chapter are specific to the study area, the ideas presented may find applicability in the exploration and production for hydrocarbons of deepwater sandstone reservoirs in other parts of the world.

2.3. Geological setting

The study area is located in the Eastern Mediterranean on the continental margin offshore Israel (Figure 2.1). This margin occupies an active tectonic and complex stratigraphic setting due to its location at the zone of interaction between the Anatolian, African and Arabian plates (Figure 2.1). A complex geological history dominated by the opening and subsequent closure of the Tethyan Ocean marks its overall tectonic evolution from the Late Triassic onwards (Ben-Avraham, 1989; Garfunkel and Derin, 1984; Robertson et al., 1996). Since then, intense tectonic activity, including plate convergence during the Late Cretaceous (Syrian Arc system), rifting during the mid-Cenozoic and subsidence since the Neogene, has resulted in a complex structural setting.

The mounded structures are confined to the Lower Yafo Formation (Lower Pliocene in age; Figure 2.2) and are restricted to an area underlain by the Afiq Submarine Canyon (Figures 2.3 and 2.4). The Afiq Submarine Canyon is one of a series of canyons (e.g., Afiq, el-Arish and Ashdod) that were incised into Cretaceous to Eocene shelf edge strata of the Israeli continental margin during the Early Oligocene (e.g., Druckman et al., 1995). It extends for over 120 km, trending in a basinwards direction NW from Beer Sheva to Gaza and into the offshore area (Druckman et al., 1995; Figure 2.3). Within the study

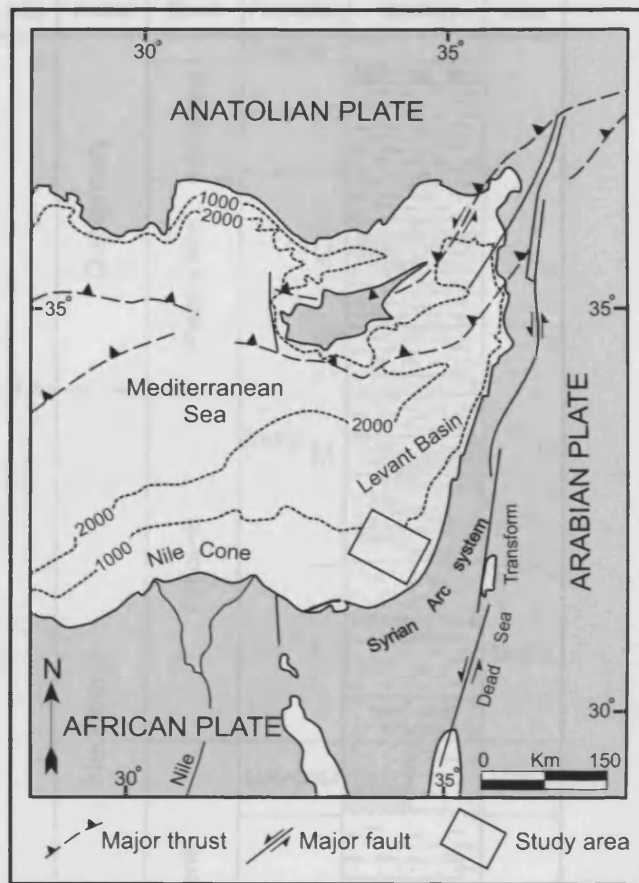


Figure 2.1 Geological sketch of part of the Eastern Mediterranean showing the main structural elements, tectonic plates and study area. Modified from Garfunkel (1998).



Figure 2.2 Generalized chrono-stratigraphic and lithological scheme of the post-Eocene continental margin of Israel. The lithological column is based on unpublished well reports. The time-scale is non-linear.

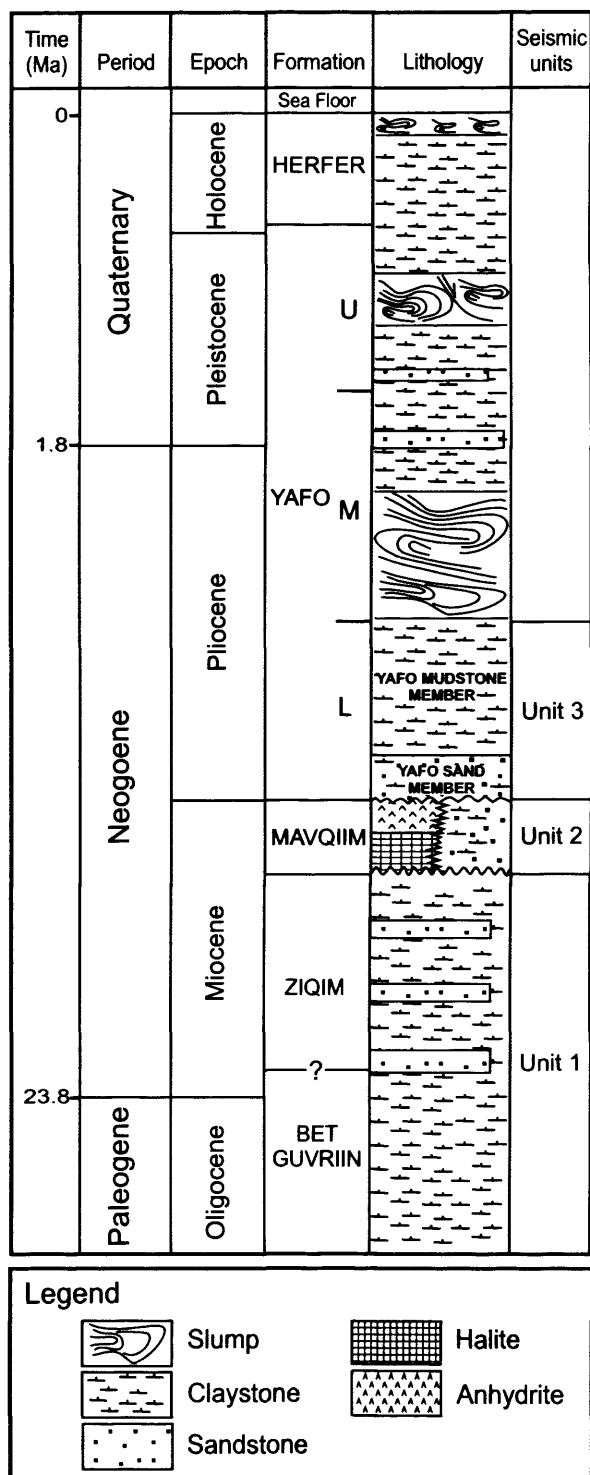


Figure 2.2 Generalized chrono-stratigraphic and lithological scheme of the post-Eocene continental margin of Israel. The lithological column is based on unpublished well reports. The time-scale is non-linear.

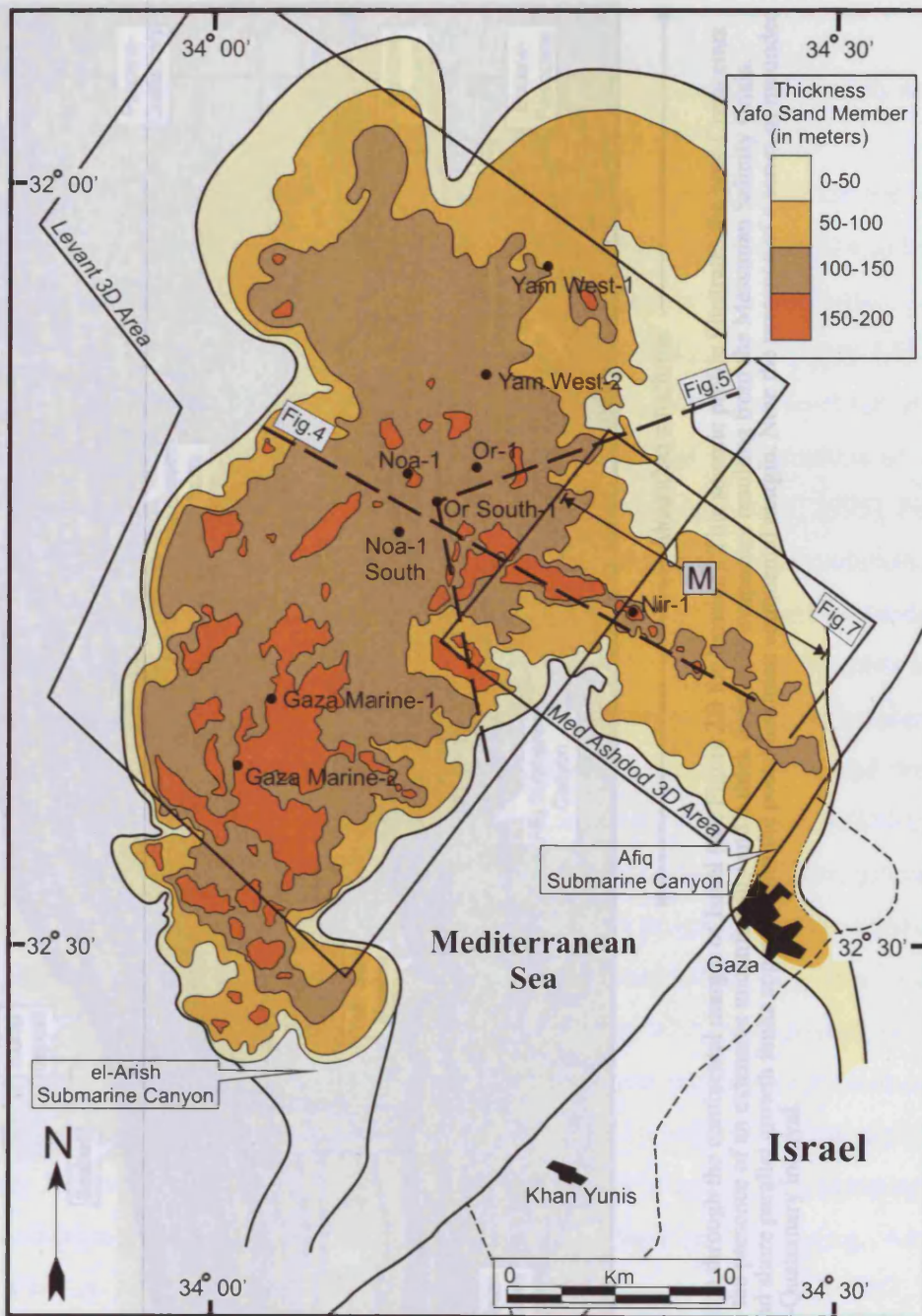


Figure 2.3 Map showing the areal distribution of the Yafo Sand Member offshore Israel. The gross of the Yafo Sand Member was supplied from the southern Levant hinterland via the Afiq and el-Arish Submarine Canyons, and deposited in deepwater as base-of-slope submarine fans. The mounded structures (marked M) are distributed along the Afiq Submarine Canyon in the Med Ashdod 3D area.

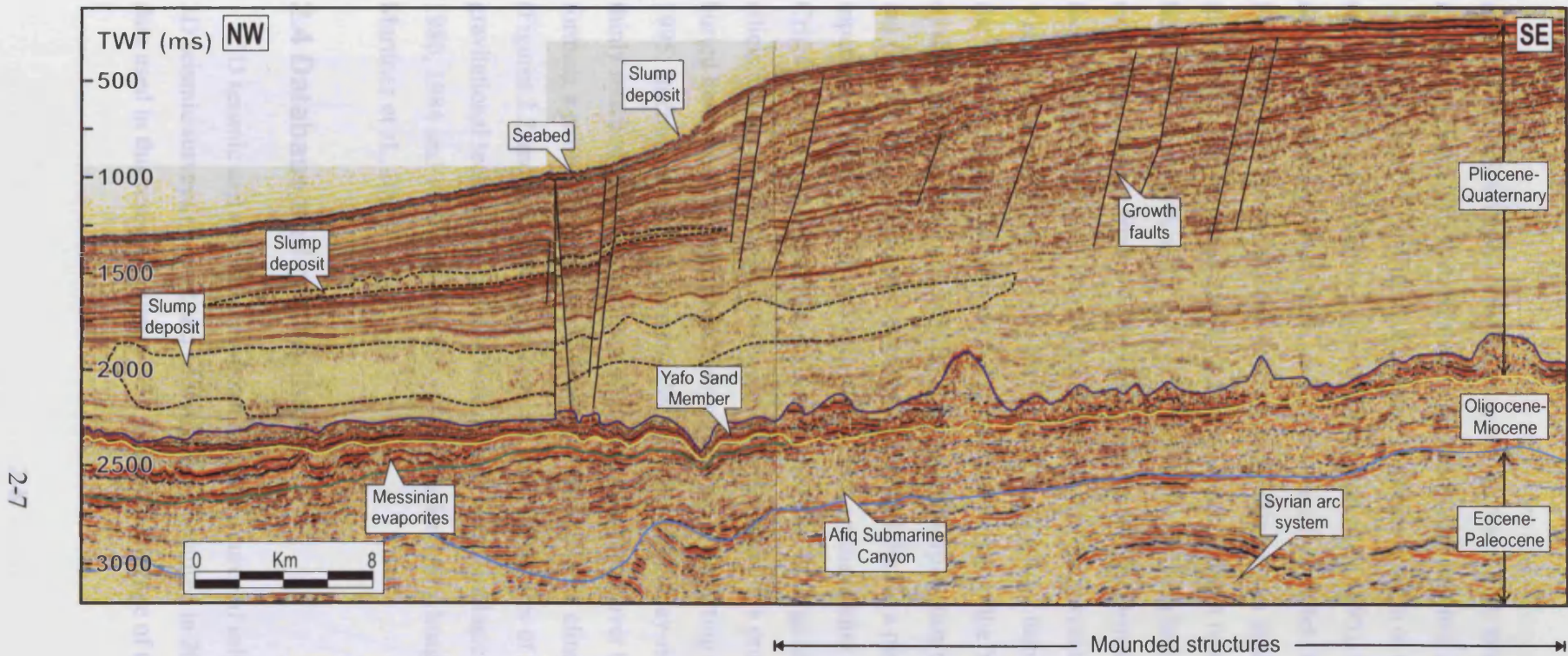


Figure 2.4 Regional dip seismic section through the continental margin of Israel (see Figure 2.3 for location). This seismic profile illustrates the post-Cretaceous configuration of the study area. Note the presence of an extensive unconformity and a thick deposit of evaporites resulting from the Messinian Salinity Crisis. Several large-scale slump deposits and shore parallel growth faults appear within the post-Messinian continental margin. Note the presence of a series of mounded structures at the base of the Pliocene-Quaternary interval.

area, the Afiq Submarine Canyon ranges from 6 to 12 km in width and reaches its maximum depth (c. 500 m relative to its shoulders) (Figures 2.3 and 2.5).

During most of the Early Miocene, submarine erosion or non-deposition prevailed within the Afiq Submarine Canyon (Druckman et al., 1995). This was followed by deposition of pelagic marls and mud-rich debris-flows (Bet Guvrim and Ziqim Formations) in the Middle and Late Miocene (Druckman et al., 1995; Figure 2.2). During the Messinian Salinity Crisis (Latest Miocene, 5.5 Ma), a relative sea-level fall of up to 800 m below the rim of the Afiq Submarine Canyon resulted in the formation of evaporitic deposits from the Mavqim Formation (e.g., Druckman et al., 1995). Following the Messinian Salinity Crisis, normal marine deposition resulted in accumulation of the Yafo Formation which includes the important deepwater turbiditic reservoir sandstone: the Yafo Sand Member (Figure 2.2). The distribution of the Yafo Sand Member in a base of slope position is consistent with core-based interpretation of this unit as a submarine fan (Figure 2.3). These sediments were deposited during a period of increased clastic input in the first stages of refilling of the Mediterranean after the Messinian Salinity Crisis. From mid-Pliocene onwards, sedimentation of large amounts of fine-grained siliciclastics and carbonates of the Yafo Formation built a progradational succession that buried both the Afiq Submarine Canyon and the pre-existing slope (e.g., Druckman et al., 1995; Buchbinder and Zilberman, 1997) (Figure 2.4). Clay-rich marls passed upwards to thinly interbedded sandstones and claystones deposited over the slope and basin areas forming a strongly aggradational system, with sigmoidal clinofolds linking shelf to slope (Figures 2.2 and 2.4). During this period, several episodes of large-scale slumping and gravitational tectonics alternated with periods of hemipelagic deposition (e.g., Almagor, 1980, 1984 and 1986; Garfunkel, 1984; Garfunkel and Almagor, 1985 and 1987; Frey-Martínez et al., 2005).

2.4 Database and methodology

3D seismic and well data represent the main source of information for this study. Two 3D seismic surveys (Levant and Med Ashdod), acquired in 2000, comprise the seismic data used in this research (Figure 2.3). The total coverage of these two datasets amounts

2-9

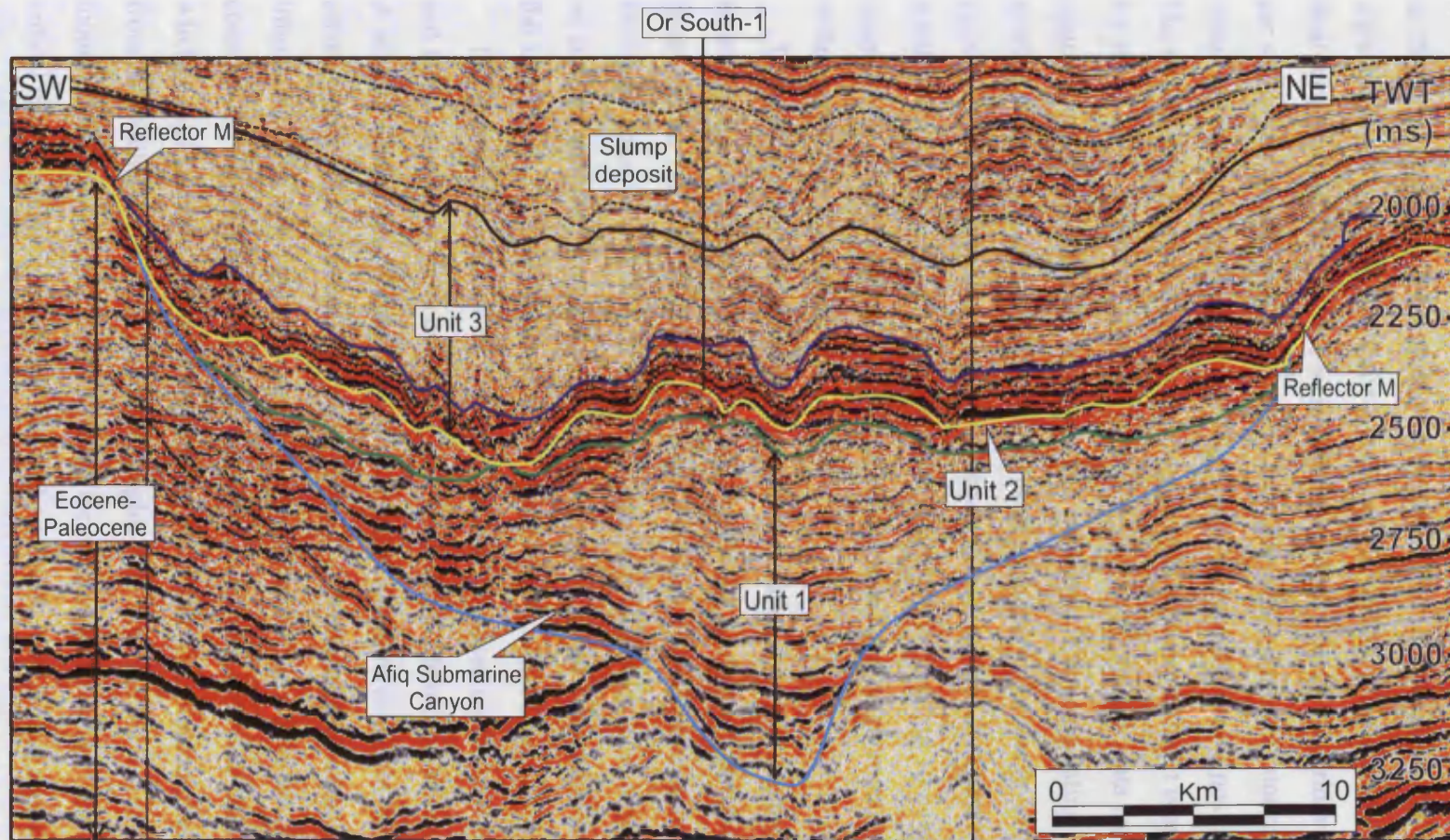


Figure 2.5 Seismic profile across the Afq Submarine Canyon (see Figure 2.3 for location) showing the three main seismic units defined in this paper (Units 1-3). Unit 1 are composed of sub-horizontal, continuous and aggradational seismic reflections that onlap the margins of the canyon. Unit 2 is an uneven veneer of discontinuous to transparent seismic reflections that pinch out against the flanks of the canyon. Unit 3 consists of continuous, high-amplitude seismic reflections onlapping and downlapping the flanks of the canyon. Further discussion on unit architecture is given in the text. The colors used for the seismic unit boundaries are consistent throughout this paper.

to 2500 km², extending from shelf to deepwater. The Levant and Med Ashdod surveys were acquired with an in-line trace interval of 6.25 m and a line spacing of 25 m. The final data for these two surveys were defined on a 12.5 by 12.5 m grid with 6400 bin cells per sq km after processing. The data are near zero phase with SEG normal polarity, meaning that an increase in acoustic impedance is represented by a positive amplitude. The dominant frequency of the seismic data varies with depth, but it is approximately 50 Hz at the level of interest (2500-1750 ms TWT). The 3D seismic data have been time-migrated and the data quality is regarded as excellent. When calculating the resolution, an average seismic velocity of 2000 m/s has been assumed within the level of interest. This velocity is derived from the checkshot measurements made in the Gaza Marine-1 well. Vertical ($\lambda/4$) and lateral (λ) resolutions are estimated to be about 10 m and 40 m, respectively. In this chapter, all stratal thicknesses and depths given in seismic time are in milliseconds two-way travel time (TWT).

The well data used in this study come from nine hydrocarbon exploration wells located in the study area (Figure 2.3). These well data consist of petrophysical well logs (γ -ray, sonic, velocity, resistivity and checkshots), along with paleontologic and biostratigraphic information. Unpublished commercial stratigraphic reports, mainly based on cuttings analyses, were also available from seven of the exploration wells located in the area (Nir-1, Or-1, Or South-1, Noa-1, Yam West-1, Gaza Marine-1 and 2).

The methodology followed in the present study is based on the seismic stratigraphic and facies analysis of the sedimentary intervals of Upper Miocene-Middle Pliocene age. A seismic stratigraphic framework for the mounded structures within these intervals was established by two different approaches. Firstly, a combination of seismic and lithostratigraphic analysis was employed in order to provide a detailed stratigraphic context. The 3D seismic data interpretation was calibrated with well data by integrating wireline logs and core sedimentological interpretations with biostratigraphic information from the available well data. Lithostratigraphic data from the Nir-1 well (drilled through a mounded structure) were extensively used for detailed calibration of the lithologies in the critical intervals above, below and within the mounds. The second approach employed accurate 3D mapping and seismic attribute analysis to investigate the external and internal seismic geometry, fabric and lithology of the mounded structures. This was undertaken by

means of timeslice and coherence volume generation within representative case studies.

2.5 Stratigraphic context of the mounded structures

The seismic-stratigraphic analysis of the mounded structures resulted in the identification of three seismic units within the Oligocene to Middle Pliocene successions (Units 1-3 in Figures 2.2 and 2.5). These seismic units are defined primarily on their seismic facies, thickness variations and spatial reflection patterns. The boundaries between the seismic units are identified based on their physical discontinuity, i.e. onlap, downlap, toplap and truncation terminations. Checkshot surveys and calibrated wireline logs provided direct well ties with the interpreted seismic units, which have been correlated with the lithostratigraphic framework established for the Afq Submarine Canyon by Druckman et al. (1995).

2.5.1 Unit 1 (Canyon fill)

Unit 1 is bounded at its base by a conspicuous erosional unconformity at which it is possible to distinguish clear reflection terminations (base of the Afq Submarine Canyon; Figure 2.5). The upper boundary is coincident with a very irregular and discontinuous seismic reflection of moderate to low amplitude (Figure 2.5). Unit 1 is only present within the Afq Submarine Canyon where it forms a NE-SW trending 15 km long x 7 km wide depocenter with up to 500 m of sediments. Internally, Unit 1 is composed of sub-horizontal, medium to low amplitude, continuous and aggradational seismic reflections that onlap the canyon margins (Figure 2.5).

Petrophysical log data and completion reports show that Unit 1 is principally composed of grey-brown, glauconitic and pyritic, pelagic marls interbedded with grey-brown, soft to firm, deep-marine claystones, limestones and medium grained turbiditic sandstones. Unit 1 corresponds to two lithostratigraphic formations as defined in the available wells: the Bet Guvrim Formation (Oligocene to Middle Miocene) and the Ziqim Formation (Middle Miocene) (Figure 2.2). However, lack of accurate dating does not allow clear recognition of the boundary between them, and makes correlation of the lithostratigraphic markers with the seismic stratigraphy highly problematic. The

completion log from Nir-1 describes the upper parts of the Ziqim Formation as a c. 400 m succession of 10-15 m thick intervals of hemipelagic shales interbedded with chert-bearing conglomerates and very coarse to medium grained turbiditic sandstones.

2.5.2. Unit 2 (Messinian deposits)

Unit 2 is bounded at its top by an irregular reflection of high amplitude that marks a basinwide erosional unconformity surface (Reflector M) caused by subaerial exposure during the Messinian Salinity Crisis (Ryan et al., 1971) (Figure 2.5). Unit 2 forms a thin and uneven veneer that irregularly covers Unit 1 and pinches out with onlap against the flanks of the Afiq Submarine Canyon (see Figure 2.5). Internally, Unit 2 mainly comprises discontinuous to transparent low-amplitude seismic reflections that are locally interbedded with continuous and moderate-amplitude reflections.

Unit 2 is correlated to the Mavqim Formation in several exploration wells within the study area (Figure 2.2). The Mavqim Formation within the Afiq Submarine Canyon is interpreted as the time equivalent of thick deposits of evaporites that were deposited over the former abyssal plain during the Messinian Salinity Crisis (Druckman et al., 1995). According to Druckman et al. (1995), the Mavqim Formation consists of thin interbeds of compacted nodular anhydrite interbedded with medium to dark grey and moderately firm claystones, limestones and sandstones (Figure 2.2). However, the completion log from Nir-1 describes the Mavqim Formation as loose and poorly sorted sandstones interbedded with light-medium grey claystones and soft powdery limestones. Importantly, there is no conclusive evidence from the seismic or the well data for any significant accumulations of primary evaporites at this stratigraphic level.

2.5.3 Unit 3 (Lower Yafo Formation)

The upper boundary of Unit 3 corresponds to a high amplitude seismic reflection that marks the top of the Middle Pliocene sedimentary fill within the Afiq Submarine Canyon (Figure 2.5). Unit 3 consists of a c. 500 m thick interval that is part of a prograding and aggrading slope wedge onlapping and downlapping the lateral flanks of the Afiq Submarine Canyon (Figure 2.5). All the wells located in the study area have penetrated

Unit 3, which is correlated to the Lower Yafo Formation and dated as Lower to Middle Pliocene (Figure 2.2).

The basal part of Unit 3 consists of a package of high amplitude, continuous, sub-parallel and high-frequency seismic reflections with an approximately constant thickness of 70 m (Figure 2.5). This package has been penetrated in six exploration wells in the study area, and it is informally termed the Yafo Sand Member (Lower Pliocene) in well completion reports (Figure 2.2). 3D mapping calibrated with borehole data indicates that the Yafo Sand Member is geographically restricted to the offshore extension of the Afiq and el-Arish submarine canyons (Figure 2.3). The Yafo Sand Member consists of grey, soft to firm marls interbedded with siltstones and sandstones and overlain by a succession of up to three thick units of very fine to medium grained, clean and well-sorted, thinly bedded turbiditic sandstones (Figure 2.2). Deposition of the Yafo Sand Member was strongly influenced by the underlying Afiq and el-Arish submarine canyons, which at that time still formed deep depressions along the continental margin and provided conduits for fine-grained siliciclastics to be deposited onto the basin floor. According to well completion reports, the turbiditic sandstones at the top of the Yafo Sand Member were supplied from the southern Levant hinterland via the Afiq and el-Arish submarine canyons, and accumulated in deepwater as base-of-slope submarine fans (Figure 2.3).

The basal part of Unit 3 is overlain by a conformable interval of moderate to low amplitude, sub-parallel continuous and medium frequency aggradational seismic reflections (Figure 2.5). This interval reaches up to c. 400 m in thickness and is herein informally termed the Yafo Mudstone Member of Lower to Middle Pliocene age (Figure 2.2). The bulk of the Yafo Mudstone Member comprises deep-marine limestones, claystones and siltstones that locally alternate with sandstones, limestones and marls. The Yafo Mudstone Member was deposited during a major transgression that inundated the exposed Late Miocene shelf (e.g., Buchbinder and Zilberman, 1997).

2.6 General appearance of the mounded structures

The mounded structures presented here are delimited in the 3D seismic data by mapping the two seismic reflections that correspond to their lower and upper boundaries.

The main key recognition criteria for these two boundaries are illustrated with reference to Figure 2.6. The lower boundary of the mounded structures is defined in this study as the base of the Yafo Sand Member as calibrated in the available well data. This boundary generally forms a relatively concordant, continuous and flat-lying strong negative amplitude seismic reflection that underlies all the mounded features (Figure 2.6). Accurate mapping of this reflection is relatively straightforward as it is only rarely deformed in the study area.

The upper boundary of the mounded structures is defined in this chapter as a surface of stratal discontinuity between the concordant seismic reflections of the underlying Yafo Sand Member and the convergent onlap terminations of the overlying Yafo Mudstone Member (Figure 2.6). This boundary is correlated with the top of the Yafo Sand Member based on calibration of the seismic data at the Nir-1 exploration well. In 3D seismic data, the upper boundary corresponds to a convex upwards and moderately continuous seismic reflection that overlies all the mounded structures (Figure 2.6). Mapping of this boundary across the mounds is locally problematic due to significant variations in its seismic response. On the crest of the mounds, it generally corresponds to an easily traced, continuous and strong negative seismic amplitude reflection. Towards the flanks, the reflection is more difficult to detect; in some places it is represented by a weak trough, in others it is absent (Figure 2.6). This is probably due to the steeply dipping nature of the flanks of the mounded structures and the lack of a strong seismic impedance contrast between the structures and the overburden. In this study, the upper boundary has thus been identified by mapping the stratal terminations between the steeply dipping reflections dominant within the flanks of the mounded structures and the continuous seismic reflections of the overburden. Following this approach, this boundary has been followed from the top of the Yafo Sand Member up the flanks of the mounded structures and across their crestal parts (Figure 2.6). This pick is consistent with the lithology encountered in the Nir-1 well as further discussed in a later section.

Based on mapping at the top of the Yafo Sand Member and the recognition that mounds are defined by localised structural culminations at this surface, seventeen discrete mounded structures have been identified in the Med Ashdod 3D area. A time-structural map at this stratigraphic level (e.g., Figure 2.7) shows the mounded structures as elliptical

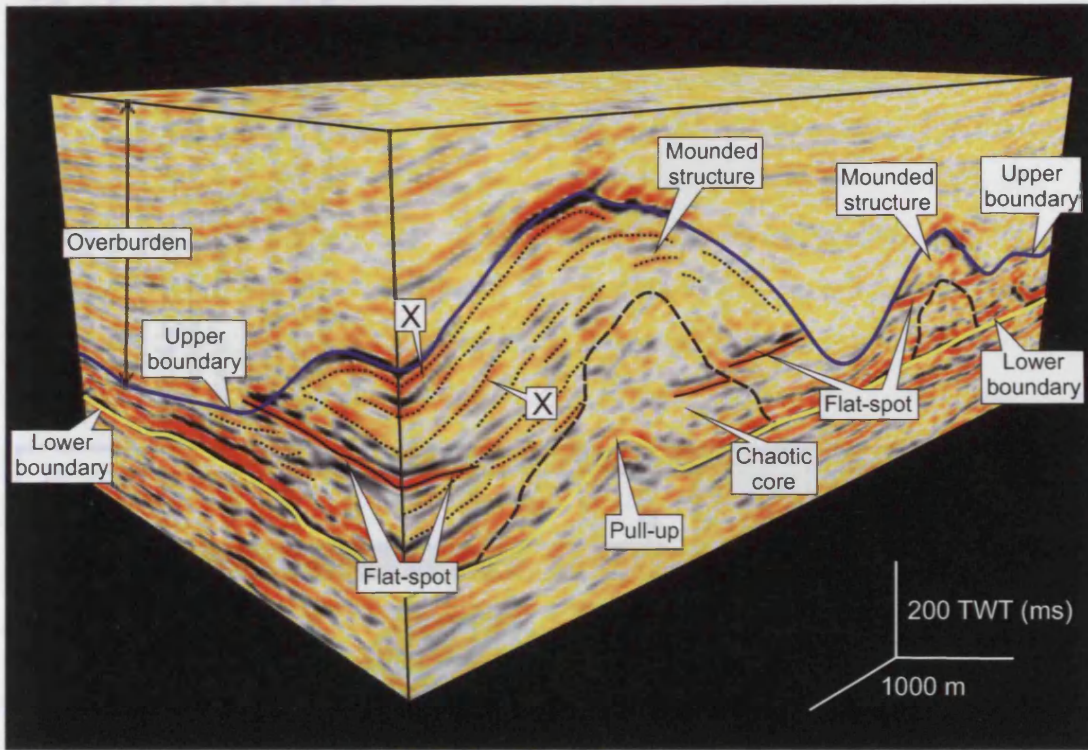
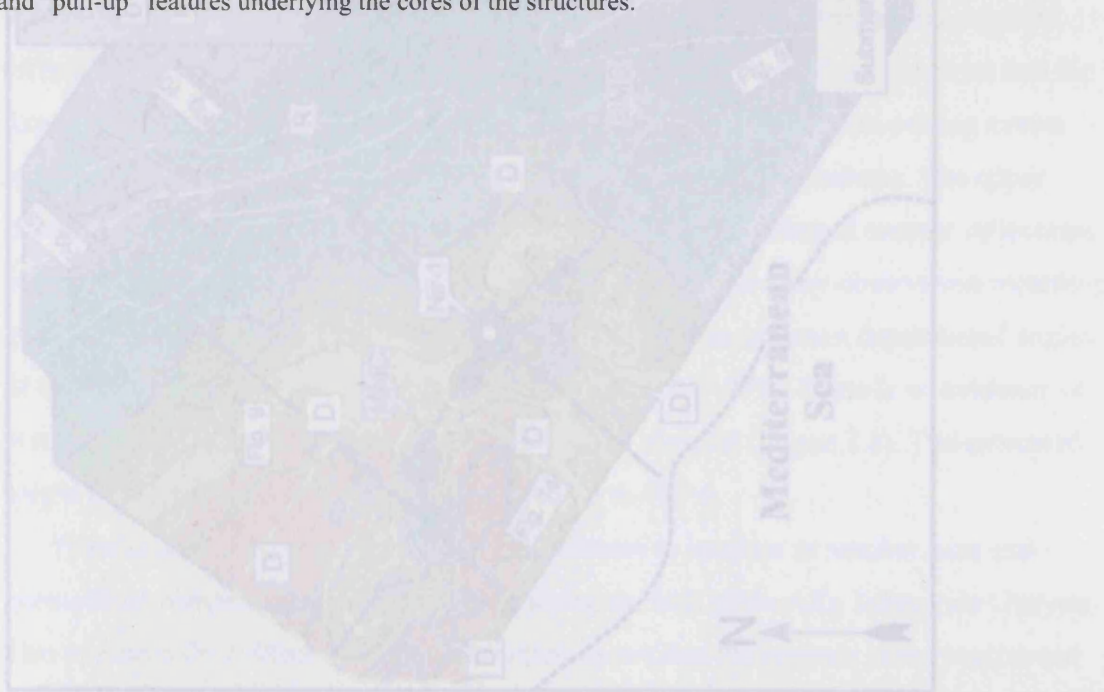


Figure 2.6 3D visualization of two representative mounded structures in the study area. Mounded structures are delimited by a relatively concordant, continuous and flat-lying lower boundary and by a convex-upward and discontinuous upper boundary. The lower and upper boundaries correspond to the base and top of the Yafo Sand Member respectively. The internal parts of the mounded structures show chaotic seismic reflections in the cores (enclosed by dashed black lines) and more continuous seismic reflections in the flanks and crests (marked X). Note the presence of flat-spots crosscutting the flanks and “pull-up” features underlying the cores of the structures.



2-16

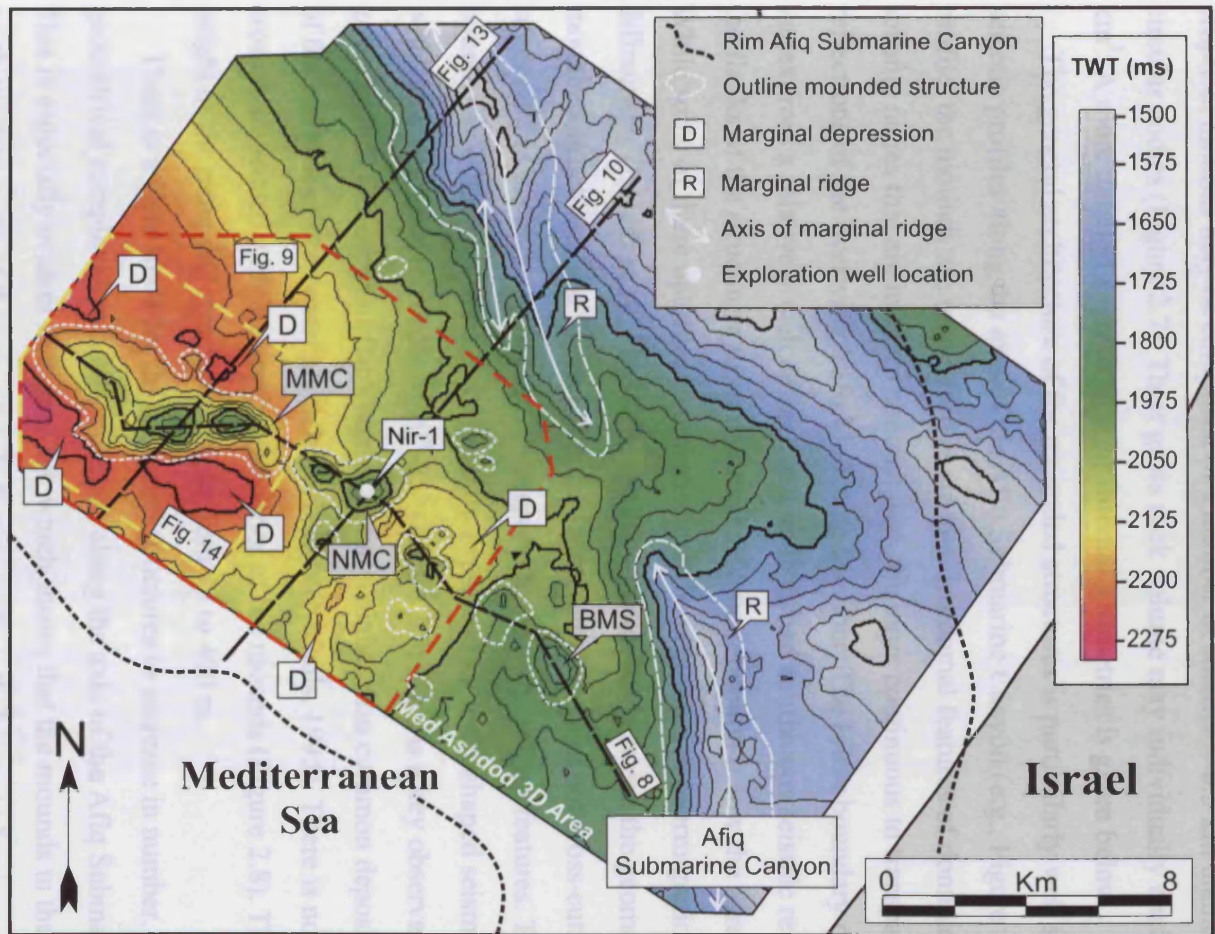


Figure 2.7 Structural map in two-way time of the top of the Yafo Sand Member in the Med Ashdod 3D area (TWT, 2000 ms= ~1700 m). The mounded structures appear as circular to elongated culminations flanked by marginal depressions. The mounds form both isolated and complex features. The majority of the structures are aligned in a NW-SE trend along the axis of the Afiq Submarine Canyon. Note the presence of ridge-like shale diapirs parallel to the northern rim of the Afiq Submarine Canyon.

(max. c. 1.2 ellipticity ratio) to circular culminations in plan-view with diameters at their base of 0.5-2 km. Some are isolated four-way dip closures; others coalesce to form arrays of up to three linked bodies. The majority of the mounded structures form a SE-NW trending arrangement coinciding with the axis of the underlying Afq Submarine Canyon (Figures 2.3 and 2.7). The more elliptical mounded structures generally occur in the north-westernmost region of the canyon axis arrangement, whereas the near circular ones appear in its central and south-easternmost parts (Figure 2.7). In detail, the larger elliptical mounds may be composed of a number of smaller (~0.5 km diameter), aligned circular bodies (Figure 2.7). Their gross rock volume may individually reach up to c. 0.75 km³. A more detailed analysis of their internal geometries is given below.

The general architecture of the mounded structures is particularly well seen on seismic profiles along the axis of the Afq Submarine Canyon (e.g., Figure 2.8). On this profile, the mounds are recognised as steep-sided domal features of dominant chaotic seismic facies that are in sharp contrast with the more continuous to transparent reflections of the overlying Yafo Mudstone Member. The lower boundary of the mounds varies from a relatively well defined and undisturbed continuous seismic reflection below the flanks of the structures, to an upturned seismic reflection below the cores (Figure 2.8). While some of these upturned geometries may be attributed to overmigration of point diffractions (Løseth et al., 2003), the spatial coincidence between the geometries and the mounded structures, and the fact that they form antiforms and not cross-cutting events suggests that the majority of them correspond to velocity pull up features. The upper boundaries of the mounds are consistently expressed as dome-shaped seismic reflections with flank angles of the order of 20°-25° (Figure 2.8). This is a key observation regarding genesis since this range of flank angles is much higher than common depositional angles of the margins of deepwater siliciclastic bodies (Nichols, 1995). There is no evidence of erosion associated with the upper boundaries of the mounds (Figure 2.8). The estimated height of the mounded structures ranges from 75 to 400 m.

There is a clear trend for the mounded structures to increase in number, size and geometrical complexity in a NW direction along the axis of the Afq Submarine Canyon. This is especially evident in Figure 2.8, which shows that the mounds in the central and north-western parts of the canyon axis form significantly larger and more complex

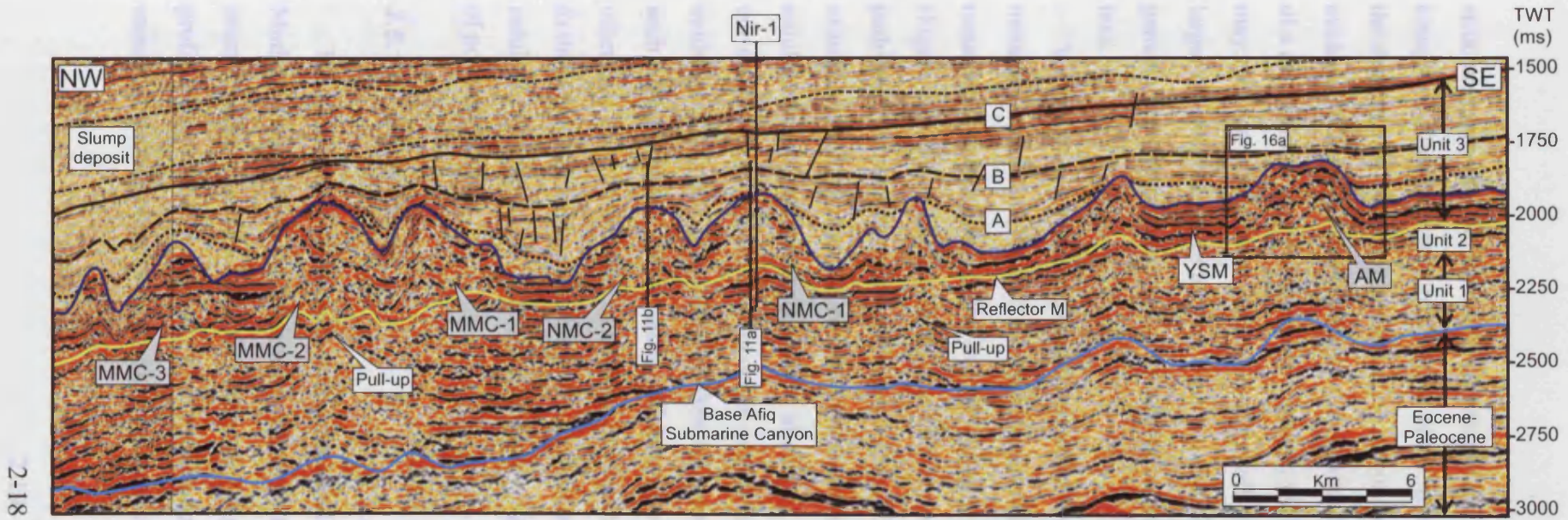


Figure 2.8 Seismic section along the axis of the Afq Submarine Canyon in the Med Ashdod 3D area (see Figure 2.7 for location). There are ten mounded structures confined to the Yafo Sand Member (YSM) and the Yafo Mudstone Member. They all form dome-like features delimited by the base and top of the Yafo Sand Member (lower and upper boundaries respectively). Note the presence of “pull up” features underlying the cores of the mounded structures. The overburden is significantly deformed above the structures. Further discussion of the geometrical relationships of the mounded structures to the overburden is given in the text. Mairi Mound Complex (MMC), Nir Mound Complex (NMC) and Alpha Mound (AM).

structures than those in the south-eastern parts. This differentiation in dimension and complexity could be interpreted as the result of erosional or depositional processes along the canyon axis. However, these can be discounted as possibilities since there is no evidence of erosion associated with the mounded structures and these are too steep to be of a depositional origin (see above). Instead, we prefer the interpretation that such a trend may reflect a gradation in the timing of growth of the mounds along the canyon axis (i.e. larger mounds are active longer). This is a significant conclusion for understanding the genetic mechanism of the mounded structures and will be discussed further later in the text.

Vertical zones of chaotic seismic reflections are repeatedly observed below the mounded structures (Figure 2.8). These are restricted to the areas overlain by the mounded structures and extend in depth down to the Palaeocene and Eocene intervals (Figure 2.8). These chaotic zones could be interpreted as some form of fluid migration pathway from deeper stratigraphic levels (i.e. Palaeocene-Eocene). Gas chimneys, for example, resulting from the vertical movement of gas-rich fluids are known to have similar seismic expressions (Løseth et al., 2003). In the case of the vertical noise zones in our study area, however, such an origin cannot be invoked, provided that there is no evidence of increased gas content below the mounds. Well Nir-1, which penetrated one of such vertical chaotic zones, had significantly low gas readings and no indication of any other type of hydrocarbons. In addition, the fact that the vertical chaotic zones are limited to the areas overlain by the mounded structures suggests that they are more likely the result of ray bending and scattering caused by high velocity contrasts and overmigration of point diffractions.

2.6.1 Overburden

The sedimentary overburden of the mounded structures is defined here as the Yafo Mudstone Member and is delimited upwards by the upper limit of visible deformation of seismic reflections associated with the underlying mounds (horizon C). On seismic dip profiles (Figure 2.8), it appears as a c. 350 m interval of continuous to discontinuous seismic reflections that terminate sharply against the upper boundary of each of the

mounds (Figure 2.8). The relationships of the overburden to the mounded structures are highly complex and variable. In some areas, these relationships can be interpreted locally as onlap and be conveniently explained by a depositional origin. Evidence of deformational processes (i.e. folds and faults) however has been repeatedly observed in several locations. 3D mapping, for instance, reveals that the overburden is clearly folded directly above the flanks and the crest of the mounded structures (Figures 2.6 and 2.8). It is also clearly seen, that small-offset normal faults affect the overburden particularly near the large-scale mounded structures. In plan view, these faults appear as clusters of concentric and radial features surrounding the mounds (Figure 2.9), indicative of forced folding (*sensu* Jackson and Talbot, 1991). The main radial faults are dominant near the flanks of the mounded structures, whereas the concentric faults are most concentrated above their crests.

The overburden shows localised variations in thickness adjacent to the mounded structures. These thickness variations are especially evident on strike profiles where the overburden can be seen to form wedges that thin against the flanks of the mounds by convergent onlap (Figure 2.10). The detailed geometry of these thickness variations, together with the deformed terminations previously mentioned, is critical when assessing the mode and timing of formation of the mounded structures and will be discussed in more detail in the context of the timing in a later section.

2.6.2 Marginal depressions

Mapping at the top of the Yafo Sand Member shows the presence of bowl-shaped marginal depressions flanking the mounded structures. These depressions are elongate and crescentic in plan view and are well defined near the major mounded structures (marked D in Figure 2.7). The largest examples are up to c. 20 km² in area (mean length 6 km, mean width 4 km), 150 m in depth and may individually reach up to 0.3 km³ in gross volume (calculated above a local undeformed datum). On seismic profiles, they are bowl-shaped features with marginal flank dips of between 3° and 5° (marked D in Figure 2.10). No evidence of erosion (i.e. reflection truncations) is observed associated with the marginal depressions. Importantly, mapping indicates that the thickness of the Yafo Sand

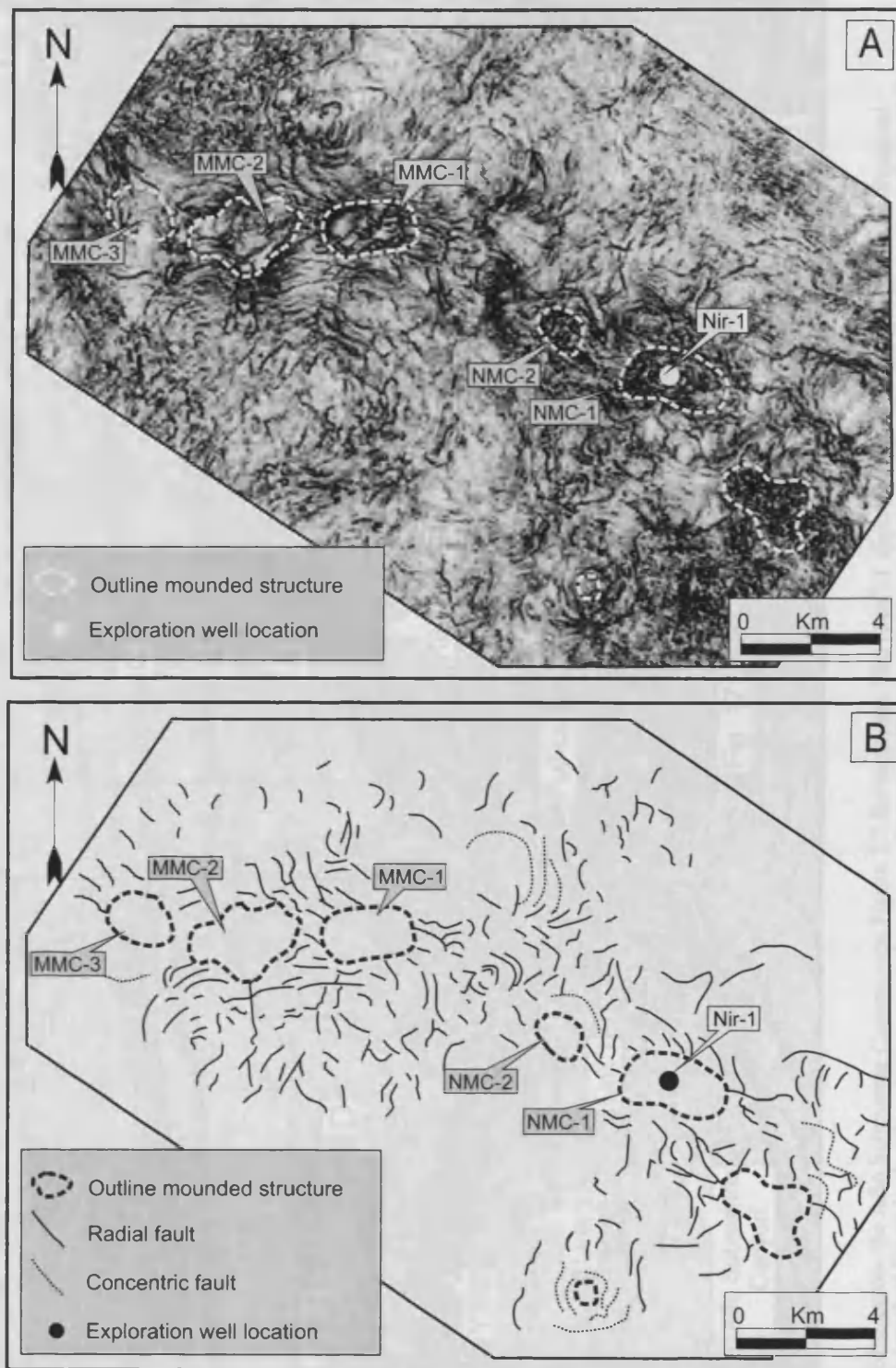


Figure 2.9 (a) Structurally flattened horizontal coherence-slice across the overburden of the mounded structures in part of the Med Ashdod 3D area (see Figure 2.7 for location). Note the presence of radial and concentric faults within the overburden of the mounded structures. The faults surround the crests and flanks of the largest mounded structures in the area (outlined by white dashed lines). (b) Schematic depiction illustrating the plan view of the fault systems around the mounded structures.

2-22

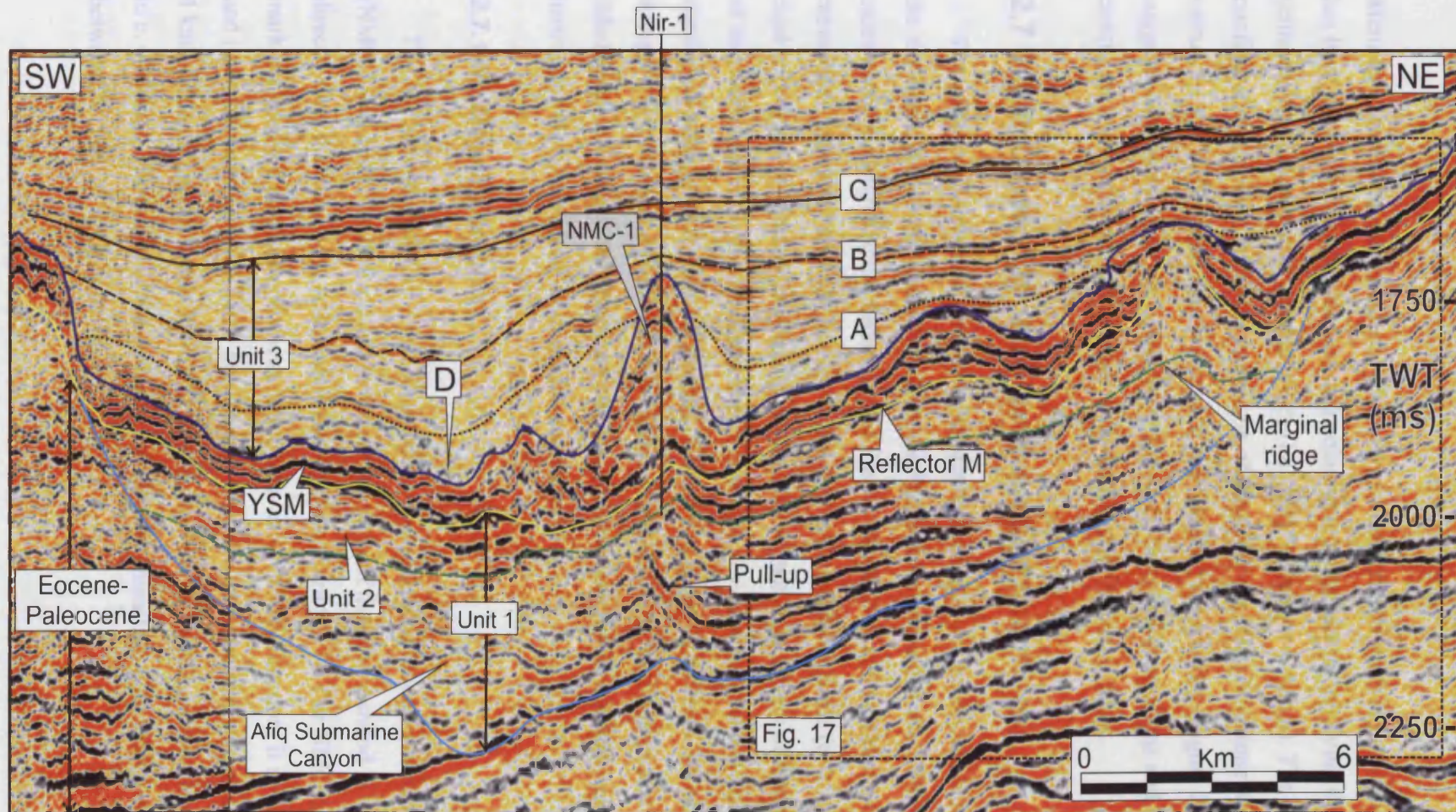


Figure 2.10 Seismic profile across the Afq Submarine Canyon (see Figure 2.7 for location). The NMC-1 appears in its central parts. There are marginal topographic depressions (marked D) on both sides of the mounded structure. Note the presence of a small-scale diapiric structure in the northern flank of the Afq Submarine Canyon. There are “pull up” features below the NMC-1. The overburden is clearly folded towards the flanks and crest of the NMC-1 and shows significant thickness variations towards the structure.

Member does not vary across them. This is a key observation implying that no material has been removed from this interval and pointing to a mechanism involving depletion of sediment from deeper stratigraphic levels (i.e. Afq Submarine Canyon). The reflection configurations and the thickness variations of the overlying Yafo Mudstone Member are vertically concordant with the geometry of the marginal depressions (Figure 2.10). This suggests downwarping of the overburden above the marginal depressions and is consistent with sediment volume loss from the Afq Submarine Canyon.

2.7 Detailed description of the mounded structures

Three representative case studies were selected to highlight the key characteristics of the mounds and their relationship to the underlying and overlying strata. The first two cases are of the Mari Mound Complex and the Nir Mound Complex, which are remarkable in several respects, not least of which is their large volume (c. 0.75 km³). The third case study is of the much smaller Alpha Mound, which is mainly of interest because of its much simpler geometry. This simpler structure provides insights that have a significant bearing on the overall genesis of the entire group of mounds. 3D seismic interpretation calibrated with well data allows highly detailed morphological and lithological analysis of the three case studies, and reveals a highly complex genetic history for the whole group of mounded structures.

2.7.1 Nir Mound Complex

The Nir Mound Complex (NMC) comprises two coalesced mounded structures (NMC-1 and NMC-2). It is located in the central parts of the Med Ashdod 3D area, lying directly over the axis of the Afq Submarine Canyon (Figure 2.7). The NMC has a marked elongated planform geometry that trends in a NW-SE direction; it is 4 km long and its width ranges from 1.5 to 3 km (Figure 2.7). The total structure covers an area of c. 4 km², has a maximum height up to 375 m and involves an overall gross rock volume up to c. 0.45 km³. The flanks of the structure are almost symmetric, with slopes ranging between 20° and 25° (Figure 2.10).

2.7.1.1 Seismic character of the NMC

In seismic dip-sections, the NMC appears as two interlocked, approximately symmetric upwards conical-shaped bodies (NMC-1 and NMC-2; Figure 2.8). The lower boundary of both component mounds appears as a moderately deformed continuous high-amplitude seismic reflection (Figures 2.8 and 2.10). The deformed appearance of this boundary increases below the cores of the structures, where it forms small-scale antiforms (Figure 2.10). These geometries are interpreted as seismic velocity pull up features. The upper boundary of the NMC corresponds to a discontinuous domed-like moderate- to low-amplitude seismic reflection against which the reflections of the overburden terminate by deformed onlap (cf. Figures 2.8 and 2.10).

The internal seismic reflection character of the NMC is dominated by low amplitude and chaotic seismic facies (Figures 2.8 and 2.10). The internal chaotic pattern is locally broken by short and disconnected block-like segments that appear as parallel-bedded high-amplitude reflections in seismic profiles (marked X in Figure 2.11). These block-like reflections can only be traced for short distances (< 1 km) along the flanks and crest of the NMC and dip systematically parallel to the outer boundary of the mounded structure (Figure 2.11). 3D data reveal that the contact between the chaotic seismic facies and the block-like reflections is significantly steep (c. 15°-20°) and irregular (Figure 2.11). It is difficult to explain such a geometrical relationship by any known depositional process, simply because the observed contact is too vertical to be of a clastic depositional origin. Instead, we prefer the interpretation that such a contact is the result of some type of forceful intrusion process of clastic sediments within the NMC. Within this interpretation, the chaotic internal reflections represent the intruded clastic sediments, whilst the block-like reflections are remnants of the primary stratification that has been broken and distorted due to the intrusion. From measurements made on serial depth converted seismic sections, we estimate that up to a c. 50% of the total gross rock volume within the NMC corresponds to intruded material (Figure 2.11). This is a highly significant observation that helps to constrain the origin of the mounded structures since it clearly excludes a depositional origin, and forms the basis for inferring a dominant role for diapirism.

No clear evidence of Direct Hydrocarbon Indicators (DHI) is observed within the

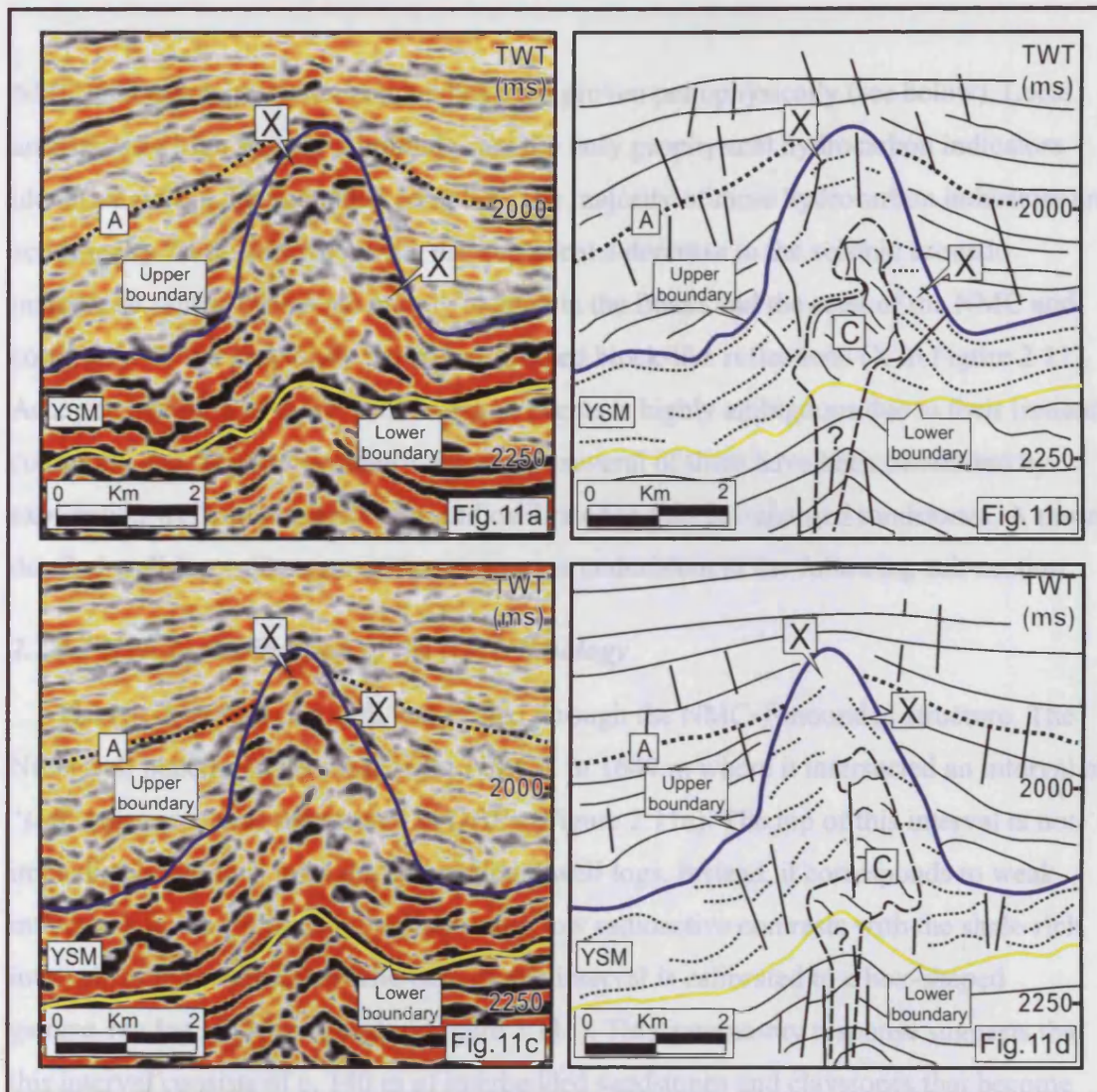


Figure 2.11 Catalogue of seismic sections through the NMC illustrating the seismic appearance of its internal parts (see Figure 2.8 for location). The internal seismic reflections within the Yafo Sand Member (marked YSM) are truncated and bent-up toward the cores of the NMC. Note the presence of several fractures underlying the mounds. (A) Seismic section across the NMC-1. The flanks and crest of this mound contain many resolvable block-like seismic events (marked X) that can be traced up to the preserved parts of the YSM. The core consists of chaotic seismic facies (marked C). There are several “soft” seismic events corresponding mainly to the block-like seismic events (X) along the flanks and crest. (B) Seismic section across the NMC-2 showing an internal appearance that is highly equivalent to that of the NMC-1.

direction throughout the crest of the structure (Figure 2.11). This change in the azimuthal direction clearly correlates with the top of the NMC-1 and is interpreted as an inhomogeneity.

Beneath this interval of “soft” seismic events, the Nir-1 well penetrates a c. 185 m thick unit of claystones that are interbedded in a highly complex manner with loose sands and slightly calcareous cemented sandstones. This unit correlates on seismic data with the

NMC although a gas-water contact has been proven petrophysically (see below). Local anomalously high seismic amplitudes are the only geophysical hydrocarbon indicators identified within this mounded complex. The majority of these hydrocarbon indicators are acoustically “soft” seismic events that represent a decrease in the seismic acoustic impedance. These events are mainly located in the flanks and the crest of the NMC and correspond to the previously described isolated block-like reflections (X in Figure 2.11). Accurate mapping of these “soft” seismic events is highly ambiguous due to their limited continuity and intricate geometry. However, several of them have been penetrated by exploration wells in the study area and calibrated to thin gas-charged sandstones. A more detailed well-log calibration of these events is undertaken in the following sub-section.

2.7.1.2 Well-log calibration of the NMC lithology

The Nir-1 exploration well was drilled through the NMC-1 mounded structure. The Nir-1 well penetrated the crest of the NMC-1 at 1649 m where it intersected an interval of “soft” seismic events interpreted as DHI’s (Figure 2.11a). The top of this interval is not immediately obvious from the conventional well logs. Instead, it corresponds to weak inflections in the gamma ray log indicating low radioactive contrasts with the shale-rich intervals of the overburden. The base of this interval is calibrated to a box-shaped gamma-ray log motif (arrowed in Figure 2.11a). This gamma-ray response suggests that this interval consists of c. 140 m of interbedded sandstones and claystones that become more sand-rich towards the bottom. The completion log describes these sandstones as highly-fractured, gas-charged and moderately cemented interpreted as giving rise to the brightening observed in the seismic data. Analysis of the azimuth and dip trends within the NMC-1 indicates that at c. 1649 m, there is a small angular change in dip and a clear variation in azimuth from a NW direction dominant within the overburden to a SSW direction throughout the crest of the structure (Figure 2.11). This change in the azimuth direction clearly correlates with the top of the NMC-1 and is interpreted as an unconformity.

Beneath this interval of “soft” seismic events, the Nir-1 well penetrates a c. 185 m thick unit of claystones that are interbedded in a highly complex manner with loose sands and slightly calcareous cemented sandstones. This unit correlates on seismic data with the

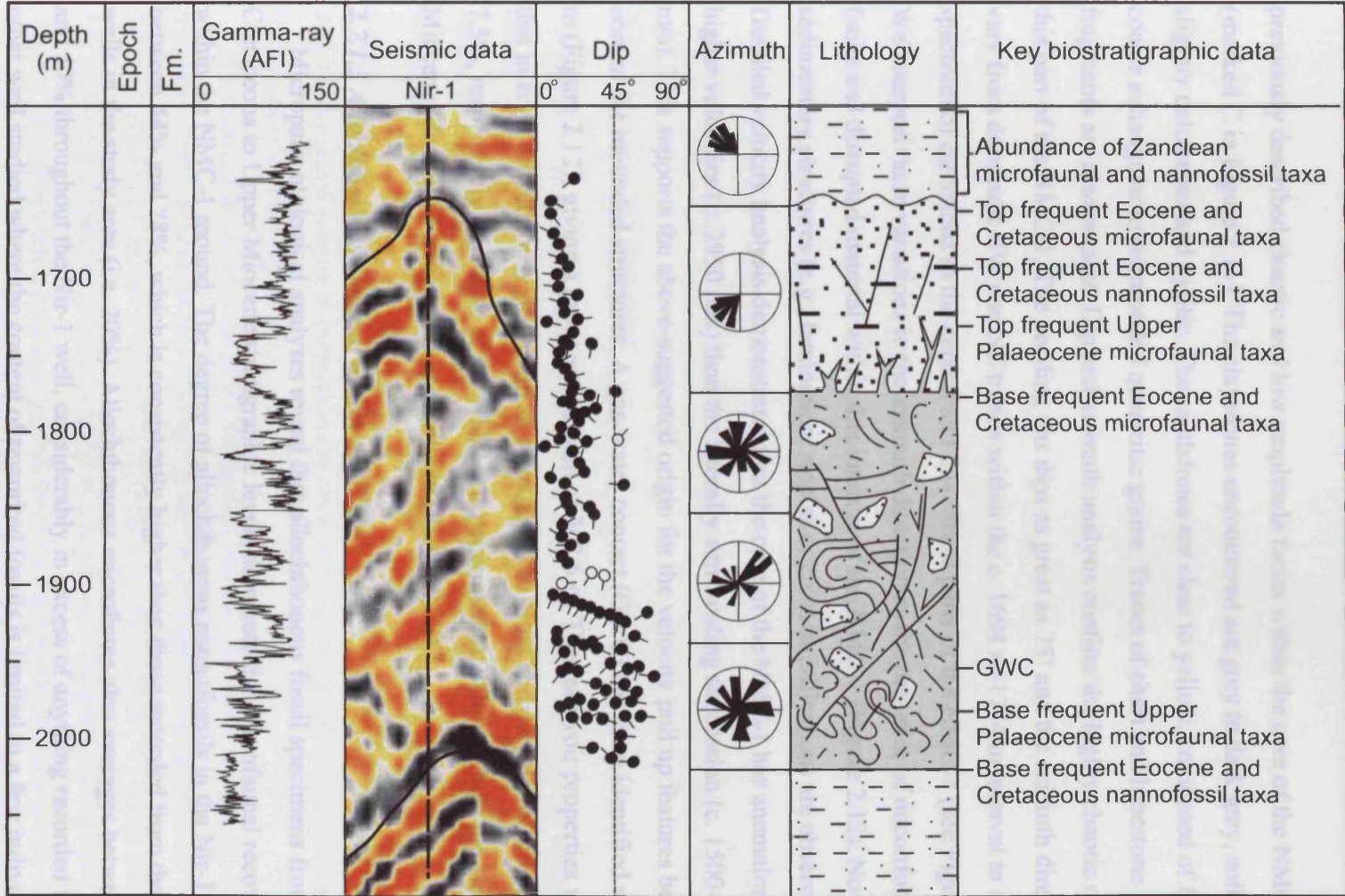


Figure 2.12 Log of exploration well Nir-1, showing depth of the NMC-1. Note the presence of box-shaped gamma log motifs suggesting presence of clean sandstones within the structure. Dip and azimuth indicate highly disturbed sediments especially towards the core of the mound. Note the presence of allochthonous microfaunal and nannofossil taxa within the structure. A gas-water contact (marked GWC) has been penetrated at 1951.6 m.

previously described chaotic and low amplitude facies within the core of the NMC (marked C in Figure 2.11). The claystones encountered are grey to dark grey, soft plastic, slightly calcareous and pyritic. The sandstones are clear to yellow, composed of fine to coarse subangular to subrounded quartzitic grains. Traces of chert and limestone fragments are also present. Dip and azimuth analysis confirm the highly chaotic nature of this part of the NMC-1. The bedding has dips as great as 75° and the azimuth directions vary from dominant NW and NE trends within the c. 1694 m-1774 m interval to a wide spectrum of directions in the central and lowermost parts of the NMC-1 (see Figure 2.12). We interpret these variations in the azimuth direction as the presence of unconformities, faults and disrupted material within this interval of the NMC-1 (Figure 2.12). No sedimentary structures (e.g., lamination, ripples or cross-stratification) are observed. Detailed velocity analysis demonstrates that the core of the NMC-1 has anomalously higher velocities (c. 2950 m/s) than the laterally surrounding succession (c. 1500-1800 m/s). This supports the above-suggested origin for the velocity pull up features below the core of the mounded structures. A gas-water contact (GWC) has been identified at 1951.6 m (Figure 2.12); giving a gross gas column of 302.6 m. The reservoir properties within this interval are relatively poor with an average net to gross and porosity of 0.56 and 7.5%, respectively. The base of the NMC-1 is penetrated at 2026 m where the Upper Miocene Mavqim Formation is encountered (Figure 2.12).

2.7.1.3 Allochthonous material within the NMC

Micropaleontological analyses reveal that allochthonous fossil specimens from Cretaceous to Upper Miocene stratigraphic levels dominate the microfaunal recovery within the NMC-1 mound. The degree of allochthonous nannofossils in the Nir-1 well is between 44% and 78%, which is consistently higher than those recorded from the other wells in the study area (i.e. 20%). Allochthonous microfauna also averages between 40% and 50% throughout the Nir-1 well, considerably in excess of anything recorded in any other well studied where the content of reworked fossils is limited to a few individual specimens. The taxa composing the reworked assemblages within the Nir-1 well also contrast markedly with those recorded from the other wells. This variation is most clearly seen in the microfauna. The first microfaunal evidence of reworking within the NMC is

recorded between 1649 m and 1770 m where Early and Middle Eocene foraminifers (*Acarinina* spp., *Morozovella* spp., *Nummulites* spp. and Operculinids) and Upper Cretaceous planktic and benthic species (*Bolivinoidea draco*, *Gavelinella* spp., *Globotruncana ventricosa*) are encountered. Upper Palaeocene reworking is also indicated by the planktic *Morozovella velascoensis* that occurs consistently between 1728 m and 1980 m (Figure 2.12).

A similar pattern is repeated in the nannofossil record, which shows a major influx of reworked samples from 1671 m to the base of the NMC-1. The dominant specimens are primarily of Late Cretaceous age (*Arkhangelskiella cymbiformis*, *Ceratolithoides aculeus*, *Quadrum trifidum*, *Reinhardtites levis* and *Zeughrabdiotus compactus*) and Eocene taxa (*Discoaster kuepperi*, *D. barbadiensis* and *Helicosphaera seminulun*). Early Miocene to Oligocene taxa (*Sphenolithus belemnoides*, *Cyclicargolithus abisectus* and *Reticulofenestra scissura*) are also recorded in significant numbers throughout the NMC-1.

2.7.2 Mari Mound Complex

The Mari Mound Complex (MMC) is the largest and most conspicuous mounded feature in the study area with a gross volume of c. 0.75 km³. It is located in the western corner of the Med Ashdod 3D area (Figure 2.7), directly above the axis of the Afiq Submarine Canyon. In plan view, the MMC forms a WNW-ESE trending elongated feature covering an area of c. 16 km² (Figure 2.7). The MMC is flanked by two well-defined elongated marginal depressions as observed in a structural map of the top of the Yafo Sand Member (Figure 2.7).

3D mapping shows that the MMC comprises three large coalesced mounded structures. Two of these (MMC-1, MMC-2) are clearly seen on a time-structure map of the top Yafo Sand Member (Figure 2.7). The third structure (MMC-3) is less obvious on this map but is evident on seismic profiles as a small-scale mound flanking MMC-2 (Figure 2.8). The planform geometry of all three mounds is circular to sub-circular with diameters ranging from 0.75 km (MMC-3) to 1.5 km (MMC-1, MMC-2). These mounds are all near symmetric dome-like structures, with flank dips of c. 20° and a maximum height of c. 400 m (MMC-1; Figure 2.8).

2.7.2.1 Seismic character of the MMC

In seismic dip-sections (e.g., Figure 2.8), the MMC is seen as an array of three coupled upwards dome-shaped structures (MMC-1, MMC-2 and MMC-3). The lower boundary of the MMC forms a continuous negative high amplitude seismic reflection that underlies all three component mounds. Evidence of velocity pull up features is seen at the lower boundary and in the underlying strata, directly beneath the cores of the MMC (Figures 2.8 and 2.13). However, these are significantly smaller than those observed for the NMC (cf. Figure 2.10). The significance of this observation is that it strongly suggests lower seismic velocities within the MMC compared to those of the NMC. The upper boundary of the MMC is a mounded, strong negative amplitude seismic reflection that forms a continuous surface in three-dimensions (Figures 2.8 and 2.13).

The internal seismic reflection character of the MMC is most clearly seen on flattened horizontal coherence slices across the structure (e.g., Figure 2.14). On this coherence slice, the internal parts of the MMC can be seen to consist of two dominant seismic facies. The first corresponds to incoherent and chaotic seismic reflections that are dominant in the core of each component mound (marked C in Figure 2.14b). The second corresponds to seismically resolvable reflections that are confined to the flanks of the structures and form concentric and continuous reflections around the three chaotic cores (marked X in Figure 2.14b). On seismic cross-sections (Figure 2.15), these resolvable reflections can be traced continuously over the crests of each mound where they are broken up into block-like segments with possible reverse and normal faults interpreted at the hinges of maximum deflection. The geometrical relationship between the chaotic cores and the parallel-stratified facies in the flanks and crests is interpreted as intrusive because the reflection terminations define very irregular contacts that are too steep (c. 15°-20°) to be depositional in origin (Figure 2.15). Following this interpretation, the chaotic reflection pattern represents the intruded sediment. Based on measurements on a series of depth converted seismic sections, we estimate that the intruded material represents an average of c. 35% of the gross rock volume in the MMC (Figure 2.15). In the MMC-3 mound (Figures 2.15e and f), the coherent seismic reflections are clearly seen to correspond to the overall parallel-stratified Yafo Sand Member that is deflected up and overlies the chaotic core of the structure. The Yafo Sand Member can be traced

2-31

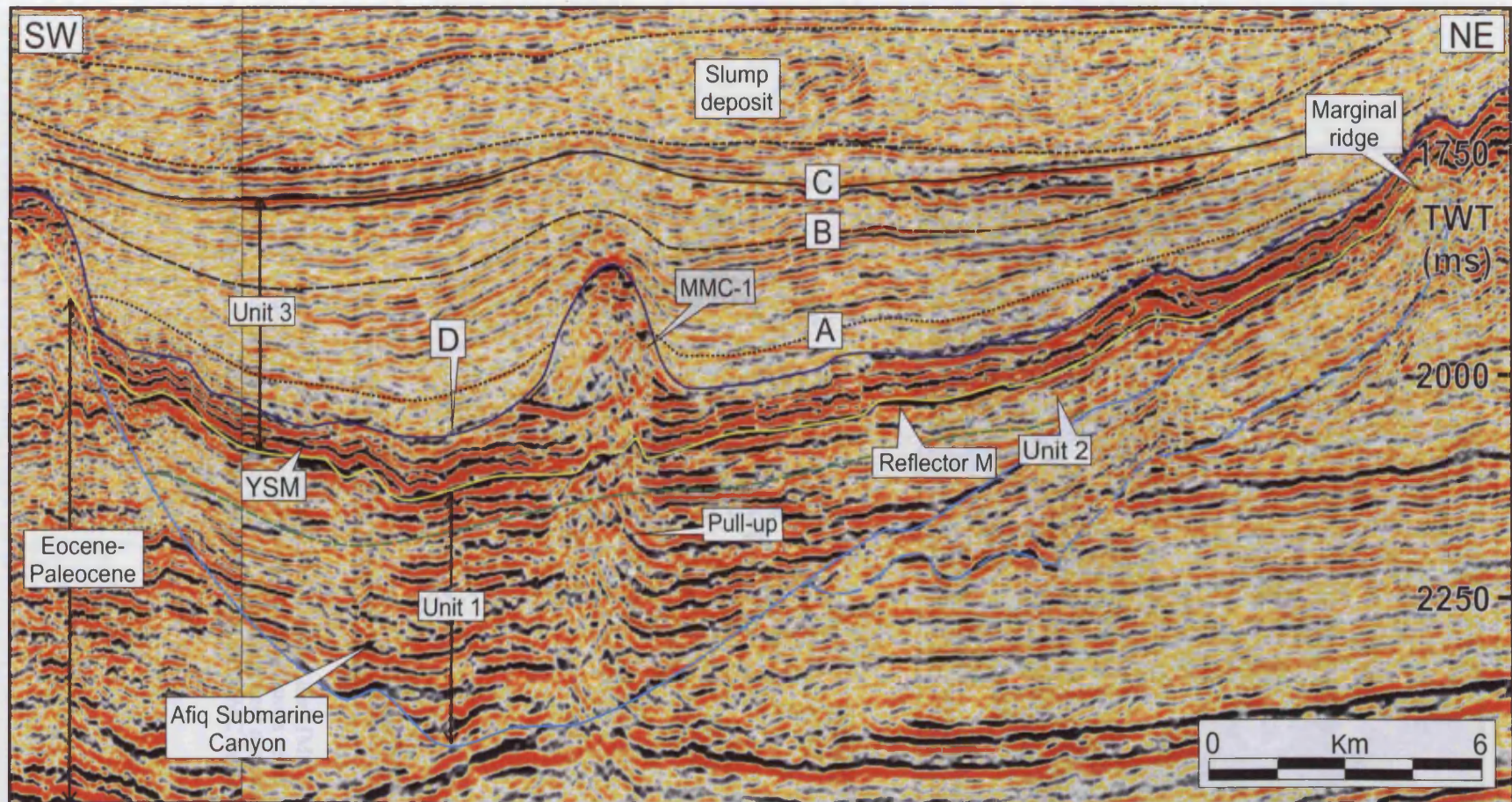


Figure 2.13 Seismic profile across the Afiq Submarine Canyon (see Figure 2.7 for location). The MMC-1 appears in its central parts. Note the presence of marginal topographic depressions (marked D) on both sides of the mounded structure. There are small-scale diapiric structures towards the northern flank of the canyon. There are clear “pull up” features below the NMC-1. The overburden is folded towards the flanks and crest of the MMC-1 and shows substantial thickness variations towards the structure.

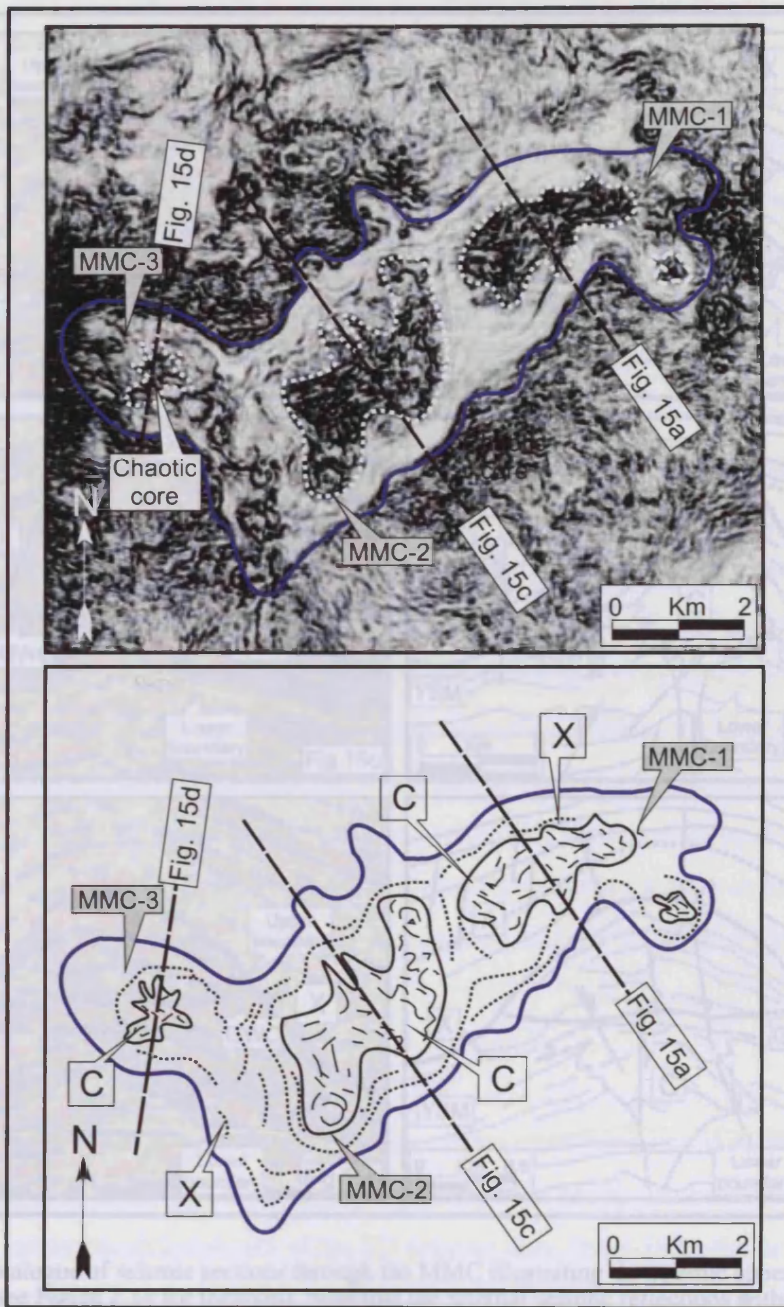


Figure 2.14 (A) Structurally flattened horizontal coherence-slice across the MMC (see Figure 2.7 for location). The internal parts of the MMC consist of concentric and continuous seismic events in the flanks (marked X) that surround three chaotic cores (one for each component mounded structure, marked C). (B) Schematic depiction illustrating the internal parts of the MMC in plan view.

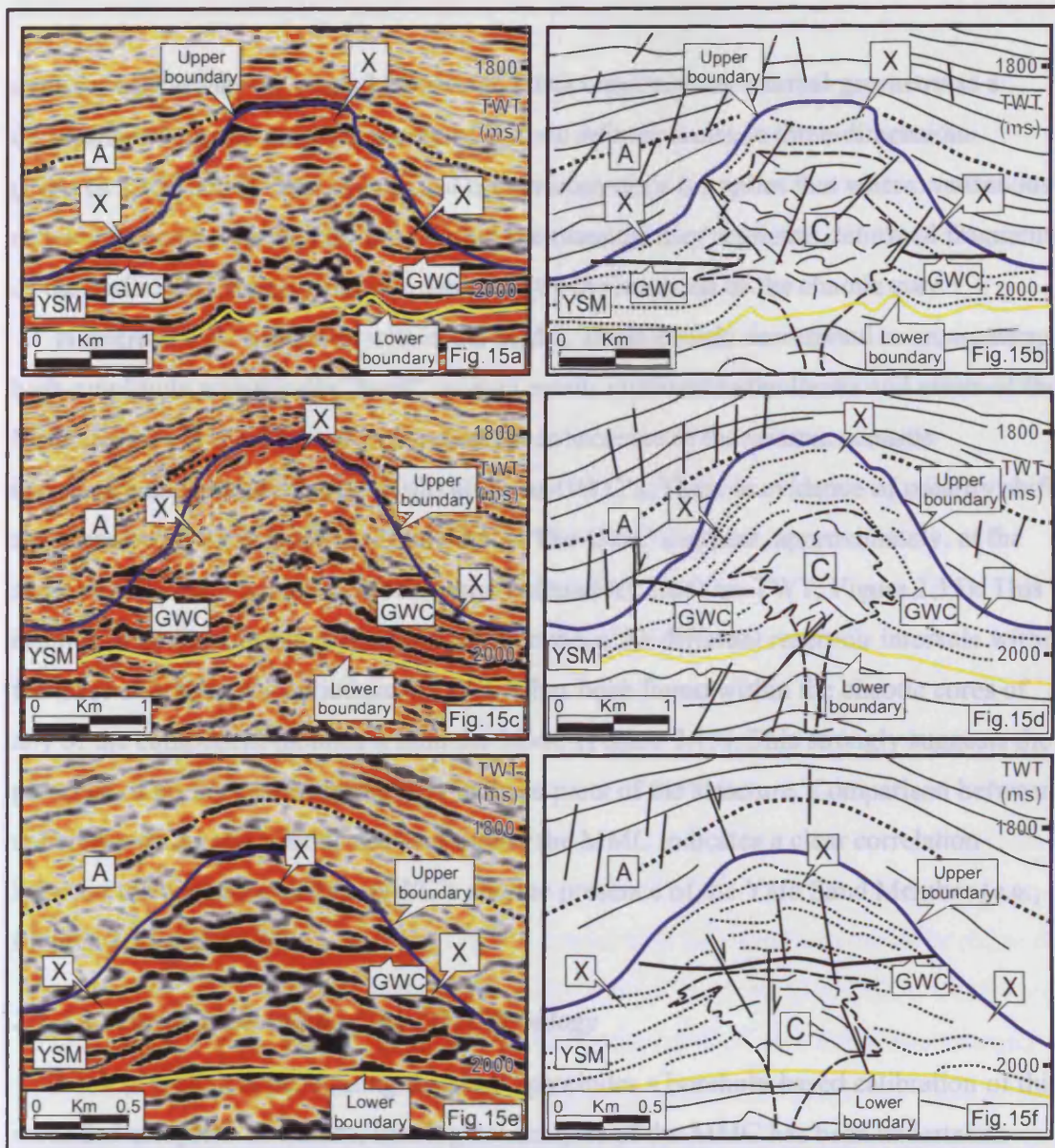


Figure 2.15 Catalogue of seismic sections through the MMC illustrating the seismic appearance of its internal parts (see Figure 2.14 for location). Note that the internal seismic reflections within the Yafu Sand Member (marked YSM) are truncated and bent-up toward the cores of the MMC. (a) Seismic section across the MMC-1. The flanks and crest of this component mound show many resolvable seismic events (marked X) that can be traced up to the preserved parts of the YSM. The core consists of chaotic seismic facies (marked C). There are two clear flat-spots restricted to the flanks of the structure. These represent gas-water contacts (marked GWC). (b) Seismic section across the MMC-2 showing an internal appearance that is highly equivalent to that of the MMC-1. (c) Seismic section across the MMC-3. Note the presence of continuous seismic reflections in the flanks and crest of the mound (X). The internal seismic reflections within the YSM are truncated against the basal central parts of the structure. There is a clear gas-water contact (GWC) continuously traceable across the crest of the mound.

first corresponds to gas-bearing sandstones that are restricted to the flanks and crests of the mound complex. This interpretation is supported by the recognition of well-defined GWC's crosscutting the flanks of the MMC (Figure 2.15). It is highly unlikely for any

continuously across the mound interior and thus constrains its internal geometry as a dome-shaped feature encasing a core of chaotic seismic facies in three-dimensions (Figures 2.15e and f). This is a critical observation since it implies that where continuous reflections can be traced internally within the mounds, they represent deformed fragments of the Yafo Sand Member that are disrupted by the intrusion of the chaotic core.

Numerous DHI's are seen within the MMC. These mainly correspond to crosscutting high-amplitude acoustically "hard" seismic events confined to the flanks and crests of the MMC (Figure 2.15). These events represent an increase in the seismic acoustic impedance and are interpreted in this study as GWC's. There is evidence of polarity shifts associated with these GWC's (Figure 2.15). The GWC's appear, approximately, at the same vertical level within each component mound (c. 2000 ms TWT; Figure 2.15). This implies some level of intercommunication between the different reservoir intervals within the three structures. No evidence of GWC's has been found within the chaotic cores of any of the component mounds within the MMC (Figure 2.15). This strongly suggests the presence of poorer reservoir qualities in these parts of the structure. Comparison between coherence slices and seismic sections across the MMC indicates a clear correlation between the occurrence of the GWC's and the presence of the Yafo Sand Member (e.g., Figures 2.14 and 2.15).

2.7.2.2 Seismic calibration of the MMC lithology

Lack of well data penetrating the MMC precludes a borehole-based calibration of this mounded complex. Therefore, lithological analysis of the MMC has been undertaken based on the previous observations of the 3D seismic data, those from the nearby Nir-1 well, and the supporting evidence of the analogous NMC. The internal reflection geometry of the MMC is clearly imaged in seismic profiles and allows for reasonable inferences to be made as to its lithological composition on the basis of the amplitude, continuity and geometry of the seismic reflections.

Following this approach, two dominant lithologies are inferred within the MMC. The first corresponds to gas-bearing sandstones that are restricted to the flanks and crests of the mounded complex. This interpretation is supported by the recognition of well-defined GWC's crosscutting the flanks of the MMC (Figure 2.15). It is highly unlikely for any

other reservoir lithology to produce clear GWC's equivalent to those recognised in the MMC. In addition, the upper boundary of the MMC invariably corresponds to a high amplitude seismic trough (Figure 2.15). This indicates a decrease in seismic acoustic impedance between the MMC and the clay-dominated overburden (Yafo Mudstone Member). Such a decrease strongly suggests that the material in the outer parts of the mound is of lower velocity than that of the overburden (claystones) and strengthens the argument for gas filled sandstones occupying the outer portion of the MMC. Moreover, well calibration from the Nir-1 well indicates that a similar decrease in acoustic impedance in the NMC-1 (cf. Figure 2.11) results from a contact between gas-bearing sandstones within the structure and claystones from the overburden (see previous section). We interpret these sandstones as mainly corresponding to the remnants of the Yafo Sand Member within the structure (see above). However, a minor percentage of intruded origin should not be excluded.

The second lithology within the MMC is inferred to correspond to clay-dominated sediments within the cores of each component mound (MMC-1, MMC-2 and MMC-3). This interpretation is based on three main observations. (1) GWC's are absent within the cores of all the constituent mounds of the MMC (cf. Figure 2.15). This strongly suggests a variation in terms of lithology, pore fluid generation or cementation content between the cores and the gas filled sandstones on the flanks and crests of the MMC. (2) Velocity pull up features are repeatedly observed directly below the cores of each component mound (cf. Figure 2.8). These are most likely due to higher seismic velocities in the cores of the mounds compared to the gas-bearing sandstones that encase them. Such a response of the seismic velocities is easily reconcilable with a clay-rich lithology in the central parts of the mounds. (3) Well calibration from the Nir-1 well shows that equivalent seismic responses drilled within the core of the NMC-1 correlate to clay-rich sediments (see previous section).

2.7.3 Alpha Mound

The Alpha Mound (AM) is an isolated four-way dip closure located in the SE corner of the Med Ashdod 3D area (Figure 2.7). The AM is a moderately sized feature compared

with the other examples in the study area (e.g., MMC and NMC). It is approximately elliptical in plan view and covers an area of c. 1.5 km² (mean length c.2 km, mean width c. 0.5 km) (Figure 2.7). The AM has a maximum height up to 100 m, lateral flanks dipping up to 10°-15° (Figure 2.8) and involves a total volume of c. 0.25 km³.

2.7.3.1 Seismic character of the AM

The lower boundary of the AM corresponds to a strong and continuous, negative high amplitude seismic reflection (Figure 2.8). This reflection can be laterally traced below and near the AM and is only locally affected by minor deformational structures below the apex of the structure (Figure 2.8). Low amplitude pull up amounting to a maximum of 50 ms TWT is seen to affect this lower boundary and the underlying reflections (Figure 2.8). The upper boundary of the AM is defined by a continuous, strong negative amplitude reflection against which the reflections of the overburden sharply terminate by onlap (Figure 2.8). The onlap geometry is parallel rather than convergent, with onlapping reflections being concordant to the top of the undeformed Yafo Sand Member (Figure 2.8).

The internal seismic appearance of the AM is highly reminiscent of that previously described from the MMC and, to a lesser extent, to that of the NMC. The core of the structure is dominated by chaotic seismic facies (marked C in Figure 2.16) whilst the flanks and crest show individual continuous and well-defined seismic reflections (X in Figure 2.16). On seismic profiles across the AM (e.g., Figures 2.16a and c), these well-defined reflections are clearly seen to correspond to the parallel-bedded Yafo Sand Member. On these profiles, the Yafo Sand Member can be continuously traced within the AM as a package of approximately constant thickness that is deflected up towards the centre of the structure and is concordant with the upper boundary of the mound. We also interpret a series of possible reverse and normal faults that fragment the Yafo Sand Member in several block-like segments (cf. Figures 2.16a and c). In plan view (Figure 2.16d), the Yafo Sand Member appears as a concentric and continuous seismic unit that surrounds the chaotic core of the structure. The Yafo Sand Member thus has a dome-like geometry in three-dimensions that encloses the core of chaotic seismic facies within the AM and represents up to 70% of the internal parts of the mound.

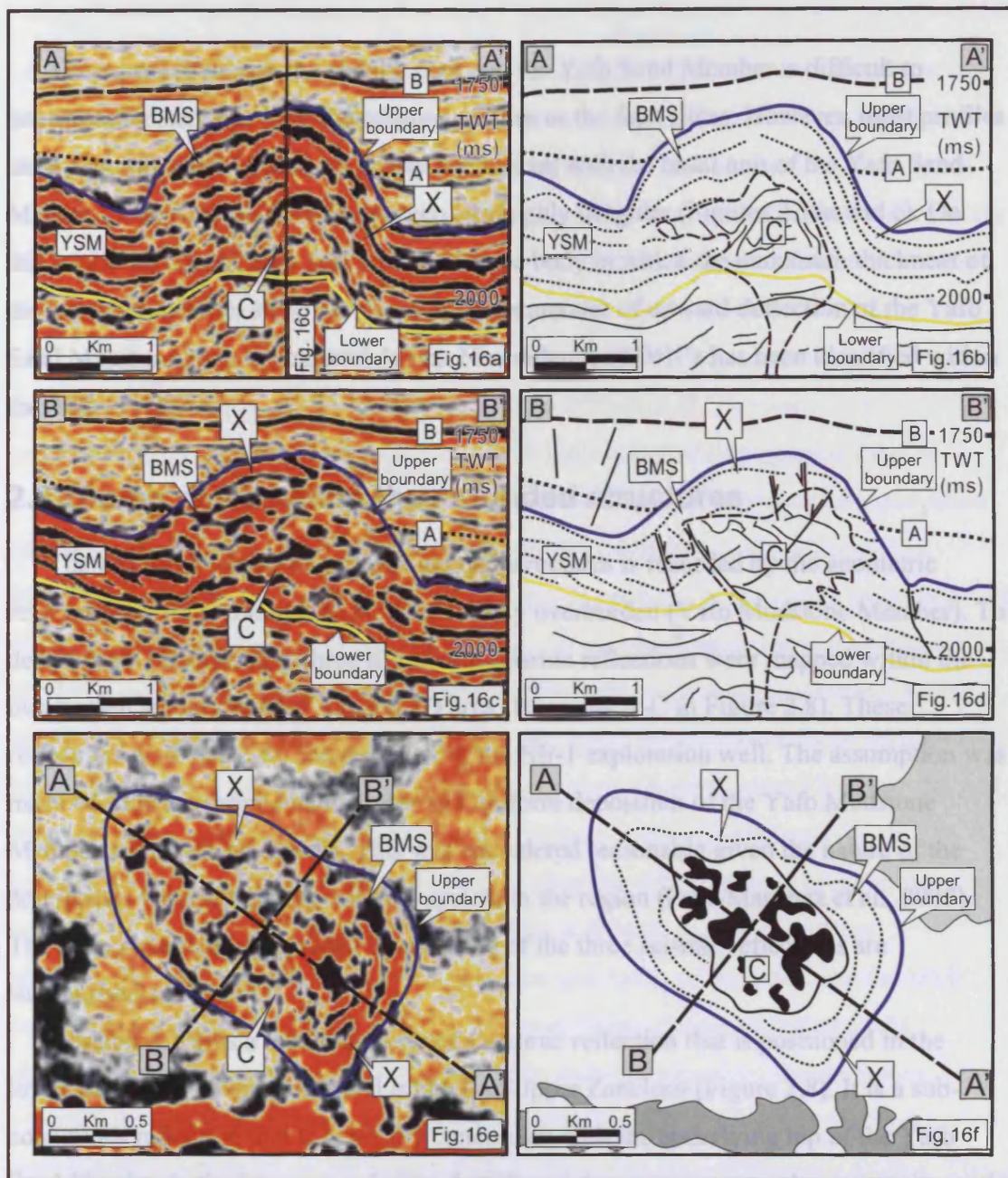


Figure 2.16 Seismic examples of the internal geometries of the BMS. Note the bulbous morphology and highly organized internal structure of this mound. (a) Seismic profile across the BMS (see Figure 2.8 for location). Note the presence of continuous seismic reflections (marked X) along the flanks and crest of the structure. These correspond to the Yafo Sand Member (marked YSM) which is deflected up toward the chaotic centre of the mound (marked C). (c) Seismic profile across the BMS perpendicular to Figure 2.16A. There are continuously traceable seismic reflections (X) across the crest of the mound from the YSM. (e) Time slice through the BMS. Note the presence of concentric and continuous seismic reflections (X) enclosing a core of chaotic seismic facies (marked C).

The contact between the chaotic core and the Yafo Sand Member is difficult to interpret precisely on either the seismic profiles or the time slices. However, most profiles show that the upper contact is crudely concordant with the basal unit of the Yafo Sand Member, whilst on the flanks it is steep and highly irregular (Figures 2.16a and c). On this basis, the chaotic core defines an intrusive body in which the maximum thickness of the intrusive mass (c. 30%) corresponds to the amount of upward deflection of the Yafo Sand Member above its regional datum. No evidence of DHI's has been identified within the AM.

2.8 Timing of formation the mounded structures

The timing of formation of the mounded structures is recorded by the geometric relationships of the mounds to the sedimentary overburden (Yafo Mudstone Member). To define these relationships, three significant seismic reflections were mapped within the overburden across the Med Ashdod 3D area (Horizons A-C in Figure 2.8). These reflections were dated by correlation with the Nir-1 exploration well. The assumption was made of constant sedimentation rates and uniform deposition of the Yafo Mudstone Member within the study area. This was considered reasonable given the nature of the dominantly hemipelagic depositional system in the region (Frey-Martínez et al., 2005). The main observations revealed by mapping of the three seismic reflections are summarised as follows.

Horizon A forms a medium-amplitude seismic reflection that is positioned in the lower parts of the overburden and is dated as Upper Zanclean (Figure 2.8). It is a sub-continuous reflection that is generally concordant with the underlying top of the Yafo Sand Member in the inter-mound areas, but shows clear convergent onlap, upturning and rotation onto the crests of the mounded structures (Figure 2.8). The onlap terminations are especially clear near the NMC and the MMC where horizon A is strongly domed with flanks dipping up to 20° (Figure 2.8). Horizon B is a moderate amplitude seismic reflection positioned in the middle parts of the overburden and is dated as Lower Piacenzian (Figure 2.8). This horizon overlies all the mounded structures and forms a continuous surface that is slightly deformed into a series of domal folds above the crests

of the mounds (Figure 2.8). The degree of structural relief on this horizon increases in a basinward direction, north-westerly along the canyon axis, being the largest over the NMC and the MMC and negligible over the AM. Horizon C is a seismic reflection that marks the upper boundary of the overburden of the mounded structures and is close to the Piacenzian-Gelasian boundary. It is a continuous, moderate-amplitude reflection that is only slightly deformed into small-scale folds over the NMC and the MMC (Figure 2.8).

The most significant of the previous observations is that horizon A exhibits convergent onlap onto all the mounded structures (Figure 2.8). This specific form of onlap demonstrates that the mounds were at the palaeo-seabed during deposition of horizon A. It is evident from this conclusion that the formation of the mounds pre-dated the deposition of horizon A. The significance of this convergent onlap relationship, therefore, is that it fixes horizon A as a minimum datum to infer the timing of initiation of the mounded structures. Provided that horizon A is dated as Upper Zanclean we can therefore establish the approximate timing for initiation of the mounded structures as Middle Zanclean. The package between horizons A and B varies laterally in thickness and has several growth wedges adjacent to the mounded structures (Figure 2.8). Near the AM, the A-B interval forms a package of constant thickness comprised by continuous, horizontal and relatively undeformed seismic reflections that terminate in parallel onlap onto the flanks of the structure (Figure 2.8). This A-B interval, however, thins significantly by convergent onlap onto the crests and flanks of the NMC and the MMC (see Figures 2.8, 2.10 and 2.13). The identification of parallel onlap onto the AM indicates the fill of an established topography by post-deformational sedimentation. In contrast, the convergent onlap onto the NMC and the MMC implies growth of a series of established topographies on the palaeo-seabed affected by syn-sedimentary folding. These observations demonstrate that growth of the AM concluded before deposition of the A-B interval while the NMC and the MMC remained active as deposition proceeded between A and B. The geometric relationships of the B-C interval to the mounded structures are equivalent to those of the A-B interval, but with diminution of the thickness variations. There is no evidence from the 3D seismic data for forcible folding at horizon C or the overlying strata throughout the study area. We interpret the small-scale folds over the NMC and the MMC (see Figures 2.8, 2.10 and 2.13) to be the result of passive down-

building of horizon C above the mounded structures by differential compaction after burial. From these observations, together with the calibration from the Nir-1 well, it is therefore interpreted that growth of the AM was completed during the Late Zanclean while the NMC and the MMC remained active up to the Early Gelasian.

From the previous observations, we can constrain the time of initiation and cessation of the mounded structures to c. 4 Ma BP and c. 2.5 Ma BP, respectively. There is evidence that growth of the mounded structures initiated simultaneously along the Afiq Submarine Canyon. It has also been observed that the mounds first became inactive at the landward parts of the Afiq Submarine Canyon (e.g., AM), while those in the seaward parts (e.g., NMC and MMC) remained active for a longer period of time. Given that growth of the AM and the MMC terminated during the Late Zanclean (c. 4 Ma) and the Early Gelasian (c. 2.5 Ma), respectively, we infer a delay in the cessation of the mounded structures along the Afiq Submarine Canyon of up to c. 1.5 Ma. The mounded structures evolved thus in, at least, two main phases of activity. The first phase took place between the Middle and Late Zanclean. It was synchronous to all the mounded structures and led to the development of a series of four-way dip closures along the axis of the Afiq Submarine Canyon. The second phase occurred between the Early Piacenzian and the Early Gelasian. It was restricted to the NMC and the MMC and probably consisted of several episodes of continued growth of the mounds interspersed with sedimentary deposition of the Yafo Mudstone Member. These growth episodes possibly decreased in number and magnitude through time as evidenced by the diminution of the thickness variations in the B-C interval.

2.9 Canyon margin ridge structures

Although the main focus of this chapter is on a series of mounded structures along the axis of the Afiq Submarine Canyon (see above), there are a number of other features observed in the study area that are of fundamental significance for the purpose of this study. These features show many of the key characteristics previously identified for the mounds (e.g., convex-upward geometry, internal chaotic facies). However, they lack a well defined lower boundary and show clear differences in terms of planform geometries,

volumes and internal character. In this section, we provide a detailed description of the 3D appearance of these features and compare them with the previously described mounded structures.

The general planform appearance of these structures is best described with reference to the structural time contour map of the top Yafo Sand Member (Figure 2.7). On this map, the structures (marked R) appear as two ridge-shaped structural culminations that are oriented in a SSE-NNW direction. The imaged portions of the two ridges cover areas of up to c. 40 km² (mean length 15 km, mean width 4 km) and have a maximum structural relief of c. 150 m. Importantly, both ridges are restricted to the areas underlain by the northern flank of the Afiq Submarine Canyon. This clear spatial coincidence strongly suggests a causative connection between this flank and the ridge structures.

On strike seismic profiles (e.g., Figures 2.10 and 2.13), the ridges appear as steep-sided domed features (marginal flank dips of up to 15°) that are invariably positioned above the highest point of the northern flank of the Afiq Submarine Canyon. Their internal seismic character is dominated by chaotic seismic reflections that are most likely derived from the canyon infill (Figures 2.10, 2.13 and 2.17). The lower boundary of the ridges is very difficult to determine because it is masked by overmigration noise (Figures 2.10, 2.13 and 2.17). However, it is tentatively suggested here that it corresponds to a relatively convex-upward reflection within the infill of the canyon. The upper boundary of the ridges is defined as the base of the Yafo Sand Member. This boundary is imaged as a convex-upwards seismic reflection that separates the chaotic seismic reflections within the ridges from the continuous reflections of the Yafo Sand Member (Figure 2.17). There is no evidence from the seismic data of any accumulation of gas (i.e. DHI's) within the ridges. There is evidence of velocity pushdown effects beneath the ridges (Figure 2.17). This could be related to the presence of overpressured fluids within the structures causing a reduction in the average interval velocity (e.g., Morley, 2003).

The sedimentary overburden of the ridge structures corresponds to the Lower Yafo Formation (Figures 2.10 and 2.13). Correlation of intra-overburden seismic reflections is possible above the ridges, and this shows that there are significant thickness variations (i.e. growth intervals) and deformational structures adjacent to them. For example, the Yafo Sand Member shows clear indication of forcible folding and rim syncline

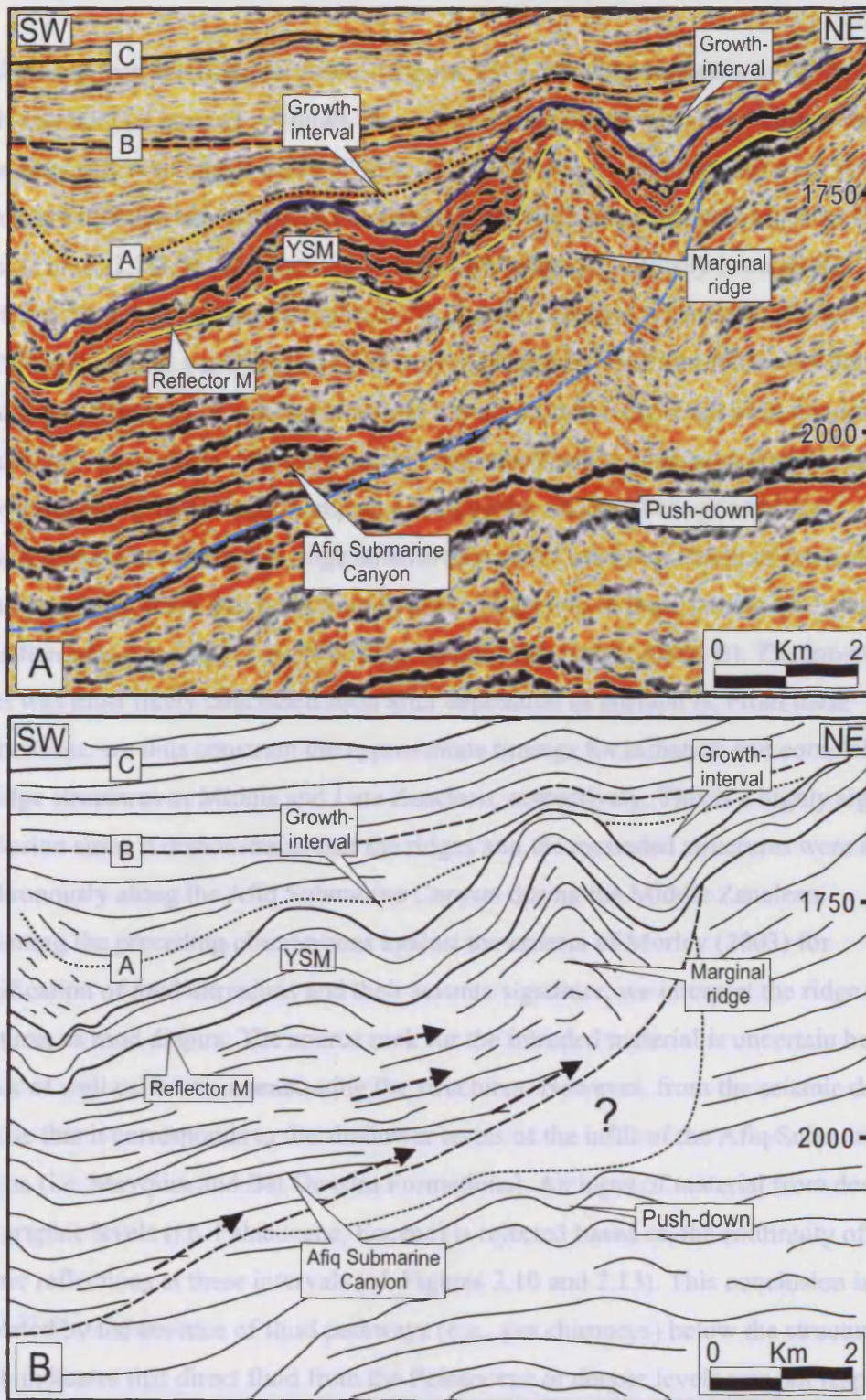


Figure 2.17 (a) Close up on the northeastern flank of the Afq Submarine Canyon (see Figure 2.10 for location) showing the internal appearance of the marginal ridges. They form steep-sided domed features (marginal flank dips of up to 15°). Note that the internal seismic character is dominated by chaotic seismic reflections most likely derived from the canyon infill. Note the presence of velocity pushdown effects beneath the structure. (b) Schematic depiction illustrating the marginal ridges and the internal parts of the Afq Submarine Canyon. Dashed arrows indicate interpreted pathways for fluidized sediment flowage.

development over the ridge structures (Figure 2.17). The interval between the top Yafo Sand Member and horizon A shows clear growth wedges that pinch out against the flanks of the ridges by convergent onlap (Figure 2.17). These thickness variations are vertically concordant with the rim synclines developed in the Yafo Sand Member adjacent to the ridges (Figure 2.17). In addition, the A-B interval thins dramatically towards the structures from the southwest (Figure 2.17). The B-C interval, in contrast, shows no significant thickness variations and it is only slightly deformed into folds over the crests of the ridge structures. We do not consider these folds to be the result of hydraulic “jacking up” through forceful intrusion but the consequence of passive down-building of the overburden by differential compaction above the ridges. These geometrical relationships demonstrate that ridge structures initiated after deposition of the Yafo Sand Member and that there was an important phase of growth of these structures during the deposition of the younger Yafo Mudstone Member (horizons A and B). The growth of the ridges was most likely concluded soon after deposition of horizon B. From these observations, we thus constrain the approximate timings for initiation and completion of the ridge structures as Middle and Late Zanclean, respectively. This is a highly significant conclusion since it demonstrates that the ridges and the mounded structures were initiated synchronously along the Afiq Submarine Canyon during the Middle Zanclean.

Setting the preceding observations against the criteria of Morley (2003) for classification of mud intrusions and their seismic signature, we interpret the ridge structures as mud diapirs. The source rock for the intruded material is uncertain because of lack of well calibration penetrating the structures. However, from the seismic data, we propose that it corresponds to the shallower levels of the infill of the Afiq Submarine Canyon (i.e. Mavqim and Bet Guvrim Formations). An input of material from deeper stratigraphic levels (i.e. Palaeocene, Eocene) is rejected based on the continuity of the seismic reflections at these intervals (cf. Figures 2.10 and 2.13). This conclusion is also supported by the absence of fluid pathways (e.g., gas chimneys) below the structures which indicates that direct fluid from the Palaeocene or deeper levels was not responsible for their formation. The ridged planform morphology of the mud diapirs (Figure 2.7) suggests that some form of alignment of feeding sources must have created the structures. In addition, the close spatial coincidence between the ridges and the northern flank of the

Afiq Canyon (e.g., Figure 2.17) indicates that this flank could have effectively acted as a preferential pathway for remobilised mud to move vertically and built the ridge diapirs.

We are unable to offer a conclusive explanation for why the diapiric ridges are restricted to the northern flank of the Afiq Submarine Canyon, other than to suggest that it might be connected to differential behaviour of fluid migration and pressure gradients within the canyon infill. The Afiq Submarine Canyon consists of a relatively continuous succession of marls, claystones, limestones and turbiditic sandstones (see above). This could have created differential permeabilities within the canyon infill such that fluids did not reach the eastern parts of the canyon, which consequently did not mobilise. There are no significant thickness variations or any specific structures (i.e. faults, folds or stratigraphic discontinuities) within or adjacent to the Afiq Submarine Canyon that could explain such a differentiation in diapirism along its flanks.

There are several conclusions to be drawn from the identification of these diapiric ridges along the Afiq Submarine Canyon that are of great significance for the overall understanding of the mounded structures. The most important conclusion is that the presence of such diapirs clearly indicates that soft-sediment deformation played a critical role in reshaping the overall appearance of the Afiq Submarine Canyon during the Early Pliocene. Secondly, the fact that the diapiric ridges appear distributed along a flank of the canyon points clearly to a system in which lateral and vertical flowage of mud-rich sediments was dominant. Thirdly, the clear spatial correspondence between the Afiq Submarine Canyon, the mounded structures and the ridge diapirs strongly suggests that their coexistence is not coincidental, but the result of a causative connection between them. Finally, the close concurrence in time between the mounded structures and the diapiric ridges indicates that their triggering mechanisms and overall genesis could have been similar.

2.10 Discussion

The most important observations undertaken from seismic interpretation of the mounded structures within the study dataset are summarised as follows as the basis for the discussion below:

- Seventeen discrete examples of kilometre-scale mounded structures are recognised within the Lower Pliocene offshore Israel. The majority of these mounded structures are aligned NW-SE over the axis of the Afiq Submarine Canyon (Figure 2.7).
- The mounded structures are circular to elliptical in plan view and appear as culminations at the top of the Yafo Sand Member stratigraphic level (Figure 2.7). These structures may appear as isolated four-way dip closures (e.g., AM) or as complexes of up to three coalesced features (e.g., MMC and NMC).
- In seismic profiles, the upper boundaries of the mounded structures are invariably expressed as dome-like reflections with flank angles up to 20°. These boundaries are correlated on exploration wells to the top of the Yafo Sand Member (Figure 2.6). The basal boundaries correspond to a common continuous, sub-horizontal and high amplitude reflection that is correlated with the base of the Yafo Sand Member (Figure 2.6).
- The internal seismic reflection character of the mounded structures consists of two dominant seismic facies. The first corresponds to incoherent and chaotic seismic reflections that are dominant in the core of the structures. The second corresponds to more coherent and continuous seismic reflections that are dominant on the flanks and the crests of the mounds. These continuous reflections correspond to the Yafo Sand Member, which is deflected up above the mounded structures.
- Flat and bright events of positive amplitude crosscut some of the internal parts of the mounded structures. These events are interpreted as hydrocarbon-related fluid contacts (flat-spots) and correlated to the GWC in the Nir-1 exploration well. These hydrocarbon indicators are mainly restricted to the flanks and crests of the mounded structures and are absent in the central and chaotic parts (Figure 2.15).
- Based on seismic analysis and lithological calibration from the Nir-1 exploration well, clay-rich lithologies mixed with loose sands are dominant within the core of the mounded structures (cf. Figures 2.11 and 2.15). Gas-bearing sandstones are encountered in the flanks and crest of the structures.
- The internal parts of the mounded structures are dominated by allochthonous material from Cretaceous to Upper Miocene stratigraphic levels. Evidence of

external input of material within the mounds principally consists of reworked nannofossils and microfauna recorded from the Nir-1 exploration well.

- Seismic data evidence clear “pull-ups” in time below the NMC and less pronounced below the MMC (cf. Figures 2.10 and 2.13). These “pull-ups” are most pronounced beneath the core of the mounded structures, suggesting poorer reservoir within the core and improved reservoir on the flanks. This correlates with the lithological information extracted from the Nir-1 well.
- The sedimentary overburden of the mounded structures corresponds to the Yafo Mudstone Member. Evidence of syn- and post-depositional deformation (e.g., tilted onlap, forced folding and faulting) has been observed within this interval in areas adjacent to the mounds.
- Elongated and crescent-shaped depressions bound the majority of the mounded structures in plan view (Figure 2.7). These depressions are depicted in seismic profiles as downward-bent reflections from the Yafo Sand Member mimicked by the overburden (Figures 2.10 and 2.13). Importantly, the thickness of the Yafo Sand Member remains constant in the areas affected by the topographic depressions whereas the thickness of the overburden is markedly variable (Figures 2.10 and 2.13).
- Kilometre-scale mud diapiric ridges develop along the northern flank of the Afiq Submarine Canyon (Figure 2.7). These ridges form domed-like structures at the Yafo Sand Member (Figures 2.10 and 2.13). Their formation is coeval to the initiation of the mounded structures along the canyon axis.

2.10.1 Origin of the canyon axis mounded structures

The unusual geometry and high flanking angles of the mounded structures in the study area strongly suggests that these are not primary depositional features but are the product of post-depositional deformational processes (*sensu* Brooke et al., 1995). There are a number of genetically distinct post-depositional geological features that are mounded in cross-section, circular to sub-circular in planform and similar in scale to the observed structures. These, amongst others, comprise igneous, salt and mud diapirs, mud

volcanoes, sand mounds and slumps. In the case of the mounded structures observed in this study, the number of possible interpretations is constrained by seismic and well data. For instance, the internal parts of the mounded structures are composed of well-mixed sands and clays. There is no evidence from the well data of salt or igneous lithologies, which rules out an igneous or salt diapir origin for the structures (e.g., Alsop et al., 2000; Davies et al., 2002). An origin as sand mounds (e.g., Jenssen et al., 1993; Brooke et al., 1995; Dixon et al., 1995, Huuse et al., 2004) is also precluded on the basis that large amounts of clay have been recorded from the mounded structures. Slump deposits may appear as chaotic mounded geometries in seismic profile. However, they are excluded as an origin for the mounded structures in the study area as there is no evidence of a basal shear plane, a headscarp and a toe region, which are essential elements of slump deposits *sensu* Varnes (1978).

The overall geometries of the mounded structures could suggest mud volcanism as a possible origin. However, this is precluded as an option based on several important observations previously presented. For instance, there is no evidence of erosion associated with the upper boundaries of the mounds. This strongly suggests that the upper boundaries were unlikely to be exposed at the seabed. In addition, it is evident from the examples presented here that the Yafo Sand Member is invariably domed upwards above the mounded structures. This observation, together with the identification of a steep (c. 15°-20°) and irregular contact between the chaotic core and the Yafo Sand Member (c.f. Figures 2.11, 2.15 and 2.16) suggests a forceful intrusive origin for the mounds. Moreover, the overburden (Yafo Mudstone Formation) is deformed into a series of folds and faults against the flanks and crests of the mounded structures (c.f. Figure 2.8). These styles of deformation are morphologically consistent with the characteristics of upwarped domes through flexure and folding due to forceful intrusion of material into shallow-level sedimentary strata (Price and Cosgrove, 1990). Alternatively, it could be argued that such deformational styles may be partly the result of differential compaction of the overburden after burial of the mounds being formed on the palaeo-seabed as mud volcanoes. However, the high angles of the folds against the structures (20°-25°), and the recognition of concentric and radial faults systems are clear indications of brittle deformation of the overburden by hydraulic “jack up”. It is obvious therefore that the mounded structures are

the result of some form of intrusive processes and only this possibility is considered in any further discussion.

Another fundamental observation that can help constrain the origin of the mounded structures is their lithological composition. Well data have revealed the presence of large amounts of allochthonous clastic sediments within the NMC. Nannofossils and microfauna recorded from the Nir-1 well indicate that these sediments are polygenetic and originate from various stratigraphic levels (Cretaceous to Upper Miocene). This strongly suggests an external input of material within the mounded structures and forms the basis for inferring two possible origins for these sediments: horizontal or vertical reworking. The evidence for a pre-existing depositional fairway (Afiq Submarine Canyon) could suggest that the allochthonous material within the mounds resulted from horizontal canyon fill reworking. However, this is excluded as a possibility, because of the presence of a much higher ratio of allochthonous fossils within the mounded structures compared with the same stratigraphic levels nearby the mounds. Furthermore, in such a depositional environment, sedimentary structures (e.g., lamination, ripples or cross-stratification) would be expected and these have not been observed in the available well data. Instead, dip and azimuth analysis from the Nir-1 well have revealed that the material within the mounded structures is highly chaotic and remixed, which strongly suggests some type of post-depositional remobilisation process. It is proposed therefore that the allochthonous material was derived vertically from deeper stratigraphic sections and injected into shallower levels to create the mounded structures. A vertical input of material would require a vertical feeder system for fluids and rock being mobilised upwards from deeper stratigraphic levels and intruded into the mounded structures. No evidence of structures such as pipe-like features that could act as migration pathways (e.g., Hanken et al., 1996; Graue, 2000; Løseth et al., 2001; Netoff, 2002; Draganits et al., 2003) has been observed. However, this can easily be explained by the difficulty of making any primary observation of vertical feeders within the highly disturbed zones directly beneath the mounds due to a combination of chaotic sediments and gas accumulations within the structures. The lack of any mapped feeder does not therefore preclude the presence of such features directly beneath each major mounded structure.

3D mapping has shown the presence of elongated and crescent-shaped marginal

topographic depressions surrounding most of the mounded structures (c.f. Figures 2.7 and 2.10). These depressions could be interpreted as some form of erosional features. However, the absence of any evidence of erosional truncation and the bowl-like geometry of these marginal depressions do not support such an origin. Instead, we prefer the interpretation that these topographic depressions represent zones affected by withdrawal-induced subsidence of material being intruded within the mounded structures. These depressions are thus the result of local subsidence produced around the area of emission (feeder system) because of the accommodation of the palaeo-seafloor to the loss of material at depth. Similar depressions have been documented around feeder systems elsewhere (e.g., Nichols et al., 1994; Netoff, 2002; Davies, 2003). Importantly, the thickness of the Yafo Sand Member remains constant across the topographic depressions, which indicates that no material has been removed from this stratigraphic interval. We thus propose that remobilisation affected the intervals beneath the level of the Yafo Sand Member, which subsided as coherent layers due to undermining by deeper depletion. This mechanism requires the volume of allochthonous material within the mounded structures to be approximately balanced by the loss of an equivalent volume from the topographic depressions excluding the loss of any pore fluid from the system. From measurements made on isopach maps and depth converted seismic sections, we estimate the volume of sediment intruded within the mounds to approximately balance with the material depleted from the surrounding topographic depressions. This evidence strongly suggests that the material injected within the structures was remobilised from the Afq Submarine Canyon and reinforces an injection origin for the mounded structures.

Based on the previous observations and discussion, the mounded structures in the study area are interpreted to have formed by clastic forceful intrusion into shallow-level sedimentary host rocks (Yafo Sand Member). From the microfauna records, the sources for the intruded material were most probably the Bet Guvrim and Ziqim Formations within the Afq Submarine Canyon. Comparable structures involving forceful intrusion by diapirism have been generated in theoretical modelling (e.g., Schultz-Ela, 2003), and described from outcrop and seismic-based studies (e.g., Jenyon, 1986 and 1988; Kempler et al., 1996; Alsop et al., 2000; Davison et al., 2000; Cartwright et al., 2001; Van Rensbergen and Morley., 2003). Diapiric intrusion is morphologically consistent with the

styles of deformation observed in the Yafo Sand Member and the overburden of the mounded structures presented here. Diapirism can cause the overburden layers to upturn against the diapir flanks by frictional drag forces exerted at the structure interface (e.g., Davison et al., 2000). For instance, forced-folds caused by frictional drag in diapirs are well-documented geological features (e.g., Jenyon, 1986 and 1988; Kempler et al., 1996; Alsop et al., 2000; Davison et al., 2000; Cartwright et al., 2001; Morley, 2003; Schultz-Ela, 2003; Stovba and Stephenson, 2003; Van Rensbergen and Morley., 2003) and correspond closely with the deformational structures observed in the mounded geometries of the study area (cf. Figure 2.8). Radial and concentric normal faulting, similar to the examples previously presented, is another important mechanism of overburden deformation related to diapiric intrusion (e.g., Davison et al., 2000).

2.10.2 Genetic model and evolution

The arguments advanced in the previous section point to a genesis for the structures presented here in which mud remobilisation and injection within the Afq Submarine Canyon played a key role. Clastic injection occurs when fluidised sediment is depleted from a source area and flows through a series of feeder systems (e.g., fractures, blow-out pipes) to be entrained into a host rock. Sediment becomes mobilised because it is in a condition of insufficient strength to resist the forces driving it to move (Maltman and Bolton, 2003). A high overpressure must be then maintained for clastic intrusions to propagate and develop (Morley, 2003). Three main potential factors controlling the development of high overpressure regimes have been described from a variety of sedimentary basins and could be invoked for the study area:

- Hydrocarbon generation – overpressure development by the generation of methane in mud-rich sediments.
- Earthquake activity – overpressure development by dynamic liquefaction.
- High-sedimentation rates – overpressure development due to rapid deposition of underconsolidated mud-rich sediments.

The mounded structures presented in this chapter occur within a hydrocarbon province. A detailed description of the source rock goes beyond the scope of this chapter.

However, basin modelling and well data indicate that it is likely to be the Bet Guvrim and Ziqim Formations within the Afiq Submarine Canyon. This strongly suggests that mud mobilisation and injection could have been driven by gas buoyancy and migration within the canyon infill. The involvement of methane is widely reported to be associated with many mud volcanoes and diapirs elsewhere (e.g., Kopf, 2002) and could be easily be invoked for the mounded structures in the study area. It should be noted, however, that it is extremely unlikely that the present-day hydrocarbon accumulations within the mounds were involved in their formation as these correspond to biogenic gas that almost certainly migrated to the mounds significantly afterwards.

A direct link between earthquakes and mobilisation of clastic sediments has been widely described in the literature (e.g., Bankwitz et al., 2003; Yassir, 2003). Earthquakes would significantly increase the fluid pressure and weaken the seals within the canyon infill, thus facilitating seal rupture and clastic injection. Because of its position at the zone of interaction between the Anatolian, African and Arabian plates, the continental margin of Israel is a seismically active region. Local earthquakes along structures underlying the Afiq Canyon such as the Syrian Arc system could have caused local overpressures and triggered sediment mobilisation. A high probability exists that the region was seismically active during the Early Pliocene. Palaeoseismic activity is to have been expected in this region, because tectonic studies give evidence for active geodynamic processes in Pliocene times (e.g., Garfunkel and Almagor, 1985; Garfunkel, 1998; Robertson, 1998; Vidal et al., 2000; Huguen et al., 2001).

Build-up of excess pore pressure in fine-grained sediments because of high-sedimentation rates is proposed as one of the main causes for mud mobilisation along continental margins (e.g., Morgan et al., 1968; Hedberg, 1974; Evamy et al., 1978; Knox and Omatsola, 1989; Yassir, 2003). Rapid deposition can result in underconsolidation of buried layers of clay-rich sediment in which upward hydraulic gradients reduce the internal shear strength of the sediment and lead to mobilisation. Interpretation of seismic and well data states that the infill of the Afiq Submarine Canyon is up to 500 m thick. Our estimations from this thickness suggest an average for the accumulation rate of about 20 cm/kyr. According to these values, the sedimentation rates are not likely to be sufficient to build up significant excess in pore pressure within these deposits and to generate the

observed mounded structures.

We thus propose that overpressures were generated within the Afq Submarine Canyon probably due to earthquake activity, hydrocarbon generation or a combination of both factors. Fluids were trapped in the sand-rich intervals (i.e. turbiditic sands) interbedded with poorly permeable claystones of the canyon infill. The clay-rich intervals built a series of permeability barriers that prevented drainage and consolidation of the sand-rich units. This induced the formation of overpressured compartmentalised sandstone reservoirs that created a meta-stable pore fluid regime within the Afq Submarine Canyon (Figure 2.18a). Eventually, fluid overpressure approached lithostatic pressure and the seals failed by hydraulic fracturing (e.g., Mandl and Harkness, 1987). This created a differential pressure gradient within the canyon that triggered rapid vertical movement of fluids. Fluids migrating through the canyon infill fragmented and mobilised sediments along their path. As a result, a low-density mixture of fluids and fine-grained sediments (fluidised sediment) were mobilised and moved upwards (Figure 2.18a). In most of the cases, the fluids moved discordant to the bedding of the canyon infill (Figure 2.18a). However, they probably also utilised high permeability levels (e.g., turbiditic sandstones) as preferential pathways to migrate sub-horizontally along them. This created a lateral dissipation of the overpressures along the infill of the canyon and would explain the presence of fluidised sediments along its northern flank (Figure 2.18a). At this point, a major episode of mud injection ensued.

The fluidised sediments migrating upwards exerted a continuous stress to the base of the Yafo Sand Member along the Afq Submarine Canyon (Figure 2.18a). Eventually, this level failed in tension and fractured, leading to catastrophic intrusion of fluidised sediment (Figure 2.18a). In the northern flank of the canyon, this intrusion occurred through an alignment of feeding points that built the ridge structures whilst, in the axis, intrusion occurred through discrete feeders that created the mounds (Figure 2.18a). During emplacement, the fluidised sediment moved upwards, probably in a convective way, to hydraulically deform the overall parallel-bedded strata of the Yafo Sand Member (Figure 18a). This resulted in a series of four-way dip mounds and elongated ridges being created at the palaeo-seabed (top Yafo Sand Member; Figure 2.18b). After this first major episode of mud injection, growth of the canyon margin ridge structures and of those

mounds positioned in the eastern parts of the canyon axis (e.g., AM) terminated. Concurrently, relief at the palaeo-seabed was almost eliminated by deepwater sedimentation (horizon A; Figure 2.18b). Growth of the mounded structures, however, continued in the western axis of the canyon (e.g., NMC and MMC) for a more protracted period of time (Figure 2.18c).

It is highly probable that a number of discrete, probably earthquake-induced, episodes of mud remobilisation and injection continued up to the Early Gelasian in the western axis of the Afiq Canyon. Evidence for diachronous growth of the mounds along the canyon axis has been presented in the form of thickness variations and deformational structures in the sedimentary overburden (see previous sections). As intrusion of fluidised sediment persisted in these areas, the mounded structures increased in volume, the marginal depressions renewed by downsagging and the overburden was progressively deformed by faulting and folding (Figure 2.18d). Within the mounds, the Yafo Sand Member was intensively fragmented into a series of block-like segments with preserved primary bedding that surrounded the core of forcefully intruded clay-rich sediment (Figure 2.18d). This model would help to explain the occurrence of block-like segments of parallel-bedded high-amplitude seismic reflections within the NMC and the MMC and the previously argued difference in reservoir qualities between the cores and the flanks of the structures. Finally, as several mounded structures formed closely in space, they merged and intersected to form complex arrays (e.g., NMC and MMC) that were flanked by elongated and bowl-shaped topographic depressions.

A final and important point to be addressed regarding the genesis of the mounded structures is the burial depth at which they formed. It has been previously argued that the first, major episode of mud injection along the Afiq Submarine Canyon ensued during the middle Zanclean. At this time, the top of the Yafo Sand Member was exposed at seabed within the study area. Considering that the injected mud reached the base of the Yafo Sand Member and that the average thickness of this interval is about 70 m (see previous section), it is clear that mud injection occurred up to very shallow depths (c. 50-70 m). Such a superficial occurrence raises the question of why the injected material did not extrude to the seabed. It is possible that a minor part of the injected material reached the seabed. However, this cannot be observed in the seismic data, and it would seem unlikely

that muds would intrude at the base of the Yafo Sand Member if there was already a connection to seabed allowing the mud to flow along the pressure gradient between seabed and the overpressured canyon fill. Mud extrusion at seabed is thus in conflict with the previously presented observations that proved many of the mounds to occur through a number of discrete episodes of mud intrusion during a protracted period of time. Another possibility is that mobile muds may have been restricted in their vertical ascent by a sealing unit within the Yafo Sand Member. The Yafo Sand Member consists mainly of a succession of marls, siltstones and sandstones that are overlain by thick units of turbiditic sandstones (see above). Limestones can have excellent sealing properties specially where mixed with shale-rich lithologies, but we do not consider the thin carbonate stringers present in the Yafo Sand Member to be sufficiently competent by themselves to prevent extrusion to the seabed in a fast and highly overpressured system. An alternative possibility that appears more plausible is that when muds intruded vertically they encountered the highly bedded lower Yafo Sand Member and the permeable massive sandstones of the upper Yafo Sand Member. It is possible that the highly permeable sandstones allowed overpressure to dissipate thus diminishing the intrusion drive in a manner analogous to an interval blow-out. In this context, bedding anisotropy and lateral spreading of the intruded mud mass within the Yafo Sand Member may have interacted to form the mounded structures presented here. This assertion is supported by idealised mechanical theory of clastic intrusion undertaken by Jolly and Lonergan (2002). According to these authors, the intrusion of dykes is favoured at large burial depths whilst sills tend to form at relatively shallow depths where the effects of bedding anisotropy exceed the effects of the vertical stress. In a system where mobile muds intrude vertically and encounter a highly bedded succession close to seabed (such as the lower-Zanclean Yafo Sand Member) this theory would thus predict the formation of laccolithic bodies that jack-up the overburden in preference to dyke intrusion to the seabed.

2.10.3 Implications for hydrocarbon exploration and production

Complex deformational features of the type discussed here are important to understand in the context of hydrocarbon exploration and production. The most important

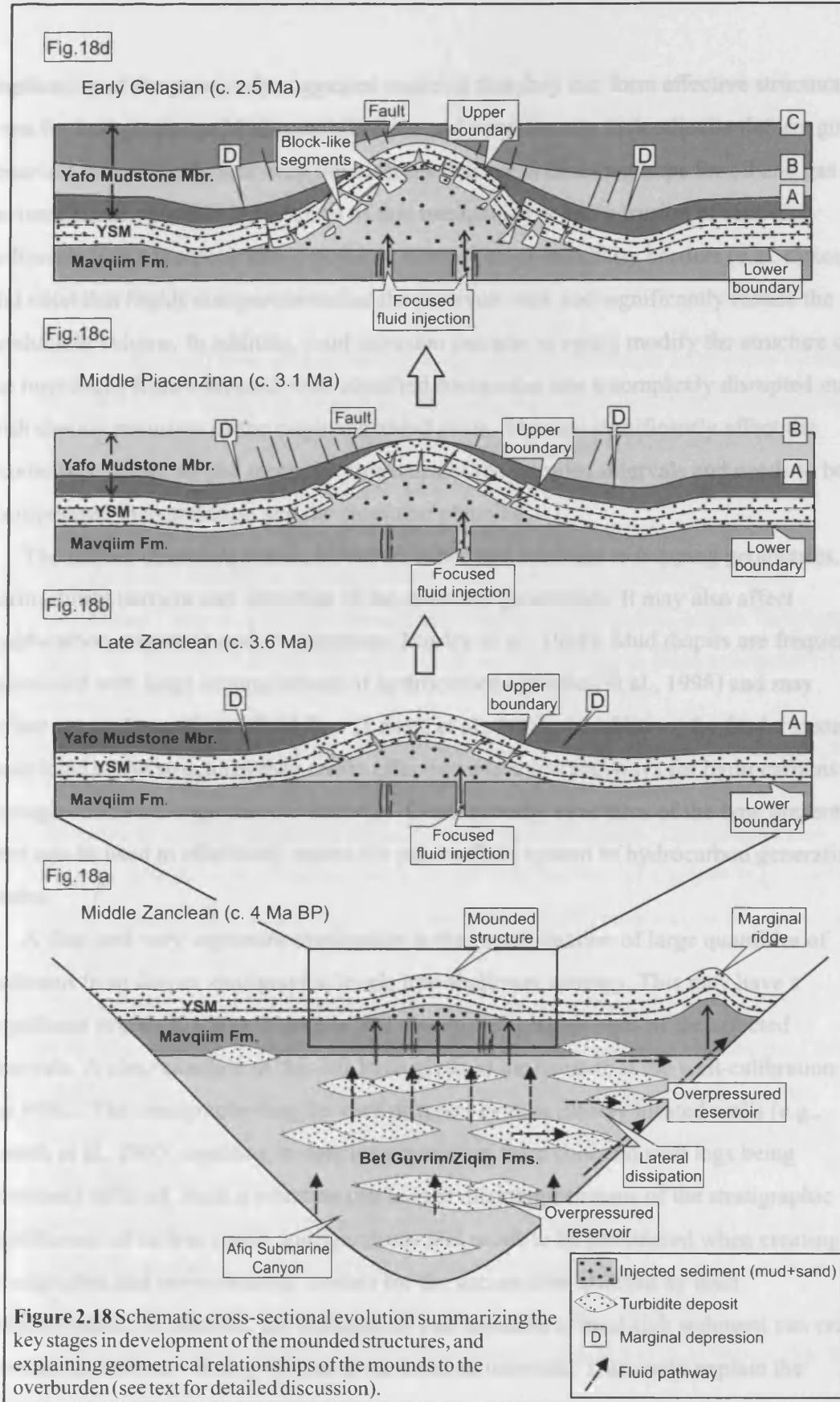


Figure 2.18 Schematic cross-sectional evolution summarizing the key stages in development of the mounded structures, and explaining geometrical relationships of the mounds to the overburden (see text for detailed discussion).

implication of the previously suggested model is that they can form effective structural traps for hydrocarbons. Mud remobilisation and intrusion can hydraulically deform good reservoir intervals into four-way dip closures that act as excellent traps for oil and gas accumulations. Another implication of this mechanism is that intrusion of mud-rich sediments into a reservoir may result in a network of permeability barriers (e.g., dykes and silts) that highly compartmentalise the reservoir rock and significantly reduce the producible volume. In addition, mud intrusion can also severely modify the structure of the host-rocks from a layered, well-stratified succession into a complexly disrupted mass with chaotic remnants of the original bedded strata. This can significantly affect the geometries, thickness and reservoir properties of the intruded intervals and needs to be incorporated in exploration and development planning.

The impact of mobile shales, however, is not just confined to trapping geometries, permeability barriers and alteration of the reservoir geometries. It may also affect hydrocarbon migration and re-migration (Morley et al., 1998). Mud diapirs are frequently associated with large accumulations of hydrocarbons (Morley et al., 1998) and may reflect areas of significant fluid flow (Løseth et al., 2003). In addition, the feeder systems associated to the structures may create effective migration pathways for hydrocarbons through otherwise impermeable intervals. Consequently, structures of the type presented here can be used to effectively assess the palaeo-fluid system of hydrocarbon generating basins.

A final and very important implication is the remobilisation of large quantities of sediment from deeper stratigraphic levels into shallower settings. This may have a significant impact in the stratigraphy and the biostratigraphic ages of the affected intervals. A clear example of this has been given in the context of the well-calibration of the NMC. The stratigraphy may be very different even in closely located wells (e.g., Løseth et al., 2003) resulting in detailed correlation from core and well logs being extremely difficult. Such a situation can lead to misinterpretations of the stratigraphic significance of certain stratal configurations and needs to be considered when creating stratigraphic and environmental models for the successions affected by mud remobilisation. In addition, the intrusion of vast amounts of mud-rich sediment can create anomalous seismic velocity effects in the affected intervals. This could explain the

observed seismic velocity artefacts (i.e. pull ups and push downs) associated with the mounded structures. Løseth et al. (2003) reported similar seismic imaging effects from the Hordaland Group (North Sea) and concluded that accurate velocity analysis should be undertaken in areas affected by these processes.

2.11 Conclusions

- Seismic and well data have revealed the presence of seventeen large-scale mounded structures with diameters of up to 4 km affecting the Lower Pliocene offshore Israel.
- These mounded structures are interpreted to have formed by clastic forceful intrusion into shallow-level sedimentary host rocks (Yafo Sand Member) and subsequent hydraulic “jack-up” of the overburden (Yafo Mudstone Member).
- The mounded structures are restricted to an area 40 x 20 km along the Afiq Submarine Canyon, a former depositional fairway Oligocene in origin. They may appear as isolated four-way dip closures or as arrays of up to three coalesced structures.
- Growth of the mounded structures was active between the Middle Zanclean (c. 4 Ma BP) and the Early Gelasian (c. 2.5 Ma BP). Growth consisted in several episodes of activity alternated with deepwater sedimentation. The mounds first became inactive at the landward parts of the Afiq Submarine Canyon (e.g., AM), while those in the seaward parts (e.g., NMC and MMC) remained active for a longer period of time.
- The initiation of the mounded structures was coeval with the formation of large-scale ridge-like mud diapirs along the northern flank of the Afiq Submarine Canyon.
- The localised occurrence of the mounded structures is attributed to the spatial constriction of clastic successions that accessed overpressure regimes within the Afiq Submarine Canyon.
- Development of high overpressure regimes within the Afiq Submarine Canyon was probably controlled by hydrocarbon generation, seismicity or a combination of both.
- The mounded structures presented here are amongst the largest and most complex examples of clastic intrusion features described to date. It has been shown that they

may create good trapping geometries capable of hosting large volumes of hydrocarbons. However, they may also result in a complex network of permeability barriers that highly compartmentalise the reservoir rock and significantly reduce the producible volume. In addition, they can severely affect the geometries, thickness and reservoir properties of deepwater sandstones.

Chapter Three: 3D seismic interpretation of slump complexes¹

3.1 Abstract

This chapter uses 3D seismic data from the continental margin of Israel (Eastern Mediterranean) to describe a series of slump deposits within the Pliocene to Holocene succession. These slumps are linked to the dynamics of subsidence and deformation of the transform margin of the eastern Mediterranean. Repeated slope failure occurred during the post-Messinian, when a clay dominated progradational succession was forming. This resulted in large-scale slump deposits accumulating in the mid-lower slope region of the basin at different stratigraphic levels. It is probable that the slumps were triggered by a combination of slope oversteepening, seismic activity and gas migration.

The high spatial resolution provided by the 3D seismic data has been used to define a spectrum of internal and external geometries within slump deposits. Importantly, we recognise two main zones for many of the slumps on this margin: a depletion zone and an accumulation zone. The former is characterised by extension and translation, and the latter by complex imbricate thrusts and fold systems. Volume-based seismic attribute analysis reveals transport directions within the slump deposits, which are predominately downslope, but with subtle variations particularly at the lateral margins. Basal shear surfaces are observed to ramp both up and down stratigraphy. Slump evolution occurs both by retrogressive upslope failure, and by downslope propagation (out-of-sequence) failure. Slump anatomy and the combination of factors responsible for slump failure and transport are relatively poorly understood, mainly because of the limited 3D of outcrop control, hence this sub-surface study is an example of how improved understanding of the mechanisms and products can be obtained using this 3D seismic methodology in unstable margin areas.

¹Published as:

J. Frey-Martinez et al., 2005, *3D seismic interpretation of slump complexes: examples from the continental margin of Israel*, *Basin Research*, 17, p. 83-108.

3.2 Introduction

Submarine slump deposits are widely recognised from several continental margins and are an important component of many slope systems (Moore *et al.*, 1976; Field *et al.*, 1982; Bugge, 1983; Jansen *et al.*, 1987; Barnes & Lewis, 1991; Field & Barber, 1993; Evans *et al.*, 1996; Smith *et al.*, 1999). Large-scale submarine slumping represents an important mechanism in shaping both active and passive margins whereby vast amounts of sediment are transported and redistributed into deepwater from an originally shallow-water setting.

Although slumping processes have been studied since the early 1920's, much of the research has been conducted on ancient slumps preserved in outcrop, and the incompleteness of the preserved slump bodies has been a persistent obstacle to a fuller, process based analysis of the slump system (Locat & Lee, 2002; Strachan, 2002). In the last few decades, increasing use has been made of geophysical techniques such as 2D seismic interpretation and sonar and multibeam imaging to characterise submarine slump deposits (e.g. Almagor & Wiseman, 1977; Prior & Coleman, 1978, 1979 and 1982; Garfunkel *et al.*, 1979; Nardin *et al.*, 1979; Garfunkel, 1984; Moore *et al.*, 1989, 1994a,b; Booth & O'Leary, 1991; Lee *et al.*, 1991; O'Leary 1991 and 1993; Watts & Masson, 1995; Hampton *et al.*, 1996; Lee *et al.*, 1999; Bøe *et al.*, 2000; McAdoo *et al.*, 2000). Many valuable insights have been accrued from these approaches, but they are essentially 2D and suffer from many of the same limitations as the field-based analysis. In particular, 2D seismic data have inherent problems with the spatial aliasing of slump deposits and the geological structures within them. This has left many unresolved questions with regards to the detailed morphology, internal geometries and accurate areal extent of slump deposits, which limits our ability to construct more sophisticated kinematic and dynamic models for slumping.

3D seismic technology offers a fundamentally novel method for investigations of both modern and subsurface slump deposits that promises to add significantly to our understanding of the mechanisms and results of slope instability processes. Modern, high-resolution 3D seismic surveys are now acquired on many continental margins for hydrocarbon exploration purposes, and often in areas that are or have been prone to slope

failure. The remarkable high spatial resolution that 3D seismic data provides (tens of metres in all three dimensions) can thus be used to define both the full areal extent and the external and internal morphology of submarine slump deposits to a high degree of precision in a way that cannot be achieved with any other combination of methods.

The principal aim of this chapter, therefore, is to illustrate the potential for 3D seismic interpretation of slump systems by describing the geometry and distribution of a suite of slump deposits from the post-Messinian continental margin of Israel. This area is ideal for such an analysis because it contains many well-preserved examples of both deeply buried and shallow slump deposits. A secondary aim is to examine the stratigraphic evolution of slumping and its role in the overall development of the margin. The chapter commences with an overview of the geological setting and a description of the stratigraphic context of the slump deposits in the study area. The main arguments are subsequently developed through detailed 3D seismic analysis focused on two representative case studies.

3.3 Regional tectono-stratigraphic context

The study area is located offshore Israel, and comprises the continental margin that bounds the onshore platform of Israel with the oceanic lithosphere of the Eastern Mediterranean Sea (Figure 3.1a). This margin is situated in an active tectonic setting at the zone of interaction between the Anatolian, African and Arabian plates (Figure 3.1a). Its early development is related to a sequence of rifting events from the Early Permian to the Middle Jurassic, during the first stages of disintegration of Pangea (Garfunkel, 1998). Throughout this period, opening of the Tethys Ocean caused rifting to the north of the African plate resulting in break-up of the extensive shallow-water carbonate platform that had dominated the paleogeography of the area. The subsequent continental break-up that led to the initiation of spreading in the eastern Mediterranean region resulted in the formation of a passive continental margin from the end of the Middle Jurassic (Garfunkel & Derin, 1984). During this period, high-energy carbonate platforms bordered by deepwater basins developed until the Late Cretaceous (Garfunkel, 1998).

In the Late Cretaceous, a change in the relative motion of the African plate with respect to the Eurasian plate led to a compressive stress regime and the formation of the

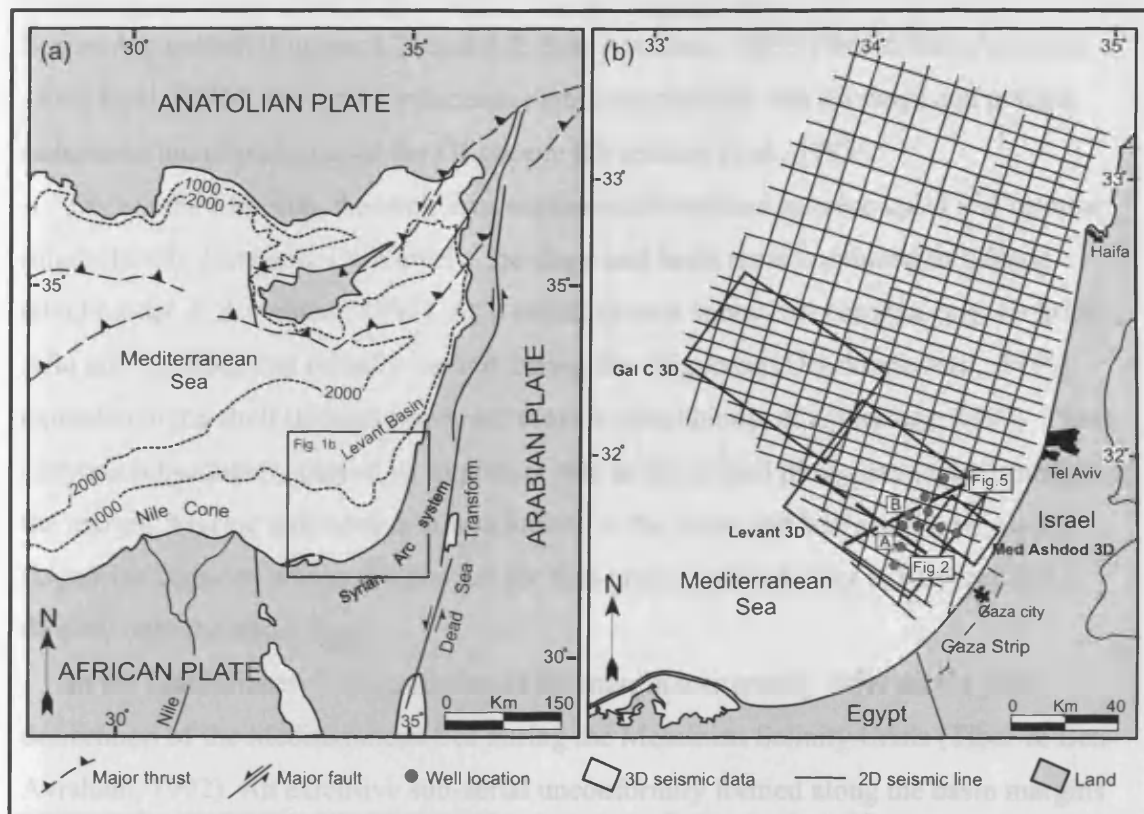


Figure 3.1 (a) Geological sketch of part of the Eastern Mediterranean showing the main structural elements. The box marks the approximate location of the study area. Modified from Garfunkel (1998). (b) Location map for the study area showing the 2D and 3D seismic database used in the study and locations of key exploration wells (A and B mark the location of the Gaza Marine-1 and the Or-South-1S wells respectively). Dashed lines indicate the location of seismic profiles (Figures 3.2 and 3.5).

Zilberman, 1997). Clay rich marls are seen to pass upwards into thinly interbedded sandstones and claystones deposited in the slope and basin areas (Yafu Formation; Figure 3.5). During this period, the gross configuration of the margin constituted a strongly aggradational system, with sigmoidal configurations linking shelf to slope (Figure 3.2). Several episodes of large-scale slumping and gravitational tectonics (e.g. Almogor, 1980, 1984 and 1986; Garfunkel, 1984; Garfunkel & Almogor, 1985 and 1987) alternated with periods of tectonically deposition.

During the Pliocene, global eustatic sea-level oscillations and local vertical tectonic movements resulted in repeated advances and retreats of the shoreline. Consequently, interbedded sands, clays and marls accumulated in the shelf under alternating terrestrial and marine conditions (Sivan *et al.*, 1999) (Herzli Formation, Figure 3.3). A Holocene

Syrian Arc system (Figures 3.1a and 3.2; Ben-Avraham, 1989; Tibor & Ben-Avraham, 1992; Eyal, 1996). The Late Cretaceous carbonate platform was drowned and pelagic sedimentation prevailed until the Oligocene (Druckman *et al.*, 1995).

During the Miocene, the shelf area experienced localised tectonic uplift and became intermittently emergent. Conversely, the slope and basin areas continued to subside (Buchbinder & Zilberman, 1997). As a result, several submarine canyons (e.g. el-Arish, Afiq and Ashdod) that initially incised during the Oligocene (Druckman *et al.*, 1995) extended to the shelf through headward erosion (Buchbinder & Zilberman, 1997). These canyons subsequently played an important role in the overall progradation and stability of the margin. Marine sedimentation was limited to the slope and basin areas, where the submarine canyons provided a conduit for fine-grained siliciclastics to be deposited directly onto the basin floor.

In the Late Miocene, the evolution of the margin was greatly influenced by the desiccation of the Mediterranean Sea during the Messinian Salinity Crisis (Tibor & Ben-Avraham, 1992). An extensive sub-aerial unconformity formed along the basin margins whilst thick evaporitic deposits (Mavqiim Formation) were laid down over the former basin floor (Hsü *et al.*, 1978; Montadert *et al.*, 1978) (Figures 3.2 and 3.3).

During the Pliocene, the vertical tectonic movement reached its peak (Almagor, 1993) and a major transgression submerged the exposed Upper Miocene shelf (Buchbinder & Zilberman, 1997). Clay-rich marls are seen to pass upwards into thinly interbedded sandstones and claystones deposited in the slope and basin areas (Yafo Formation; Figure 3.3). During this period, the gross configuration of the margin constituted a strongly aggradational system, with sigmoidal clinoforms linking shelf to slope (Figure 3.2). Several episodes of large-scale slumping and gravitational tectonics (e.g. Almagor, 1980, 1984 and 1986; Garfunkel, 1984; Garfunkel & Almagor, 1985 and 1987) alternated with periods of hemipelagic deposition.

During the Pleistocene, global eustatic sea-level oscillations and local vertical tectonic movements resulted in repeated advances and retreats of the shoreline. Consequently, interbedded sands, clays and marls accumulated in the shelf under alternating terrestrial and marine conditions (Sivan *et al.*, 1999) (Herfer Formation; Figure 3.3). A Holocene

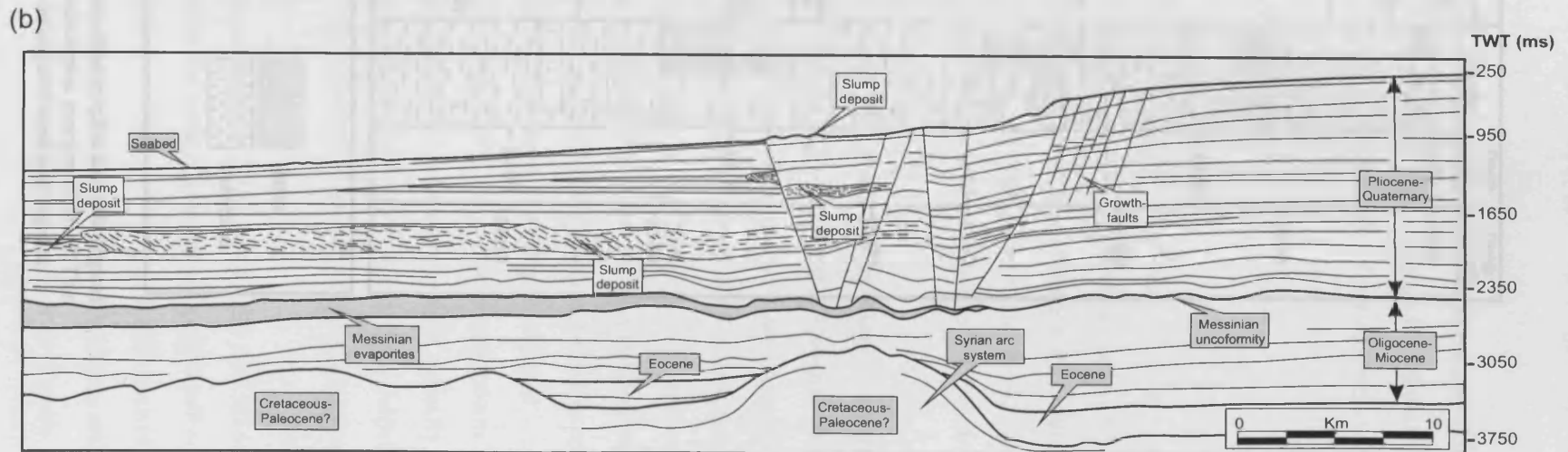
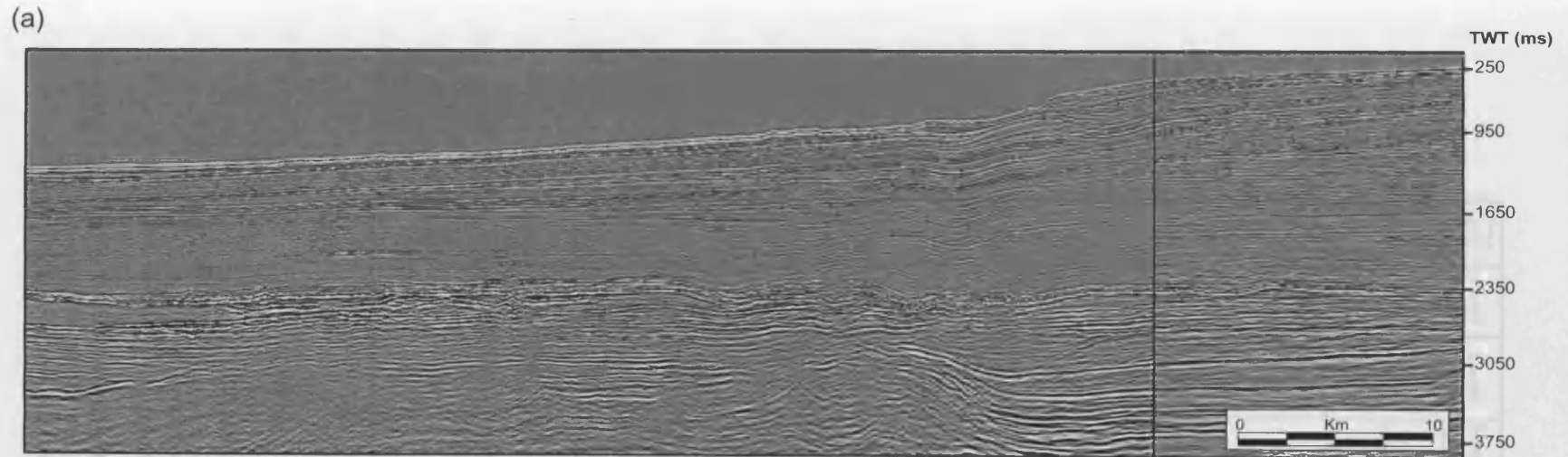


Figure 3.2 Regional dip seismic section through the continental margin of Israel (see Figure 2. 1b for location). This seismic profile illustrates the post-Cretaceous configuration of the study area. Note the presence of an extensive uncoformity and a thick deposit of evaporites resulting from the Messinian Salinity Crisis. Listric shore parallel growth faults are related to gravity-driven deformation of the Pliocene-Holocene continental margin and to salt tectonics.

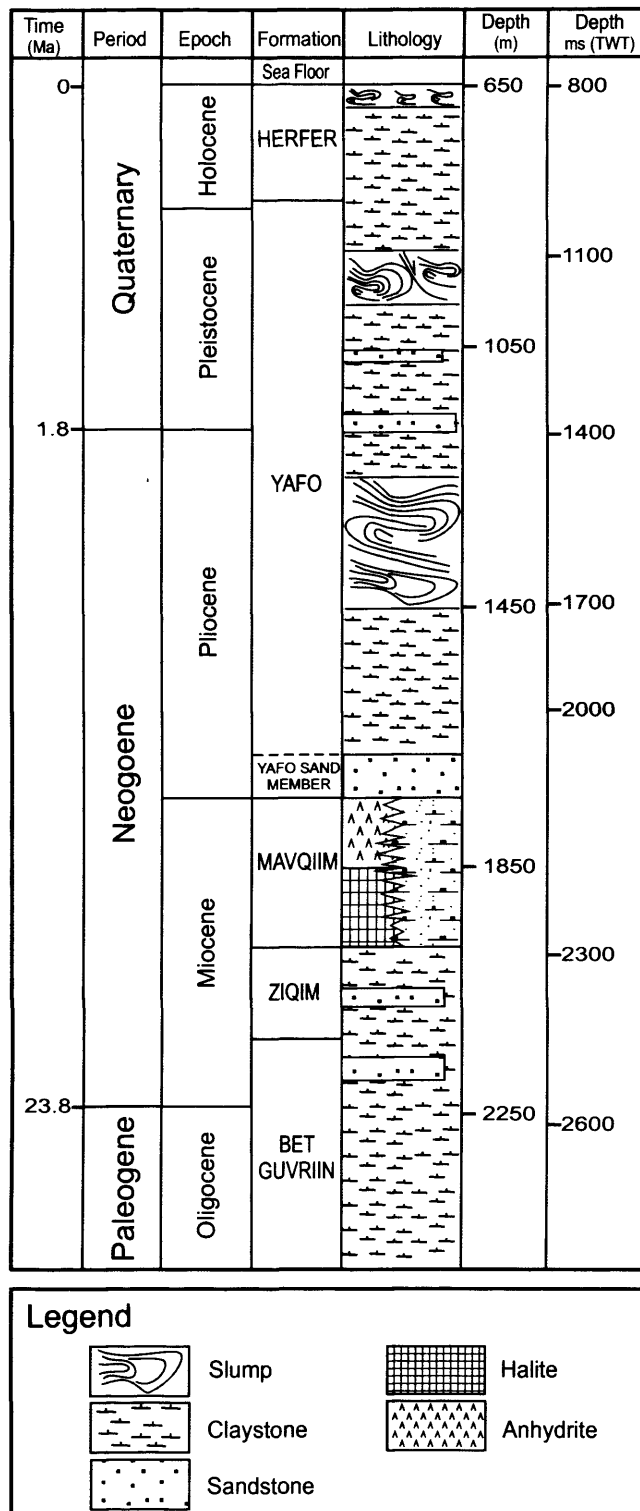


Figure 3.3 Generalised chrono-stratigraphic and lithological scheme of the post-Eocene continental margin of Israel. The lithological column is based on unpublished well reports.

transgression resulted in sedimentation of silt-rich clays over the present-day continental terrace. The gross configuration of the margin was similar to that in the Pliocene, i.e. a strongly aggradational system affected by slumping and gravitational tectonics (Figure 3.2).

3.4 Data and methodology

Conventional 2D and high-resolution 3D seismic data represent the main source of information for this study. Wireline logs (gamma-ray, sonic and resistivity) and commercial stratigraphic reports, mainly based on cuttings analyses, were available from 10 exploration wells located in the study area (Figure 3.1b). The regional 2D seismic database of offshore Israel used for this study comprises approximately 18,000 km in a 10 km by 10 km grid (Figure 3.1b).

Three 3D seismic surveys were available for this study (Med Ashdod, Levant and Gal C) and constitute the high-resolution data (Figure 3.1b). The total 3D seismic coverage amounts to 3200 km², extending from the shelf to the deep basin areas. These datasets, in comparison with the 2D seismic data, allow considerably better seismic-stratigraphic resolution because of improved acquisition and processing methods. All three surveys were acquired with an in-line trace interval of 6.25 m and a cross-line spacing of 25 m. Final processing yielded a time-migrated 12.5 m by 12.5 m grid (i.e. 6400 bin cells per km²). The dominant frequency of the seismic data varies with depth, but it is approximately 50 Hz at the base of the Pliocene. Vertical and lateral resolutions are estimated to be about 10 m and 100 m respectively. An average seismic velocity of 2000 m/s has been assumed within the first 2.5 seconds of the 3D datasets. This velocity is derived from the check-shot measurements made from the Gaza Marine-1 exploration well.

Firstly, regional mapping at different stratigraphic levels on the 2D and 3D seismic datasets was undertaken to identify and map the main slump deposits. Secondly, a detailed seismic-stratigraphic framework was established by tying the 3D seismic interpretation of the slumps and the intervening sedimentary units with litho- and biostratigraphic information from the ten wells located in the study area (Figure 3.1b).

Detailed 3D seismic mapping of slump deposits was undertaken by correlating the base and the top of the selected slumps. Subsequently, flattened horizontal coherence slices and seismic attribute extractions were generated in representative areas to analyse the external seismic geometry of individual slump deposits and to examine their transport directions and internal fabrics.

3.5 Recognition of slump deposits on 3D seismic data

There is considerable overlap and confusion in the literature in the usage of the terms “slump” and “slide”. In this chapter, slumps are defined after Stow (1986) as downslope movements of sediments above a basal shear surface where there is significant internal distortion of the bedding. Mulder & Cochoat (1996) divided slump deposits into two end members: simple and complex. Simple slump deposits are those in which slumping operates as an isolated and single event and does not generate other significant failures (e.g. Knebel & Carson, 1979). In contrast, complex slump deposits are those in which the motion of the main sedimentary block leads to instability of neighbouring areas, and the volume of such induced successive events is similar to the volume of the initial slump (e.g. Lewis, 1971; Barnes & Lewis, 1991). All the examples of slump deposits presented in this chapter belong to this latter complex type.

Slump units are recognised on seismic data using some simple criteria established from a number of previous studies (Embley & Jacobi, 1977; Woodcock, 1979; Embley, 1980; Field *et al.*, 1982; Prior & Coleman, 1982; Prior *et al.*, 1984; Bugge *et al.*, 1987; Jansen *et al.*, 1987; Kenyon, 1987; Normark & Gutmacher, 1988; Trincardi & Normark, 1989; Evans *et al.*, 1996; Hampton *et al.*, 1996; Smith *et al.*, 1999; Lee *et al.*, 2002). Most important of these is the recognition of a body that is characterised internally by chaotic or highly disrupted seismic facies that covers a large enough area to be identifiable as a discrete stratigraphic unit (Figure 3.4). Scale is thus important because of the limitations of seismic resolution: if a slump is so small that it is beyond vertical and horizontal seismic resolution, then clearly it is impractical to interpret it as a slump *per se*. The external geometry of the chaotic unit is therefore a critical parameter allowing slump masses to be distinguished from other types of depositional units that often exhibit

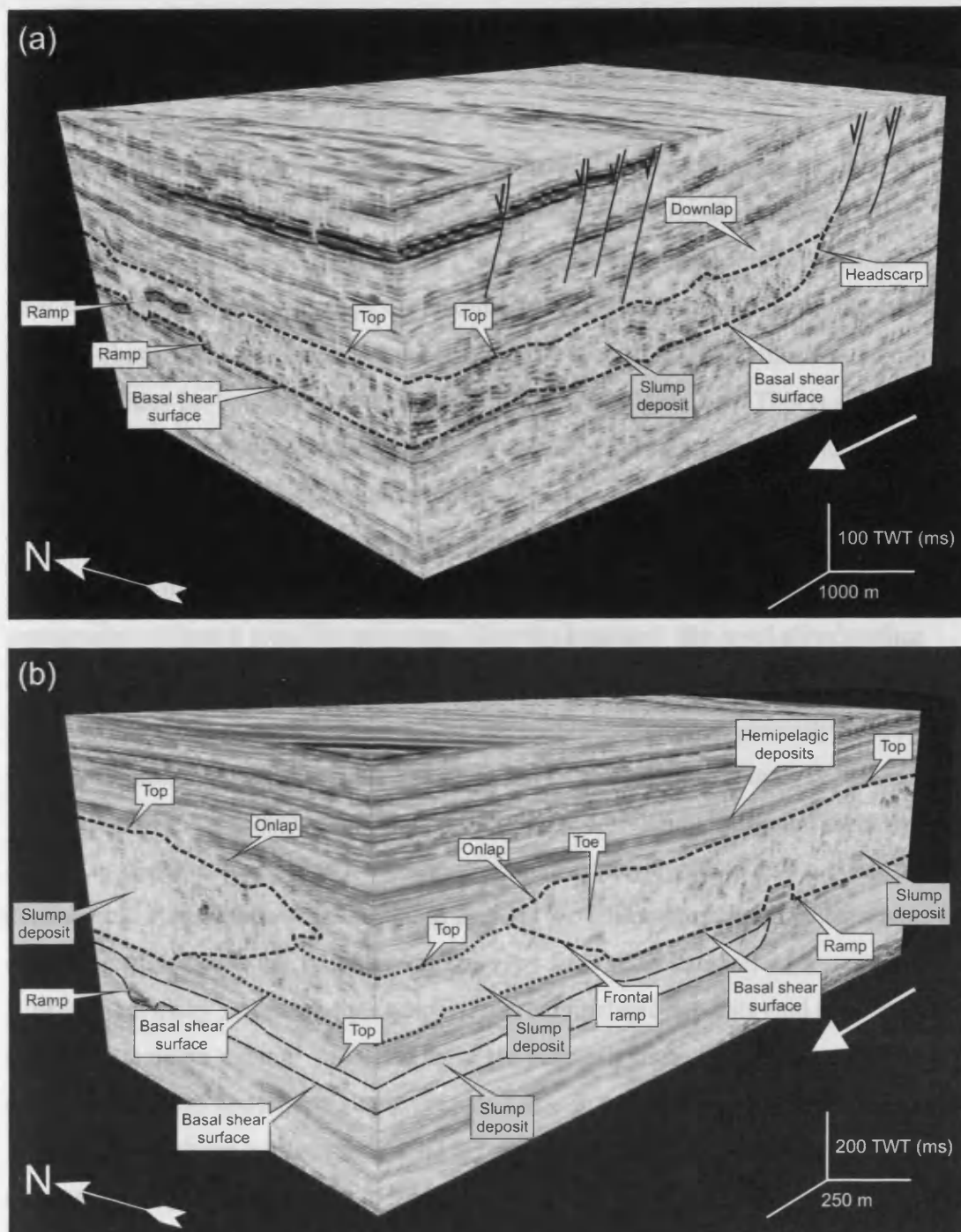


Figure 3.4 3D visualization of representative slump deposits in the study area. Slump masses form intervals of disrupted and chaotic seismic facies enclosed by the basal shear and the top surfaces. White arrows mark the main downslope direction of movement. (a) 3D seismic block showing the upslope parts of a slump deposit. Note the listric character of the basal shear surface towards the headscarp and the irregular morphology of the top surface. Presence of downlap from the overlying strata. (b) 3D seismic volume showing the downslope parts of a slump deposit. Note the presence of other older slump deposits being intersected. The basal shear and the top surfaces mark the limits between the chaotic seismic facies within the slump deposits and the continuous reflections of the outer undeformed strata. Note the presence of a frontal ramp towards the toe of the slump mass.

chaotic seismic facies, such as canyon fills, channel fills or talus wedges as, for example, described by Brown and Fisher (1977).

The basal shear surface is perhaps the most critical aspect leading to the correct identification of a slumped mass. Discrete slump events are usually associated with specific basal shear surfaces (e.g. Farrell, 1984), so an accurate definition of these surfaces offers a potential method for discriminating between successive slump events within a slump complex. The basal shear surface is identified in a similar way to unconformities i.e. by termination of stratal reflections (Figure 3.4). This is aided by the often significant contrast between the chaotic facies of the slump and the much more continuous seismic facies of the undeformed slope deposits (Figure 3.4). Over much of the area of a slump deposit, the basal shear surface forms a continuous plane that dips parallel to the underlying strata. However, this surface may locally ramp up and down the stratigraphy to form a step-like geometry. Near the headwall, the basal shear surface exhibits a listric, concave upward appearance, cutting the upslope strata (Figure 3.4a). Approaching the toe (*sensu* Varnes, 1978), the basal shear surface generally ramps upwards crosscutting the downslope strata to form a frontal ramp (Figure 3.4b).

The top of the slumped unit is simply defined by correlating the boundary between the chaotic or disrupted facies and the more continuous overlying strata. In the event that the depositional system following the slump episode is itself comprised of discontinuous or chaotic seismic facies, this boundary can be very difficult to interpret with accuracy. However, on many slopes where slumps occur, hemipelagic deposits tend to be the first sediments to drape a slump mass, and these are generally highly continuous, and easily separated from the underlying slump (Figure 3.4b). In many cases in the study area, the top surfaces of slump bodies correspond to irregular and mounded surfaces with localised depressions where it is common to find onlap or downlap of the overlying units (Figure 3.4).

3.6 Stratigraphic context of slump deposits in the study area

Using the diagnostic criteria described in the previous section, over 40 slump complexes have been identified within the post-Messinian succession of the southern

Israeli continental margin. It is apparent that there are distinct regions of the margin where these slump complexes are concentrated; in particular the presence of a slump deposit influences the position of succeeding slumps. This section describes these gross stratigraphic relationships using a combination of regional 2D and detailed 3D seismic interpretation.

The post-Messinian succession of the southern parts of the study area has been divided into three seismic-stratigraphic units as a basis for discussing the distribution of slump deposits in this part of the study area (Figure 3.5). These three units (T30, T20 and T10) correspond approximately to the Pliocene, the Early-Late Pleistocene and Late-Pleistocene-Recent respectively. The Plio-Pleistocene boundary is based on biostratigraphic data tied to the seismic data from 10 exploration wells, and is a remarkably consistent seismic reflection throughout the basin. The boundary between the upper two units is not constrained by biostatigraphy, but it is assumed to be of Late Pleistocene age based on the average thickness of the upper unit and an extrapolation of sedimentation rates from the exploration wells. The areal distribution of the main slump complexes within these three units as mapped within the 3D seismic data sets is summarised in Figure 3.6.

3.6.1 Unit T30

Unit T30 consists of a c.750 m thick accumulation of mainly fine clastic sediments that are part of a prograding and aggrading slope wedge (Figure 3.5). The basal part of this unit is devoid of any slumps, and consists of sandstones interbedded with thin glauconitic claystones and marls interpreted as basin floor turbiditic fan deposits (Yafo Sand Member; Figure 3.5). The seismic character of the Yafo Sand Member is expressed as a package of high frequency, continuous, high amplitude seismic reflections that are restricted to the areas of the Afiq and el-Arish canyons. Overlying this is a c. 700 m thick package consisting mainly of continuous high amplitude reflections representing the main phase of hemipelagic and turbiditic slope wedge deposition, with strongly aggradational reflection configurations (Figure 3.5).

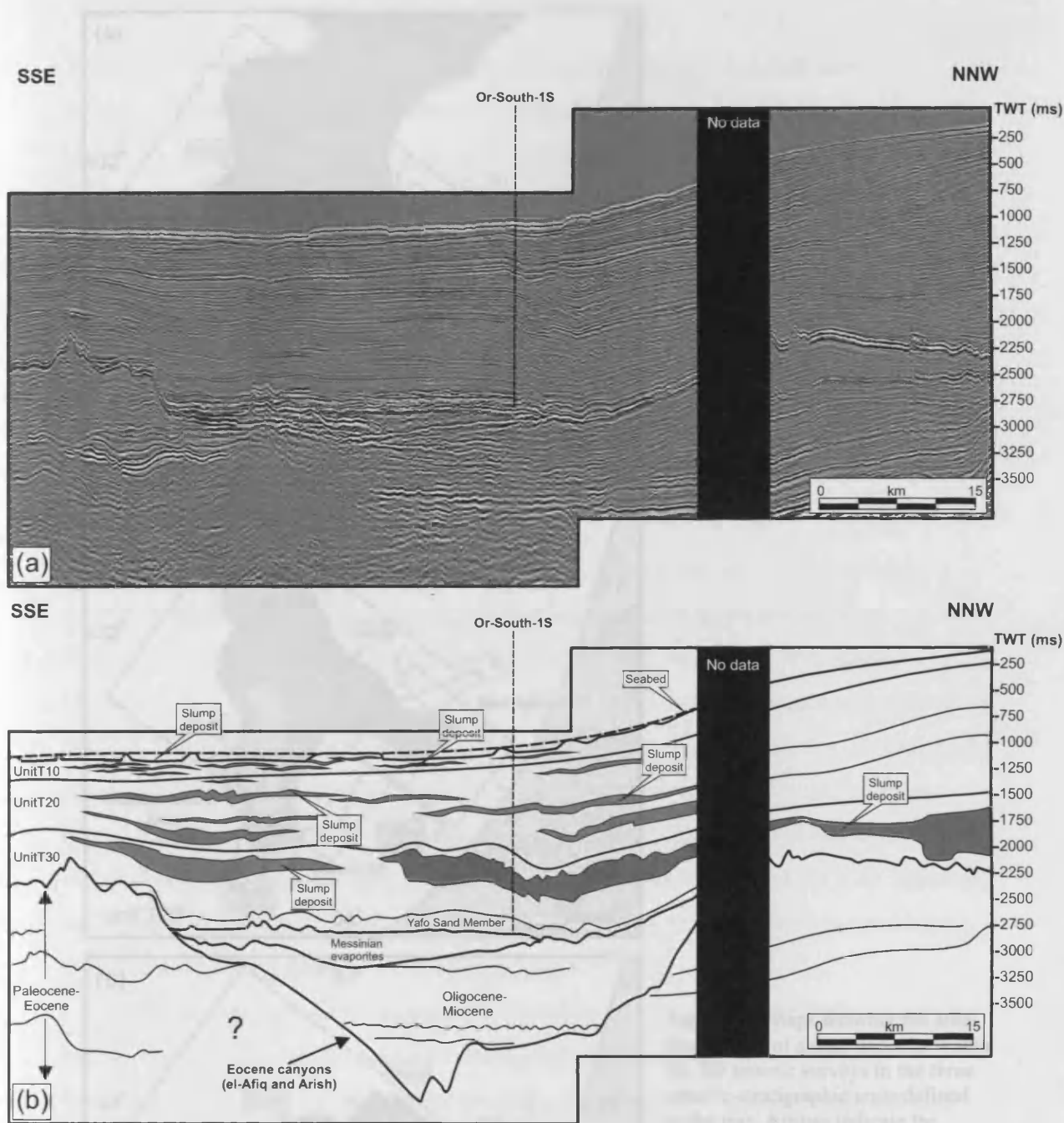


Figure 3.5 Seismic section (a) crossing the central parts of the Levant 3D area (see Figure 3.1b for location) and (b) interpretation showing the stratigraphic context of slump deposits in the study area. Shaded areas correspond mainly to simple slump deposits. Note that there is a concentration of slump deposits in the locations overlying pre-Messinian canyons. Slumps increase in number and decrease in size upwards (see text for discussion).

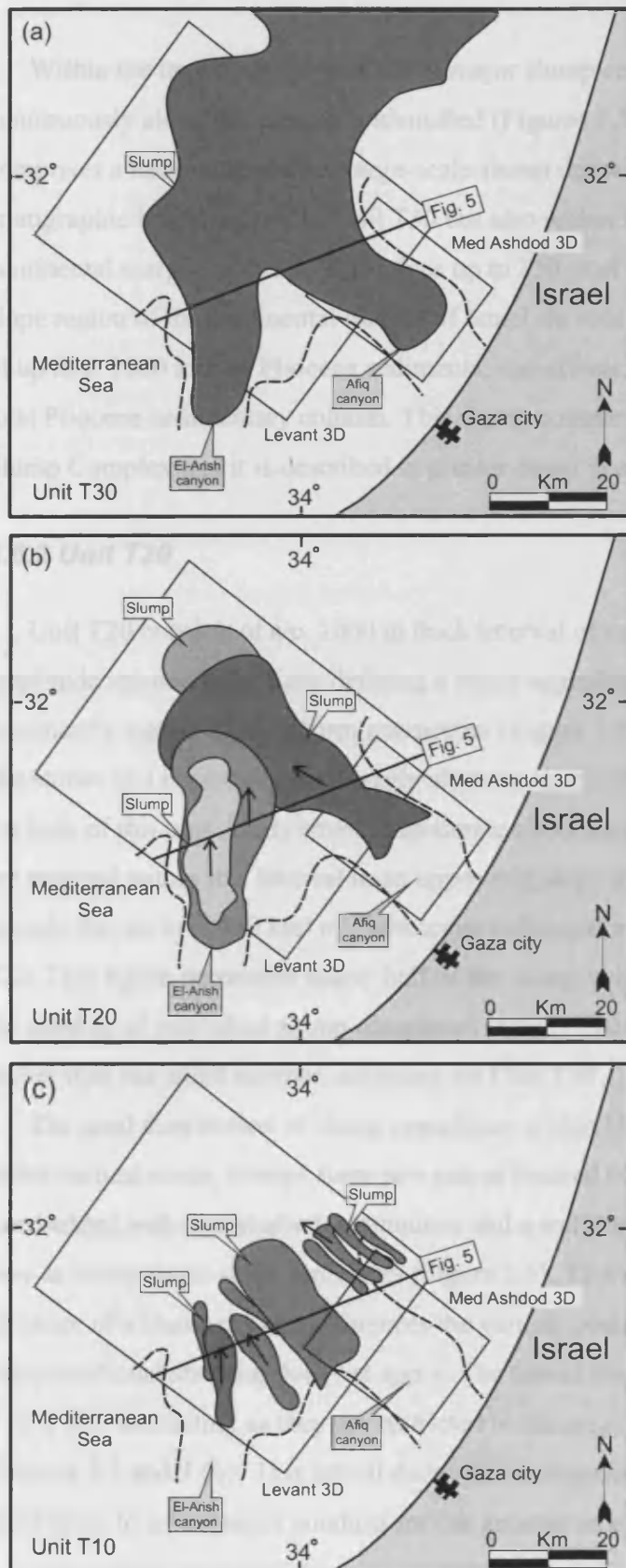


Figure 3.6 Maps showing the areal distribution of slump deposits within the 3D seismic surveys in the three seismic-stratigraphic units defined in the text. Arrows indicate the interpreted directions of movement. Dashed lines represent the flanks of the Afiq and el-Arish canyons. (a) Areal distribution of a major slump complex within Unit T30. (b) Areal distribution of slump deposits within Unit T20. Note the concentration of slump deposits in the areas underlain by the Arish and el-Arish canyons. (c) Areal distribution of slump deposits within Unit T10.

Within the upper part of Unit T30 a major slump complex extending almost continuously along the margin is identified (Figures 3.5 and 3.6a). This slump complex comprises a minimum of three large-scale slump deposits and creates the biggest seismic stratigraphic break not just in Unit T30 but also within the entire post-Messinian continental margin of Israel. It involves up to 350 m of sediments and covers most of the slope region of the continental margin of Israel. In volume, this slump complex consists of up to c. 1000 km³ of Pliocene sediments, and affects, therefore, up to c. 30% of the total Pliocene sedimentary column. This slump complex is herein termed as the Israel Slump Complex and it is described in greater detail in a later section.

3.6.2 Unit T20

Unit T20 consists of a c. 1000 m thick interval of continuous, moderate to high amplitude seismic reflections defining a major aggradational slope wedge with dominantly sigmoidal clinoform geometries (Figure 3.5). Shallow to deep-marine claystones and limestones that locally alternate with sandstones, siltstones and marls form the bulk of this unit. Many small to moderate sized slump bodies (typically <100 m thick) are mapped within this interval in an upper-mid slope position. A volumetric analysis reveals that up to c. 400 km³ of Pleistocene sediments are affected by slump units in Unit T20. This figure represents nearly half of the slump volume of that in Unit T30. However, the number of individual slump complexes in Unit T20 is over 15, which is considerably higher than the small number computed for Unit T30.

The areal distribution of slump complexes within Unit T20 is particularly interesting. In the vertical sense, slumps form two sets of stacked bodies that are commonly interbedded with undisturbed, continuous and a well-bedded seismic facies interpreted here as hemipelagic slope sediments (Figure 3.5). This distribution suggests that the presence of a slump deposit influences the vertical position of succeeding slumps and that compensational stacking does not apply. The lateral distribution of slumps within Unit T20 is also interesting as they are restricted to the areas of the Afiq and el-Arish canyons (Figures 3.5 and 3.6b). This lateral distribution suggests some sort of intrinsic control for these areas to act as major conduits for the generation of slump complexes.

3.6.3 Unit T10

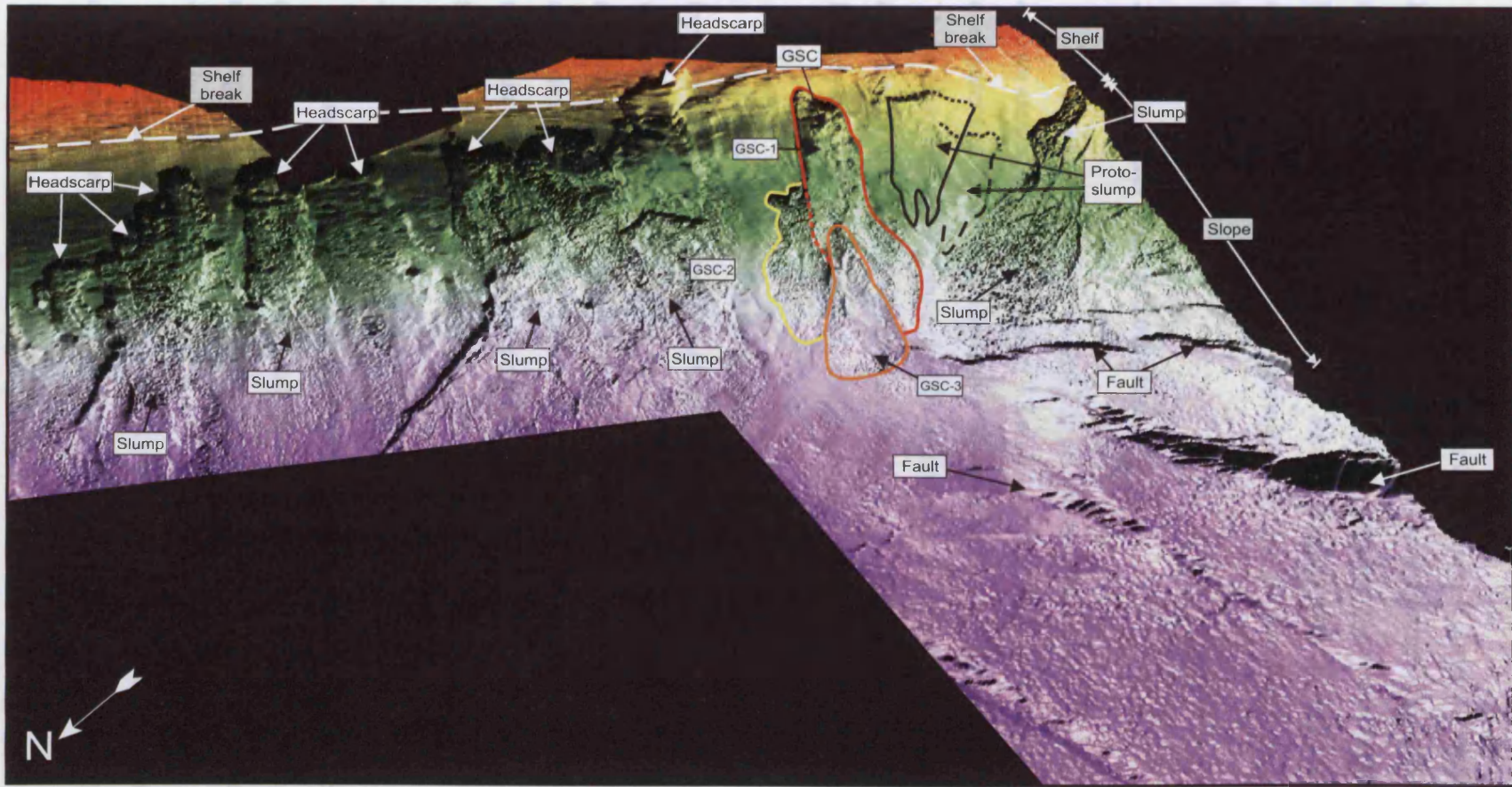
Unit T10 is the uppermost 100-200 m of the post-Messinian section consisting of mainly fine-grained clastic sediments deposited in an aggrading sigmoidal clinoform configuration (Figure 3.5). Piston core testing carried out in the study area (e.g. Almagor and Wiseman, 1977; Almagor and Schilman, 1995) shows that the present-day shelf and slope sediments consist mainly of normally consolidated dark grey claystones (up to 75%) comprising 60-80% montmorillonite, 20-40% kaolinite, 1-15% illite, and very low carbonate content. Geotechnically, the sediments are characterised by bulk density of $\rho=1.44-1.51 \text{ g/cm}^3$, water content of 90-110%, liquid limit of 70-95% and plasticity index of 45-65% (Frydmand *et al.*, 1982).

Numerous slump bodies have been mapped within Unit T10. These are particularly well imaged on the present day seabed as described in the following section (Figure 3.7). The slump bodies are distributed over the entire Upper Pleistocene-Recent section forming complexes that extend from the shelf break to the base of slope (Figures 3.6c and 3.7). The dimensions of these slump complexes are considerably smaller than those in Units T20 and T30, typically with individual surface areas of c. 80 km^2 . However, their total number (c. 25) is significantly higher than that of Units T30 and T20 (c. 1 and c. 15 respectively).

Within Unit T10, one slump complex extends almost continuously from the shelf-break to the base of slope areas. This consists of a composite of three different slumps that form an intricate cross-cutting array. In this chapter, it is referred as the Gaza Slump Complex (GSC in Figure 3.7) and will be described in detail in the following section.

3.7 Detailed 3D mapping of slump deposits

Two slump complexes display typical characteristic on 3D seismic data and are described here. The first case study is of the Israel Slump Complex of Early Pliocene age, which is remarkable in several aspects, not least of which is its enormous volume (c. 1000 km^3), placing it amongst the world's largest slump deposits (i.e. Storegga Slide; Bugge,



3-17

Figure 3.7 3D perspective view of the present day seabed in the Levant 3D area. Note the presence of several slump complexes covering the slope region. These form arrays of elongated slump deposits extending from the shelf to the base of slope areas. Note the presence of headscarps and secondary crown cracks. Inset shows the Gaza Slump Complex (marked by GSC).

1983). The second is of the much smaller Gaza Slump Complex of Late Pleistocene/Holocene age, which is expressed at the present seabed. This allows for a much higher resolution of surface topography, comparable to modern multibeam bathymetry data. The combination of surface imagery with the vertical seismic profiles allows for very detailed morphometric analysis that has revealed a complex kinematic history.

3.7.1 The Israel Slump Complex

The Israel Slump Complex (ISC) is a large-scale buried slump complex that extends over an area of 4800 km² (Figures 3.8 and 3.9). The ISC affects in excess of 300 m of deepwater claystones from the Upper Pliocene and has a volume of up to c. 1000 km³. These enormous values make the ISC comparable to some of the largest documented examples of submarine mass-wasting deposits (e.g. Woodcock, 1979; Bugge, 1983; Bugge *et al.*, 1987; Jansen *et al.*, 1987; Kenyon, 1987; Evans *et al.*, 1996; Hampton *et al.*, 1996).

The ISC is positioned at the transition between two distinct morpho-structural zones: the Syrian Arc system and the Levant basin (Figure 3.8). The first zone underlies the upslope parts of the ISC, where the Pliocene margin consists of steep slopes with maximum gradients of c. 6° (Figure 3.9a). The second zone lies beneath the downslope and central parts of the ISC. Here, the undisturbed Pliocene strata dip at c. 1° and are underlain by thick (> 800 m) deposits of Messinian evaporites (Figure 3.9a). The gross transport direction of the ISC is W-NW.

3.7.1.1 Seismic character of the Israel Slump Complex

The limitations of the coarse regional grid of the 2D seismic data preclude any accurate mapping of the northern and central parts of the ISC. Therefore, detailed mapping and seismic analysis was undertaken in its southern parts where 3D seismic data were available (Figure 3.8).

The seismic expression of the ISC is recognisable as a zone of chaotic to discontinuous seismic reflections bounded above, below, and laterally by continuous

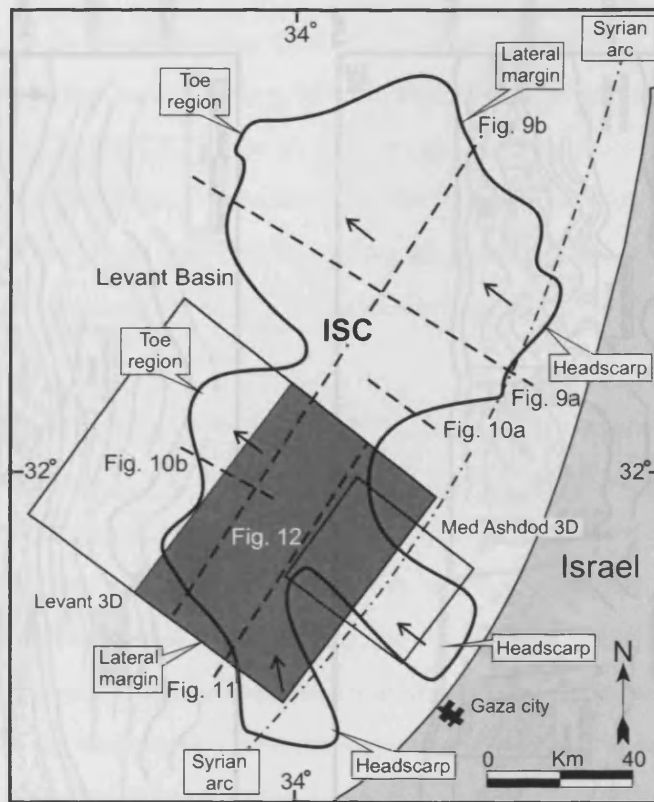


Figure 3.8 Map of the ISC showing its areal extension. Note its enormous areal extent (c. 4800 km²). The dashed line (parallel to the coastline) marks the general trend of large tectonic structures from the Syrian Arc system. Arrows indicate the gross transport direction of the slump mass. Seismic sections (indicated with thick dashed lines) are used to illustrate the regional seismic appearance of the ISC (Figures 3.9-3.11). The area where detailed 3D seismic interpretation has been undertaken is indicated by the shaded box (Figure 3.12).

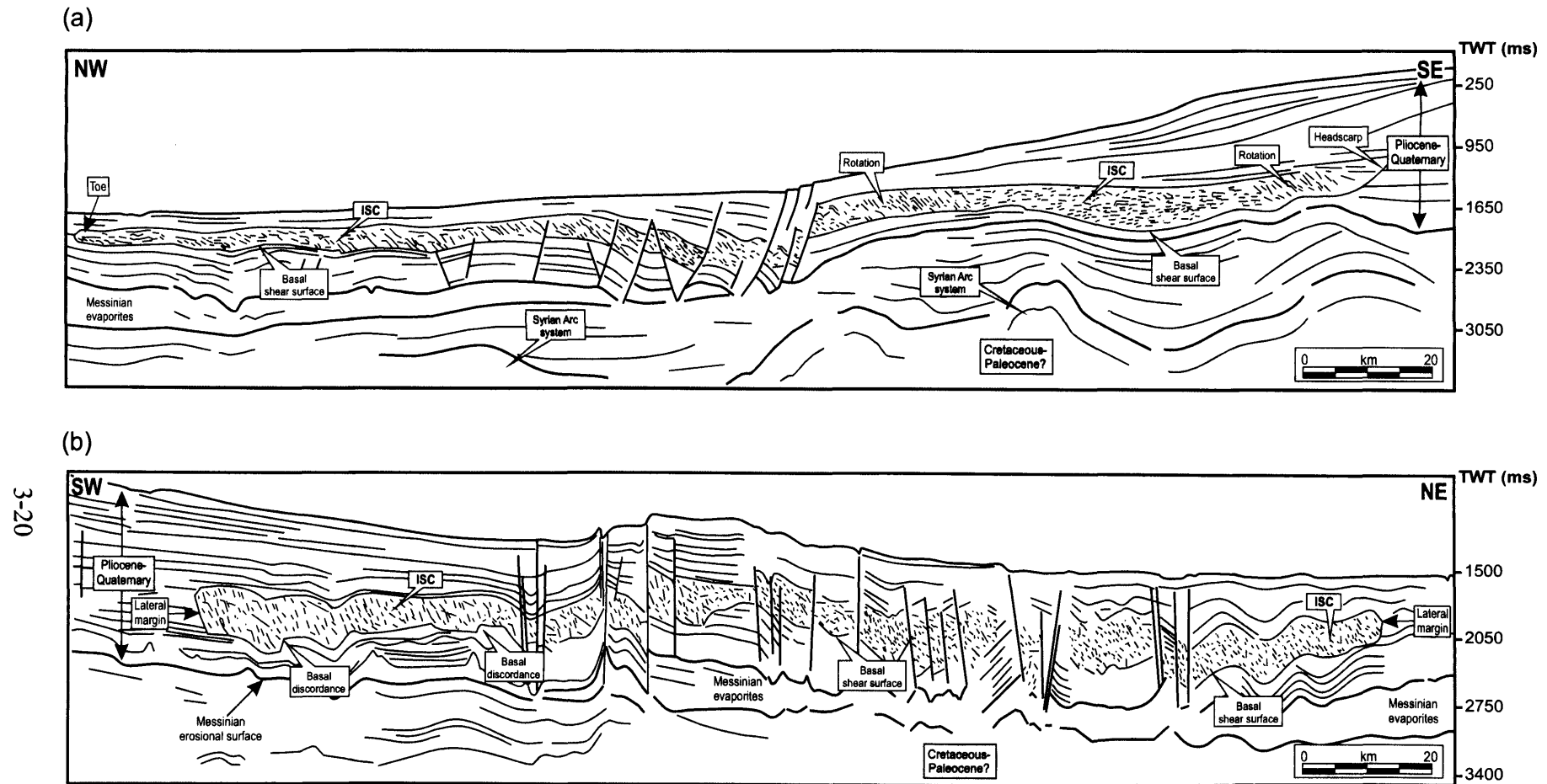


Figure 3.9 (a) Dip geo-seismic section through the continental margin of Israel (see Figure 3.8 for location). The profile images the Israel Slump Complex (ISC) as a package of chaotic seismic facies within the Lower Pliocene slope system. Reflections within the ISC exhibit local rotation away from the headscarp. The toe region forms an abrupt change from chaotic facies (ISC) to continuous facies (base of slope units). Note the presence of salt-detachment growth faults deforming the ISC. (b) Strike geo-seismic section through the continental margin of Israel (see Figure 3.8 for location). The profile images the ISC as a continuous body extending from the southern to the northern parts of the margin. The lateral margins of the ISC appear as limits to the chaotic facies within the slump mass. Note the presence of discordances in the basal shear surface and faults deforming the slump mass.

strata of Unit T30. In the downslope direction (Figure 3.9a), the ISC is seen as a continuous package that extends for c. 150 km along the continental margin. On strike profiles (Figure 3.9b), the ISC forms an approximately rectangular body dominated by a chaotic seismic facies sharply in contrast with the more continuous seismic reflections from the undisturbed strata. The ISC shows significant variations in thicknesses that are spatially related to large-scale steps at its basal shear surface (Figure 3.9b).

Headscarp

The headscarp of the ISC is located between 2 and 20 km offshore the present day coastline of Israel (Figure 3.8). In plan view, it is mapped as an irregular boundary, with three main salients suggesting that the ISC consists, at least, of three major slump bodies (Figure 3.8). Unfortunately, the lack of high seismic resolution data has precluded a more detailed analysis of their spatial distribution and chronology. On seismic profiles, it is recognisable as a concave upwards surface that separates the chaotic seismic facies of the slump body from the undisturbed surrounding strata (Figures 3.9a and 3.10a). Its upper tip is generally between 200 and 300 m above the level of the basal shear surface and has a gradient ranging from c. 2° in the southern parts of the ISC to c. 15° in the north. Near the headscarp, the top of the ISC is depressed with respect to the undeformed region of the slope and it is overlapped by post-slump deposits, suggesting that the ISC is thinned relatively to the pre-slump slope template (Figure 3.10a).

Toe

The toe of the ISC is positioned between 100 and 140 km offshore Israel (Figure 3.8). On downslope seismic profiles, it is very well constrained by an abrupt change from the chaotic seismic facies within the ISC to the continuous seismic reflections at the base of the slope areas (Figures 3.9a and 3.10b). In some parts of the toe region, the ISC is seen to affect various intervals of chaotic seismic facies interpreted as older slump deposits (see Figure 3.10b).

In the toe region, the basal shear surface steepens dramatically to form a frontal ramp seen as a boundary between the chaotic seismic facies within the ISC and the continuous seismic facies outside. In this region, the slump mass appears buttressed against the outer continuous strata. Only locally developed evidence of slumped material overlying the

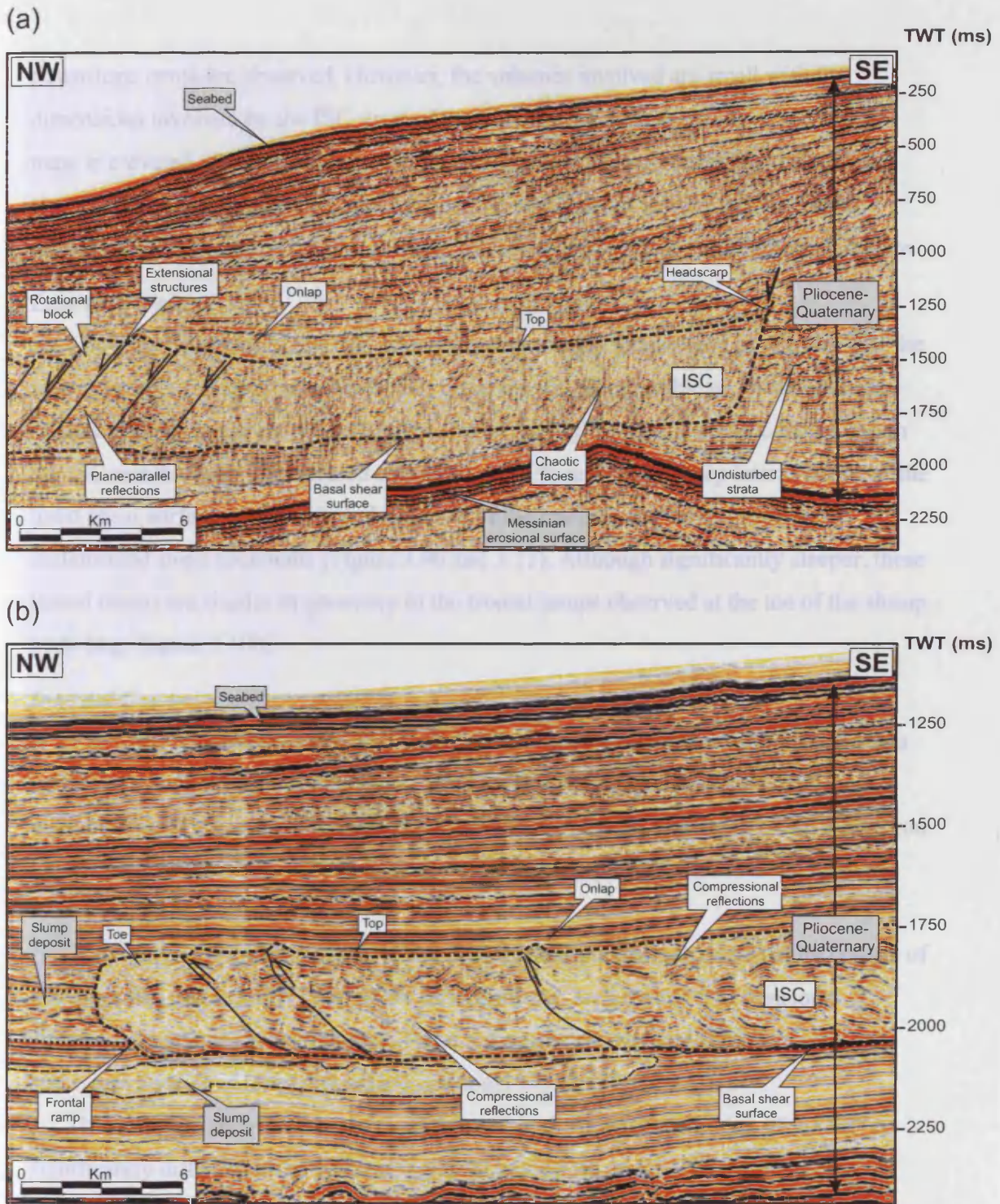


Figure 3.10 Seismic profiles along the ISC. (a) 2D seismic profile in the upslope parts of the ISC (see Figure 3.8 for location). The headscarp forms a steeply dipping interface forming the updip boundary between the chaotic seismic facies within the slump body and the continuous reflections of the upper slope. Clear onlap of the headscarp by post-slump sediments is observed. (b) 3D seismic profile through the toe region of the ISC (see Figure 3.8 for location). The toe region appears as the downslope boundary between chaotic seismic facies of the ISC and the continuous reflections of the base of slope. Note the presence of a clear frontal ramp and the slump mass being buttressed against the downslope strata. Older slump deposits appear affected by the ISC.

downslope strata are observed. However, the volumes involved are small with the dimensions involved by the ISC. In the area surrounding the toe, the top of the slump mass is elevated with respect to its lateral correlative reflection within the undeformed region of the slope and it is overlapped by post-slump deposits (Figure 3.10b). These relationships suggest that the ISC is thickened relatively to the pre-slump slope template.

Lateral Margins

The lateral margins of the ISC are only approximately constrained by the limits of the seismic grid in the study area. However, these are still recognisable on strike-oriented seismic profiles as abrupt lateral limits between the highly chaotic seismic facies within the ISC and the outer undeformed strata (Figure 3.9b and 3.11). Steep lateral ramps of the basal shear surface are observed along most of the margins abutting against the undeformed slope sediments (Figure 3.9b and 3.11). Although significantly steeper, these lateral ramps are similar in geometry to the frontal ramps observed at the toe of the slump body (e.g. Figure 3.10b).

Internal Geometry

The seismic character of the ISC is dominated by a chaotic facies. However, there is sufficient coherence of individual intra-slump seismic reflections to allow local recognition and mapping of deformational features. These are particularly well imaged on the 3D seismic data, but can also be seen on 2D seismic profiles wherever the quality resolution of the data permits.

Throughout the upslope region of the ISC, the internal geometries generally consist of plane-parallel and laterally continuous reflections that are affected by extensional structures (e.g. listric normal faults). These are approximately parallel to the headscarp and create a series of tilted downslope rotational blocks (Figure 3.10a).

The dominant internal seismic character within the downslope region of the ISC is significantly different to the upslope region (Figures 3.9b and 3.10b). Highly deformed and discontinuous seismic reflections are seen to be affected by compressional structures that contribute to a substantial thickening of the downslope parts of the ISC (e.g. thrusts and folds, Figure 3.10b). The thrust systems detach from the basal shear surface and

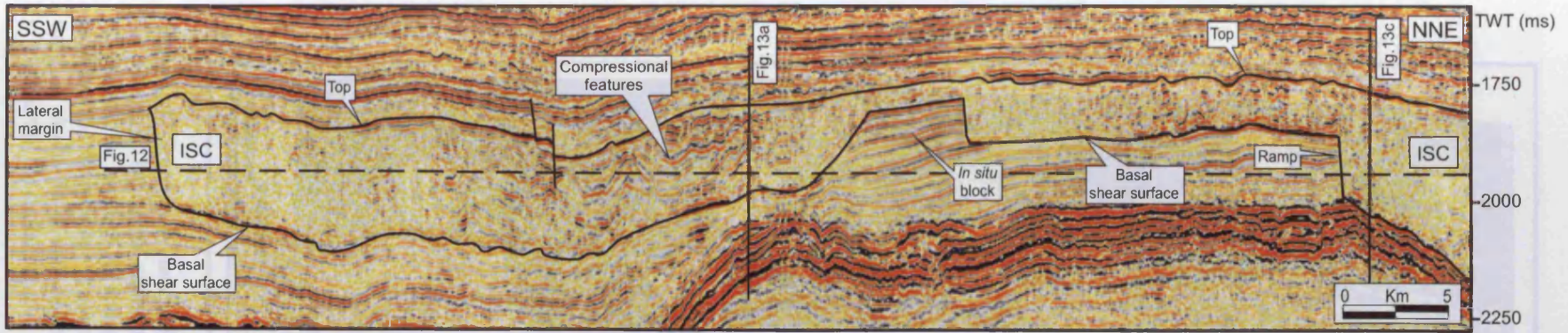


Figure 3.11 3D seismic profile across the ISC (see Figure 3.8 for location). Note the intensively chaotic seismic facies of the internal parts of the ISC bounded above and below by the top and basal shear surfaces, respectively. A lateral flank of the ISC forms a highly steep ramp separating chaotic from continuous seismic facies. Note the presence of a ramp indenting the basal shear surface and a block of undisturbed reflections within the ISC (see text for discussion). A horizontal coherence-slice (Figure 3.12) and three seismic profiles (Figure 3.13) are used to further illustrate the internal geometry of the ISC.

...analysis reveals the ... 3D view (see Figure 3.8 ... of the ... clearly observable. Sharp lateral ... and the ... the ... and to develop compressional ... the interpreted direction



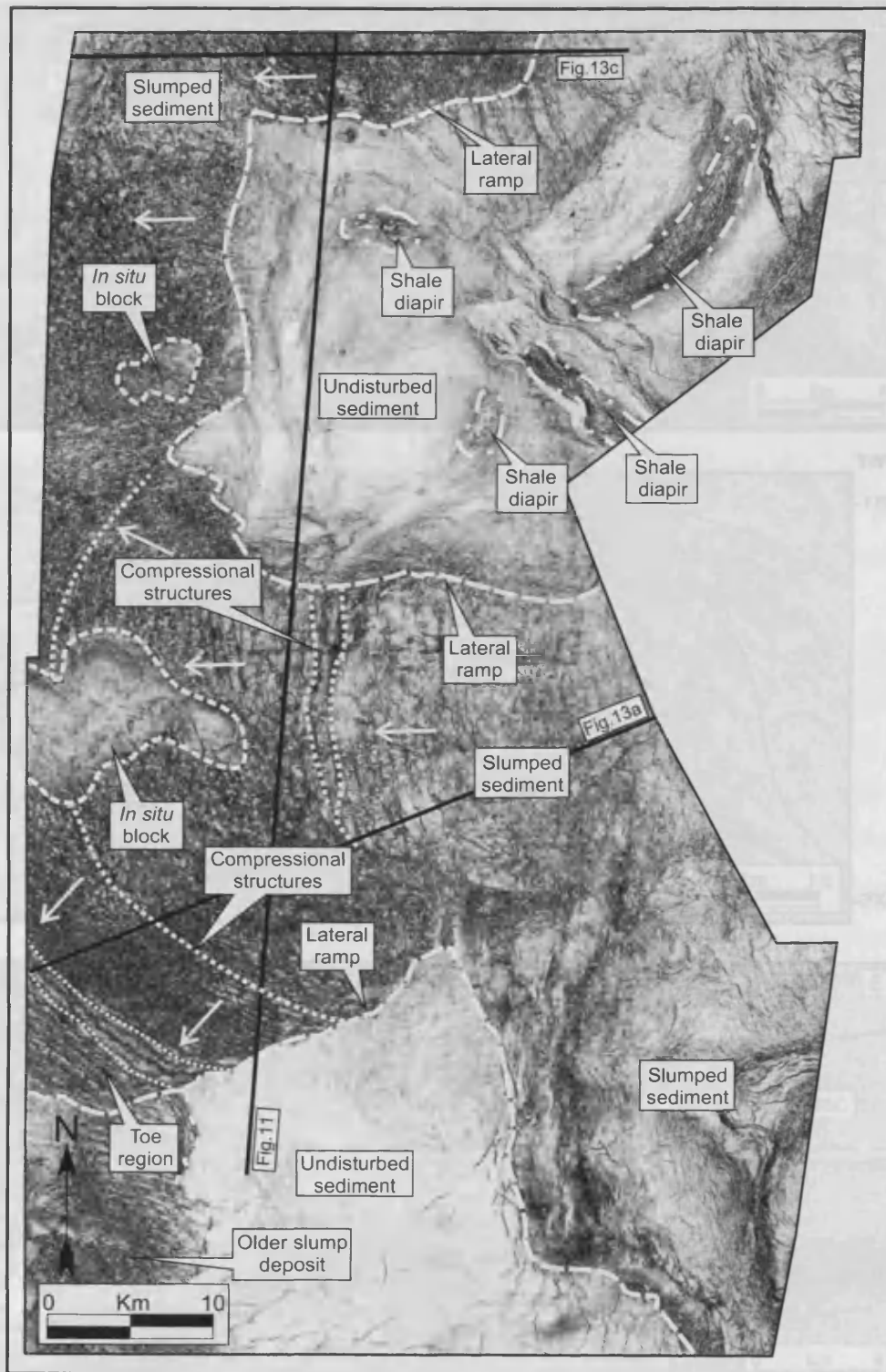


Figure 3.12 Structurally flattened horizontal coherence-slice across the Levant 3D area (see Figure 3.8 for location). The internal geometry of the lower region of the ISC is clearly observable. Sharp lateral ramps mark the limits of the slump mass. Note the contrast between the slumped and the undisturbed sediment and the presence of concentric arcs of ridge-like structures due to downslope compressional stress. *In situ* blocks of undisturbed sediments are observed. Arrows indicate the interpreted direction of transport of the slump mass.

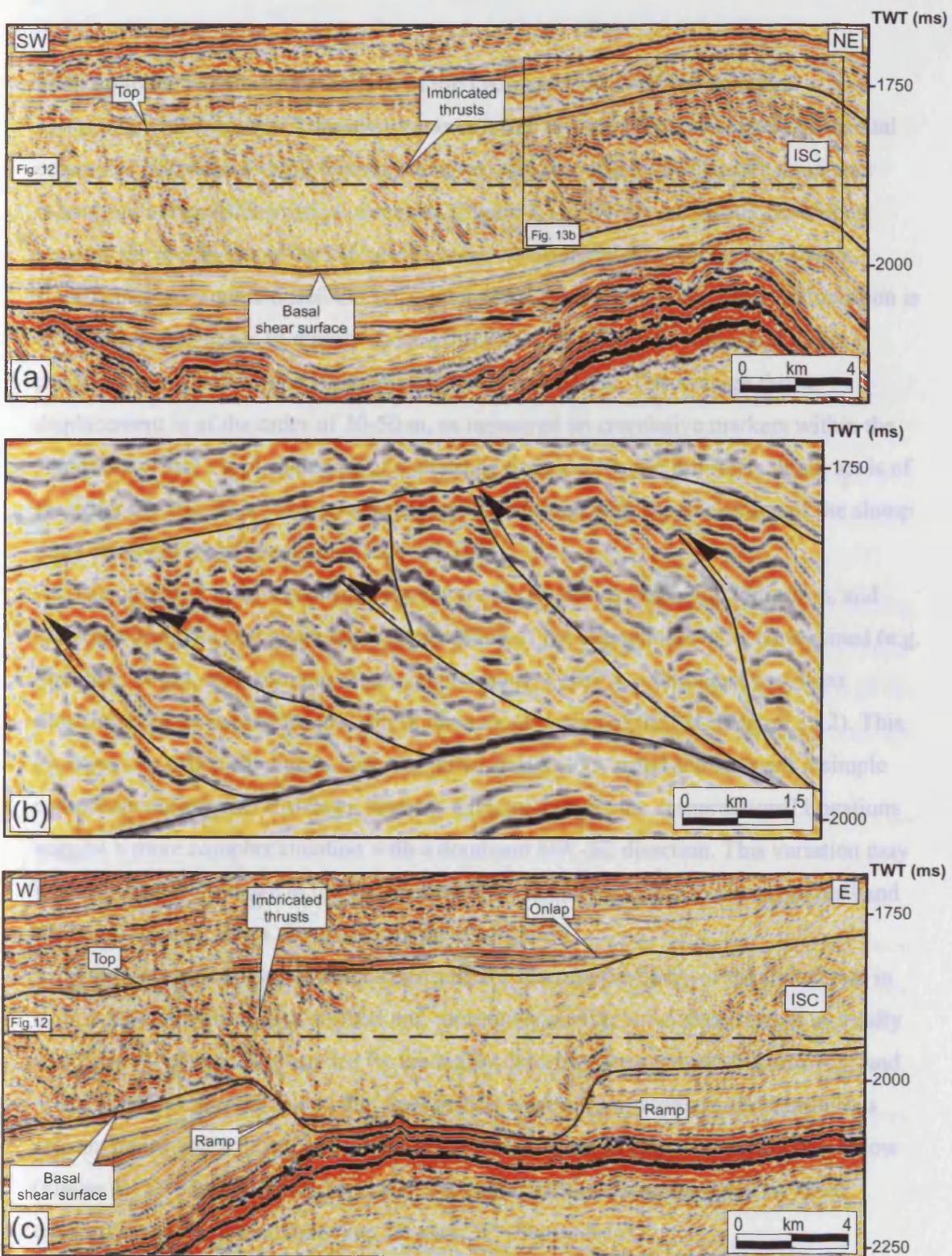


Figure 3.13 Seismic examples of the internal geometries of the ISC (see Figure 3.12 for location). The direction of movement is northeast-southwest. (a) Dip seismic section showing imbricated series of closely spaced thrusts. (b) Enlargement of the section across a group of thrusts. Note that thrusts ramp up from the basal shear surface (see text for discussion). (c) Dip seismic section showing a large-scale ramp in the basal shear surface. Note the presence of imbricated thrusts propagating in the direction of movement and an onlapped depression.

ramp up to deform the upper surface of the ISC, such that localised mounded topographies and overlapped depressions are created (Figure 3.10b). Flattened horizontal coherence slices show these thrust systems as concentric arcs of ridge-like structures extending in a gross downslope direction (Figure 3.12). These are mainly developed towards the toe region of the ISC and in areas where the basal shear surface shows significant topographic relief. On seismic profiles, their typical structural configuration is of an imbricated series of closely spaced thrusts (c. 500-1000 m) with small thrust propagation folds developed at the thrust tips (Figure 3.13). The average thrust displacement is of the order of 30-50 m, as measured on correlative markers within the slump body, and a typical degree of shortening expressed in the imbricate thrust set is of the order of 10%. This value of shortening accords well with the thickening of the slump body observed in the toe region (Figure 3.10b).

The observed thrusts and fold systems are invaluable as kinematic indicators, and allow the direction and magnitude of translation of the slump mass to be constrained (e.g. Strachan, 2002). According to these compressional systems, a dominant east-west direction is observed within the overall downslope region of the ISC (Figure 3.12). This direction accords well with the inferred down-palaeoslope trend and suggests a simple compressional regime. However, towards a lateral margin, the compressional lineations suggest a more complex situation with a dominant NW-SE direction. This variation may be indicative of a change in the kinematics of the slump mass due to compressional and frictional stress-regimes along the interfaces of the ISC.

Another important observation regarding the internal geometry of the ISC is that in certain areas, blocks of undisturbed and continuous seismic reflections remain as totally undeformed 'islands' surrounded by the highly deformed slump mass (Figures 3.11 and 3.12). These are remarkable in that they exhibit a laterally concordant and continuous seismic facies and are clearly coupled to the undeformed sedimentary succession below (Figure 3.11). The blocks are separated from the surrounding slump body by steep outward dipping flanks of between 20° and 25° (Figure 3.11).

These blocks could be interpreted as intact masses of sediment that have been translated as rafts within the more highly deformed slump mass. However, this interpretation can be discounted as a possibility, because their internal stratigraphy is

clearly rooted to the strata directly below, and there is no visible detachment surface present at their base. An alternative interpretation that appears more plausible is that they represent isolated cores that have not experienced failure, and that the failed material propagated around them. This interpretation places significant constraints on the local kinematics of the slump mass surrounding these cores, and it is unlikely from this argument that large-scale translation could have occurred within these parts of the ISC.

Basal Shear Surface

The basal shear surface of the ISC forms a continuously traceable seismic reflection that separates the highly deformed seismic units within the slump body from the underlying and undeformed strata (Figures 3.9-3.11). On seismic profiles, it appears as a high-amplitude negative reflection that cuts up and down the stratigraphy in a staircase-like geometry (Figure 3.11). Towards the headscarp region, the basal shear surface becomes increasingly steeper forming a concave upwards-surface that cuts the overlying stratigraphic interval (Figures 3.9a and 3.10a). In the toe region, it steepens dramatically to form a frontal ramp (Figure 3.10b). The lithology within the basal shear surface of the ISC is unknown; however the significant acoustic impedance contrast suggests an abrupt lithologic or diagenetic contrast at this stratigraphic level.

Large-scale ramps (e.g. 80-90 m) that form indentations in the basal shear surface are recognised in several sectors of the ISC (Figures 3.9b and 3.11). These are most clearly delimited within the downslope parts of the ISC although their presence should not be ruled out in other areas where the resolution of the data is inferior. Seismic sections, both parallel and perpendicular to the main direction of slump movement, exhibit these ramps as conspicuous erosional features against which underlying seismic reflections are truncated. They have remarkably steep flanks that dip at between 20° and 25° and connect the deepest segments of the basal shear surface to shallower stratigraphic levels (Figures 3.11 and 3.13c). Above the ramps, the slump mass undergoes folding in order to accommodate the topographic gradient of the basal shear surface (Figure 3.13c). We propose that these ramps are related to changes in the mechanical properties of the slumped material, the basal shear surface or the interaction of these factors.

In summary, the ISC constitutes a buried and buttressed large-scale slump complex within the Upper Pliocene succession. From the data available, we suggest that it is

comprised of a minimum of three large-scale slump bodies, although smaller scale episodes of mass wasting should not be ruled out. A continuous basal shear surface that corresponds to a strong negative and continuous seismic reflection underlies the entire slump mass. This basal shear surface is affected by several ramps that form a staircase-like geometry. The ISC is divided into two main zones according to its seismic character. The first is located in a steep upslope region (c. 6°) underlain by folded structures from the Syrian Arc system. This zone is characterised by extensional deformational structures (i.e. listric normal faults) and by thinning of the slump mass. Its upslope perimeter is well constrained by the presence of a continuously mapped headscarp. In this chapter, this area is interpreted as the depletion zone of the ISC (*sensu* Varnes, 1978). The second zone is situated in a gentle (c. 1°), downslope area that is underlain by thick accumulations of Messinian evaporites. This sector is dominated by compressional structures (i.e. folds and thrusts) and by thickening of the slump body. Its downslope limit is marked by the toe region. Blocks of undeformed seismic reflections that are rooted to the underlying strata and topographic ramps are locally observed. This area is interpreted as the accumulation zone of the ISC (*sensu* Varnes, 1978). The main features of the ISC are summarised in Figure 3.14.

3.7.2 The Gaza Slump Complex

The Gaza Slump Complex (GSC) is an array of three slump bodies observed on the present day seabed of the study area (Figures 3.7 and 3.15). Morphometric analysis of the seabed map combined with cross-sectional interpretation has led to the recognition of these three component slumps. Their cross-cutting relationships have been used to define the sequence of slumping events.

The GSC is located 40 km offshore from Gaza city, in a water depth ranging from 500 to 1150 m, with slope gradients between 2° and 0.5° respectively. The failure zone trends N-W and covers an area of c. 110 km² (mean length 22 km, mean width 5 km; Figure 3.15b). The GSC affects up to 80 m of fine-grained claystones within Unit T10. It is, therefore, a moderately sized feature compared with other reported submarine slope instability products (e.g. Dingle, 1977; Bugge, 1983; Bugge *et al.*, 1987).

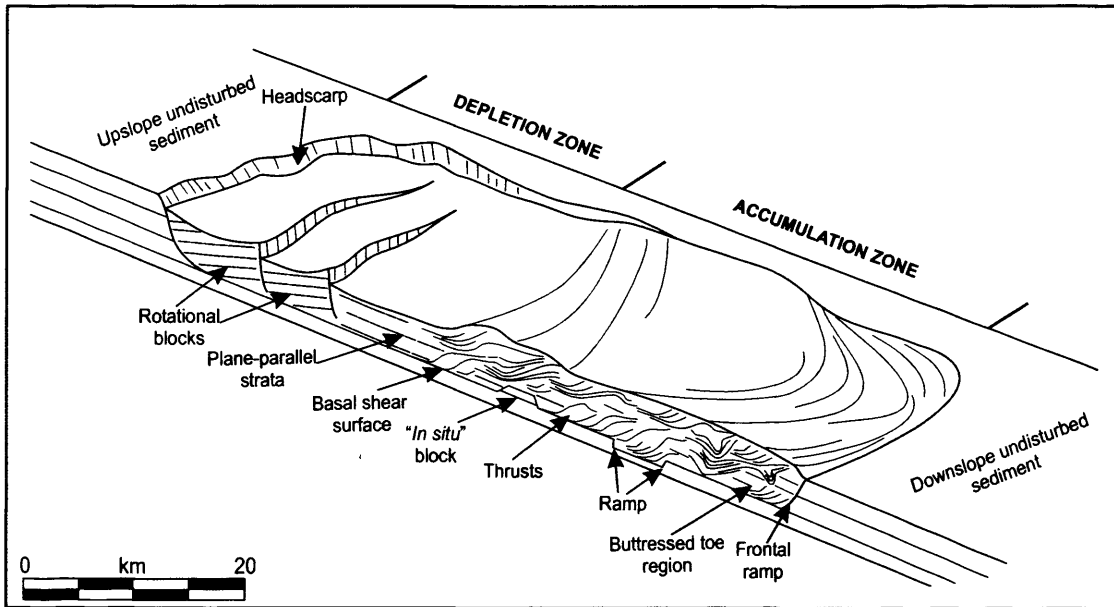


Figure 3.14 Schematic depiction of part of the ISC. The upslope parts of the slump mass correspond to the depletion zone. This is characterized by extensional deformational structures and thinning of the slump mass. Note the presence of listric faults forming a series of rotational blocks that are tilted downslope. The downslope part of the slump body corresponds to the accumulation zone. This is characterized by compressional structures and thickening of the slump mass. The slump mass is buttressed against the downslope strata in the toe region. Note the presence of individual "in situ" blocks, which have been interpreted as indicators of a limited downslope displacement.

3.7.2.1 Seismic character of the Gaza Slump Complex

Headscarp

Three different headscarps are recognised within the GSC based on the abrupt offsets of the seabed topography (Figures 3.7 and 3.15b). Two of these (GSC-1, GSC-2) are clearly seen on the dipmap of the seabed (Figure 3.15b). The GSC-1 is confirmed in seismic cross-sections (Figure 3.16a) as an excisional feature, where there is an abrupt reduction of stratigraphic section in a downslope direction. The third headscarp within the GSC (GSC-3), is less obvious on the dipmap (Figure 3.15b), but is observable on the seismic profiles as an excisional scarp with c. 10-20 m loss of stratigraphic section (Figure 3.16a). The planform geometry of all three headscarps is crescentic, with either single salients (e.g. GSC-1 and GSC-3) or a double salient (e.g. GSC-2; Figure 3.15a). Immediately downslope of the headscarps GSC-1 and GSC-2, there is a region of marked extensional thinning, where the slump bodies are cut by minor listric faults that have a distinct seabed scarp of up to 70 m height (Figure 3.16a). The geometry of these faults bears a close relationship to the respective headscarps immediately updip, and are interpreted as retrogressive failure surfaces, that are widely recognised on other slump deposits (e.g. Evans *et al.*, 1996; Mulder & Cochonat, 1996).

Upslope of the headscarp of GSC-1 is a region affected by elongated and subtle topographic depressions that are parallel to the headscarp and reach a length of c. 4 km (Figure 3.15). On seismic sections, these appear as small-scale faults and fractures that are locally coincident with larger-scale fault systems (Figure 3.16a). By comparison with subaerial analogues (e.g. Farrell, 1984; Fitches *et al.*, 1986; Martinsen & Baken, 1990) and previous models for slump deposits (e.g. Varnes, 1978), these features are interpreted here as crown-cracks. Crown-cracks may form in the undisplaced material adjacent to the headscarp of a slump deposit due to development of extensional stresses by undermining and represent the upslope propagation of slumping during retrogressive failure.

The spatial distribution of the three main headscarps and their cross-cutting relationships are the major criteria to constrain the relative timing of the slump bodies within the GSC. A lateral margin of GSC-1 is clearly seen on Figure 3.15b to be crosscut by the headscarp of GSC-2. The headscarp of GSC-3 cuts into the seabed topography associated with both GSC-1 and GSC-2 in their combined toe region (Figure 3.15b). The

3-32

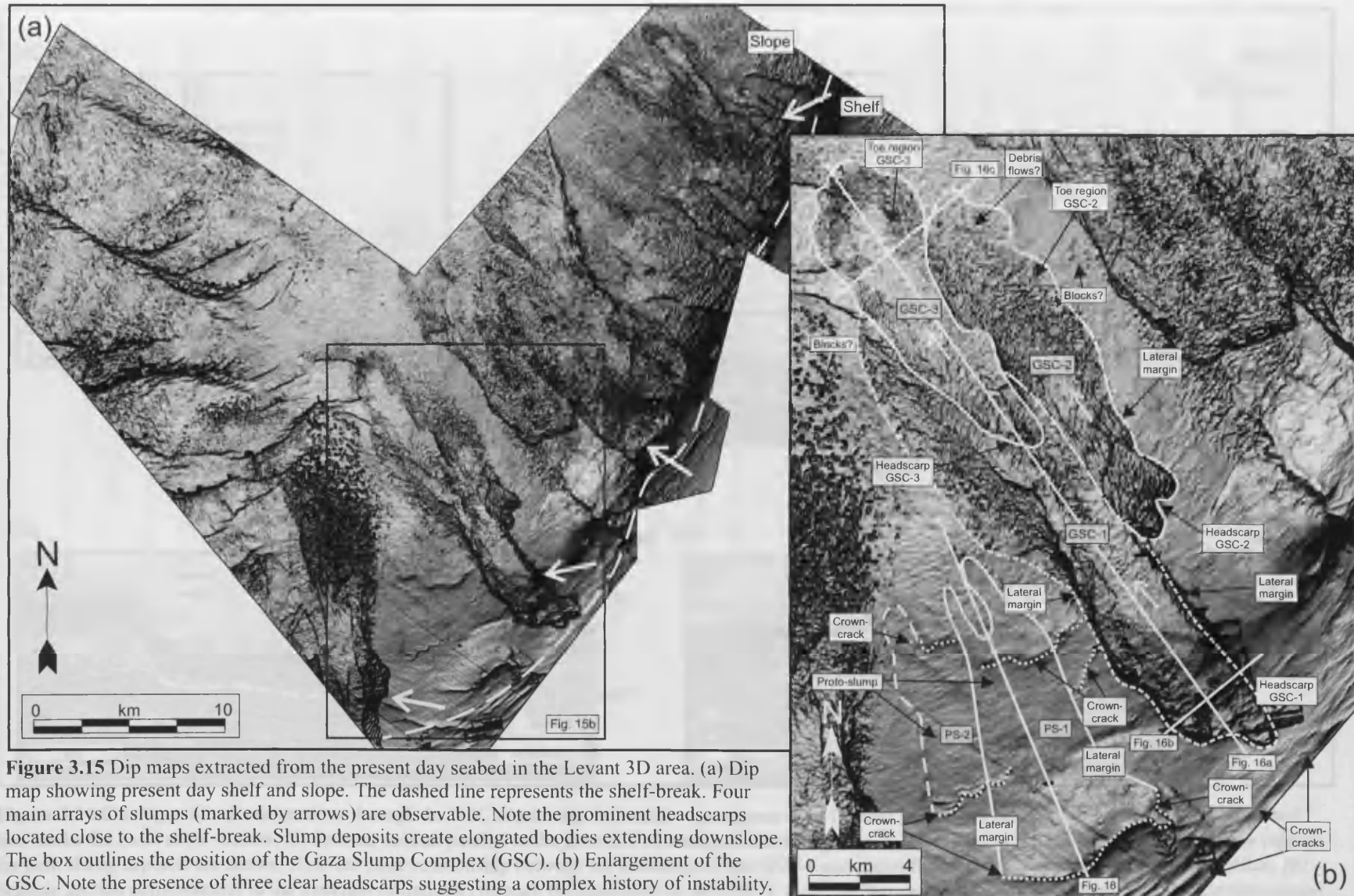


Figure 3.15 Dip maps extracted from the present day seabed in the Levant 3D area. (a) Dip map showing present day shelf and slope. The dashed line represents the shelf-break. Four main arrays of slumps (marked by arrows) are observable. Note the prominent headscarps located close to the shelf-break. Slump deposits create elongated bodies extending downslope. The box outlines the position of the Gaza Slump Complex (GSC). (b) Enlargement of the GSC. Note the presence of three clear headscarps suggesting a complex history of instability. The strike-parallel lineaments upslope of the headscarps GSC-1 and GSC-2 are interpreted as crown-cracks. Note the presence of two elongated bodies interpreted as proto-slumps (PS-1 and PS-2). The continuous straight lines indicate the position of seismic profiles used to interpret the internal appearance of the GSC and the PS-1 (Figures 3.16 and 3.18, respectively).

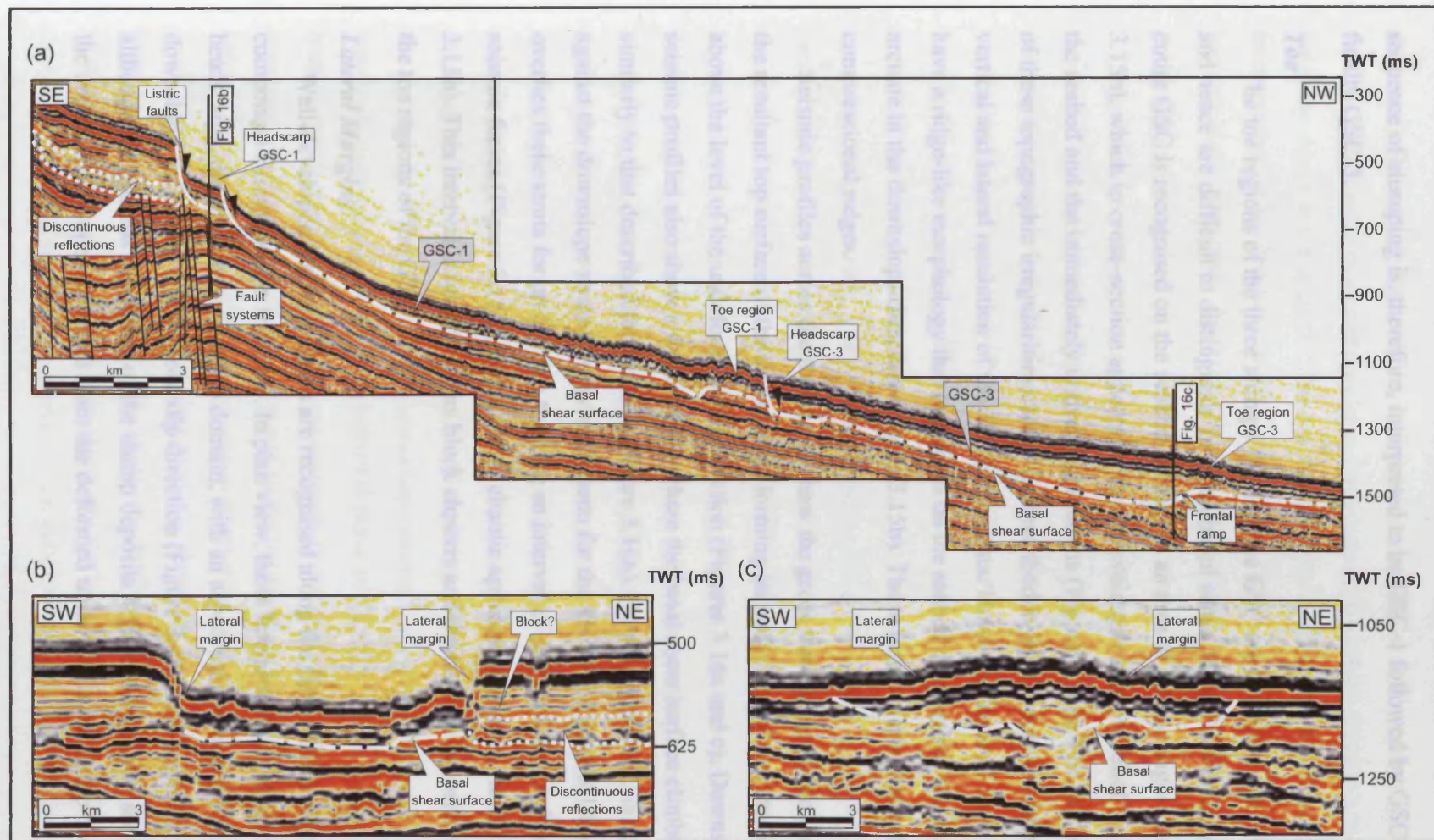


Figure 3.16 Catalogue of seismic sections through the GSC illustrating the seismic appearance of its internal parts (see Figure 3.15b for location). The dashed line marks the basal shear surface. (a) Seismic section parallel to the direction of transport illustrating the GSC-1 and the GSC-3. The headscarps and toe regions for both slump deposits are shown. Note the close relationship between the headscarp of the GSC-1 and minor faults updip suggesting retrogressive failure. (b) Seismic section perpendicular to the direction of transport through the headscarp of the GSC-1. Note the two clear lateral margins creating a negative topography and the presence of a block-like feature. (c) Seismic section perpendicular to the direction of transport through the toe region (see Figure 3.15b for location). The lateral margins form a positive topographic relief. The seabed appears crenulated.

sequence of slumping is, therefore, interpreted to be GSC-1 followed by GSC-2 and finally GSC-3.

Toe

The toe regions of the three slumps forming the GSC are to a great extent overlapping and hence are difficult to distinguish. In a combined sense, the gross toe region for the entire GSC is recognised on the seabed dipmap as an area of intense rugosity (Figure 3.15b), which in cross-section appears as short wavelength and low relief 'crumpling' of the seabed and the immediately underlying sections (Figure 3.16a). The precise geometry of these topographic irregularities cannot be described in detail because of the limits of vertical and lateral resolution of the 3D seismic data. However, some of these 'crumples' have a ridge-like morphology that is evident on the seabed dipmap and are approximately arcuate in the downslope direction (Figure 3.15b). These features are interpreted here as compressional ridges.

Seismic profiles across the toe region show the gross thickening within the GSC, with the resultant top surface of the slump body forming an irregular and elevated region above the level of the undeformed slope section (Figures 3.16a and c). Downslope seismic profiles also show a frontal ramp where the basal shear surface climbs up section similarly to that described for the ISC (Figure 3.16a). However, the GSC is not buttressed against the downslope strata as previously seen for the ISC (c.f. Figure 3.10b). Instead, it overlies these strata for up to 2 km forming an interval of diffuse and very low amplitude seismic facies (Figure 3.16a), with a rather chaotic appearance in plan view (Figure 3.15b). This interval is interpreted as block clusters and debris flow deposits derived from the toe regions of the GSC.

Lateral Margins

Well-developed lateral margins are recognised along the flanks of all the three-component slumps within the GSC. In plan view, these lateral margins, together with the headscarps, define a chute-like slip domain, with an aspect ratio strongly elongated downslope, indicating a NW gross slip direction (Figure 3.15b). On seismic profiles, although the internal resolution of the slump deposits is poor, they can be seen to separate the undeformed slope sediments from the deformed units within the slump bodies

(Figures 3.16b and c). Their aspect varies from steep scarps in the upslope parts of the GSC (Figure 3.16b), to smooth positive topographies downslope (Figure 3.16c). Often, the steep scarps in the upslope areas are flanked by subparallel groups of smaller-scale fractures that define blocks of well-layered strata (Figure 3.16b). These are interpreted as hanging blocks that might be metastable to rigid lateral collapse along the lateral margins.

Basal Shear Surfaces

Three different basal shear surfaces (one for each slump) can be correlated throughout the GSC. These are all defined as the lower boundary of the deformed and chaotic stratal seismic reflections within each slump body abutting against the undeformed underlying slope strata (e.g. Figure 3.16). These basal shear surfaces are generally highly concordant with the underlying stratigraphy, except near the headscarps, where they cut up section and exhibit a listric geometry, and along the toe region, where they are seen to ramp downslope (Figure 3.16a). The original lithology of the basal shear surfaces is unknown, because of the lack of petrophysical calibration of the shallow section in the available exploration wells. However, it is noteworthy, that all three basal shear surfaces correlate laterally with intervals of discontinuous and low amplitude seismic reflections (Figures 3.16a and b). These intervals could be interpreted as a buried slump or slide deposits formed initially at the seabed. However, this is discounted as a possibility because they form continuously traceable intervals of constant thickness that are concordant with the surrounding strata throughout the study area and have no evidence of significant downslope displacement. Another possible interpretation is that they correspond to gas-saturated sediments. This possibility, however, is rejected here since such intervals are not associated with any high amplitude seismic anomalies (typical from gas saturated sediments in the area) and no gas-readings at these stratigraphic levels have been reported from the exploration wells. Instead, we propose the interpretation that these intervals represent weak or incompetent layers due to the liquefaction of fine grained clastic sediments (i.e. sands) that lead to the loss of internal coherence of the material.

In summary, the GSC forms a medium-scale slump complex comprised by three simple slump deposits from the Late Pleistocene-Holocene. Each slump deposit consists of an upslope region characterised by gross volume loss and extensional structures, and a downslope region dominated by gross volume gain and compressional features (Figure

3.17). These areas are interpreted here as the depletion and accumulation zones (*sensu* Varnes, 1978) of the GSC, respectively. The majority of extensional structures correspond to listric normal faults that die out on the basal shear surface and involve retrogressive failure. The compressional structures correspond to arcuate and compressional ridge-like geometries that propagate in the downslope direction (Figure 3.17). The sequence of slumping within the GSC is interpreted to be GSC-1 followed by GSC-2 and GSC-3 respectively. This is a highly important observation since it implies that slump evolution within the GSC occurs by downslope propagation failure. Three different basal shear surfaces are identified within the GSC (one for each component slump). They all correlate laterally into intervals of discontinuous and low amplitude seismic reflections that are interpreted here as incompetent layers characterised by loss of coherence in the sediment.

3.8 Proto-slumps

In this chapter, a proto-slump is defined as the resulting product (as imaged on 3D seismic data) of an immature or failed stage of slumping. We consider proto-slumps to be the result of long-term strength degradation processes of dipping strata or an aborted episode of slumping. They can be potential precursors to future downslope mass movements. Proto-slumps may display many of the diagnostic structures identified from slump deposits (e.g. lateral margins, crown-cracks). However, they lack a basal shear surface and clear extensional or compressional deformational structures, since their downslope displacement is highly restricted or absent.

In the study area, two main proto-slumps (PS-1 and PS-2) are observed in a region of the present day seabed that is not affected by slump deposits (Figure 3.15b). In plan view, these proto-slumps appear as chute-like features that extend from the shelf-break to the mid-slope area with an aspect ratio strongly elongated in the downslope direction (Figure 3.15b). The planforms of the PS-1 and PS-2 are defined by two groups of lineations that are parallel and perpendicular to the downslope direction (Figure 3.15b). By analogy with the GSC, these lineations are interpreted as lateral margins and crown-cracks respectively.

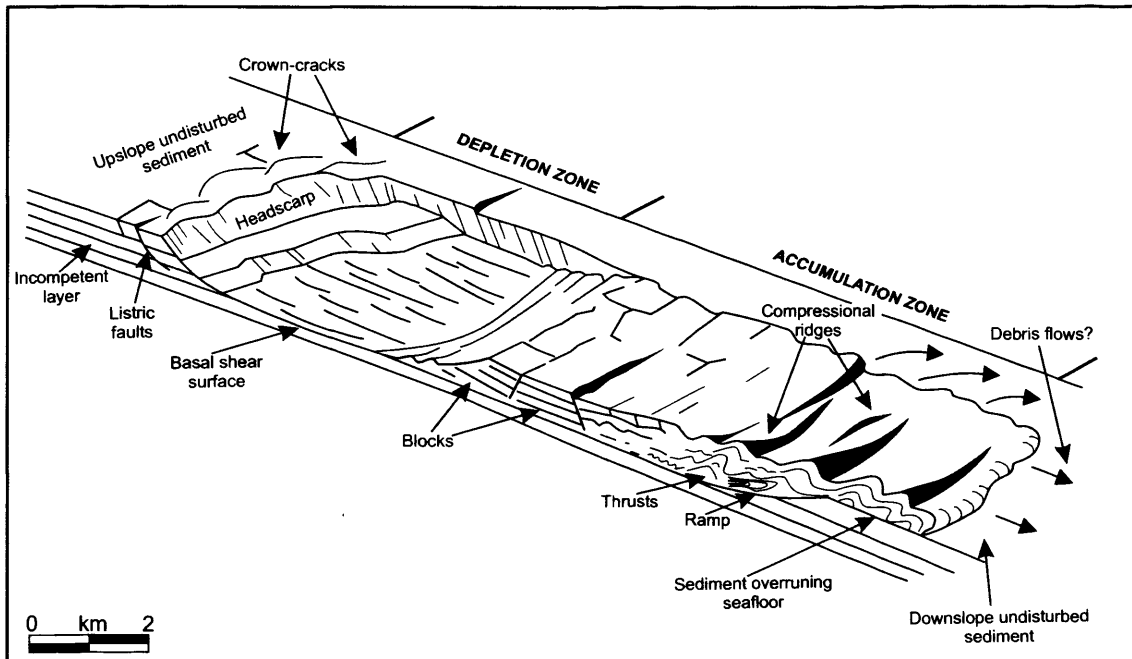


Figure 3.17 Schematic depiction of part of the GSC. The slump body is divided into two main parts: the depletion zone and the accumulation zone. The depletion zone shows a spoon-shaped depression suggesting reduction of the sediment column. Note the presence of a clear headscarp and evidences of retrogressive failure in the upslope parts. The accumulation zone is characterized by compressional structures and gain of material. In the toe region the slumped material over runs the previous seabed. Inspired by O'Leary (1991).

On seismic profiles, the PS-1 and PS-2 do not show a chaotic seismic facies as those described from slump deposits. Instead, they appear as intervals of slightly irregular, continuous and well-layered strata that overly a unit of discontinuous and medium amplitude seismic reflections interpreted here as an incompetent layer (Figure 3.18). Small-scale faults and fractures are the only deformational structures observed within the PS-1 and PS-2. These are rooted in the incompetent layer and are locally expressed on the seabed as small topographic depressions that correspond to the crown-cracks previously described (Figure 3.18). No indication of loss or gain of material is observed in any part of the PS-1 and PS-2, which is compelling evidence to indicate a very restricted downslope displacement.

3.9 Discussion

The most important observations undertaken from seismic interpretation of the slump complexes within the study dataset are summarised as follows:

- Several discrete examples of medium to large-scale slump complexes (c. 40) have been identified within the Pliocene to Holocene succession of the Israeli continental margin.
- In seismic profiles, these slump complexes appear as intervals of chaotic or highly disrupted seismic facies in sharp contrast with the laterally continuous and undeformed strata. They are bounded by an erosional basal shear surface and by a continuous and mounded top surface.
- The majority of these slump complexes are composed of several (~3) discrete slump deposits of (approximately) the same order of magnitude.
- Each slump deposit is divided into an upslope and a downslope region. The first is dominated by extensional deformational structures and thinning of the slump mass. The second is characterised by compressional structures and thickening of the slump mass.
- Slump complexes are distributed along the entire post-Messinian Israeli margin and extend from the shelf to the base of slope areas. In the vertical sense, they

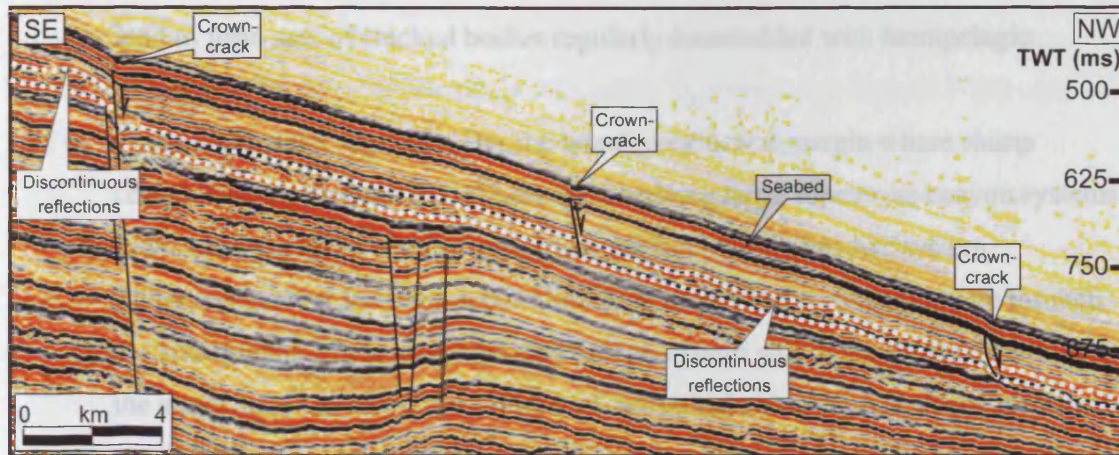


Figure 3.18 Seismic profile through the PS-1 (see Figure 3.15b for location). Note the small topographic depressions on the seabed interpreted as crown-cracks. These correspond to faults and fractures that are rooted in an interval of discontinuous seismic reflections interpreted here as an incompetent layer.

includes a large multi-lobed slump body that is composed of a mixture of three large-scale slump deposits.

- The GSC (Late Pliocene-Holocene) corresponds to a slump complex on the present day continental margin of Israel. It forms a medium-scale array of three slump deposits that exhibit evidence of upslope and downslope propagation failure.

The foregoing observations demonstrate that the entire post-Messinian continental margin of Israel is intrinsically affected by processes of slope instability. The most outstanding resultant elements are a series of large-scale slump complexes that extend from the shelf-break to the base of slope areas involving an average of c. 15% of the total post-Messinian sediments. Analysis of their stratigraphic context in the southern continental margin has revealed that these slump deposits diminish in size and increase in number towards the shallowest intervals. It has also been shown that there are regions of the margin where slump deposits concentrate and the presence of a slump body influences the position of succeeding events. These regions correspond mainly to the parts of the margin overlaying regional structures from the Syrian Arc system or large pre-Messinian canyons (e.g. the Afiq and el-Arish submarine canyons).

Large-scale slumping initiated during the Late Pliocene with the ISC, which represents the largest slump complex in the region and is comparable to some of the biggest documented examples of submarine mass-wasting deposits in the world (i.e.

tend to form sets of stacked bodies regularly interbedded with hemipelagic sediments.

- There are distinct regions along the Israeli continental margin where slump complexes are concentrated. These are overlying large submarine canyon systems in the pre-Messinian section and structures from the Syrian Arc system.
- There is a general increase in the number of slump bodies on moving up through the stratigraphy of the post-Messinian slope system within the southern parts of the study area. However, the volume of individual slump bodies clearly decreases upwards.
- The ISC (Late Pliocene) is the oldest large-scale slump complex identified along the Israeli continental margin and involves large amounts of material (c. 1000 km³ in volume). It forms a buttressed slump body that is comprised by a minimum of three large-scale slump deposits.
- The GSC (Late Pleistocene-Holocene) corresponds to a slump complex on the present day continental margin of Israel. It forms a medium-scale array of three slump deposits that exhibit evidence of upslope and downslope propagation failure.

The foregoing observations demonstrate that the entire post-Messinian continental margin of Israel is intrinsically affected by processes of slope instability. The most outstanding resultant elements are a series of large-scale slump complexes that extend from the shelf-break to the base of slope areas involving an average of c. 15% of the total post-Messinian sediments. Analysis of their stratigraphic context in the southern continental margin has revealed that these slump deposits diminish in size and increase in number towards the shallowest intervals. It has also been shown that there are regions of the margin where slump deposits concentrate and the presence of a slump body influences the position of succeeding events. These regions correspond mainly to the parts of the margin overlaying regional structures from the Syrian Arc system or large pre-Messinian canyons (e.g. the Afiq and el-Arish submarine canyons).

Large-scale slumping initiated during the Late Pliocene with the ISC, which represents the largest slump complex in the region and is comparable to some of the biggest documented examples of submarine mass-wasting deposits in the world (i.e.

Storegga Slide; Bugge, 1983). The most striking characteristic of the ISC is that the slump mass is clearly entrenched within the underlying strata (e.g. Figures 3.10b and 3.14). This is especially clear in its toe region where the ISC buttresses against the undisturbed sediments, which trap the slump mass preventing its movement farther downslope. This observation raises important implications for the mechanism and kinematics of movement and emplacement of the slump body. A detailed mechanical analysis of the ISC goes beyond the scope of this chapter. However, from the previous observations, it is likely that the ISC resulted from a confined type of slumping that experienced a very limited downslope movement (c. 5-15 km). The presence of blocks of undisturbed and continuous reflections that are coupled to the undeformed sedimentary succession corroborates this interpretation.

Previous investigators have reported other submarine mass-wasting deposits presenting this characteristic style of emplacement and have interpreted them as the result of quasi *in situ* deformation processes (e.g. Suvero Slide; Trincardi & Normark, 1989; Gela Slide; Trincardi & Argnani, 1990). The previous examples considered morphological obstacles as the main contributing factor for confinement of the respective slumped masses. In this chapter, however, this is precluded as the cause for the entrenching of the ISC within the underlying sediments since the toe region is built in a near horizontal area where there is no morphological barrier able to create such a topographic confinement. Instead, we propose that a major contribution to the style of emplacement of the slumped mass resulted from relatively deep rooting of the basal shear surface within the underlying strata probably due to an abrupt lithological variation at that stratigraphic level combined with the general morphology of the strata.

Since the deposition of the ISC, slump events continued episodically up to the Holocene. As a result, tens of slump deposits and complexes formed at different stratigraphic levels interbedded with periods of normal hemipelagic deposition. The GSC is the most representative example of one of these slump complexes. It is located on the present day seabed of the study area and is composed of several different elements, resulting from an orderly sequence of linked slumping events. The overall resultant assemblage comprises three cross-cutting slump deposits that are interpreted as Late Pleistocene to Holocene in age. Each of these deposits includes an upslope area

characterised by gross volume loss and extensional structures (depletion zone; Figure 3.17), and a downslope region dominated by gross volume gain and compressional features (accumulation zone; Figure 3.17). The architecture and geometry of each slump deposit indicate that slump evolution was controlled by a combination of retrogressive upslope and downslope propagation of failure. The relative ages of the three component deposits have been determined from their cross-cutting relationships, with the interpreted ordered sequence: GSC-1 followed by GSC-2 and GSC-3 respectively. Three basal shear surfaces, one associated with each component slump, have been observed and correlated with intervals of incompetent layers. This critical observation strongly suggests that movement in the GSC took place along surfaces of weakness and was controlled and limited by the number and distribution of these planes.

The occurrence of such a large number of slump deposits as that observed in the study area raises the obvious question of what internal or external factors predisposed the post-Messinian continental margin of Israel to be so susceptible to repeated failure. Previous studies have identified a number of possible causes controlling the development of submarine slump deposits along continental margins. These include:

- Destabilization of gas hydrates (e.g. Andreassen *et al.*, 1990, Laberg & Vorren, 2000).
- Presence of gas in the sediments (e.g. Prior & Coleman, 1978; Carpenter, 1981; Duperret *et al.*, 1995).
- High-sedimentation rates (e.g. Prior & Coleman, 1982; Aksu & Hiscott, 1989; Hiscott & Asku, 1994, Laberg & Vorren, 2000; Imbo *et al.*, 2002).
- Seismicity (e.g. Lewis, 1971; Dingle, 1977; Hampton *et al.*, 1978; Prior & Coleman, 1984; Keefer, 1994; Hasiotis *et al.*, 2002; Imbo *et al.*, 2002).
- Steepening of slope angle (e.g. Martinsen, 1989; Hampton *et al.*, 1996; Imbo *et al.*, 2002).

In the case of the slump deposits presented here, the number of possible controlling factors is constrained by the available data. There is no evidence from seismic or well data of gas hydrates, which probably rules out this possibility as a controlling factor for slumping in the study area. However, abundant accumulations of biogenic gas within the post-Messinian succession have been revealed by the seismic and well data. Bubble-phase

gas has the effect of increasing pore fluid pressures and hence reducing the effective normal stress on a potential slide plane, along with increasing its susceptibility to failure when stressed by earthquakes (Whelan *et al.*, 1976; Barnes & Lewis, 1991). The presence of free gas could thus have played an important role in facilitating the mobilisation of sediments in the study area.

Rapid deposition due to high-sedimentation rates can result in underconsolidation of buried layers of clay-rich sediment in which upward hydraulic gradients reduce the internal shear strength of the sediment and lead to slope instability. The Pliocene-Quaternary section in the study area is up to 2 km thick with an average accumulation rate of about 0.5 mm/yr. According to these figures, the sedimentation rates are not likely to be sufficient to build up significant excess in pore pressure within these deposits in order to generate the observed large-scale slump deposits. However, the role of temporal variations in the sedimentation rates within the study area should not be discounted. During the Pliocene and Pleistocene period, the margin was affected by several episodes of global eustatic sea-level oscillations and local vertical tectonic movements that resulted in repeated transgressions and regressions (e.g. Almagor, 1993; Buchbinder & Zilberman, 1997). In such situations, sedimentation rates could have been considerably higher than the average rates, and could have thus facilitated mass wasting processes.

The direct link between seismicity and instability of submarine slopes have been widely described in the literature (e.g. Lewis, 1971; Prior & Coleman, 1984; Edwards *et al.*, 1993; Keefer, 1994; Hasiotis *et al.*, 2002; Imbo *et al.*, 2002). Earthquakes have two effects on the sediments of a slope system (Hampton *et al.*, 1978). Firstly, violent earthquakes generate intermittent horizontal and vertical acceleration stresses that produce a direct loading on the sediment. Secondly, earthquakes can increase fluid pressure in the sediment that causes a reduction in the effective stress and therefore friction in the basal shear surface.

Because of its position at the zone of interaction between the Anatolian, African and Arabian plates, the continental margin of Israel is a seismically active region. Recent seismic activity in the area is presently concentrated in a broad zone off the coasts of Israel and Lebanon (Arieh, 1967) and along the Dead Sea Transform (Al-Tarazi, 1999). In the investigated area, the main seismic hazard is associated to the Syrian Arc system

and the Dead Sea Transform, which is the result of a rifting process active in the region since the Miocene (e.g. Garfunkel, 1981; 1998).

Despite the importance of slope gradient in slope stability assessment (e.g. Hampton *et al.*, 1996) our results show that occurrence of slope instability in the study area does not correspond with regionally increased slope gradients. The average slope angle within the post-Messinian succession is modest compared to many unstable slopes ($\alpha=2^{\circ}$ - 6°). Slopes are stable as long as the angle of internal friction (Φ) is greater than the slope angle (α). Considering a typical total angle of internal friction for a claystone of $\Phi=15^{\circ}$, it is evident that the slope angles in the study area are not sufficient to cause large-scale instability under static gravitational loading alone. However, local increases in the slope angle appear to control the occurrence of slumping in specific areas. As previously argued, the majority of slump deposits within the study area are concentrated in regions underlain by regional structures from the Syrian Arc system and by pre-Messinian canyons. In these regions locally accentuated slope angles occur ($\alpha=5^{\circ}$ - 6°). This concurrence might suggest a link between local oversteepening and higher occurrence of slope failure.

3D seismic interpretation has proved to be a very powerful tool for analysing slumping processes and results. It has provided excellent coverage of both recent and ancient slump deposits, allowing for a better understanding of their basinal distribution and geological setting. In addition, the high spatial resolution provided by the 3D seismic data has offered a better definition of the basal shear surface of individual deposits, which is critical for unravelling the chronology of events within slump complexes. 3D seismic data have also allowed a greater understanding of the geometries (external and internal) and a more accurate volumetric analysis of slump deposits, which are critical aspects for modelling the kinematics and dynamics of slumping processes. The value of 3D seismic data as a tool for submarine slope instability risk assessment has also been proved in this chapter. An interesting aspect of this approach is the possibility to map the extent of zones where diagnostic features of mass movement (i.e. proto-slumps) can be inferred, thus highlighting potential areas affected by slope instability.

3.10 Conclusions

- Slumping is an intrinsic facet of the slope system of the Israeli continental margin from the Early Pliocene to the present day.
- Simple and complex slump deposits occur at many different stratigraphic levels within the post-Messinian succession of the Israeli continental margin.
- Large-scale slumping in the Israeli continental margin commenced in the Late Pliocene with the ISC, which is one of the largest slumps in the world (c. 1000 km³ in volume) described to date.
- Since then, slumping processes repeatedly occurred up to the Holocene. Slumping events increased in number through time although the resulting products decreased in size.
- The high occurrence of slumping processes was possible due to a combination of seismic activity and presence of gas within the sediments. The degree of interaction between these triggering mechanisms may have varied through time.
- Evidence of potential slope instability occurring in the future in the study area is indicated by the presence of proto-slumps.
- 3D seismic interpretation has proved to be a powerful tool when analysing slump processes and results. The availability of a 3D understanding of slump deposits is critical to evaluate the geological context and architectural elements of slump deposits. From this geometrical foundation, many aspects related to the mechanics, processes and controlling factors of slumping seem likely to be inferred.

Chapter Four: Compressional toe regions in submarine landslides¹

4.1 Abstract

Three-dimensional (3D) seismic data from the continental margin offshore Israel (Eastern Mediterranean) have been used to analyse the compressional structures within the toe regions of two major buried submarine landslides. The high spatial resolution provided by these data has allowed a detailed analysis of the geometries and deformational structures within the two toe regions, which has been used to erect a comprehensive mechanical model for their development. Importantly, it has been recognised that submarine landslides may be divided into two main types according to their form of frontal emplacement: *frontally confined* and *emergent*. In the former, the landslide undergoes a restricted downslope displacement and does not overrun the undeformed downslope strata. In the latter, in contrast, significant downslope translation occurs since the landslide is able to abandon its original basal shear surface and translate freely over the seafloor. The division of submarine landslides into *frontally confined* and *emergent* features is of critical importance as the mechanisms of formation, downslope propagation and emplacement of the two types are fundamentally different, and hence need to be taken into consideration when analysing their genetics and kinematics. Although evidence of similar differentiations of submarine landslides has been previously observed from other continental margins worldwide, this is the first inclusive analysis of their 3D geometries, causes and formational mechanisms.

¹ Submitted to *Marine Geology* as:
J. Frey-Martinez et al., *Compressional toe regions in major submarine landslides imaged with 3D seismic data: implications for slide mechanics*

4.2 Introduction

In submarine landslides, downslope translation of unconsolidated fine-grained sediments along a basal shear surface leads to the development of domains of upslope extension and downslope compression (e.g. Lewis, 1971; Farrell and Eaton, 1987; Martinsen, 1989; Moore et al., 1989; Martinsen and Bakken, 1990; Booth & O'Leary, 1991; O'Leary 1993; Strachan, 2002). This has also been demonstrated in theoretical models (e.g. Farrell, 1984) and scaled physical experiments (e.g. Crans et al., 1980). While the processes responsible for the development of deformational structures in the upslope extensional domain (headscarp) are rather well understood, the mechanisms occurring in the downslope compressional domain (toe region) remain a matter of debate. This is mainly due to the lack of three-dimensional (3D) data, which has been a persistent obstacle to an in depth understanding of the detailed morphology and areal extent of the deformational structures. Even in areas with substantial exposure of slide deposits such as County Clare in Ireland (e.g. Martinsen and Bakken, 1990; Strachan, 2002), field-based approaches to analysis of the deformational geometries in the toe regions are limited in their 3D capacity. As a result, many questions regarding the mechanisms for the initiation and propagation of compressional strain regimes in sliding masses, and the controls for sediment deformation and resulting geometries remain unresolved.

Compressional toe regions in submarine landslides are commonly dominated by thrust and fold systems (e.g. Lewis, 1971; Varnes, 1978; Martinsen, 1989; Strachan, 2002; Frey-Martínez et al., 2005). These structures are critical as kinematic indicators since they allow the direction and magnitude of translation of the sliding mass to be constrained (e.g. Strachan, 2002). In addition, the architecture of such compressional structures is diagnostic of the mode of emplacement of the sliding mass and can be used to determine palaeoslope directions (e.g. Martinsen, 1989; Bradley and Hanson, 1998). The question of how such compressional structures initiate and propagate is also critical for understanding the dynamics of motion and arrest of submarine landslides. Traditional models (e.g. Farrell, 1984) state that compressional structures in submarine landslides can form if the sliding mass halts at its downslope margin first, thereby generating a compressional strain wave which propagates from the front to the rear of the unit. This model, however, is only

partially valid for *frontally emergent* submarine landslides (Figure 4.1a) in which the sliding mass ramps out the basal shear surface onto the seabed and is free to travel considerable distances over the undeformed slope position (e.g. Rettger, 1935; Gill and Kuenen, 1958; Morgenstern, 1967; Piper et al., 1999). In this context, landsliding involves the upslope depletion, downslope translation and base-of-slope accumulation of a sedimentary mass that abandons its initial failure region to form a positive feature on the seafloor. Recent investigations, however, have shown that submarine landslides can also develop *frontally confined* toe regions (Figure 4.1b) in which the slide mass is buttressed against the downslope undisturbed strata, has a relatively limited displacement and does not correspond to a significant topographic expression on the undeformed slope section (e.g. Trincardi and Argnani, 1990; Huvenne et al., 2002; Lastras et al., 2004; Frey-Martínez et al., 2005). The mechanisms for the formation of compressional structures in this latter type of submarine landslides are currently poorly understood and we lack any clearly defined natural example of how they proceed kinematically. In particular, one of the most important unknowns is the mechanism controlling frontal confinement i.e. why some submarine landslides become confined, how confinement occurs and what effect this has on the sliding mass. In addition, recent investigations (e.g. Lastras et al., 2004) have revealed substantial deficiencies when assessing the runout distance of *frontally confined* submarine landslides. This has been attributed to errors resultant from measuring their runout distance as the length between the headscarp and the slide toe (*sensu* McAdoo et al., 2000). Such an approach may induce significant overestimations of the actual transport distance leading to imprecision in slide modelling.

We use 3D seismic data to discuss the development of large-scale compressional structures in the toe regions of two major submarine landslides from the post-Messinian succession offshore Israel. Both landslides are defined here as slump deposits *sensu* Stow (1986). The first case study corresponds to the Israel Slump Complex, a *frontally confined* feature that extends almost continuously along the continental margin of Israel. The second belongs to the T20 slump deposit, which consists of a medium-size *frontally emergent* feature located in the southern parts of the margin. The compressional structures in both cases consist of complex arrangements of thrust and fold systems that are approximately parallel and extend for tens of kilometres in the dip direction.

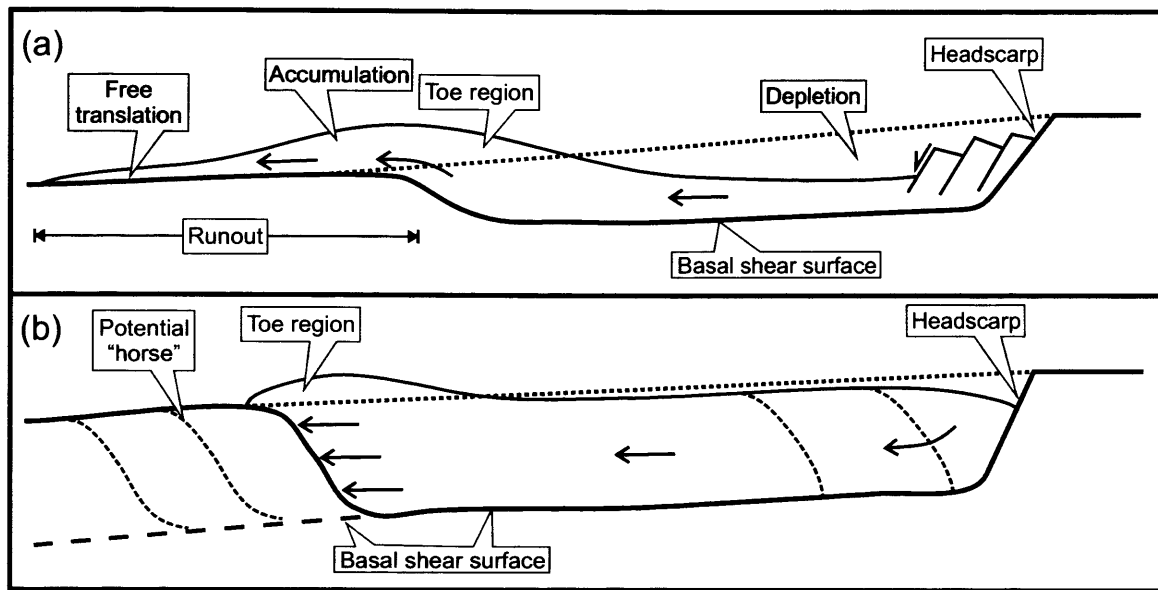


Figure 4.1 Schematic depiction of the two main types of submarine landslides according to their frontal emplacement. (a) Frontally emergent landslide. Note that the material ramps out the basal shear surface onto the seabed and is free to travel considerable distances over the undeformed slope position. (b) Frontally confined landslide. The mass is buttressed against the frontal ramps and does not abandon the original basal shear surface.

Nevertheless, detailed 3D analysis reveals a series of variations between the compressional features of the two landslides that suggest significantly different formational mechanisms. The main aim of this chapter is thus to describe the geometry and structural styles of these compressional features, with special emphasis on proposing a kinematic model for their formation. A further aim is to assess the main parameters and mechanisms involved in the development of *frontally confined* submarine landslides. The chapter commences with a brief description of the geological setting of the study area and a seismic-stratigraphic framework of the post-Messinian succession. The main arguments are subsequently developed through detailed 3D analysis of two very different landslides. The chapter concludes with a geomechanical model for the formation of the compressional toe regions of *frontally confined* submarine landslides taking into account the observations presented here.

4.3 Geological setting

The submarine landslides presented in this chapter occur within the Pliocene to Pleistocene sediments of the Yafo Formation, Israeli continental margin. The geological context and a post-Messinian lithostratigraphy of the Israeli margin are shown in Figures 4.2a and 4.3, respectively. Figure 4.4 is a representative dip-oriented seismic profile throughout the study area. The Yafo Formation was deposited during a period of increased clastic input into a rapidly increasing accommodation space (Buchbinder and Zilberman, 1997). Such increase in clastic sedimentation resulted from a major Pliocene transgression that inundated the Upper Miocene shelf following the Messinian Salinity Crisis (Buchbinder & Zilberman, 1997). During the Pliocene transgression, normal marine deposition of Nile-derived fine-grained siliciclastics combined with secondary basinward sedimentation from the Israeli continental margin to build up a thick sedimentary wedge, with up to 80 km of north-east progradation and a total thickness of c. 1200-2500 m over the Messinian intervals (Mavqim Formation; Figures 4.3 and 4.4). During the Late Pliocene, subsidence along the margin increased as a result of the large volumes of sediment been deposited in the area (see Tibor and Ben-Avraham, 1992). Simultaneously, several episodes of large-scale sliding and gravitational tectonics (e.g.,

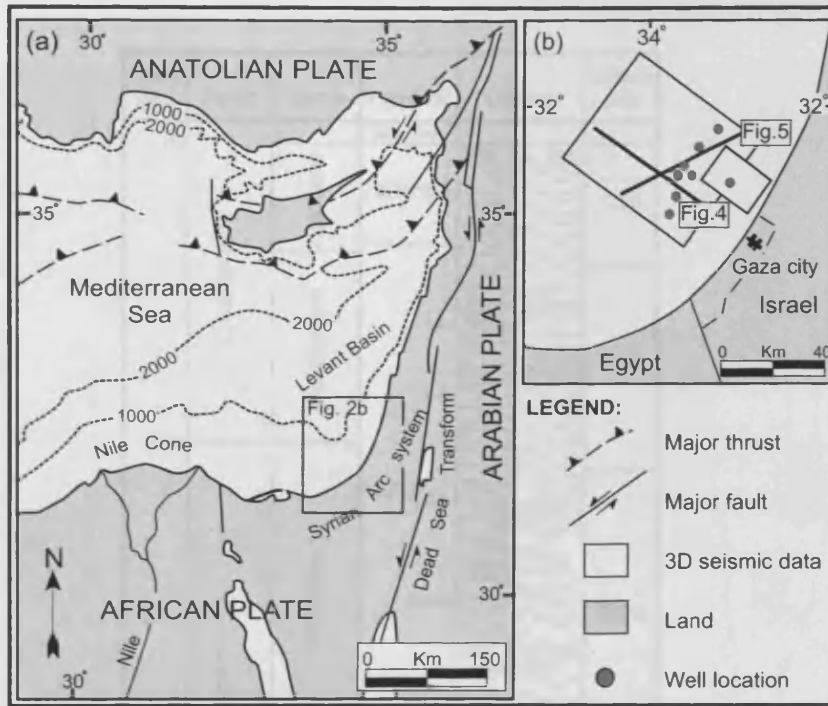


Figure 4.2 (a) Geological sketch of part of the Eastern Mediterranean showing the main structural elements. The box marks the approximate location of the study area. Modified from Garfunkel (1998). (b) Location map for the study area showing the 3D seismic database used in the study and the locations of the key exploration wells. Solid lines indicate the position of seismic profiles (Figure 4.4 and 4.5).



Figure 4.3 Generalized chrono-stratigraphic and lithological scheme of the post-Miocene continental margin of Israel. The lithological column is based on unpublished well reports.

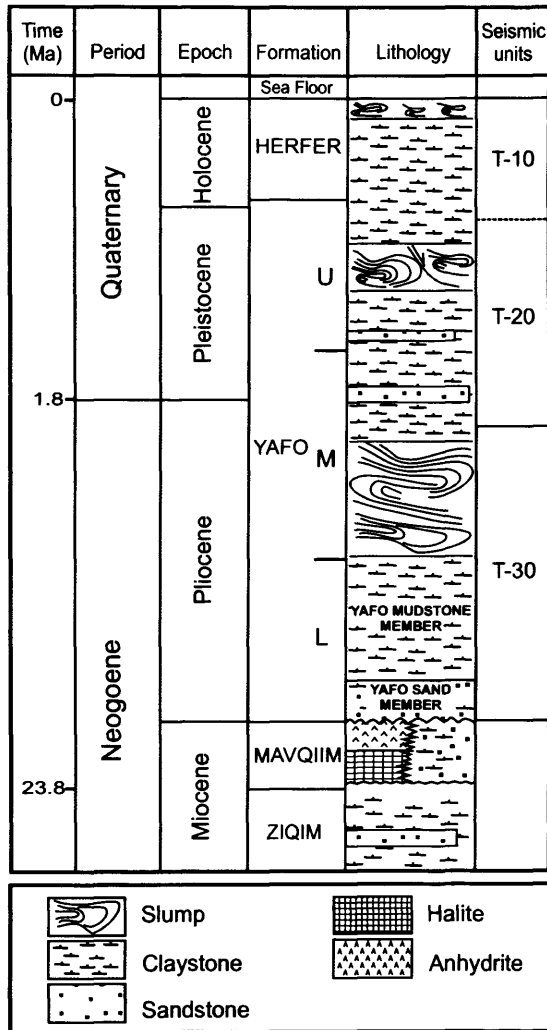


Figure 4.3 Generalised chrono-stratigraphic and lithological scheme of the post-Miocene continental margin of Israel. The lithological column is based on unpublished well reports.

4-8

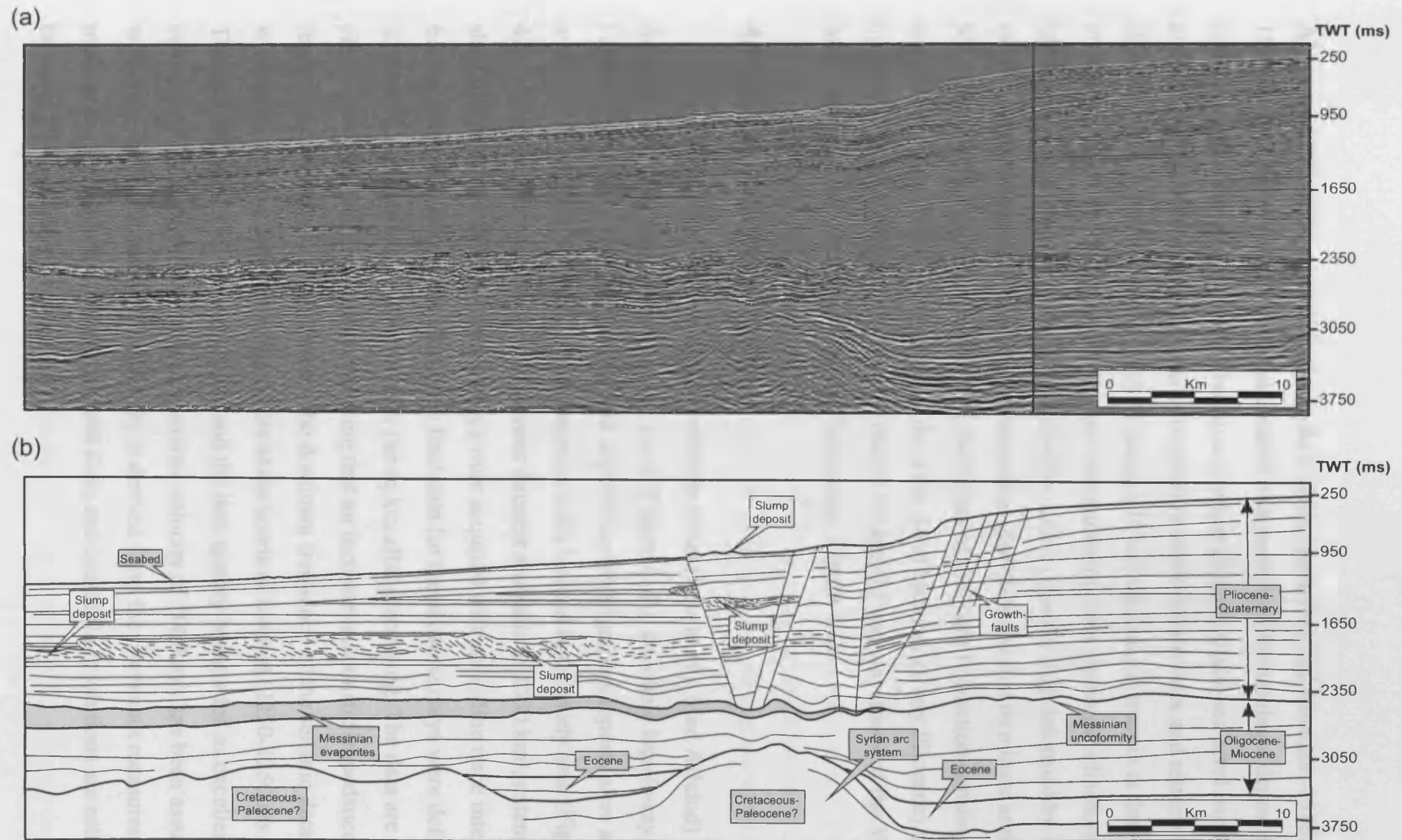


Figure 4.4 Regional dip seismic section through the continental margin of Israel (see Figure 2. 1b for location). This seismic profile illustrates the post-Cretaceous configuration of the study area. Note the presence of an extensive uncoformity and a thick deposit of evaporites resulting from the Messinian Salinity Crisis. Listric shore parallel growth faults are related to gravity-driven deformation of the Pliocene-Holocene continental margin and to salt tectonics.

Almagor, 1980, 1984 and 1986; Garfunkel, 1984; Garfunkel and Almagor, 1985 and 1987; Frey-Martínez et al., 2005) alternated with periods of hemipelagic deposition. This situation persisted until the Late Pleistocene, when global eustatic sea-level oscillations and local vertical tectonic movements resulted in repeated advances and retreats of the shoreline. The resultant overall post-Messinian Israeli continental margin is thus characterised by a strongly aggradational configuration, with sigmoidal clinofolds linking the shelf to slope areas. These clinofolds are considerably deformed by large to medium-scale slump deposits and shore-parallel growth faults that terminate at the Messinian sequences (Figure 4.4). The sediments of the Yafo Formation consist of thick submarine fans and turbiditic sands of the Yafo Sand Member (Early Pliocene) that pass upward to thinly interbedded clay-rich marls, sandstones and claystones of the Yafo Mudstone Member (Middle Pliocene-Pleistocene; Figure 4.3).

4.4 Data and methodology

3D seismic data from two surveys offshore Israel (Levant and Med Ashdod) represent the main source of information for this study (Figure 4.2b). Borehole logs (γ -ray, sonic, velocity, resistivity and checkshots) and unpublished stratigraphic reports were also available from eight hydrocarbon exploration wells located in the study area (Figure 4.2b). The total coverage of the 3D seismic datasets amounts to 2500 km², extending from shelf to deepwater. Both seismic surveys were acquired with an in-line trace interval of 6.25 m and a line spacing of 25 m. The final data for these two surveys were defined on a 12.5 by 12.5 m grid with 6400 bin cells per sq km after processing. The data are near zero phase with SEG normal polarity, meaning that an increase in acoustic impedance is represented by a positive amplitude. The dominant frequency of the seismic data varies with depth, but it is approximately 50 Hz at the levels of interest (2250-1250 ms TWT). The data are post-stack time-migrated and the data quality is regarded as excellent. When calculating the resolution, an average seismic velocity of 2000 m/s has been assumed within the level of interest. This velocity is derived from the checkshot measurements made in the Gaza Marine-1 well. Vertical ($\lambda/4$) and lateral (λ) resolutions are estimated to be about 10 m and 40 m, respectively.

The methodology used in this chapter is based on interpretation of 3D seismic data calibrated with the available well data. This allows the identification and correlation of the main internal deformational structures within the slump deposits over thousands of square kilometres and at a resolution of a few tens of meters. It also constrains the investigation of the kinematic indicators within the slump masses since it allows the examination of the transport directions, and relative timing of deformation. The interpretation of such deformational structures on seismic profiles can however be notoriously complex, principally because the highly disrupted and discontinuous patterns of the internal parts of the slump deposits. Such difficulties were overcome by interpreting a combination of differently orientated seismic profiles and attribute maps. Flattened horizontal coherence slices and seismic attribute extractions were generated in particularly complex areas of the slump deposits to assist the interpretation. Other seismic attributes, including dip and azimuth, were utilised in mapping of the internal geometries of the submarine landslides but did not resolve their 3D configuration better than the previously mentioned maps.

4.5 Seismic stratigraphic framework

In this chapter, we use the three seismic-stratigraphic units defined by Frey-Martínez et al. (2005) for the post-Messinian succession of the Israeli continental margin (T30, T20 and T10 in Figure 4.3). Their general architecture is illustrated by a regional 3D seismic profile (Figure 4.5). This transect is located on Figure 4.2b; it is orientated approximately parallel to the strike of the basin. These data calibrated with the wells located in the study area provide important evidence for the basinal distribution and timing of occurrence of the submarine landslides presented here.

A regional conspicuous erosional unconformity surface marks the base of the post-Messinian succession in the study area. Regional mapping has established that this surface corresponds to Reflector M, a basinwide marker caused by subaerial exposure during the Messinian Salinity Crisis (Ryan et al., 1970). Unit T30 is the lowermost seismic-stratigraphic unit within the post-Messinian succession. It consists of a c.750 m thick package of high frequency, continuous and high amplitude seismic reflections with

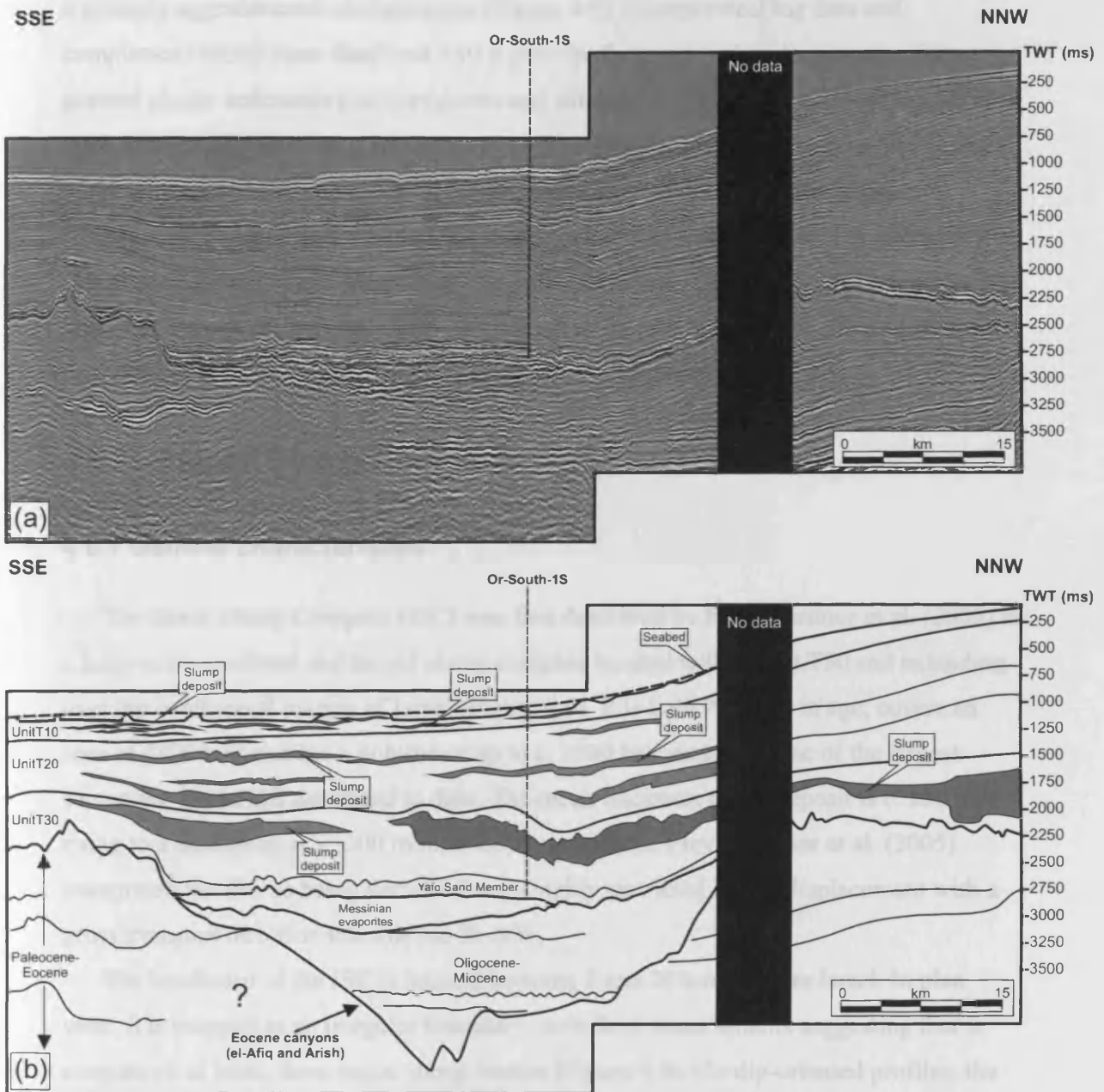


Figure 4.5 Seismic section (a) crossing the central parts of the Levant 3D area (see Figure 4.1b for location) and (b) interpretation showing the stratigraphic context of slump deposits in the study area. Shaded areas correspond mainly to simple slump deposits. Note that there is a concentration of slump deposits in the locations overlying pre-Messinian canyons. Slumps increase in number and decrease in size upwards.

a strongly aggradational configuration (Figure 4.5). Petrophysical log data and completion reports show that Unit T30 is principally composed of deep-marine fine-grained clastic sediments (i.e. claystones and siltstones). Unit T20 consists of a c. 1000 m thick interval of continuous, moderate to high amplitude seismic reflections that define a major aggradational slope wedge with dominantly sigmoidal clinoform geometries (Figure 4.5). Shallow to deep-marine claystones and limestones that locally alternate with sandstones, siltstones and marls form the bulk of this unit. Unit T10 is the uppermost 100-200 m of the post-Messinian section consisting of mainly fine-grained clastic sediments deposited in an aggrading sigmoidal clinoform configuration (Figure 4.5).

4.6 The Israel Slump Complex

4.6.1 General characteristics

The Israel Slump Complex (ISC) was first described by Frey-Martínez et al. (2005) as a large-scale confined and buried slump complex located within Unit T30 and extending over the continental margin of Israel (Figure 4.6). It is Late Pliocene in age, covers an area of 4800 km² and has a volume of up to c. 1000 km³ making it one of the largest submarine landslides described to date. The mean thickness of the deposit is c. 200 m, rising to a maximum of c. 300 m in its downslope parts. Frey-Martínez et al. (2005) interpreted the ISC as being derived from a highly restricted lateral displacement with a gross transport direction towards the W-NW.

The headscarp of the ISC is located between 2 and 20 km offshore Israel. In plan view, it is mapped as an irregular boundary; with three main salients suggesting that it consists of, at least, three major slump bodies (Figure 4.6). On dip-oriented profiles, the headscarp is recognised as a stratal termination between the chaotic seismic facies within the slump mass and the undisturbed seismic reflections of the upslope strata (Figure 4.7a). It forms a concave upwards plane that originally connected the basal shear surface with a level of undeformed slope section interpreted here as the original seabed. Its upper tip reaches up to 300 m above the level of the basal shear surface and has a gradient ranging

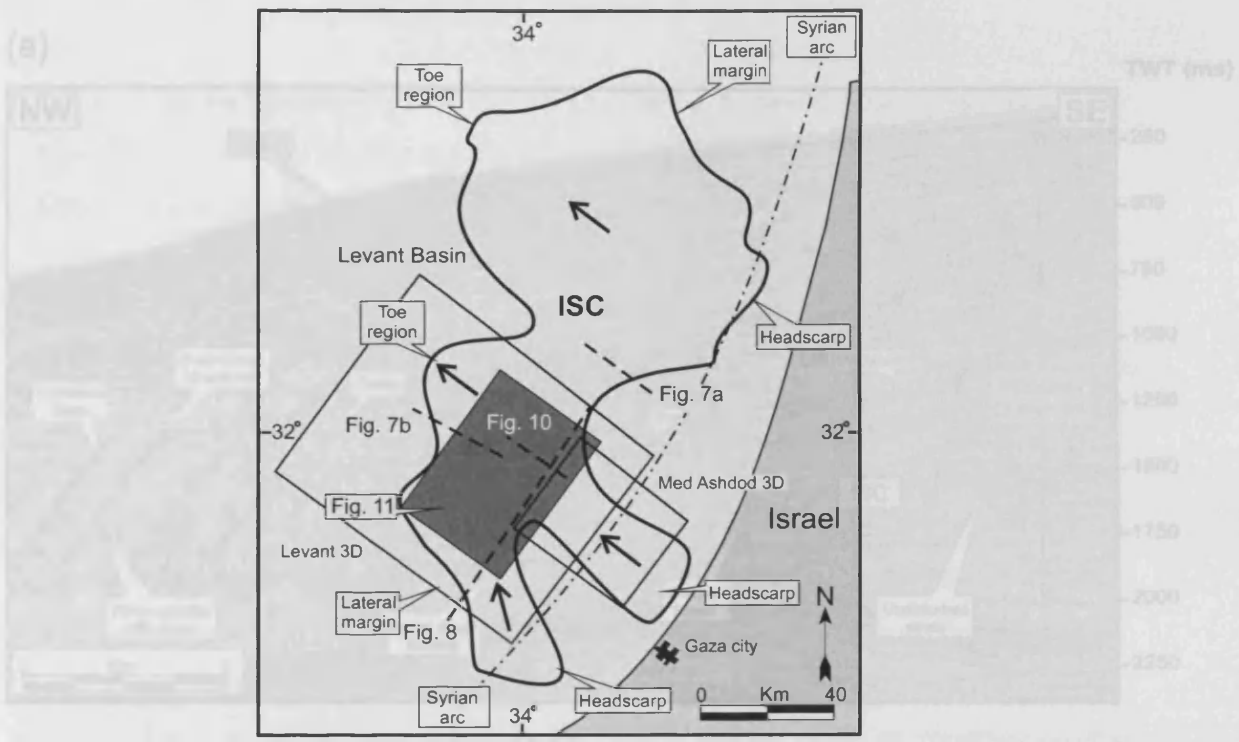


Figure 4.6 Map of the ISC showing its areal extension. Note its enormous areal extent (c. 4800 km²). The dashed line (parallel to the coastline) marks the general trend of large tectonic structures from the Syrian Arc system. Arrows indicate the gross transport direction of the slump mass. Seismic sections (indicated with thick dashed lines) are used to illustrate the region seismic appearance of the ISC (Figures 4.7-4.8).

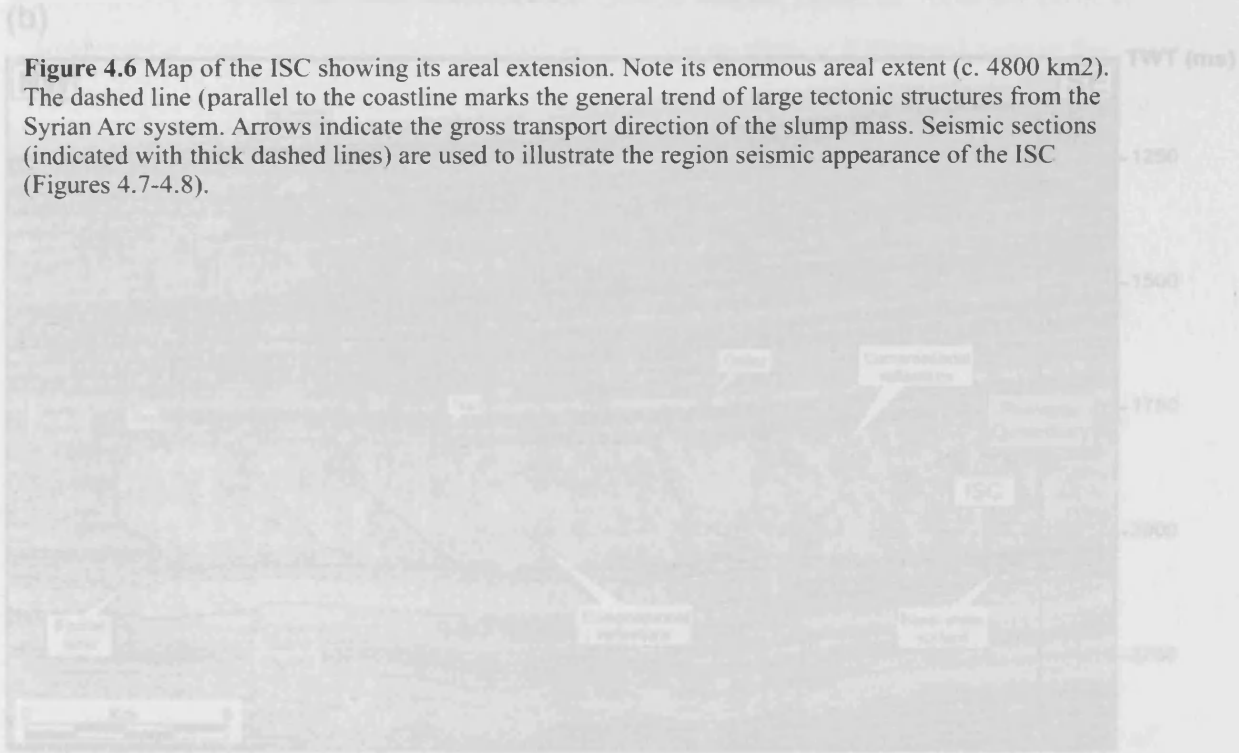


Figure 4.7 Seismic profiles along the ISC: (a) 3D seismic profile in the upslope part of the ISC (see Figure 4.6 for location). The headscarp forms a steeply dipping interface forming the upslope boundary between the chaotic seismic facies within the slump body and the continuous reflectors of the upper slope. Clear onlap of the headscarp by post-slump sediments is observed. (b) 3D seismic profile through the toe region of the ISC (see Figure 4.6 for location). The toe region appears as the downslope boundary between chaotic seismic facies of the ISC and the continuous reflectors of the base of slope. Note the presence of a clear frontal ramp and the slump mass being buttressed against the downslope strata. Other slump deposits appear affected by the ISC.

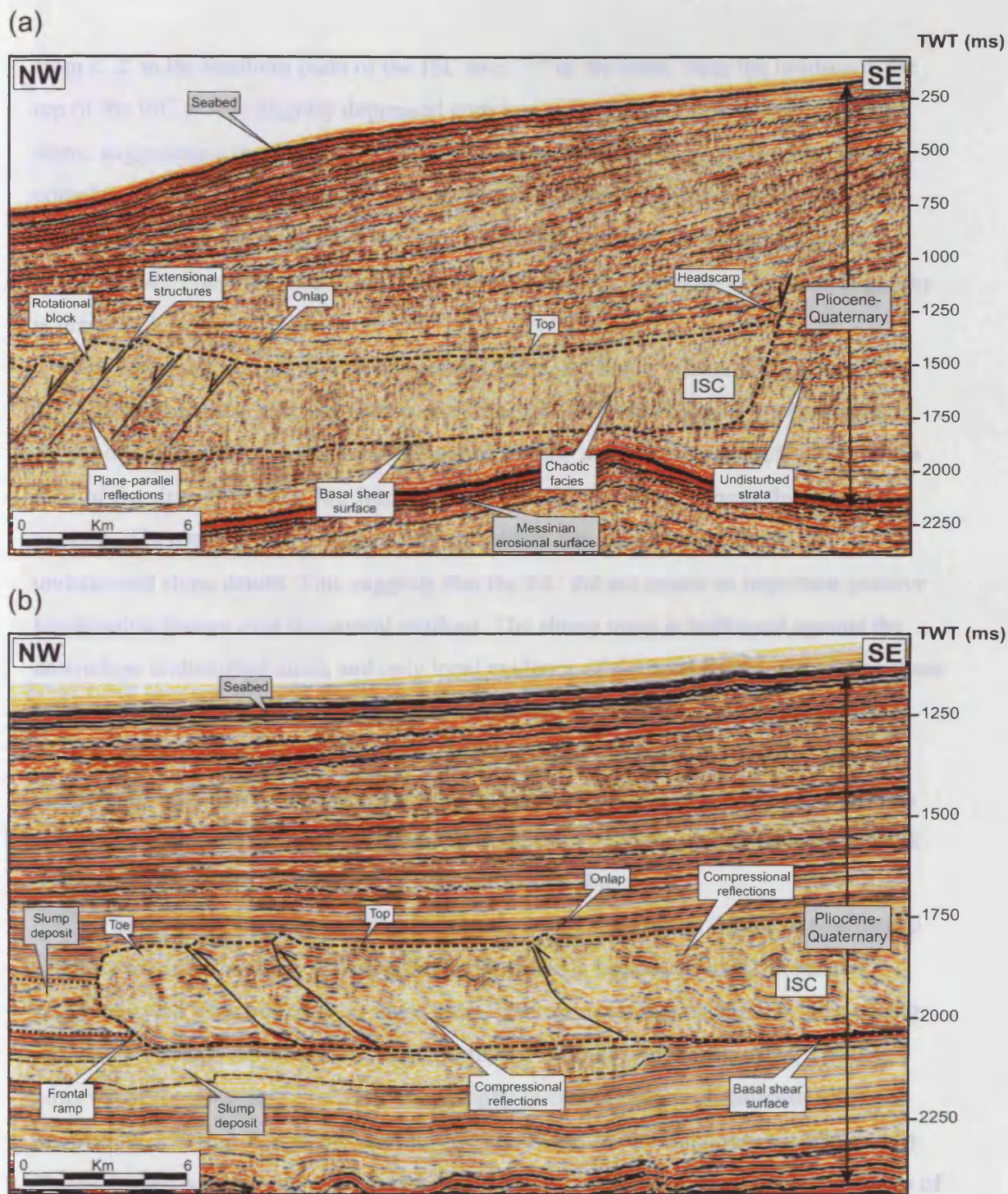


Figure 4.7 Seismic profiles along the ISC. (a) 2D seismic profile in the upslope parts of the ISC (see Figure 4.6 for location). The headscarp forms a steeply dipping interface forming the updip boundary between the chaotic seismic facies within the slump body and the continuous reflections of the upper slope. Clear onlap of the headscarp by post-slump sediments is observed. (b) 3D seismic profile through the toe region of the ISC (see Figure 4.6 for location). The toe region appears as the downslope boundary between chaotic seismic facies of the ISC and the continuous reflections of the base of slope. Note the presence of a clear frontal ramp and the slump mass being buttressed against the downslope strata. Older slump deposits appear affected by the ISC.

from c. 2° in the southern parts of the ISC to c. 15° in the north. Near the headscarp, the top of the ISC is only slightly depressed with respect to the undeformed region of the slope, suggesting a very limited depletion of sediment within these parts of the slump complex (Figure 4.7a). Tilted downslope rotational blocks of plane-parallel reflections that are separated by extensional structures (e.g. listric normal faults) are observed (Figure 4.7a). These are interpreted here as rotated blocks where the original stratigraphy is preserved.

The toe of the ISC is positioned between 100 and 140 km offshore (Figure 4.6). On dip-oriented profiles, it is very well constrained by an abrupt change from the highly disturbed seismic facies within the slump body to the outer continuous reflections at the base of the slope (Figure 4.7b). Importantly, although the slump deposit thickens considerably towards the toe region; its top seldom lies significantly above the undeformed slope datum. This suggests that the ISC did not create an important positive topographic feature over the coeval seafloor. The slump mass is buttressed against the downslope undisturbed strata and only local evidence of slumped material overlying these strata is observed. The lateral margins of the ISC are generally seen on strike-oriented seismic profiles as abrupt and steep (c. 25°) limits between the highly chaotic seismic facies within the slump mass and the outer undeformed strata (Figure 4.8). These limits commonly lie below the level of the undeformed slope section, confirming that the bulk of the slump deposit is entrenched within the surrounding strata.

The basal shear surface can be continuously traced with a high degree of confidence (Figures 4.7 and 4.8). This surface exhibits remarkable lateral variations in seismic amplitudes and geometries. Over large areas, it forms a continuous and flat-lying strong negative amplitude reflection that is conformable with the underlying strata. Locally, however, it ramps up and down the stratigraphy to create a series of staircase-like geometries, where it is possible to observe clear reflection terminations (see Figure 4.8). The geometric complexity of the basal shear surface increases where it exploits a series of horizons that exhibit kilometre-wavelength undulations and have a marked upslope accreting configuration (Figure 4.9). These horizons are interpreted here as contourite drift deposits by comparison with similar structures described by Faugères et al. (1999) and Knutz and Cartwright (2004). In the areas where the ISC overlies these deposits, the

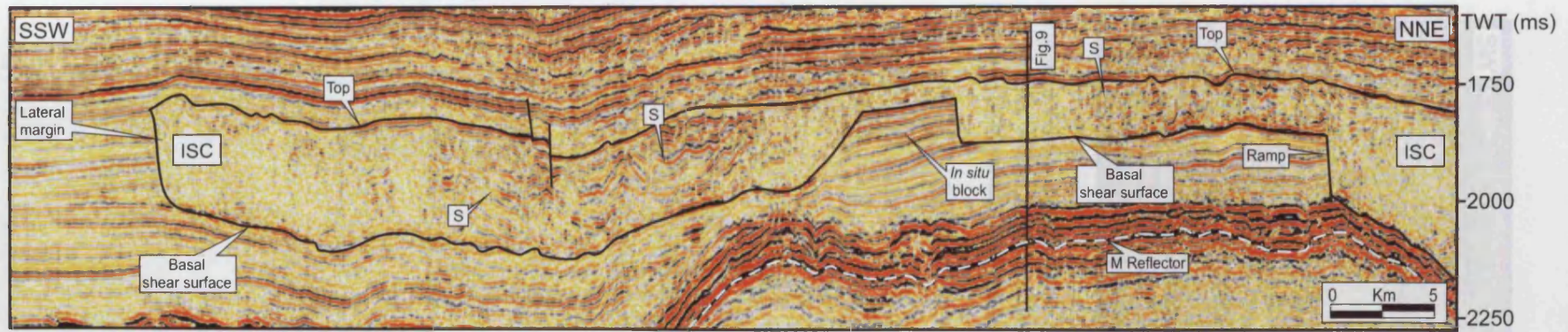


Figure 4.8 3D seismic profile across the ISC (see Figure 4.6 for location). Note the intensively chaotic seismic facies of the internal parts of the ISC bounded above and below by the top and basal shear surfaces, respectively. A lateral flank of the ISC forms a highly steep ramp separating chaotic from continuous seismic facies. Note the presence of a ramp indenting the basal shear surface and a block of undisturbed reflections within the ISC (see text for discussion). A seismic profile (Figure 4.9) is used to further illustrate the internal geometry of the ISC.

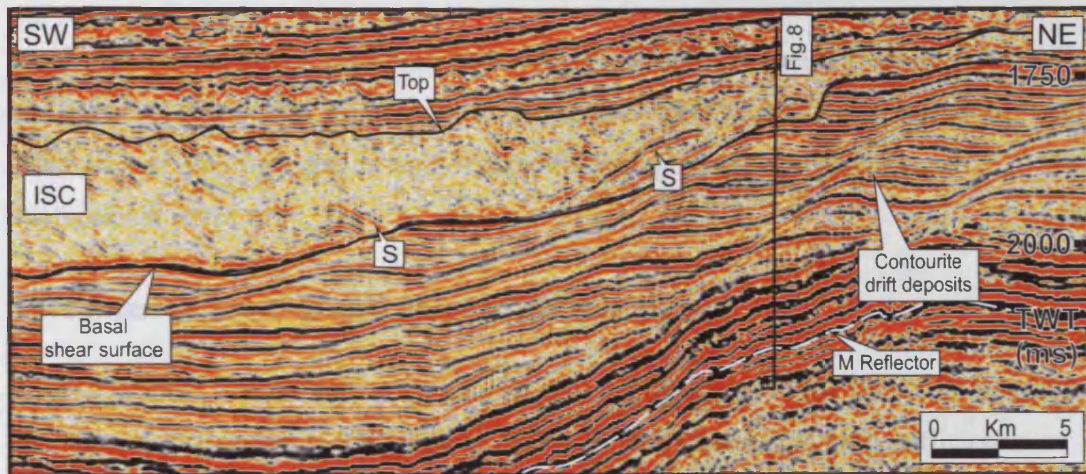


Figure 4.9 Seismic profile in the dip direction along the ISC. Note the presence of resolvable seismic reflections within the slump deposit (marked S). These are significantly similar to the surrounding strata. The basal shear surface follows the strata of the underlying contourite drift deposits.

These events are generally not significantly tilted. Near the frontal parts of the toe region, they are more easily traceable than towards the central and rear (in some places they correspond to weak troughs, in others they are almost opaque). There is a considerable similarity of form and seismic response between these reflections and the undisturbed strata outside the slump mass. This is particularly evident in areas where the ISC affects contourite drift deposits (see Figure 4.9). This observation suggests that the continuous reflections within the ISC correspond to portions of sediment that have been deformed and transported within the slump mass but still preserve their primary stratification.

A minor crease of continuous reflections within the toe region of the ISC is formed by a series of tilted (<20°) and significantly deformed events (Figure 4.7b). These are particularly distinct in areas of rapid change of gradient of the basal shear surface (see Figure 4.10). When viewed in detail, the tilted reflections are ubiquitously offset and dip upslope. Towards the lower parts of the slump body, they are seen to ramp up the basal shear surface and steepen vertically thus creating a listric morphology (Y in Figure 4.10). In many parts of the slump, the reflections exhibit small-scale folded geometries (X in Figure 4.10). This appearance has been consistently observed across many spatially correlated seismic profiles and this is taken as evidence of a genuine structural characteristic and not a processing (e.g. overmigration) or interpretational artefact. 3D

basal shear surface has a markedly undulating geometry; it increases significantly in dip and becomes considerably entrenched. The precise lithological contrast across the basal shear zone is unknown due to lack of accurate petrophysical calibration at this stratigraphic level.

4.6.2 Internal seismic character of the toe region

The internal seismic reflection character of the toe region of the ISC is dominated by chaotic and transparent facies (Figures 4.7b-4.9). Nevertheless, there is sufficient coherence of individual moderately continuous reflections to allow correlation of internal features. The majority of reflections correspond to parallel-bedded and sub-horizontal events that are mainly concordant with the basal shear surface and the top of the slump deposit (S in Figure 4.9). These events are generally not significantly tilted. Near the frontal parts of the toe region, they are more easily traceable than towards the central and rear (in some places they correspond to weak troughs, in others they are almost opaque). There is a considerable similarity of form and seismic response between these reflections and the undisturbed strata outside the slump mass. This is particularly evident in areas where the ISC affects contourite drift deposits (see Figure 4.9). This observation suggests that the continuous reflections within the ISC correspond to portions of sediment that have been deformed and transported within the slump mass but still preserve their primary stratification.

A minor group of continuous reflections within the toe region of the ISC is formed by a series of tilted ($<20^\circ$) and significantly deformed events (Figure 4.7b). These are particularly distinct in areas of rapid change of gradient of the basal shear surface (see Figure 4.10). When viewed in detail, the tilted reflections are ubiquitously offset and dip upslope. Towards the lower parts of the slump body, they are seen to ramp up the basal shear surface and steepen vertically thus creating a listric morphology (Y in Figure 4.10). In many parts of the slump, the reflections exhibit small-scale folded geometries (X in Figure 4.10). This appearance has been consistently observed across many spatially correlated seismic profiles and this is taken as evidence of a genuine structural characteristic and not a processing (e.g. overmigration) or interpretational artefact. 3D

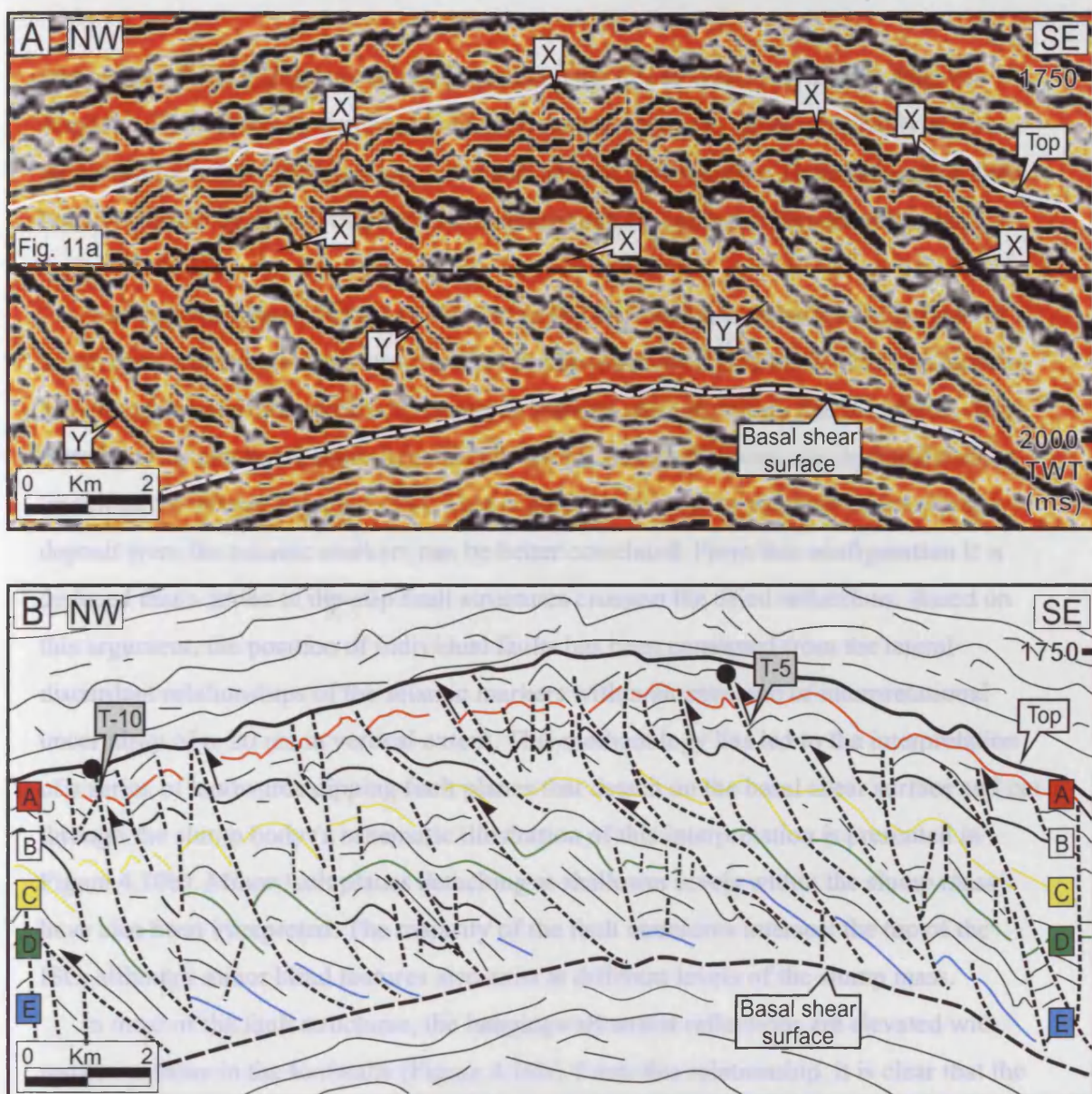


Figure 4.10 (a) Seismic profile in the dip direction along a segment of the ISC (see Figure 4.6 for location). The internal parts of the slump deposit are composed of upslope dipping tilted seismic reflections. These reflections are offset and create locally developed listric geometries (marked Y). (b) Interpretation showing five markers that have been used to undertake an accurate correlation across the ISC. Thrust structures ramping from the basal shear surface up to the top of the slump deposit are interpreted. Minor extensional structures (i.e. faults) are also interpreted.

mapping of these reflections is locally problematic due to variations in their seismic response, limited areal extent and their monotonous character. This is probably due to their dipping nature, low frequency and sub-seismic deformation. These difficulties have been overcome by correlating vertical and horizontal seismic profiles across the toe region of the ISC.

A series of seismic markers (A-E) within the tilted reflections have been defined in those areas where continuous stratification can be interpreted (Figure 4.10b). The markers have been correlated between differently orientated sections within the 3D seismic data. Based on this approach, it has been found that the tilted reflections are repeatedly offset (maximum c. 60 ms; Figure 4.10a). This is most clear in the upper parts of the slump deposit where the seismic markers can be better correlated. From this configuration it is deduced that a series of dip-slip fault structures crosscut the tilted reflections. Based on this argument, the position of individual faults has been construed from the lateral discordant relationships of the seismic markers within an envelope of interpretational uncertainty of c. 20 ms in vertical extent. This methodology has led to the interpretation of a series of landwards dipping fault planes that detach on the basal shear surface and cut through the slump body (a schematic illustration of this interpretation is presented in Figure 4.10b). Minor fault planes detaching at shallower levels within the slump mass have also been interpreted. The majority of the fault structures intersect the top of the ISC, although minor blind features also exist at different levels of the slump mass.

In most of the fault structures, the hangingwall stratal reflections are elevated with respect to those in the footwalls (Figure 4.10b). From this relationship, it is clear that the relative vertical displacement associated to the fault planes is mainly upwards. We thus interpret these dip-slip faults as thrust structures. Within this interpretation, the tilted reflections correspond to the original strata, which have been deformed by compressional stress. The folded geometries on the upper parts of the slump deposit are thrust propagation folds (e.g. Suppe and Medwedeff; 1990). Minor faults with a normal component of displacement have also been interpreted.

The thrusts overlap one on another basinwards to generate a “domino-like” succession (Figure 4.10b). This structural style shows a marked resemblance with the geometry of imbricate fans associated with foreland fold-and-thrust belts (e.g. Croot, 1987; Dahlen,

1990), fronts of prograding deltas (e.g. Morley, 2003) and glaciotectonic thrust complexes (e.g. Pedersen, 1987; Van der Wateren, 1995; Huuse and Lykke-Andersen, 2000; Andersen, 2004). No evidence of roof thrusts is observed hence no duplex zones are interpreted here. The tips of all the thrust structures appear at the same vertical level. Therefore, they do not construct a critical wedge such as some classic imbricate fans described, for instance, from foreland fold-and-thrust belts (i.e. Restrepo-Pace et al. 2004; Turrini and Rennison, 2004).

From the geometries observed, it is not possible to give a definitive indication of the direction of thrust propagation within the toe region of the ISC (i.e. foreland, hinterland or out-of-sequence). It is also possible to infer a “concertina” mechanism through which thrusting occurs simultaneously along the entire toe region. However, based on the previous analogy with imbricate fans, we propose that the most likely direction is foreland. If this is the case, it would mean that the ISC translated downslope by the sequential propagation of its frontal parts into the foreland. In this mechanism, each episode of downslope translation would be represented by a thrust structure. At each increment of movement, the sole of the toe and the adjacent sediment would compress rapidly and overpressure would rise thus allowing for new downslope propagation along the sole direction into previously undeformed sediment to occur significantly easier. This is an important argument from a genetic viewpoint, and will be referred to in more detail later.

A final and important observation from the seismic profiles across the toe region of the ISC is the presence of blocks of continuous reflections that remain as totally undeformed ‘islands’ and are surrounded by the highly deformed slump mass (Figure 4.8). The blocks are clearly coupled to the undeformed sedimentary succession below and are separated from the surrounding slump body by steep outward dipping flanks (c. 20°-25°; Figure 4.8). These features were interpreted by Frey-Martínez et al. (2005) as isolated cores of intact sediment that have not experienced failure. These authors also proposed that the presence of such blocks were indicative of low distances of downslope translation.

The internal planform appearance of the toe region of the ISC is illustrated in Figure 4.11a; a flattened horizontal coherence slice through the slump body at 1875 ms TWT.

Faced with such a complex fabric, the interpretational approach consisted of marking the limits between the different coherence facies, and correlating them with vertical profiles. The frontal parts of the toe region are dominated by low coherence facies. These are interpreted here as intensively deformed sediments that have totally lost their original stratification. The central parts of the toe region and one of its lateral margins show linear coherent reflections (C in Figure 4.11a). Nearly 80 of these linear reflections have been recognised in the imaged portions of the toe region of the ISC. The reflections can be traced over c. 20 km and have two main strike directions: N-S and SE-NW. The first form rectilinear features in the core of the toe region; the second create concentric arcs running parallel to the frontal parts of the slump. All the lineaments are convex basinwards. Calibration of the lineaments with vertical profiles reveals that they can be systematically correlated with the previously described thrust structures. From such high degree of correlation, we interpret the linear coherent reflections as thrust fault planes. A NW-SE trending alignment separating the two sets of thrust fault planes is also observed (D in Figure 4.11a). This alignment is interpreted as a longitudinal shear plane (i.e. strike-slip fault). Finally, several areas of coherent facies are identified in Figure 4.11a. These correspond to the previously mentioned isolated cores of undisturbed sediment. A schematic illustration of all these interpretations is illustrated in Figure 4.11b. Comparable geometries to those observed in Figure 4.11a have been reported by Huvenne et al. (2002) from a buried submarine landslide in the western Porcupine Basin (offshore SW Ireland).

Based on mapping at flattened horizontal coherence slices across the toe region of the ISC (e.g. Figure 4.11a) and the recognition that thrust fault planes are defined by lineaments in these surfaces, an interpretation of the main transport direction of the slump mass has been undertaken. For this purpose, it has been assumed that the direction of translation is approximately perpendicular to the strike of the thrust fault planes (after Ramsey and Lisle, 2000). Based on this rationale, a dominant East to West direction is interpreted in the central parts of the toe region (Figure 4.11b). This direction accords well with the inferred down-palaeoslope trend and suggests a simple compressional regime in these parts of the slump body. Towards the frontal parts of the toe region, however, the thrust fault planes suggest a more complex situation with two dominant

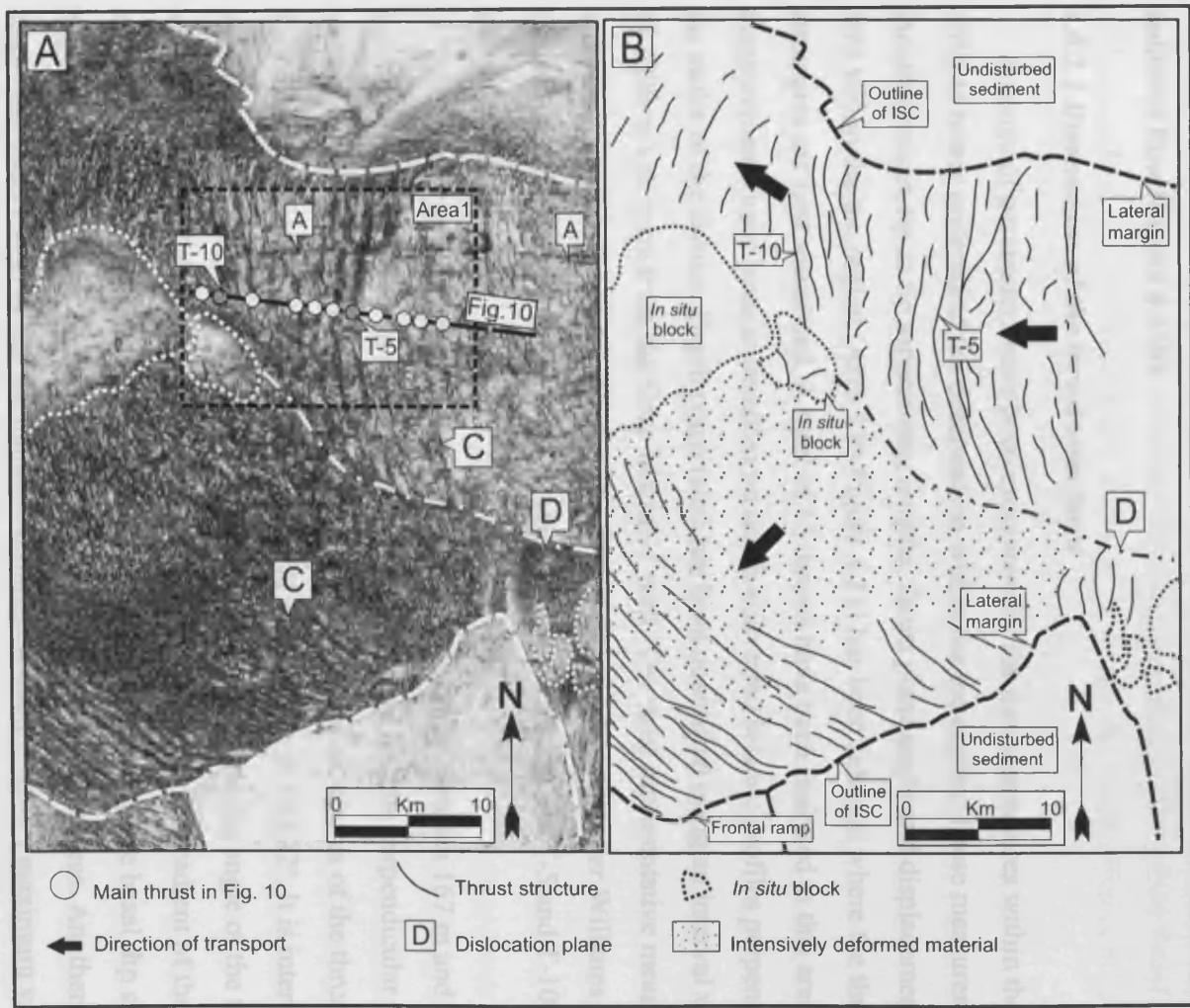


Figure 4.11 (a) Structurally flattened horizontal coherence-slice across part of the toe region of the ISC (see Figure 4.6 for location). Note the presence of arc-like concentric structures (marked C). These are interpreted as thrust fault planes. There are also coherent parts of the slump deposit interpreted as "in situ" blocks. It is important to note the presence of planes of dislocation within the slump mass (D). These act as strike-slip faults. A marks a seismic artifact. (b) Interpretation. The black arrows indicate the inferred direction of displacement of the slump mass. T-5 and T-10 correspond to two thrust fault planes studied in detailed in this chapter.

transport directions: NW-SE in the south and SW-NE in the north (Figure 4.11b), suggesting that these parts moved partially independently at some stage. The parallelism between these thrust fault planes and the perimeter of the frontal parts of the slump strongly suggests that there is a genetic link between the propagation of the ISC and the growth of the ridge structures. This strengthens the previous argument for a relationship between the sequential propagation of thrusting and the downslope advance of the ISC. We also believe that the presence of blocks of undisturbed sediment within the ISC may have influenced the direction of transport of the slump mass by locally dividing the sediment flow (Figure 4.11b).

4.6.2.1 Dimensions of the thrust structures

A series of parameters have been measured for the thrust structures within the ISC in order to better understand the deformation within the toe region. These measurements include: height, tip to tip separations, lengths, thrust plane angle and displacement. An area within the toe region (Area 1 in Figure 4.11) has been selected where the thrust structures are best visualised. A total of 15 thrusts have been analysed in this area. All the measurements have been undertaken on depth-converted seismic profiles perpendicular to the strike of the thrusts. Depth conversion has been quantified using an interval velocity of 2000 m/s derived from the Gaza Marine-1 well. The most representative measurements are summarised in Table 4.1. Two displacement-distance graphs (*after* Williams and Chapman; 1983) produced for two representative thrust structures (T-5 and T-10) are also presented.

The thrust structures within Area 1 have heights ranging between 167 m and 236 m (average ~194 m), tip to tip separations of 400-600 m and lengths perpendicular to the strike varying from c. 550 m to c. 1200 m (Table 4.1). Typical angles of the thrust planes (as measured from a flattened lower boundary) are between 9° and 22°. It is interesting to note that there is an inverse relationship between the length and the angle of the thrust structures. This relationship is, at least partly, an expression of the gradient of the basal shear surface because thrusts overlying points of rapid increase in the basal dip show higher angles and lower plane lengths than those occurring in flat areas. Another important observation is that the majority of thrust structures have a maximum value of

displacement at the basal shear surface, with a gradual decrease towards the top of the thrust plane (see displacement-distance graphs for T-5 and the T-10 in Figure 4.12). No evidence of thrust faults nucleating above their sole thrust is observed. 3D seismic data reveal that the displacement maxima are ubiquitously associated with clearly deformed stratal terminations immediately adjacent to the thrust planes (see Figure 4.10). Only minor folding is seen at the tips of the thrusts (X in Figure 4.10). The observed displacement patterns, together with the deformation associated with the thrust planes, strongly suggest that the thrust structures propagated from the basal shear surface towards the top of the slump. From the presence of minor folding at the tips of the thrust planes we propose that, as the displacement decreases upwards, the thrust offset is progressively replaced by ductile deformation (ductile bend; Elliott, 1970).

The displacement of individual thrust structures varies laterally. Figure 4.13 shows a series of measurements along the strike of the T-5 thrust structure. The measurements have been undertaken at marker C across five seismic profiles perpendicular to the strike of the thrust. The displacement varies from c. 10 m to c. 60 m (Figure 4.13). The displacement has a maximum in the central portion of the thrust structure and decreases gradually towards its flanks. This characteristic has been consistently observed in many other thrust structures across the toe region of the ISC. The observed lateral variation in displacement suggests that the central parts of the slump mass have undergone higher levels of translation than those in the flanks. This may be caused by the difference in flow rates and shear friction between the centre and the flanks of the slump mass. At the flanks of the slump, the flow rates tend to be lower than in the core due to higher levels of friction against the surrounding strata and the possible expulsion of lubricating fluids along the margins. Such scenario would explain the tendency of the thrust structures to form convex geometries in plan view (Figure 4.11). Ramsay and Lisle (2000) employed similar arguments to attribute the generation of flow ridges on the surface of extrusive bodies of magma.

The amount of bedding-parallel slip represented by the accumulative displacement on the thrust structures presented here is difficult to quantify. This is due to a general lack of marker horizons which can be correlated from thrust to thrust across the full extent of the toe region, and to appreciable variations in displacement vector between the various link

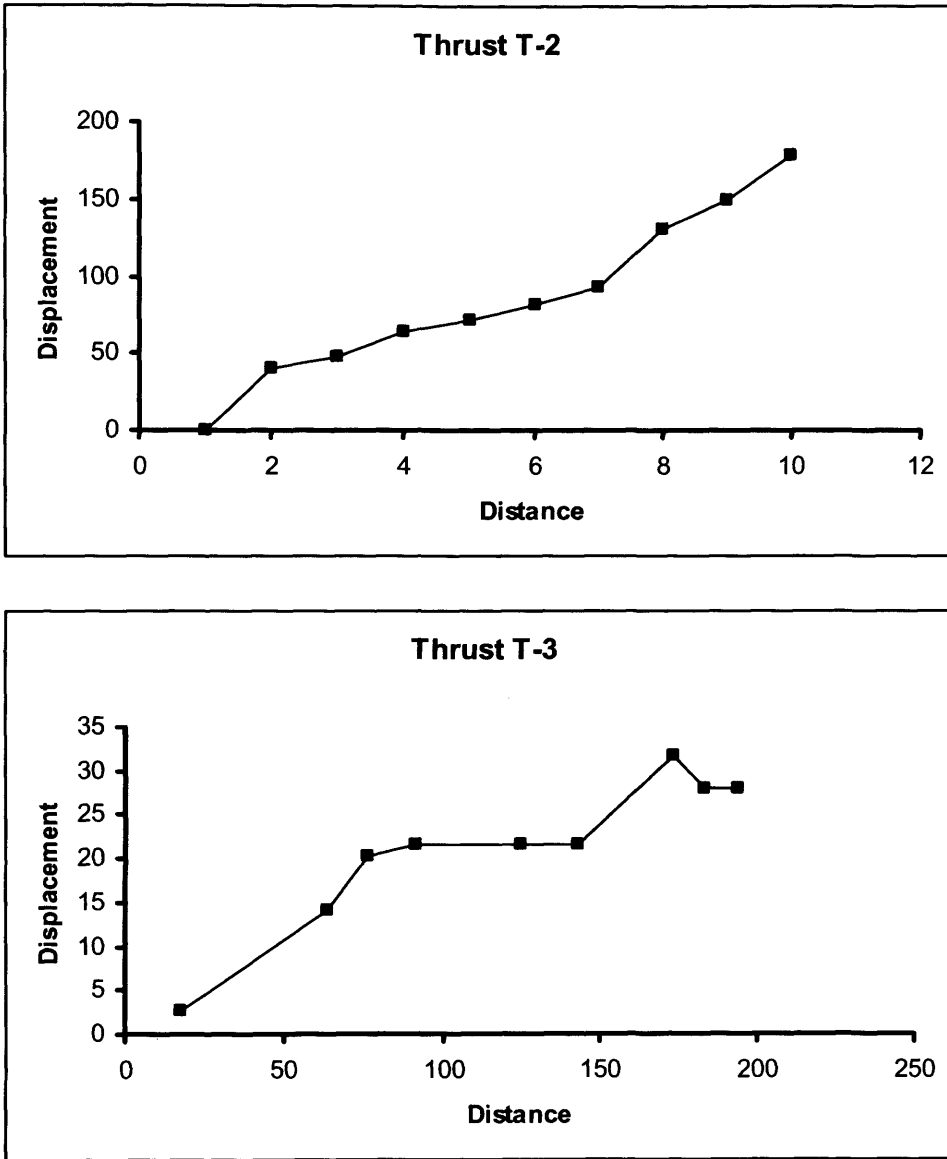


Figure 4.12 Displacement vs distance of two representative thrust structures within the toe region of the T20 slump deposit. The displacement has been measured from the tip of the thrust planes.

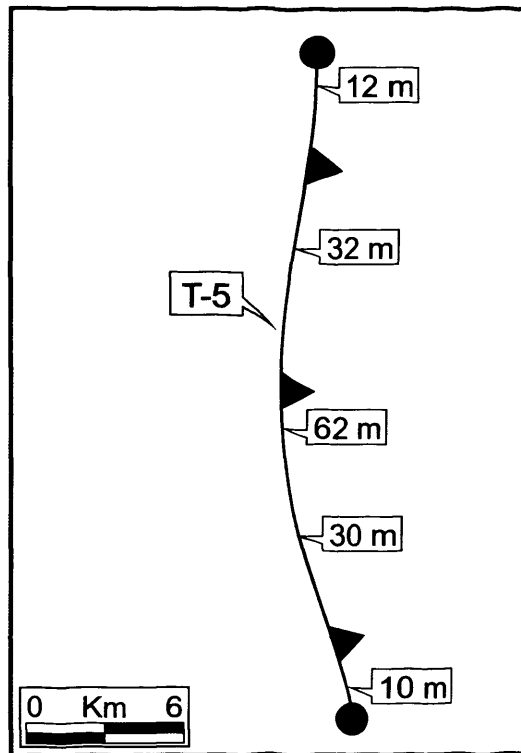


Figure 4.13 Representation of the displacement along a representative thrust structure (T-5). The maximum displacement is in the centre of the structure suggesting higher levels of translation in the central parts of the slump mass than in the flanks (see text for discussion).

Thrust	Height (m)	Length (m)	Plane angle (degrees)	Maximum displacement (m)
1	236	653	20	25
2	215	757	22	31
3	228	553	16	62
4	218	869	14	27
5	167	900	10	24
6	194	912	12	28
7	176	653	15	32
8	187	939	11	24
9	170	1154	9	25
10	188	1010	10	51
11	190	1187	9	24
12	184	1200	9	23
13	184	1027	10	26
14	189	1011	11	21
15	192	1087	10	25

Table 4.1 Measurements undertaken at fifteen different thrust structures within the toe region of the T20 slump deposit.

thrusts. Therefore, the shortening within the toe region of the ISC has been calculated as the amount of thrusts present, multiplied by their maximum horizontal displacement (i.e. their heave). Eighty thrust structures have been observed on the 3D seismic data, thus yielding an overall shortening of the order of 4 km. A typical degree of total shortening expressed in the imbricated set is of the order of 10%. This value of shortening accords extremely well with the thickening of the slump deposit in the toe region (Figure 4.7b); suggesting an interrelation between the thickness and morphology of the slump and the height and geometries of the thrusts.

In summary, the ISC corresponds to a large-scale *frontally confined* submarine landslide that has undergone a very restricted lateral displacement in the W-NW direction. It is Late Pliocene in age and represents one of the largest submarine landslides described to date. The ISC has a deeply entrenched and erosive basal shear surface that ramps up and down the stratigraphy and locally exploits the internal fabric of underlying contourite deposits. The upslope parts of the slump complex are characterised by extensional deformational structures (i.e. normal listric faults) and by minor thinning of the slump mass (see Figure 4.7a). The compressional toe region appears buttressed against the downslope undisturbed strata and does not have a significant bathymetric expression in terms of topographic height compared to its total thickening (see Figure 4.7b). No evidence of sediment spilling out over the seafloor has been observed. The internal parts of the toe region are dominated by large-scale imbricated thrust structures. These structures detach from the basal shear surface and ramp up to locally deform the top of the slump mass, such that irregular topographies and overlapped depressions are created. The thrust planes form by propagation from the basal shear surface towards the upper parts of the slump deposit. Blocks of undisturbed sediments that are rooted to the underlying strata have been also observed within the compressional toe region. These blocks have been interpreted as isolated cores that have not experienced failure. There is no evidence of large amounts of sediment being transported large distances downslope by the ISC.

4.7 The T20 Slump

4.7.1 General characteristics

The T20 slump was selected for detailed 3D study because it is the second biggest submarine landslide within the southern Levant continental margin and one of the best imaged examples offshore Israel. It consists of a single, large-scale *frontally emergent* feature within Unit T20 (hence Early to Late Pleistocene in age) that is located c. 60 km from the present-day coastline. The failure zone trends SW and extends from the shelf-break to the base of slope areas with slope gradients between 2° and 0.5°, respectively. The areal exposure within the two 3D seismic surveys covers a region of c. 60 km² (mean length 10 km, mean width 6 km; Figure 4.14). Maximum thickness varies from c. 50 m in the upslope areas to c. 250 m distally. The total volume of the slump deposit is estimated at about 6 km³ based on a mean thickness of 100 m. The T20 slump has been penetrated by three exploration wells, and it is mainly composed of soft and plastic, deep-marine claystones and limestones.

A time thickness map (Figure 4.14) illustrates the planform geometry of the T20 slump. On this map, the slump defines a lobe-like geometry with an aspect ratio significantly elongated downslope. 3D seismic mapping of the headscarp is complicated since it is positioned in an area heavily deformed by growth fault systems. Nonetheless, it can be mapped as a crescentic planform feature that opens towards the NNW and extends for c. 8 km in a SW-NE direction (Figure 4.14). Our mapping shows that this headscarp corresponds to a discrete feature, thus suggesting that the T20 slump consists of a single landslide event. On seismic sections in the dip direction, it forms a concave upwards surface with its upper tip up to c. 200 m above the basal shear surface and a mean gradient of c. 10° (Figure 4.15). Near the headscarp, the top of the slump is considerably depressed with respect to the undeformed slope datum and is overlapped by post-slump deposits (Figure 4.15). This configuration indicates that the upslope parts of the T20 slump are thinned relative to the pre-slide slope template, and forms the basis for inferring the depletion of large amounts of sediment from these areas. Another important

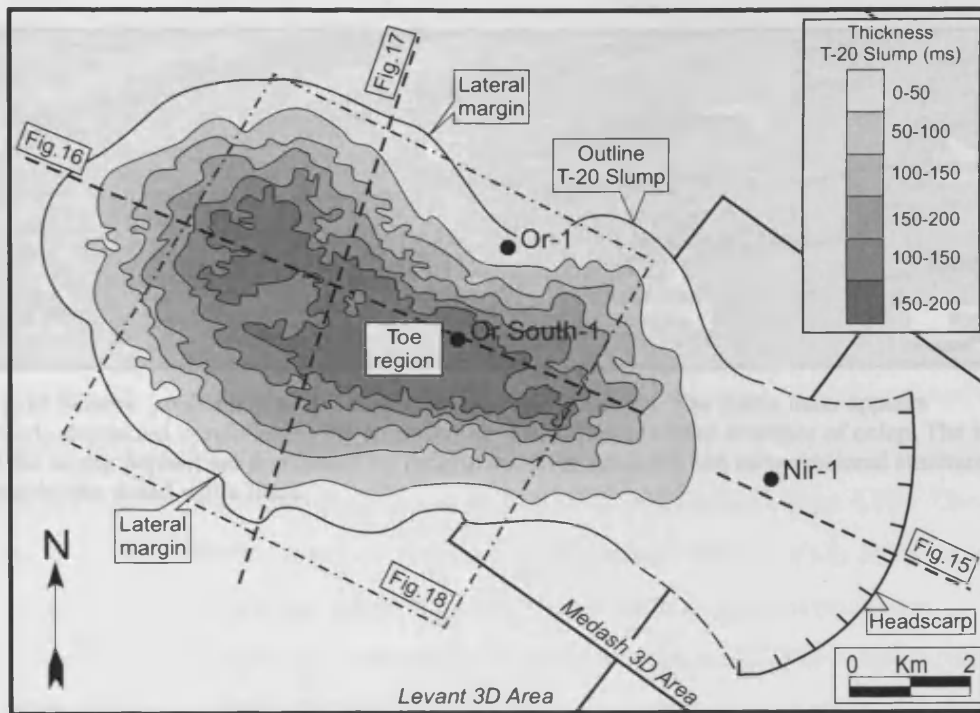


Figure 4.14 Isochron of the T20 slump deposit. The headscarp forms an arcuate feature surrounded by thin deposits of sediment. The toe region is characterised by a considerable increase in the thickness of material. The dashed lines and box (Figures 4.15-4.17, respectively) indicate the position of seismic profiles and amplitude extractions used to illustrate the internal parts of the T20 slump.

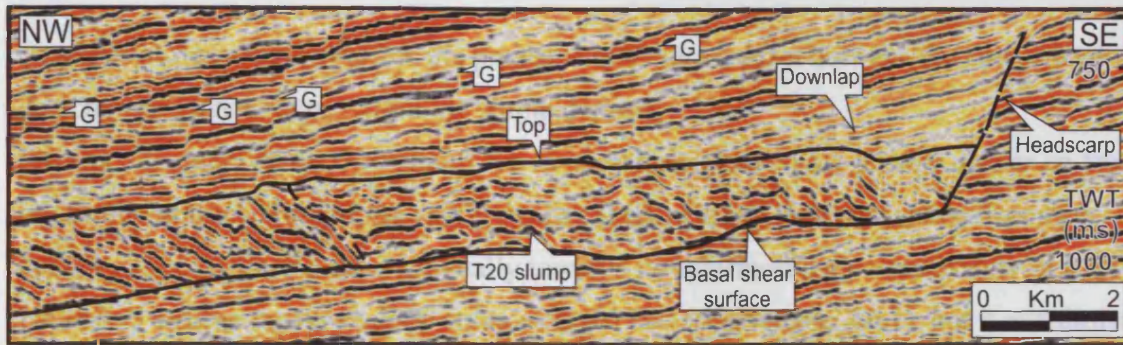


Figure 4.15 Seismic profile across the headscarp area of T20 slump. The slump mass appears significantly depressed in relation to the surrounding strata. There is clear evidence of onlap. The internal parts of the slump deposit are dominated by deformational extensional and compressional structures (separated by the dotted white line).

...ect to the undeformed slope (arrow) (Figure 4.16). The lateral margins of the T20 slump do not correspond to abrupt and vertical limits as those seen for the ISC. In particular, the area where the slump mass thins progressively and is in contact with the underlying and overlying strata (Figure 4.17). This configuration supports the argument that the slump had sufficient momentum to ramp up the basal shear surface and move downslope freely over the seabed.

The basal shear surface of the T20 slump corresponds to a distinct and continuous horizon that is generally sub-horizontal and concordant with the underlying strata. This configuration changes near the headscarp, where the basal surface cuts up section and exhibits a listric geometry (Figure 4.15), and in the frontal parts of the toe region, where it forms a minor ramp (Figure 4.16). On seismic profiles, the basal shear surface appears as a negative high-amplitude reflection that follows the same bedding planes below most of the slump deposit. No evidence of large-scale topographic ramps similar to those of the ISC is observed; indicating the same degree of erosion over the whole area and the strong influence of one bedding-plane parallel surface in controlling the basal shear plane morphology. From measurements made on serial depth converted seismic sections, we estimate that the maximum level of entrenchment of the basal shear surface of the T20 slump (measured from the undeformed slope section) is c. 50 m in the core of the toe region. Together with its generally concordant nature and minor evidence of erosion, this small amount of entrenchment suggests that the frontal parts of the T20 slump overrode its ramp, and formed a positive feature on the coeval seafloor. It is possible however that as the landslide translated downslope, it incorporated some seafloor material which would explained the minor frontal ramp on the shear plane.

observation from Figure 4.15 is the presence of a clear contact between the extensional and compressional zones within the slump deposit.

The toe region of the T20 slump can be clearly mapped on 3D seismic data as an area of prominent thickening of the slump deposit (Figure 4.14). Here, the slump deposit is thicker in the centre and thins gradually towards its outermost parts. Importantly, it is not buttressed against the downslope strata as is the ISC (see **Section 4.6.1**), but it overthrusts the undeformed slope position for up to 10 km forming an interval of highly deformed and chaotic seismic facies (Figures 4.16 and 4.17). The toe region creates a positive topographic feature with respect to the undeformed slope datum (Figure 4.16). The lateral margins of the T20 slump do not correspond to abrupt and vertical limits as those seen for the ISC, but to extensive areas where the slump mass thins progressively and is concordant with the underlying and overlying strata (Figure 4.17). This configuration supports the argument that the slump had sufficient momentum to ramp up the basal shear surface and move downslope freely over the seabed.

The basal shear surface of the T20 slump corresponds to a distinct and continuous horizon that is generally sub-horizontal and concordant with the underlying strata. This configuration changes near the headscarp, where the basal surface cuts up section and exhibits a listric geometry (Figure 4.15), and in the frontal parts of the toe region, where it forms a minor ramp (Figure 4.16). On seismic profiles, the basal shear surface appears as a negative high-amplitude reflection that follows the same bedding plane below most of the slump deposit. No evidence of large-scale topographic ramps similar to those of the ISC is observed; indicating the same degree of erosion over the whole area and the strong influence of one bedding-plane parallel surface in controlling the basal shear plane morphology. From measurements made on serial depth converted seismic sections, we estimate that the maximum level of entrenchment of the basal shear surface of the T20 slump (measured from the undeformed slope section) is c. 50 m in the core of the toe region. Together with its generally concordant nature and minor evidence of erosion, this small amount of entrenchment suggests that the frontal parts of the T20 slump overrode its ramp, and formed a positive feature on the coeval seafloor. It is possible however that as the landslide translated downslope, it incorporated some seafloor material which would explained the minor frontal ramp on the shear plane.

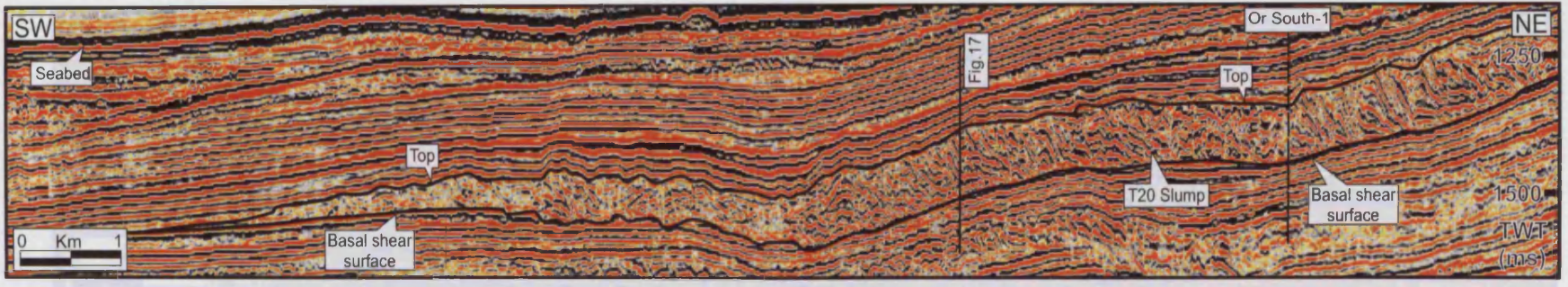


Figure 4.16 Seismic profile across the toe region of T20 slump. The slump mass overrides the coeval seafloor and thins significantly towards its distal parts. The internal parts of the T20 slump deposit are dominated by thrust structures dipping basinwards.

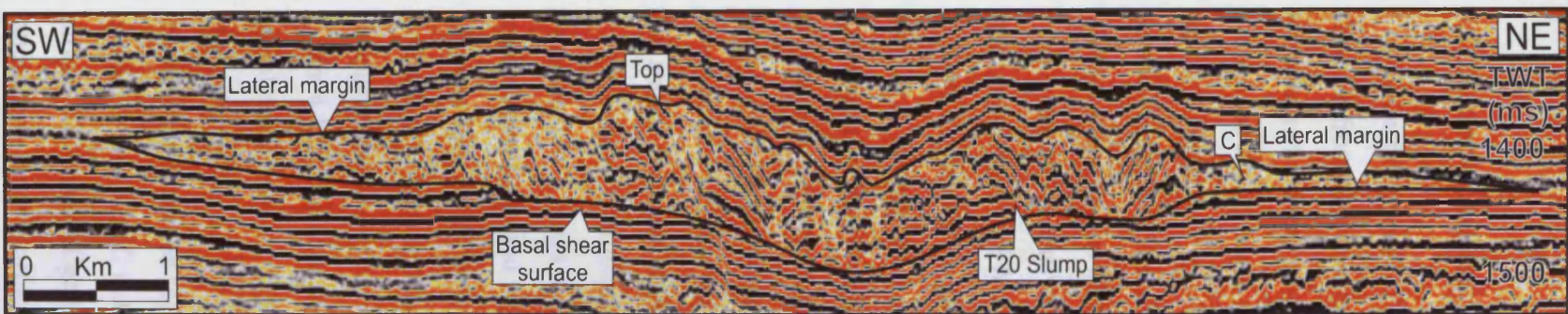


Figure 4.17 Seismic profile across the toe region of T20 slump in the strike direction. The slump mass overrides the coeval seafloor. The lateral flanks are concordant with the overlying and underlying strata and thin gradually towards the distal parts. The internal parts of the T20 slump deposit are dominated by thrust structures. C marks the position of a possible outrunner block. The direction of translation of the slump mass is approximately perpendicular to the seismic section.

4.7.2 Internal seismic character of the toe region

The best overview of the seismic character within the toe region of the T20 slump is obtained from the seismic amplitude response of its deformed interior. Figure 4.18a is an extraction of the maximum seismic amplitude computed between the basal shear surface and the top of the slump mass. From this image, it is evident that the core of the toe region is dominated by high amplitudes, whereas the outermost parts have low to medium seismic responses. This difference in seismic amplitudes is here interpreted to represent changes in the degree of deformation (i.e. high and low amplitudes correspond to moderately and intensively deformed material, respectively). When viewed in detail, there are a series of SW-NE trending lineations within the zone of high amplitudes. The contacts between the high and low amplitude areas correspond to well-defined lineations parallel to the perimeter of the slump (A in Figure 4.18a). Towards the frontal parts of the toe region, the high-amplitudes adopt a more “crumple-like” geometry and form a series of concentric features running almost parallel to the perimeter of the slump (C in Figure 4.18a). A series of lineaments trending principally in a NW-SE direction are also observed (D in Figure 4.18a). These lineaments can be traced continuously for up to 3 km and appear to fragment the core of the slump mass into a series of elongated blocks.

On seismic profiles in the dip direction (Figure 4.16), the core of the toe region is dominated by a series of inclined and continuous reflections that dip landwards, decrease in size basinwards and produce clear topographic expressions on the top of the slump. These reflections correspond to the high amplitude responses seen in Figure 4.18a. Towards the outermost parts of the toe region, the reflections diminish in size or totally disappear (Figure 4.16). This coincides with the low to moderate amplitudes observed in Figure 4.18a. The core and outermost parts of the toe region are separated by minor-scale lateral ramps (<40 m; Figure 4.17) that correlate with lineations parallel to the perimeter of the slump deposit in Figure 4.18a (marked A). The “crumple-like” geometries in the frontal parts of the toe region are correlated to small-scale block-like features of pseudo-parallel reflections (C in Figure 4.17). The blocks appear detached from the basal shear surface. This internal geometry compares locally with the interior of a major submarine landslide in the subsurface offshore Angola (e.g. Gee et al., 2004).

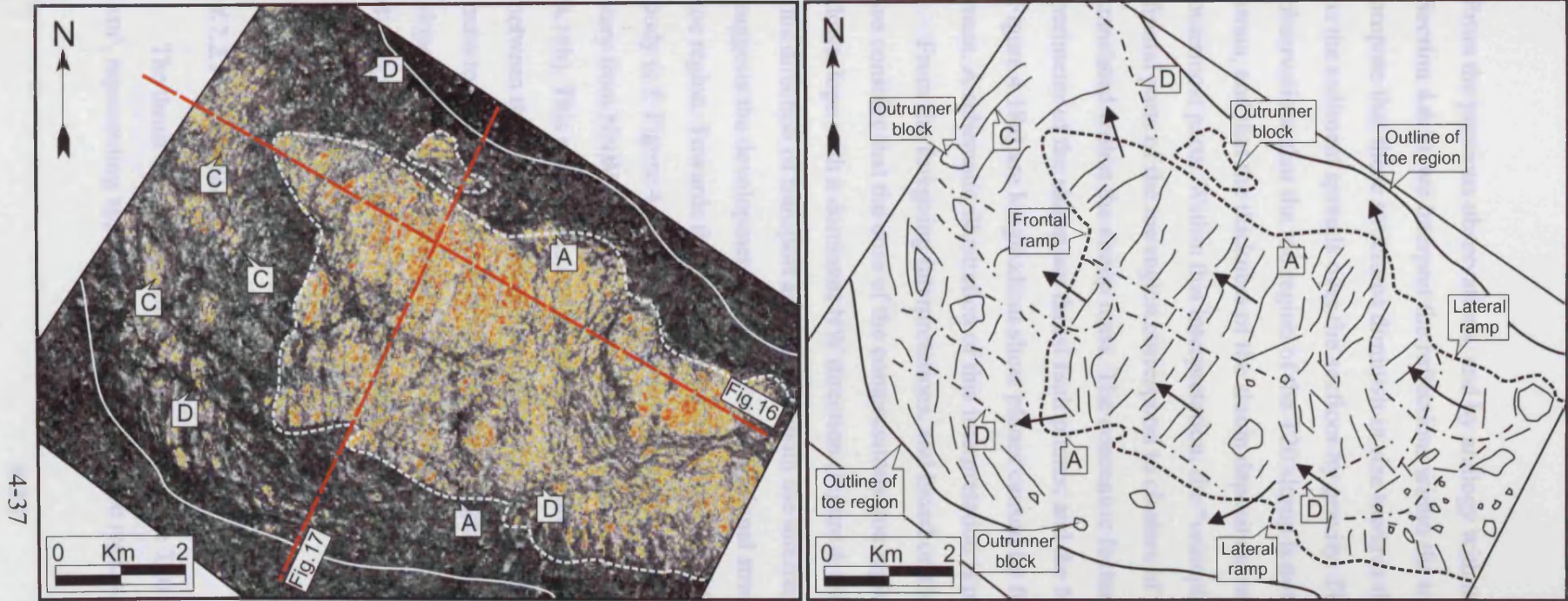


Figure 4.18 (a) Maximum amplitude seismic extraction within the toe region of the T20 slump. Note the presence of high amplitudes in the core of the toe. These correspond to an area dominated by thrust structures. Towards the lateral and frontal parts the amplitudes diminish. The core and the outermost parts are separated by a clear limit between high and low amplitudes. In the frontal parts, the slump material shows clear concentric arc-like structures, which correspond to thrust planes. There are also clear dislocation planes (marked as D). (b) Schematic depiction of the interpretation of the internal parts of the toe region of the T20 slump.

4-37

From the previous observations, and by analogy with the internal parts of the ISC (see **Section 4.6.2**), we interpret the reflections within the toe region as thrust structures. We propose that these structures diminish in size towards the outermost parts of the toe region as the sediment spreads over the seafloor by gravity. This is supported by the observations that the toe region of the T20 slump is not buttressed against the downslope strata, and that the thickness of the slump deposit decreases gradually towards its outermost parts. Within this interpretation, the “crumple-like” geometries observed in the frontal parts of the toe region correspond to clusters of rafted blocks that have been translated within the slump mass. The concentric features running parallel to the perimeter of the slump are thrust fault planes; and the NW-SE trending lineaments (D in Figure 4.18a) are longitudinal shear planes caused by frictional stresses within the slump mass. A schematic illustration of this interpretation is presented in Figure 4.18b.

From the foregoing interpretations, and based on the same rationale used for the ISC, we consider that the core of the compressional toe region of the T20 slump propagated downslope with a dominant NW direction (Figure 4.18b). As previously seen for the ISC, this direction of transport accords well with the inferred down-palaeoslope trend. This suggests the development of simple compressional stress regimes within these parts of the toe region. Towards the lateral flanks, conversely, the fan-like planform of the slump body (c.f. Figure 4.14) indicates a more complex situation with a set of directions that vary from NNW (northern flank of the toe region) to SSW (southern flank) (Figure 4.18b). This variation is considered here as indicative of a change in the kinematics between the core and outermost parts of the toe region due to the tendency of the slump mass to spread laterally under the influence of gravity due to the overall low regional slope. From the presence of NW-SE trending longitudinal shear planes (D in Figure 4.18a), we propose that different rates of downslope displacement of the slump mass were generated during its translation and these resulted in the creation of frictional stress regimes within the sediment mass.

4.7.2.1 Dimensions of the thrust structures

The thrust features within the toe region of the T20 slump extend over an area of c. 30 km², representing approximately 80% of the toe region (Figure 4.18a). In plan view,

individual thrusts can be traced for over c. 1 km in the strike direction; they are regularly closely spaced. On seismic profiles in the dip direction, individual thrusts extend over heights varying from 75 to 125 m (average ~85m), tip to tip distances are 100-150 m and lengths perpendicular to the strike direction range between c. 200 m and 1 km. Typical thrust plane angles of dip are 10°-25° and the maximum thrust displacement in each structure is c. 20-30 m. The minimum shortening associated with these thrust structures has been computed in a similar way to that of the ISC (i.e. number of thrusts multiplied by their maximum horizontal displacement). Forty-one thrusts have been observed in the core of the toe region of the T20 slump, giving an overall shortening of c. 1.25 km. Lack of correlatable marker horizons has precluded a more detailed analysis.

In summary, the T20 slump corresponds to a large-scale *frontally emergent* submarine landslide within the Early-Late Pleistocene succession. It overlies a shallow and concordant basal shear surface that corresponds to the same stratigraphic bedding over most of its areal extension. The basal shear surface ramps up the stratigraphy in the headscarp and frontal parts of the toe region. The compressional toe region forms a positive topographic feature that moved freely over the seafloor and is divided into two main areas: core and margin. The core is a high-relief zone dominated by imbricated thrust structures that extend downslope in a NNE direction. The outermost parts, instead, correspond to low-relief areas comprised by chaotic reflections where material decoupled from the main body and spilled over the seafloor to form fan-like deposits. The contacts between the two areas overlie minor-scale lateral and frontal ramps on the basal shear surface (cf. Figures 4.17 and 4.18). There is clear evidence of upslope depletion of sediment.

4.8 Discussion

The most important observations from seismic interpretation of the two compressional toe regions analysed in the previous sections are summarised as follows as the basis for the discussion below:

- The compressional toe region of the ISC is a large-scale feature that is entrenched and confined within the underlying and surrounding strata. It is flanked by abrupt

and steep (c. 25°) lateral ramps below the level of the undeformed slope section (see **Section 4.6.1**). Its frontal ramp is significantly inclined (c.50°) and continuous surface against which the slump mass is buttressed.

- The thickness of the slump mass increases considerably within the toe region. However, this does not result in the building of a significant positive topographic relief with respect to the undeformed slope datum. This suggests that the increase in volume of sediment did not occur by assimilation of material during slumping, but by the progressive entrenchment of the slump mass into the underlying strata.
- The internal parts of the compressional toe region of the ISC are dominated by moderately deformed strata. Imbricate thrusts are also observed. Discrete thrust structures are detached from a common basal shear surface, and ramp up to locally deform the upper boundary of the slump. In plan view, the thrusts link in closely related branching arrays that extend in a dominant N-S direction over an area of c. 2500 km².
- The basal shear surface of the ISC corresponds to a deeply entrenched horizon (c. 200 m) that can be traced continuously below the slump complex. This surface can be either planar and conformable horizon or ramp up and down the stratigraphy to create a series of staircase-like geometries (see Figure 4.8). Locally, it exploits the strata of contourite drift deposits where it becomes deeply entrenched (Figure 4.9).
- The compressional toe region of the T20 slump is a large-scale feature of variable thickness (thinning from its core to outermost parts) that forms a positive topographic relieve above the original seabed. It is flanked by lateral margins where the slump mass thins gradually outwards and is concordant with the underlying and overlying strata (see Figures 4.14 and 4.17). In its frontal parts, the slumped material overrides the undeformed slope datum (see Figure 4.16).
- The core of the compressional toe region of the T20 slump is dominated by imbricated thrust structures that are linked via a continuous basal shear surface. Its outermost parts are dominated by deposits of chaotic material and rafted blocks.

- The basal shear surface of the T20 slump corresponds to a shallow (c. 30 m) plane that is concordant with the underlying strata except in the outermost parts of the toe region (frontal and lateral), where it ramps up stratigraphy.

From the preceding observations, it is evident that the key difference between the two compressional toe regions described in this chapter is their mode of frontal emplacement. The toe region of the ISC corresponds to a *frontally confined* feature in which the slump mass is buttressed against the downslope undisturbed strata. Conversely, the compressional toe region of the T20 slump consists of an *frontally emergent* structure in which the sediment has been able to ramp out of the basal shear surface and travel freely over the coeval seafloor. This difference in emplacement between the two landslides demonstrates that the conventional models for submarine landsliding (e.g. Farrell, 1984) do not always apply when compressional toe regions are imaged in detail on 3D seismic data. Indeed, while the volumetric appearance of *frontally emergent* features (i.e. T20 slump) is compatible with such traditional models, the observations from a *frontally confined* toe region (i.e. ISC) have provided compelling evidence for inferring different genesis and formational mechanisms.

Over the last three decades, many previous investigators have described the mechanisms of *frontally emergent* submarine landslides (e.g. Lewis, 1971; Farrell, 1984; Jansen et al., 1987; Bugge et al. 1988; Martinsen, 1989; Moore et al., 1989; Martinsen and Bakken, 1990; Lee et al., 1999; Bøe et al., 2000; Strachan, 2002). As a result, it is now well established that landslides emerge over the seabed when they gain sufficient inertial energy to abandon their basal shear surfaces. Conversely, only four preceding studies have described what we would class as *frontally confined* submarine landslides (e.g. Trincardi and Normark, 1989; Trincardi and Argnani, 1990; Huvenne et al., 2002; Lastras et al., 2004). All these investigators have recognised that in *frontally confined* landslides, material is only slightly displaced and does not outflow significantly over the ramp. They have all attributed such configuration to a negligible downslope component of the sediment transport during landsliding.

Trincardi and Argnani (1990) used 2D seismic data to map a submarine landslide (the Gela Slide) within the Plio-Quaternary foredeep of Sicily (offshore Italy). These investigators described the internal parts of the main slide-body as maintaining their

plane-parallel and laterally-continuous reflector patterns and without evidence of significant internal deformation. In the slide toe, however, they observed coherent seismic reflections with imbrications, folds and thrusts dipping in the direction of transport. Trincardi and Argnani (1990) attributed the frontal confinement of the Gela Slide to the presence of a basinwide morpho-structural obstacle. Such confinement occurs where a positive topographic feature provides the necessary resisting forces to prevent further translation. As a result, the sliding material halts abruptly and deforms due to a compressional strain wave that propagates from the area of impact with the topographic obstacle.

Huvenne et al. (2002) employed a combination of 2D and 3D seismic data to analyse a *frontally confined* submarine landslide in the western Porcupine Basin (offshore SW Ireland). According to these authors, this landslide '*does not exhibit the traditional picture of a fully developed slump or slide*' but corresponds to a '*failure that never broke through or overthrusted the downslope sediments*'. Such configuration is strikingly analogous to that of the ISC. Huvenne et al. (2002) proposed a combination of abrupt release of the pore pressure along the failure plane and low slope angles to explain the striking architecture and mode of emplacement of this feature.

Lastras et al. (2004) used high-resolution swath bathymetry and very high-resolution seismic data to investigate the geometry and internal structures of four slides on the seafloor of the Balearic margin (offshore Spain). These investigators recognised a series of chaotic seismic facies at the slide toes, which they interpreted as a lesser degree of sediment disruption compared with the upper parts of the slides. They also demonstrated that thickening in the toe regions did not correspond to significant topographic expressions (similar observations have been presented in the present chapter for the ISC; see **Section 4.6.1**). Lastras et al. (2004) concluded that in the case of *frontally confined* submarine landslides, '*modest material transfer is accompanied by the downslope propagation of the deformation front that extensively remoulds the slope sediment without necessarily translating it very far downslope*'.

Frontally confined submarine landslides have thus been identified in a number of different continental margins worldwide. In these earlier studies, however, a lack of more extensive data has prevented a more detailed analysis being made of what parameters

control the frontal confinement of landslides. The model based on morpho-structural obstacles by Trincardi and Argnani (1990) offers a unifying explanation for the external and internal appearance of some *frontally confined* features. Such mechanism could, for instance, potentially explain many of the deformational structures observed within the ISC (see Section 4.6.2). It would, however, require the presence of a large-scale morpho-structural barrier in order to prevent the movement of such a vast volume of material (c. 1000 km³) throughout such an extensive area (c. 4800 km²). In addition, in the context of a topographic obstacle impeding the translation of the ISC, we would expect major lateral variations in the amount of contractional strain throughout the landslide mass (i.e. more intense near the topographic obstacle and less intense in further areas). Since neither of these circumstances have been observed from the 3D seismic data, topographic confinement is not considered here as a viable mechanism to explain the frontal emplacement of the ISC. This is a critical conclusion that excludes an external controlling factor and points to an internal cause related to the emplacement mechanism itself.

4.9 Mechanics

Critical insight into a possible internal controlling factor for the frontal confinement of the ISC can be derived from its morphological characterisation. 3D seismic mapping has revealed that the depth to the basal shear surface from the level of the pre-deformational slope template of the ISC is large by global standards (>400 m; Figure 4.9) when compared to the T20 slump (<50 m; Figure 4.17) or the majority of submarine landslides described in the literature (Hühnerbach and Masson, 2004). The importance of the depth to detachment for the frontal confinement of a submarine landslide lies mainly on its capacity to determine the aspect ratio of the slab of sediment affected by failure.

Landslides develop above areas where poor drainage allows slope-normal effective stress to decrease to values sufficiently below the slope-parallel effective stress of the sediment (Mandl and Crans, 1981). As a landslide moves, potential energy is lost in deforming a toe region to create accommodation space and may concurrently be gained if retrogressive failure extends the head region updip (i.e. new material is added). In this situation, the toe region deforms around a ramp where the basal shear surface reaches the

seabed thus creating a listric morphology. Immediately upslope of the ramp, the landslide creates accommodation space by lateral compaction, folding and extrusion, the latter being emergence in the terminology of this paper. For equal slope angles, where the ratio of length to height is relatively low, the deviatoric slope-parallel effective stress across the ramp will be relatively low and the surface area of the ramp relative to that of the basal slope plane will be relatively high. Resistance to motion is thus relatively large: moreover, the landslide can move only relatively short distance before its centre of gravity reaches an elevation equal to that of the lip of the ramp. Its inertia is thus relatively low and proportionately more of the available energy would be needed if material is to be raised up the ramp (where frictional resistance is far greater than along the basal slip plane). Under such conditions, it is here suggested that the most efficient use of landslide energy for further propagation is to deform the footwall rather than override it. Downslope displacement then mainly ensues by the deformation of the foreland and its integration within the frontal parts of the landslide (Figure 4.20). Within such scenario, each translational episode is conceived to correspond to a thrust structure (evidence for this has been observed from the toe region of the ISC). Emergence of landslide material is thus improbable unless the landslide behaves as a fluid. In this specific case, the top surface of the confined slide would be a palaeohorizontal and this is not observed in the ISC.

By contrast, where the ratio of length to height of the slide is high, resistance to motion across the ramp is a relatively low portion of the frictional resisting forces and the landslide has greater opportunity to acquire appreciable momentum. The increased internal shear strains thus generated probably result in far greater re-constitution of material than in the former case with resultant relative increase in its fluidity. This, together with greater momentum, makes for greater extension in the landslide depletion zone and this is observed in the T20 Slide. Both factors, and the relatively smaller elevation required to override the ramp, equally facilitate extrusion. It is here suggested in this case, that the footwall cannot deform fast enough to accommodate the sliding mass and this hence thickens until emergence and spreading result. Clearly the landslide material still retains some cohesion as subsequent downslope gravitation spreading does

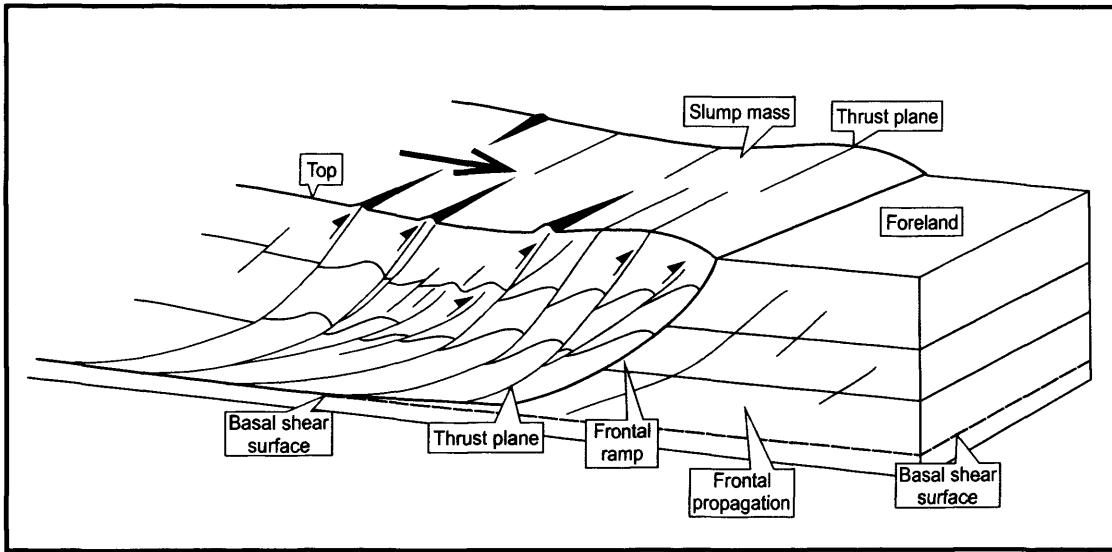


Figure 4.19 Schematic depiction of the suggested mechanism for downslope translation of frontally confined submarine landslides. The material does not override the frontal part but translates downslope by deforming and integrating the foreland into the frontal parts of the slump. In this scenario, each thrust structure correspond to a single event of downslope advance.

not totally remove the observed topographic relief above the ramp over which emergence took place.

Having presented an albeit speculative argument that the major controlling factor governing the development of frontally confined slides is the depth to detachment, a final and important question to be addressed is the possible control for the depth to detachment of submarine landslides. Martinsen (1994) proposed that the position of a basal shear surface is mainly determined by the pressure gradient in the sediment. According to Martinsen (1994) “*where the pore pressure approaches or balances the normal stress induced by the weight of the overburden, the shear strength is sufficiently reduced to allow slippage along a basal shear surface, given a sufficiently high shear stress*”. The increase in pore pressure may result from the presence of permeability barriers: such commonly occur at clay-rich intervals.

The most striking observation of the basal shear surface of the ISC is that it becomes significantly entrenched where it exploits contourite drift deposits from the Early Pliocene (see Figure 4.9). This coincidence strongly suggests that there is a genetic link between the depositional (grain) fabric of the contourite deposits and the position of the basal shear surface. Lithological calibration at the Gaza marine-1 exploration well has revealed that the contourite deposits underlying the ISC are mainly composed of fine-grained clastic sediments (i.e. claystones and siltstones). It is therefore reasonable to infer that permeability barriers could have developed along the clay-rich intervals within the contourite deposits. This could have resulted in the creation of distinct stratigraphic levels that were prone to overpressuring and hence act as basal shear surfaces. From these arguments, it is proposed that the depth to detachment of the ISC was mainly controlled by the lithologic properties of the underlying contourite deposits. Speculatively, the basal shear surface of the ISC may correspond to a stratigraphic level with a relatively impermeable mixed composition of fines and organic matter. Submarine landslides affecting contourite drift deposits are not uncommon having been extensively described, for instance, from the NW European continental margin (e.g. Storegga Slide; Bryn et al., 2003; Trænadjupet Slide; Laberg et al., 2003; Nyk Slide; Lindberg et al., 2004).

In this chapter it has been demonstrated that *frontally confined* submarine landslides occur on a basin-wide scale, and that their mechanisms of formation are significantly

different from those of *frontally emergent* features. The results presented here should be of broad interest, because the conditions for frontally confinement of submarine landslides are not unusual and similar geological contexts in which they could arise are widely developed in other continental margins (e.g. North and South Atlantic, Western Mediterranean Sea). Many of the slope instability processes in these other continental margins are attributed to “in situ” landsliding and it is an intriguing prospect that a significant proportion of the submarine landslides ascribed to these processes could also be potentially explained by frontal confinement. A further conclusion from this work is the possible importance of contourite drift deposits in controlling the occurrence and mechanisms of translation and emplacement of slope failures. Submarine landslides affecting contourite drift deposits have been observed in other deepwater environments such as the Faroe-Shetland Basin (e.g. Bryn et al., 2003; Knutz and Cartwright, 2004; Laberg et al., 2003; Lindberg et al., 2004) or the Mid-Norwegian Margin (e.g. Bryn et al., 2005) and this demonstrates the necessity for a more in depth and global analysis of their association in terms of triggering mechanisms and kinematics.

4.10 Conclusions

- 3D seismic interpretation in the Israeli continental margin has demonstrated the existence of two main types of submarine landslides: *frontally confined* and *emergent*.
- *Frontally confined* submarine landslides have their compressional toe regions buttressed by the ramp separating their fill from their foreland. They do not show a prominent bathymetric expression compared to their total thickening and imply a modest downslope transfer of sediment.
- *Frontally emergent* submarine landslides have their compressional toe regions above the coeval downslope undisturbed strata, having overridden their ramps. They show major bathymetric expressions and involve the downslope transport of significant volumes of material.
- The internal parts of both *frontally confined* and *emergent* submarine landslides show highly disrupted to chaotic seismic facies (i.e. imbricate thrust systems have

been observed in both types of submarine landslides). However, *frontally confined* submarine landslides reveal evidence of more preserved internal stratification (e.g. sub-horizontal reflections and blocks of intact strata).

- *Frontally confined* submarine landslides translate downslope by bulldozing the foreland. Downslope translation is interpreted to stop when the stress developed by the slump mass becomes lower than the strength of the foreland.
- *Frontally emergent* submarine landslides translate downslope by overthrusting the downslope undisturbed strata. They may travel freely over the undeformed slope position possibly evolving into debris flows and turbidity currents.
- Analysis of the geometries of *frontally confined* and *emergent* submarine landslides suggests that the frontal emplacement of submarine landslides depends on the position of their centre of gravity. This is in turn a function of the depth to detachment of the submarine landslide, their length and the tip of the slope. Based on this argument, it is proposed here that (under equivalent conditions) frontal confinement is more likely to occur if a landslide translates over a deeply entrenched basal shear surface relative to its length.
- Variations in the foundation of the slumps, in this case, the existence of contourite drift deposits, can play a critical role in the entrenchment of submarine landslides and hence lead to their frontal confinement.
- Similar processes of frontal confinement of submarine landslides may occur widely in other continental margins.

Chapter Five: Summary and discussion

5.1. Introduction

In this study, integrated industry seismic (2D and 3D) and well data have been employed to address the problem of soft-sediment deformation on the continental margin of Israel and its impact on the exploration and production of hydrocarbons. This research has focused on the two major types of soft-sediment deformational processes in the region: clastic diapirism (**Chapter 2**) and submarine slope instability (i.e. submarine slumping; **Chapters 3 and 4**). The combination of seismic and borehole data has provided an excellent coverage of the margin and has enabled soft-sediment deformational features to be analysed to a high degree of precision that could not have been achieved by any other combination of methods. This has provided much new insight into the typology of the soft-sediment deformational structures in the study area, their 3D geometries, internal fabrics and mechanisms of formation. The results presented in the previous chapters have thus fulfilled the aims listed in **Chapter 1**.

The main aim of the present chapter is to draw together the key scientific results presented in the preceding chapters in order to erect an integrated model for the phenomenon of soft-sediment deformation on the continental margin of Israel. A secondary aim is to examine the role of soft-sediment deformation in the petroleum geology of the area. The previous chapters are structured in three semi-independent units, in a format resulting from the different emphasis required to address the key problems raised during this research. In this final chapter, therefore, it is intended to amalgamate the observations and analysis undertaken during this study and to merge them into a unified geological model. The chapter commences with a summary of the most notable results and findings of this research which were described and discussed in **Chapters 2, 3 and 4**. The main arguments of the chapter are subsequently developed by discussing three key themes: (i) a time-space reconstruction of soft-sediment deformation on the Israeli continental margin, (ii) its effects on the exploration and production of hydrocarbons, and (iii) a review of worldwide analogues. Finally, a summation of possible future avenues of research concludes this chapter.

5.2. Summary of results

5.2.1 Results from the analysis of clastic diapirism (Chapter 2)

Chapter 2 presented a pioneering work on a process of soft-sediment deformation that had not been previously documented from the continental margin of Israel: clastic diapirism. The principal objective of this chapter was to describe and unravel the genesis of a series of intriguing mounded features confined to the Afik Submarine Canyon and restricted to the Lower Pliocene intervals. A resultant aim was to examine their possible implications for the exploration and production of hydrocarbons. Indeed, the studied features host some of the largest gas fields discovered to date offshore Israel, so an accurate understanding of their formational mechanisms and reservoir properties was believed critical to efficiently assess future operations in the area. At the commencement of this study, the exact origin of the mounded features was unknown. A number of possible explanations had been previously considered in academic and industry circles salt diapirism and sand remobilisation being the two most commonly accepted (Hall, pers. comm. 2002). These models provided a partially satisfactory account of the overall geometries and geological context of the mounded structures. However, none of them offered unifying answers for their external and internal appearance, relationship to the encasing strata and lithological composition.

The research undertaken in **Chapter 2** provided an alternative explanation that is here considered to be significantly better than the previous models. Based on the analysis of the 3D seismic and well data, it was proposed that the mounded structures were formed by the forceful intrusion of clastic sediment into a shallow-level sedimentary host rock (Yafo Sand Member). It was advocated that important amounts of mud-rich sediments from the Bet Guvrim and Ziqim Formations within the Afik Submarine Canyon were remobilised and injected at the base of the Yafo Sand Member. This process hydraulically deformed the overlying strata of the Yafo Sand Member into a series of four-way dip mounds. The continuous reactivation of this process and its simultaneity with the deposition of the Yafo Mudstone Member during the Pliocene caused a series of thickness variations and deformational structures (i.e. faults and forced folds) in the

sedimentary overburden. Similar processes were invoked to explain the presence of ridge-like structures along the northern flank of the Afiq Submarine Canyon. The conclusions obtained from **Chapter 2** highlighted, amongst others, the significance of clastic diapirism for the generation of hydrocarbons traps, the creation of permeability barriers and the alteration of reservoir geometries.

5.2.2 Results from the 3D seismic analysis of slump complexes (Chapter 3)

Chapter 3 provided a comprehensive examination of submarine slumping on the continental margin of Israel. The research efforts were focused on three main subjects. The first consisted of defining the criteria to recognise and describe slump deposits on 3D seismic data. This allowed a simple and standardised methodology that could be implemented when examining both deeply buried and shallow features to be erected. The second subject was the construction of a seismic-stratigraphic framework for submarine slumping in the southern parts of the margin where the resolution of the data was superior. Three seismic-stratigraphic units (T30, T20 and T10) were defined within the post-Messinian interval. This was undertaken in order to evaluate the temporal and spatial evolution of the slump deposits, and was attained by tying the seismic data with the information provided by the ten exploration wells located in the area. The third subject was the detailed analysis of two representative case studies of submarine slump complexes (i.e. ISC and GSC). This was done fundamentally to investigate the external and internal architecture of sediment instabilities, their failure dynamics and resulting deposits. Exceptional seismic imaging provided by the 3D seismic method allowed an accurate analysis of the two slump complexes using a wide range of modern attribute-based interpretation techniques.

The results obtained from the seismic-stratigraphic analysis of the slump deposits in the southern Israeli continental margin revealed that the entire post-Messinian interval is intrinsically affected by slope instability. It was calculated, that an average of c. 15% of the total post-Messinian sedimentary column had been affected by submarine slumping, and that this value could increase to c. 30% within the Pliocene interval. It was also recognised that individual slump complexes (i.e. ISC) could involve up to c. 1000 km³ of

sediment, placing them amongst the biggest documented examples of submarine landslides in the world (e.g. Storegga Slide; Bugge, 1983). Importantly, no evidence of failure was observed within the pre-Messinian column. It was proposed that the main factors predisposing the region to be so susceptible to recurring failure were: seismicity, presence of gas in the sediment and local slope oversteepening. Other significant results attained from the seismic-stratigraphic analysis were: (i) the recognition that the failures tend to concentrate in areas overlying regional structures such as the Syrian Arc system or large pre-Messinian submarine canyons (e.g. the Afiq and el-Arish), (ii) the identification that slump deposits form sets of vertically stacked features, and (iii) the tendency of slump deposits to diminish in size and increase in number towards the shallowest parts of the continental margin.

The most important result from the detailed 3D seismic interpretation of the ISC and GSC was the definition of a spectrum of external and internal geometries for the slump deposits in the area. It was observed that each slump body could be divided into two main zones (*sensu* Varnes, 1978): depletion zone and accumulation zone. The depletion zone is located in the upslope sectors of the slump and is characterised by extensional deformational structures and removal of sediment. The accumulation zone is situated in the downslope parts of the slump body and is dominated by compressional features and addition of material. Other critical results from the 3D seismic interpretation were: (i) the recognition of numerous representative features within the slump deposits (e.g. headscarp, toe, lateral margins, basal shear surface, crown-cracks, “*in situ*” blocks, etc.), (ii) the identification of the transport directions of the slumps, (iii) the recognition that slump reactivation may occur both by retrogressive upslope failure, and by downslope propagation (out-of-sequence) failure, (iv) the identification of potential areas for slope instability (i.e. proto-slumps), and (v) the appreciation that the ISC is a frontally buttressed feature.

5.2.3 Results from the analysis of compressional toe regions (Chapter 4)

Chapter 4 built upon many of the observations and arguments presented in **Chapter 3** in order to unravel the mechanisms and controlling factors for the frontal emplacement

of submarine landslides. One of the main objectives of this chapter was to understand why some submarine landslides become *frontally confined*, whereas others form *frontally emergent* features. For this purpose, the research was concentrated on the detailed examination of the compressional toe regions of two slump deposits (i.e. ISC and T20 slump). These were used as representative examples of *frontally confined* and *emergent* submarine landslides, respectively. The geometries of the two compressional toe regions, their relation to the surrounding strata and their internal fabrics were thoroughly analysed using the high resolution provided by the 3D seismic data. From their comparison, the two forms of frontal emplacement, their mechanisms, possible causes and the response of the sliding masses were discussed.

The most critical result from this approach was the recognition that the frontal emplacement of submarine landslides is mainly controlled by their depth to detachment. Comparison of the ISC and the T20 slump suggested that *frontally confined* landslides are more likely to occur along deeply entrenched basal shear surfaces, whilst *frontally emergent* features tend to develop along shallow detachment levels. This was explained by the position of the centre of gravity of the sliding mass: if the centre of gravity falls below a certain point, then the weight of the sliding mass will prevail over its inertial energy and frontal confinement will ensue. Instead, if the centre of gravity remains on a relatively shallow level, the inertial energy will be sufficient for the landslide to emerge and travel freely over the seafloor. Based on the internal fabrics of the two case studies and their relationships with the surrounding strata, it was proposed that *frontally confined* submarine landslides translate downslope by the deformation of the foreland and its integration in the frontal parts of the feature. Instead, the downslope advance of *frontally emergent* features was interpreted to occur by gravity spreading of the sliding mass. The connection between depth to detachment and lithostratigraphy was also highlighted in this chapter.

5.3. Time-space reconstruction of soft-sediment deformational processes offshore Israel

This thesis has demonstrated that the deformation of soft-sediments is an intrinsic facet of the Israeli continental margin. It has also established that clastic diapirism and slope failure are the two prevalent types of deformation, and that they occurred during the post-Messinian history of the continental margin. In the present section, a time-space depiction of such processes is drawn in order to evaluate their evolution through time, their location in the basin and their connection with the regional geology of the area.

Soft-sediment deformation on the continental margin of Israel commenced during the Middle Zanclean (c. 4 Ma BP) with the initiation of the mounded structures along the Afiq Submarine Canyon (Figure 5.1; see **Section 2.8**). This process remained active until the Early Gelasian (c. 2.5 Ma BP), when the two longest-lasting mounded structures (i.e. NMC and the MMC) became inactive. During this period, submarine slope failure was absent. The formation of the mounded structures coincided with an interval of intense regional seismic activity (e.g. Robertson, 1998; Vidal et al., 2000; Huguen et al., 2001), and this has been proposed herein as a possible triggering mechanism for their development (see **Section 2.10.2**). Concurrently to the formation of the mounded structures, large amounts of fine-grain siliciclastics were deposited in the basin (i.e. Yafo Mudstone Member; Figure 5.1a). These sediments were mainly derived from the Nile River and were associated with the first stages of the Pliocene transgression after the Messinian Salinity Crisis (e.g. Gvirtzman and Buchbinder, 1978; Buchbinder and Zilberman, 1997). Continuous sedimentation resulted in complete draping of the mounds and in the construction a c. 350 m thick prograding and aggrading slope wedge in which local contourite drift deposits formed.

During most of the Gelasian, siliciclastic deposition of the Yafo Formation persisted without any significant event of soft-sediment deformation. Consequently, an average of c. 350 m of hemipelagic and turbiditic sediment was uninterruptedly deposited in the slope. This resulted in a rapid basinwards progradation of the entire margin (e.g. Almagor, 1993; Buchbinder and Zilberman, 1997), which was interrupted in the Late

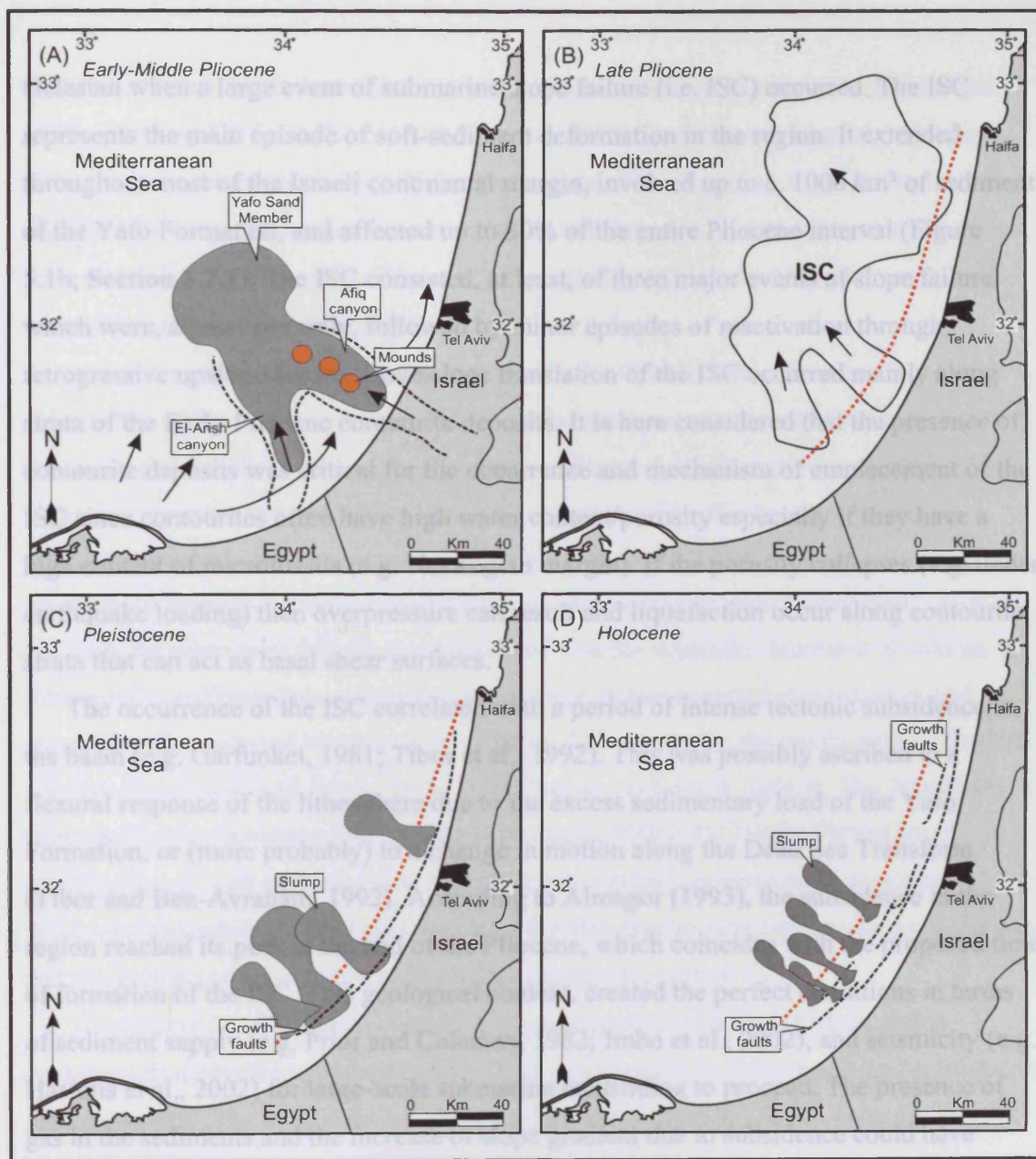


Figure 5.1 Schematic depiction of the different stages and basinal distribution of soft-sediment deformational processes offshore Israel. The red dotted line marks the approximate position of the shelf break at the different stages of the construction of the continental margin.

Gelasian when a large event of submarine slope failure (i.e. ISC) occurred. The ISC represents the main episode of soft-sediment deformation in the region. It extended throughout most of the Israeli continental margin, involved up to c. 1000 km³ of sediment of the Yafo Formation, and affected up to 30% of the entire Pliocene interval (Figure 5.1b; **Section 3.7.1**). The ISC consisted, at least, of three major events of slope failure which were, almost certainly, followed by minor episodes of reactivation through retrogressive upslope failure. Downslope translation of the ISC occurred mainly along strata of the Early Pliocene contourite deposits. It is here considered that the presence of contourite deposits was critical for the occurrence and mechanism of emplacement of the ISC since contourites often have high water content/porosity especially if they have a high content of microfossils (e.g. Norwegian margin). If the porosity collapses (e.g. under earthquake loading) then overpressure can result and liquefaction occur along contourite strata that can act as basal shear surfaces.

The occurrence of the ISC correlated with a period of intense tectonic subsidence in the basin (e.g. Garfunkel, 1981; Tibor et al., 1992). This was possibly ascribed to a flexural response of the lithosphere due to the excess sedimentary load of the Yafo Formation, or (more probably) to a change in motion along the Dead Sea Transform (Tibor and Ben-Avraham, 1992). According to Almagor (1993), the subsidence in the region reached its peak at the end of the Pliocene, which coincides with the proposed time of formation of the ISC. This geological context, created the perfect conditions in terms of sediment supply (e.g. Prior and Coleman, 1982; Imbo et al., 2002), and seismicity (e.g. Hasiotis et al., 2002) for large-scale submarine landsliding to proceed. The presence of gas in the sediments and the increase of slope gradient due to subsidence could have further facilitated slope instability. However, this hypothesis can not be verified with the data available in this research project.

During the Pleistocene, the rates of subsidence and sedimentation decreased significantly throughout the entire basin (e.g. Tibor and Ben-Avraham, 1992). Global eustatic sea-level oscillations and local vertical tectonic movements resulted in repeated transgressions and regressions of the shoreline (e.g. Almagor, 1993; Buchbinder and Zilberman, 1997). Consequently, interbedded sands, clays and marls from the Herfer Formation accumulated on the shelf (e.g. Sivan et al., 1999). Simultaneously, salt

tectonism, which had initiated during the Pliocene, increased in activity (e.g. Almagor, 1980; 1984 and 1986; Garfunkel and Almagor, 1987). In this context, submarine slope failure augmented in number while the dimensions of the resulting deposits decreased significantly compared to those occurred during the Pliocene. As a result, tens of medium-scale slump bodies formed at different stratigraphic levels interbedded with periods of normal hemipelagic deposition (Figure 5.1c).

Recurrent earthquake activity associated with the Dead Sea Transform and salt-driven deformation of the margin were probably the principal causes for the significant increase in the number of landslides during the Pleistocene (Figure 5.1d). In turn, this increase in frequency probably resulted in the volumetric reduction of the Pleistocene deposits in comparison to those of Pliocene age. It is reasonable to infer that as slope failures became increasingly frequent throughout the Pleistocene, the amount of underconsolidated sediment available for subsequent failures diminished and thus the landslides decreased in volume. A further and complementary explanation is that slope failure occurred along shallow and geographically restricted lithological boundaries. This resulted in the mobilisation of limited amounts of sediment and, hence, in the generation of small-scale deposits. This hypothesis is supported by the presence of interbedded lithologies within the Herfer Formation. A combination of both scenarios (i.e. intense seismicity and geographically restricted lithological boundaries) could also provide a feasible explanation for the change in number and dimensions of the submarine landslides during this period.

Throughout the Holocene, a similar margin evolution persisted. Slope failures continued to increase in number and diminish in volume as sedimentation and subsidence rates decreased. The triggering mechanisms for slope failure are herein considered to be identical to the Pliocene and Pleistocene. There is also compelling evidence that numerous slope failures have occurred in very recent times and that further events may occur in the future (i.e. proto-slumps; **Section 3.8**). From these arguments, it is thus clear that the slope area of the continental margin of Israel has not yet reached an equilibrium profile and that submarine failure is still an intrinsic aspect of the region.

5.4. Implications for hydrocarbon prospectivity

Soft-sediment deformation processes can have enormous implications for the exploration and production of hydrocarbons. The overpressuring and mobilisation, whether vertical (e.g. diapirism) or horizontal (e.g. slope failure), of large amounts of undercompacted sediments have the potential to radically modify their architecture, primary sedimentary properties (i.e. porosity, permeability, etc.) and position within the basin. It has been recognised both in this study and in the previous literature (e.g. Løseth et al. 2003; Morley, 2003) that understanding the mechanisms and consequences of such modifications can significantly influence exploration and production strategies. In this section, we present a review of the most relevant implications for the prospectivity of hydrocarbons of the soft-sediment deformation processes presented in this study. The insights depicted herein can also be applicable in other hydrocarbon prone sedimentary basins worldwide.

5.4.1 Implications of clastic diapirism

The implications of clastic diapirism for the prospectivity of hydrocarbons offshore Israel have been previously discussed in this thesis (see **Section 2.10.3**). Therefore, in this section only the most relevant of these implications are listed. These are:

- Clastic diapirism can form effective structural traps for hydrocarbons.
- It can compartmentalise reservoir rocks and notably reduce the producible volume. Morley (2003) proposed a similar mechanism for mudstone intrusions from the Jerudong anticline (Brunei Darussalam).
- Clastic diapirism can modify the original stratification. This can alter the geometries, thickness and reservoir properties of the intruded intervals.
- Clastic diapirism can affect hydrocarbon migration and re-migration.
- Clastic remobilisation may significantly modify the stratigraphy and biostratigraphic ages of the affected intervals and, thus, requires consideration when undertaking detailed stratigraphic correlations. This was previously outlined by Løseth et al. (2003), who studied mud mobilisation processes in the Hordaland Group (North Sea).

- Clastic diapirism can produce anomalous seismic velocity effects in the affected intervals and aliasing of the resultant structures. Morley (2003) recognised similar effects from a collection of mud diapirs in different large deltaic systems such as the Niger, the Sandakan and the Orinoco Deltas.

5.4.2 Implications of submarine slope failure

Submarine failure may involve the downslope transport and redistribution of significant amounts of sediment from shallow to deepwater settings. It has been demonstrated in this thesis that large-scale submarine landslides can affect up to c. 1000 km³ of sediment (e.g. ISC). The redistribution of such an enormous amount of material surely has a critical impact on the depositional mechanisms within the basin and thus on its hydrocarbon prospectivity. When a submarine landslide occurs, the original stratification is modified, the lithological compositions are remixed and the primary volumes of sediment are altered. In this context, possible good reservoir intervals (e.g. deepwater sandstones) can be easily remobilised or totally scattered. In addition, the transportation and deformation of landslides involves water expulsion and sediment remobilisation within the affected intervals (e.g. Martinsen, 1989; Strachan, 2002). These processes frequently cause a decrease in the porosity and permeability of the sediment (i.e. overcompaction), and an increase in its lithological complexity, with usually results in a reduction of its reservoir quality. None of the slump deposits analysed throughout this research has shown any evidence (e.g. DHI) of substantial hydrocarbon accumulations. From these arguments and observations, the submarine landslides offshore Israel are here regarded as having poor reservoir qualities and their prospectivity is thus considered low.

Submarine landslides can act as excellent traps for hydrocarbons. Slope failure usually affects clay-rich sediments, which become particularly impermeable after consolidation throughout sliding (i.e. reduction of porosity and permeability). However, in the study area, no evidence of large accumulation of hydrocarbons being associated with landslide deposits has been observed on the available seismic or well data.

Therefore, this trapping mechanism is herein excluded as a feasible play component in the region.

The occurrence of large-scale of submarine failure (e.g. ISC) can trigger seal failure and subsequent vertical migration of hydrocarbons due to rapid unloading (e.g. Ingram et al., 2004). The depletion of vast volumes of sediment during landsliding may cause a rapid drop in the lithostatic pressure (e.g. Haflidason et al., 2001). As a result, the pore fluids (or free gas) may no longer be within a stability zone, and so propagate upwards until they adjust to the new pressure conditions. This process may occur during prolonged periods of time, and involve large amounts of hydrocarbons and other fluids. In light of these arguments, the vertical migration due to slope failure is a process that potentially can influence the prospectivity of the studied region, and hence should be taken into account when planning any exploration strategy for the area.

Another major implication of slope failure for hydrocarbon exploration and production is its impact on drilling operations. As previously stated, submarine landslides tend to form overcompacted deposits. Consequently, drilling through these features can decrease drilling rates significantly. Considering an average rig cost in deepwater of \$0.25 to \$0.4 million/day, reducing the drilling time is imperative (e.g. Weimer and Slatt, 2004). Previous drilling through buried slump deposits on the continental margin of Israel have caused several problems in terms of drilling rates, borehole stability and core recovery (Hall, pers. comm. 2002). In many cases the optimal solution has been the use of bentonite and the encasing of the borehole. This approach has notably reduced borehole collapse and improved core recovery. However, it has implied considerably longer drilling times and hence a significant increase in operational costs (Hall, pers. comm. 2002). From these arguments, it seems reasonable that avoiding drilling through buried submarine landslides is, perhaps, the most straightforward approach for diminishing operational costs and risks. It is appreciated here, however, that this may not always be possible since several factors such as the prospect location or operational restrictions also play a critical role. In such cases, encasing of the borehole and the use of montmorillonite-rich clays are regarded as the best options to reduce operational risks.

Slope failure on the present day seabed can have a critical impact on production facilities (e.g. distribution pipelines, platforms), and surely constitutes a serious hazard

with potential catastrophic consequences for safety, environment and economy. A variety of submarine landslides is known to occur in the most important offshore oil provinces such as the Norwegian margin, the Gulf of Guinea, the Gulf of Mexico and the Caspian Sea (Barley, 1999). The largest gas field discovery off Norway, the Ormen Lange field, is located within the scar created by the Storegga Slide, possibly the largest submarine slide in the world ocean (Bryn et al., 2003). Diminishing the risk of slope instabilities on submarine distribution pipelines can be achieved by avoiding locations on the margin that have been recently affected by failure or show evidence of potential future events (i.e. proto-slumps, retrogressive features). These areas have been recognised in this thesis as being mainly along the slope and the shelf break. Therefore, the shelf and the base-of-slope areas are here suggested as the safest locations to place submarine pipelines. Another possibility in order to address the risks associated with slope failure is by using the appropriate relative stoutness or flexibility of pipelines and by building bridges for the distribution facilities across the potential problematic areas (e.g. Weimer and Slatt, 2004). This last option, however, may be extremely expensive and complex to implement. Reduction of the risk associated with exploration and production platforms could be attained by using floating and submersible facilities.

A final and significant implication of submarine slope failure for the prospectivity of the region is its impact on the stratigraphy and biostratigraphic ages of the affected intervals. Because of the upslope depletion, downslope transport and base-of-slope accumulation of large volumes of sediment during recurring slumping, the original stratigraphy of the margin has been considerably altered. As a result, undertaking a detailed analysis of the sequence stratigraphy of the continental margin of Israel may be of considerable complexity. This can even be the case when having good well control since the stratigraphy and biostratigraphic ages of the intervals affected by submarine slope failure can vary in the range of tens of meters. In such a situation, a three-dimensional delimitation of the areas affected by slope failure is critical in order to correctly interpret the stratigraphy of the margin.

5.5. Worldwide analogues

In this section, a review of the most representative analogues for the features documented in this thesis is presented. The aim of this review is to illustrate the global context of clastic diapirism and submarine slope instability, and to highlight the key settings in which they tend to occur. A map showing the worldwide distribution of the analogues for the two processes is shown in Figure 5.2. A table (Table 5.1) is used to summarise and catalogue the most significant examples of submarine landslides.

5.5.1 Analogues for clastic diapirism

The examples of clastic diapirism (i.e. mounded structures) presented in this thesis are believed to be unique as far as published literature goes and, therefore, no direct analogues from the existing literature are herein considered to be entirely representative. Nevertheless, there are a series of features that show interesting similarities regarding their processes, geological context and triggering mechanisms (Figure 5.2). Perhaps, the most comparable of these exemplars are a series of kilometre-scale fluidisation structures formed above the axis of a deepwater slope channel in the Niger Delta (e.g. Davies, 2003). These were described by Davies (2003) as “*a sinuous trail of 41 depressions and intervening symmetrical convex-upward hummock structures that have a regular wavelength*”. These features are clearly different to the mounded structures studied here in terms of geometry, geological context and formational mechanisms. Davies (2003), for example, stated that the fluidisation structures in the Niger Delta involved the expulsion of sediment to the coeval seafloor. Such a situation has been ruled out here for the mounded structures offshore Israel. Despite these differences, many parallelisms can be drawn regarding the causes and genetic models of the two types of features. Davies (2003) proposed that the hummock-depression structures in the Niger Delta were “*the end result of an exceptionally large-scale fluidisation process that was triggered by elevated pore pressures within buried sand, leading to seal breach and vertical fluidised sediment flow*”. A significantly similar scenario was proposed in **Chapter 2** to explain the formation of the mounded structures offshore Israel. In addition, Davies (2003) proposed that the fluidisation structures in the Niger Delta formed through a sequence of

deposition, sediment mobilisation, and overburden deformation; which is conceptually comparable to the genetic model proposed in this thesis (see **Section 2.10.2**). Another remarkable parallelism is the fact that both types of structures formed along buried submarine canyons (albeit of considerably different scales). This parallelism allows close similarities between the fluid-flow pathways in the two cases to be drawn.

Similar exemplars to the mounded structures presented herein have also been reported by Morley (2003) from the Jerudong anticline (onshore Brunei Darussalam; Figure 5.2). This author described a medium-scale mudstone laccolith which he interpreted as being caused by the intrusion of large amounts of mudstone above an inferred mudstone diapir. Morley (2003) described the laccolithic structure as having a flat base and convex top, and with stoped blocks of lithified, fissile shales inside the mudstone body. This appearance is similar to that of the mounded structures presented in here. Morley (2003) also proposed a very similar formational process to that presented in this thesis based on the forceful intrusion of mudstone into a host rock.

Other interesting features that could be partially comparable to the mounded structures offshore Israel, at least in terms of geometries and formational mechanisms, are a series of mounded features reported by Løseth et al. (2003) from the Hordaland Group (North Sea; Figure 5.2). Løseth et al. (2003) described these features as having a chaotic internal appearance and with a mounded top that was formed when the structures were at free surface. They interpreted these features as mud diapirs triggered by the vertical migration of gas, oil and formation water. Løseth et al. (2003) inferred the development of overpressured regimes by chemical compaction and hydrocarbon generation as the main triggering mechanisms for the formation of these mounded structures.

Finally, other geological settings in which similar features to the mounded structures could be expected are large river deltas (e.g. Nile, Mississippi, Mekong, Orinoco, Ganges and Bramaputra, Sandakan deltas; Figure 5.2). Large deltas involve massive fluxes of fine-grained underconsolidated sediments into basins (e.g. $1.3-1.5 \times 10^6$ km³ of sediment in the Niger Delta; Morley, 2003), and are usually associated with hydrocarbon-bearing provinces (e.g. Niger Delta, Evamy et al., 1978; Nile Delta, Wever, 2000). Under these conditions, overpressuring and subsequent remobilisation of undercompacted sediment is

to be expected, and it is possible that mounded features as those presented here could, occasionally, form.

5.5.2 Analogues for submarine slope instability

Submarine slope instability has been documented and studied from many different settings in the world (Figure 5.2; Table 5.1). As a result, it is now commonly accepted that rapid accumulations of thick sedimentary deposits, sloping seafloor, and high environmental stresses are the conditions most commonly associated with submarine landslides (e.g. Hampton et al., 1996). Certain geologic environments (e.g. deltaic systems, fjords, submarine canyons, continental margins and volcanic regions) tend to have these conditions, and consequently, submarine landslides are more common there. The largest and most abundant submarine landslides documented to date occur on the slopes of open continental margins and oceanic volcanic islands. Landslides on continental margins, for instance, have been documented from polar (e.g. Grantz and Dinter, 1980) to equatorial (e.g. Moore et al., 1976) latitudes; and in convergent (e.g. Hampton and Bouma, 1978), divergent (e.g. Booth et al., 1993), and transform (e.g. Field and Edwards, 1980) tectonic settings.

Perhaps, the most well-known example of a continental margin affected by slope failure is the Storegga region (offshore Norway; Figure 5.2). This region has been intensively affected by repeated slope failure since the late Pliocene or early Pleistocene (e.g. King et al., 1996; Evans et al., 1996; Bryn et al., 1998, 2003). As a result, numerous large-scale submarine landslides have formed (i.e. Storegga, Nyk, Trænadjupet, Andøya, Fugløy Bank, Malenebukta, Bjørnøyrenna; Table 5.1). The Storegga Slide is, certainly, one of the most renowned submarine landslides not only offshore Norway but worldwide. It was considered by Bugge (1983) as the largest exposed submarine landslide in the world, with an area of 112 000 km²; later revised by Haflidason et al. (2002) to be c. 95 000 km². The Storegga Slide is the largest landslide offshore Norway, and it has been interpreted as an instantaneous retrogressive event (within a geological time frame) dated to be 7250±250 ¹⁴C years BP (e.g. Haflidason et al. 2004). Seismicity, gas hydrate dissociation and excess pore pressure generation have been proposed as the most probable triggers

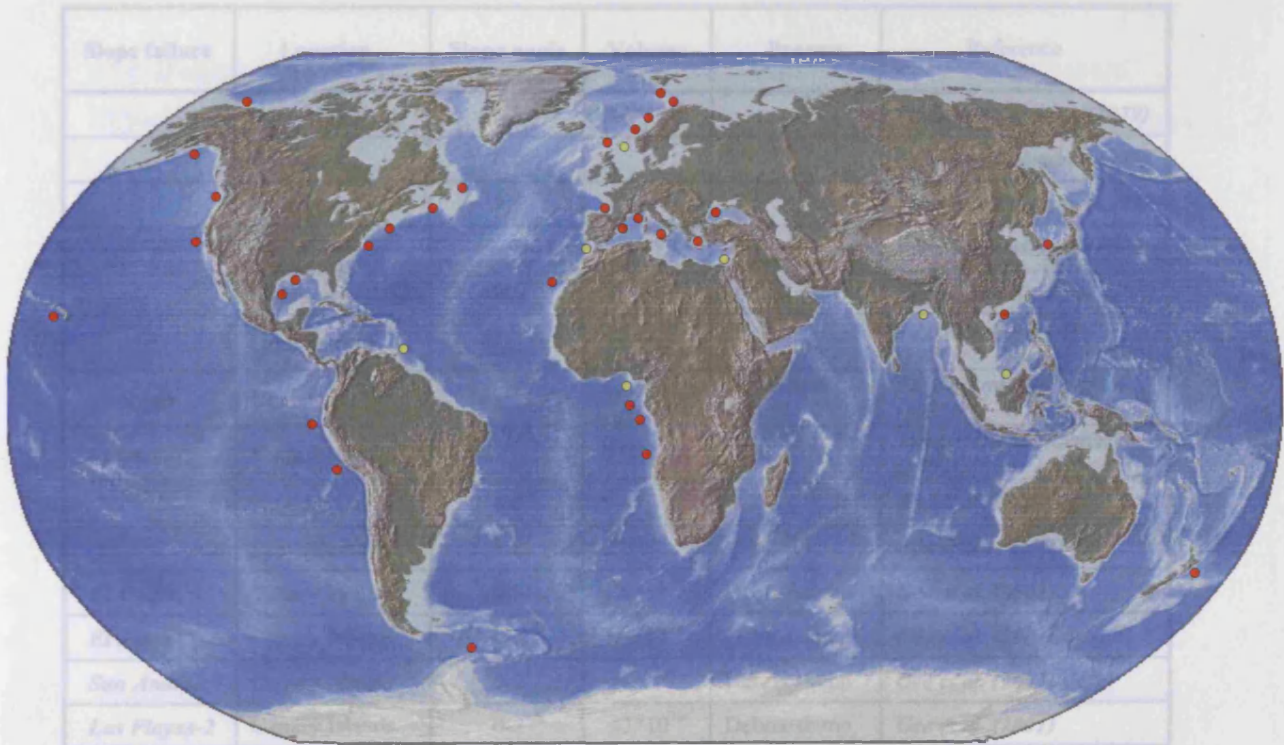


Figure 5.2 Worldwide distribution of the principal analogues for the soft-sediment deformational structures presented in this thesis. Red and green dots mark the position of submarine landslides and clastic diapirs, respectively.

Region	Analogue	Number	Volume	Structure	Reference
Angola	Ebro margin	1-5	1.5×10^5	Debris flow	Geis et al. (2001)
Arctic	Faro-Shetland Basin	2	2×10^6	Slide	Murray et al. (2003)
Asia	Ebro margin	2	1.4×10^5	Slide	Lestrus et al. (2004)
Japan	Ebro margin	2-5	4×10^5	Slide	Lestrus et al. (2004)
Norway	Ebro margin	3	3.1×10^5	Slide	Lestrus et al. (2004)
Israel	Ebro margin	1-9	1.9×10^5	Slide	Lestrus et al. (2004)
Norway	Norway				Lindberg et al. (2004)
ISC	Israel	1-6	1×10^5	Composite slump	Frey-Martinez et al. (2005)

Table 5.1 Worldwide analogues for the submarine landslides presented in this thesis.

Slope failure	Location	Slope angle (degrees)	Volume (m ³)	Process	Reference
	Grand Banks	3.5	7.6*10 ¹⁰		<i>Prior and Coleman (1979)</i>
	Hawaii	6.0			<i>Prior and Coleman (1979)</i>
	Kidnappers	2.5	8*10 ⁹		<i>Prior and Coleman (1979)</i>
	Bay of Biscay				<i>Prior and Coleman (1979)</i>
	Mississippi delta	0.5	4*10 ⁷		<i>Edgers and Karlsrud (1982)</i>
	Orkdalsfjord		2.5*10 ⁷		<i>Edgers and Karlsrud (1982)</i>
<i>Storegga</i>	Norway		3*10 ¹²	Composite slide	<i>Edgers and Karlsrud (1982)</i>
<i>Suvero</i>	Paola Basin		2*10 ¹⁰	Slide	<i>Trincardi and Normark (1989)</i>
	Atlantic Ocean	4.0			<i>Booth et al. (1993)</i>
	Santa Barbara	4.8	2*10 ⁷		<i>Edwards et al. (1993)</i>
<i>El Golfo</i>	Canary Islands	0-2	1.5*10 ¹¹	Debris/slump	<i>Gee et al. (2001)</i>
<i>El Julian</i>	Canary Islands	0-2	1.3*10 ¹¹	Debris/slump	<i>Gee et al. (2001)</i>
<i>San Andres</i>	Canary Islands	0-2		Debris/slump	<i>Gee et al. (2001)</i>
<i>Las Playas-2</i>	Canary Islands	0-2	<3*10 ¹⁰	Debris/slump	<i>Gee et al. (2001)</i>
	Angola		1.5*10 ⁷	Debris/slump	<i>Gee et al. (2001)</i>
	Ireland			Slide	<i>Huvenne et al. (2002)</i>
<i>Trænadjupet</i>	Norway	0-2	4*10 ¹¹	Composite slide	<i>Laberg et al. (2002)</i>
<i>BIG'95</i>	Ebro margin	4-17	2.6*10 ¹⁰	Debris flow	<i>Lastras et al. (2002)</i>
<i>Afen</i>	Faroe-Shetland Basin	2	2*10 ⁸	Composite slide	<i>Wilson et al. (2003)</i>
<i>Ana</i>	Ebro margin	2	1.4*10 ⁸	Slide	<i>Lastras et al. (2004)</i>
<i>Joan</i>	Ebro margin	2.5	4*10 ⁸	Slide	<i>Lastras et al. (2004)</i>
<i>Nuna</i>	Ebro margin	3	3.1*10 ⁸	Slide	<i>Lastras et al. (2004)</i>
<i>Jersi</i>	Ebro margin	1.9	1.9*10 ⁸	Slide	<i>Lastras et al. (2004)</i>
<i>Nyk</i>	Norway				<i>Lindberg et al. (2004)</i>
<i>ISC</i>	Israel	1-6	~1*10 ¹²	Composite slump	<i>Frey-Martinez et al. (2005)</i>

Table 5.1 Worldwide analogues for the submarine landslides presented in this thesis.

(e.g. Bugge, 1983; Canals et al., 2004; Sultan et al., 2004). Hühnerbach and Masson (2004) undertook an inclusive analysis of the morphology, setting and behaviour of many of the submarine landslides offshore Norway and the reader is referred to their work for further details.

Numerous continental margins in the Mediterranean basin have also shown to be extremely active in terms of slope instability (Figure 5.2). Medium to large-scale submarine landslides have been reported, for instance, from the Ebro continental margin (offshore Spain), the Paola basin (offshore Italy), and the North Aegean Trough (offshore Greece). The dimensions of the resultant deposits are considerably smaller when compared to those of the Storegga region (c. 0.31 km³; Nuna Slide), but still slope failure is regarded as one of the most significant mechanisms in shaping the margins of the entire basin. Earthquake activity, fluid migration and high sedimentation rates have been invoked as the most likely triggering mechanisms for the vast majority of the submarine landslides in the Mediterranean basin (e.g. Lastras et al., 2002; Trincardi and Argnani, 1990; Sultan et al., 2004).

As previously stated, large-scale landsliding is also regarded as one of the most important and effective processes in the destruction of volcanic oceanic islands (e.g. Gee et al., 2001). Menard (1956), for instance, argued that for many volcanic islands, the volume of deposits of gravity driven processes (i.e. slumps, debris flows and turbidites) may exceed the volume of the subaerial and submarine part of the island itself. Giant submarine landslides have been extensively reported from the Hawaiian (e.g. Lipman et al., 1988; Moore et al., 1989; Moore et al., 1994a and b; Smith et al., 1999), Reunion (e.g. Lenat et al., 1989; Ollier et al., 1998) and Canary Islands (e.g. Watts and Masson, 1995; Urgeles et al., 1997; Masson et al., 1998; Gee et al., 2001; Masson et al., 2002) (see Figure 5.2). The exact cause of these giant landslides is difficult to know (e.g. Hampton et al., 1996). While slope failure in volcanic islands is commonly regarded to be associated with intense seismic activity caused by eruptions, some investigators have demonstrated that this may not always be the case. Moore (1989), for example, proposed that seismicity can be the result rather than the cause of submarine sliding. He supported this statement with evidence that the eruption of the Kilauea volcano (Hawaii) in 1975 was triggered by a small movement of a large-scale submarine landslide: the Hilina slump.

Fjords, river deltas and submarine canyons are the other three main environments in which, although in less well described, submarine slope instability tends to occur (Figure 5.2; Table 5.1). Numerous submarine landslides have been reported worldwide from fjords such as the Resurrection Bay and Port Valdez (southern Alaska), the Kitimat Arm (British Columbia; Canada), and the Trondheim Harbour (Norway). Perhaps, the most renowned of these examples is that in the Resurrection Bay in which a catastrophic event of submarine landsliding seriously damaged the city of Seward in 1964 (e.g. Lemke, 1967). Rapid deposition of sediments, seismic activity, sea-level variations, fluid migration and anthropomorphic pressure were proposed as the main triggering mechanisms (e.g. Lemke, 1967). Submarine landsliding has been also extensively reported from the Yellow (China), the Mississippi (Gulf of Mexico; United States) and the Klamath (California; United States) river deltas (Figure 5.2; Table 5.1). In these settings, the interaction of high sedimentation rates, underconsolidated sediments, seismicity and storms has been traditionally invoked as triggers (e.g. Prior et al., 1984; Field and Barber, 1993). Finally, submarine slope failure has been described from submarine canyons in Alaska and along several margins of the United States. High-slope gradients, seismicity and high sedimentation rates have been there proposed as the main triggering mechanisms (e.g. McAdoo et al., 2000).

5.6. Limitations and future research

The work presented in this thesis is a comprehensive study, based on seismic (2D and 3D) and well data, of soft-sediment deformational processes and their resultant structures. By integrating different types of data, several soft-sediment deformational features have been examined to a high level of accuracy that could not have been attained by any other combination of methods. Comparison and discussion of various case studies in the study area has allowed numerous aspects of their typology, 3D appearance and genesis to be inferred. The conclusions presented here have then enhanced a deeper understanding of the triggers, formational mechanisms, and resultant structures of soft-sediment deformational processes that should be applicable worldwide. However, despite the advance in knowledge achieved throughout this research, some results have been partially

hindered by a series of limitations. In this section, a review of such limitations and a series of research proposals to overcome them in the future are presented.

Perhaps, the most significant limitation throughout this research has been the incomplete coverage of 3D seismic data of the study area. Accurate seismic mapping is necessary for determining the exact geographical extent and volumes of large-scale structures such as the ISC. Additionally, it is critical in order to implement attribute-based interpretation techniques and to accurately examine and compare their internal fabrics. For these purposes, 3D seismic data is required over larger extensions of the study area as 2D seismic datasets have inherent problems with the spatial aliasing of the imaged features and the geological structures within them. However, at present, large parts of the continental margin of Israel are entirely void of 3D seismic coverage and, unfortunately, it is highly unlikely that more of these data will be acquired in the future such that soft-sediment deformational structures may be confidently examined over its entire extension.

Surely the limited resolution provided by the 3D seismic data (i.e. tens of meters) has precluded a more detailed analysis of the small scale soft-sediment deformational structures. This has restricted a more inclusive analysis of their basinal distribution and external and internal geometries. Future better techniques for the acquisition and migration of the seismic data should allowed an improved visualization of such structures and hence a more complete understanding of their causes and formational mechanisms. In the meantime, comparison between those features observed on the 3D seismic data with those observed from other geophysical techniques such as multibeam or very high shallow seismic data should enhanced a better understanding of the small-scale processes of soft-sediment deformation.

Another area where significant improvements can be made is in a more rigorous analysis of the well database. Additional and more detailed biostratigraphic and well log data through supplementary soft-sediment deformational structures (especially submarine landslides) is required to fully understand their complex causes and formational mechanisms. The necessity of a more accurate well log database is especially patent when analysing the basal shear surfaces of submarine landslides. Due to lack of accurate borehole logs at these stratigraphic intervals, a more detailed examination of their physical properties has been prevented. This, in turn, has limited a further understanding

of why failure initiates and occurs along these specific strata and which is their evolution during failure. The study area is at a relatively immature stage of exploration, and a large number of exploration and appraisal wells remains to be drilled in the near future. It is highly possible that the information obtained from some of these new wells will enhance our understanding of some of these aspects.

Data hindrances have precluded a higher degree of confidence when modelling the genetics of some of the features studied in this research. This has been particularly the case when studying the physical mechanisms, timings of occurrence, and sediment behaviour of submarine landslides. Additionally, the mechanisms of shear strength propagation along the basal shear surface of submarine landslides are still poorly understood. In order to attain a greater comprehension of all these aspects, an inclusive mechanical approach is essential. Many mechanical analyses have suggested remarkable explanations for the generation of submarine landslides (e.g. Bjerrum, 1967; Puzrin et al., 2004). Puzrin et al. (2004), for instance, proposed a mechanical model based on energy balance and process zone fracture mechanics. According to these authors, slope failure can be adequately explained by considering catastrophic shear band propagation. They also proposed a series of possible measures for mitigation of the landslide hazard by controlling the dimensions of possible landslides through reduction of the sediment pore pressure. Germanovich et al. (in press) built on the concepts and principles presented by Puzrin et al. (2004) to analyze the impact of submarine slope failure in the development of tsunamis. The integration of such mechanical approaches with further geophysical analysis is here considered as the best way of improving knowledge on the generation of submarine landslides, and the mechanisms to satisfactorily mitigate the hazards associated to them.

Chapter Six: Conclusions

The investigations undertaken during the course of this research project have produced a wealth of information relating to diverse aspects of soft-sediment deformation on the continental margin of Israel. The observations and resulting conclusions provide insight ranging from the different typologies of soft-sediment deformation in the study area, to their triggers, processes, resultant structures and impact for hydrocarbon prospectivity that should be of applicability to other sedimentary basins worldwide. The following statements summarise the concluding remarks for each of the previous chapters, providing a summary of the research.

6.1. General conclusions

- Soft-sediment deformation is an intrinsic facet in the evolution of the post-Messinian Israeli continental margin.
- Two types of soft-sediment deformation are dominant in the region: clastic diapirism and slope instability.
- Soft-sediment deformation initiated during the Middle Zanclean (c. 4 Ma BP) with clastic diapirism occurring along the Afiq Submarine Canyon. At present day, soft-sediment deformation is still active almost certainly throughout the entire continental margin in the form of submarine slumping.
- It has been recognised in this thesis that soft-sediment deformation plays a critical role in the hydrocarbon prospectivity of the region.
- 3D seismic interpretation has proved to be a powerful tool when analysing soft-sediment deformational processes and results. The availability of a three-dimensional understanding of the resultant structures and their geological context has been revealed to be critical to evaluate their triggering mechanisms, genetics, timing and significance.

6.2. Clastic diapirism

- Clastic diapirism is geographically restricted to the areas underlain by the Afq Submarine Canyon.
- The clastic diapirs in the study area are generally recognised seismically as ridge and mounded structures. The latter are the most common. The mounded structures are circular to elliptical in plan view and appear as culminations at the top of the Yafo Sand Member. They may form isolated four-way dip closures or complexes of up to three features.
- The internal seismic reflection character of the clastic diapirs consists of two dominant seismic facies: incoherent and chaotic reflections in the core, and more coherent and continuous reflections on the flanks and crests. The core is dominated by allochthonous material from Cretaceous to Upper Miocene stratigraphic levels. The flanks and crest correspond to the gas-bearing Yafo Sand Member.
- It is considered here that clastic diapirism occurred by forceful intrusion of mud-rich sediment into shallow-level sedimentary host rocks (Yafo Sand Member) and subsequent hydraulic “jack-up” of the sedimentary cover sequence (Yafo Mudstone Member).
- The occurrence of clastic diapirism is attributed to the overpressuring of the sedimentary sequences within the Afq Submarine Canyon. Its spatial constriction is considered to be due to the space-time coincidence of the necessary conditions for clastic remobilisation (i.e. seal, overpressured sediment, and fluid escape pathways). Development of high overpressure regimes within the Afq Submarine Canyon was probably controlled by hydrocarbon generation, seismic activity or a combination of both.
- Clastic diapirism initiated during the Middle Zanclean (c. 4 Ma BP), and finished during the Early Gelasian (c. 2.5 Ma BP).

6.3. Submarine slope instability

- Submarine slope instability (i.e. slumping) is the most common type of soft-sediment deformation on the Israeli continental margin.
- Slump deposits are recognised on seismic data as packages of highly disrupted to chaotic facies bounded by, commonly continuous, basal shear and top surfaces.
- Submarine slump deposits have been observed to range from individual features to complexes of three or more features. They vary from medium sized (c. 110 km², GSC) to enormous features (c. 4800 km²; ISC).
- Two main zones are recognised for many slump deposits: depletion zone and accumulation zone. The former is characterised by extension and removal of sediment. The latter by compression and addition of material.
- Slump evolution occurs both by retrogressive upslope failure, and by downslope propagation (out-of-sequence) failure.
- Submarine slumping offshore Israel commenced in the Late Pliocene with the ISC, which is one of the largest slumps in the world (c. 1000 km³ in volume) described to date. Since then, slumping processes repeatedly occurred up to the Holocene.
- Slumping events have increased in number from the Pliocene to the Holocene, although the resulting products have significantly decreased in size. This has been interpreted here as the result of variations in the basinal subsidence, sedimentation rates and seismic activity.
- The triggering mechanisms for slumping have been considered to be a combination of seismic activity, presence of gas within the sediments and slope oversteepening. The degree of interaction between these triggering mechanisms may have varied through time.
- There is evidence of future potential slope instability in the study area. This is represented by the occurrence of proto-slumps, which have been defined here as the result of long-term degradation processes of dipping strata and the potential precursors to mass movement. Proto-slumps may display many of the diagnostic structures identified from slump deposits (e.g. lateral margins, crown-cracks).

6.4. Compressional toe regions in submarine landslides

- 3D seismic interpretation has proved the existence of two main types of submarine landslides according to their form of frontal emplacement: *frontally confined* and *emergent*.
- *Frontally confined* landslides imply a modest downslope transfer of sediment, and are characterised by having buttressed and confined compressional toe regions and by an insignificant bathymetric expression compared to their total thickening. On the contrary, *emergent* landslides involve the downslope transport of significant volumes of material, and are characterised by compressional toe regions above the coeval seabed that form major bathymetric expressions.
- Internally, both *frontally confined* and *emergent* submarine landslides are characterised by highly disrupted to chaotic seismic facies. However, *frontally confined* submarine landslides reveal evidence of more preserved internal stratification (e.g. sub-horizontal reflections and blocks of intact strata).
- 3D mapping suggests that *frontally confined* submarine landslides translate downslope by bulldozing the foreland. This downslope translation is considered here to stop when the stress developed by the slump mass becomes lower than the strength of the foreland. Instead, *emergent* submarine landslides translate by overthrusting the downslope undisturbed strata. They then travel freely over the undeformed slope position possibly evolving into debris flows and turbidity currents.
- Analysis of the geometries of *frontally confined* and *emergent* submarine landslides suggests that the frontal emplacement of submarine landslides depends on the position of their centre of gravity. This is in turn a function of the depth to detachment of the submarine landslide.
- The existence of contourite drift deposits has been recognised as a possible controlling factor for the depth to detachment of submarine landslides, and hence for their frontal confinement.

6.5. Implications for hydrocarbon prospectivity

6.5.1 Implications of clastic diapirism

- Four-way dip mounded structures formed by clastic diapirism can form effective structural traps for hydrocarbons.
- Clastic diapirism can compartmentalise reservoir rocks and notably reduce the producible volume. It can also modify the original stratification altering the geometries, thickness and reservoir properties of the intruded intervals.
- Clastic diapirism may have an impact on hydrocarbon migration and re-migration.
- Clastic remobilisation may lead to erroneous stratigraphic and biostratigraphic interpretations and difficulties for seismic interpretation due to anomalous seismic velocity effects and aliasing of the resultant structures.

6.5.2 Implications of submarine slope failure

- No evidence of good quality hydrocarbon reservoirs or traps associated to the slump deposits has been observed throughout the study area.
- The presence of buried submarine slump deposits is of great importance for drilling operations as they may decrease drilling rates significantly.
- Slope failure on the present day seabed can have a critical impact on production facilities (e.g. distribution pipelines, platforms), and surely constitutes a serious hazard with potential catastrophic consequences for safety, environment and economy.
- Submarine slope failure may alter their original stratigraphy and biostratigraphic ages of the affected intervals and this needs to be taken into account when undertaking a sequence stratigraphy analysis in the study area.

REFERENCES

A

- Allen, J. R. L., 1984, Sedimentary structures: their character and physical basis: *Elsevier*, Amsterdam, Oxford.
- Almagor, G., and G. Wiseman, 1977, Analysis of submarine slumping in the continental slope off the southern coast of Israel: *Marine Geotechnology*, v. 2, p. 349-388.
- Almagor, G., 1980, Halokinetic deep-seated slumping on the Mediterranean slope of northern Sinai and southern Israel: *Marine Geotechnology*, v. 4, p. 83-105.
- Almagor, G., 1984, Salt-controlled slumping on the Mediterranean slope of central Israel: *Marine Geophysics Research Letters*, v. 6, p. 227-243.
- Almagor, G., 1986, Mass transport on the continental slope of Israel: *Geo-Marine Letters*, v. 6, p. 29-34.
- Almagor, G., 1993, Continental slope processes off northern Israel and southernmost Lebanon and their relation to onshore tectonics: *Marine Geology*, v. 112, p. 151-169
- Almagor, G., and B. Schilman, 1995, Sedimentary structures and sediment transport across the continental slope of Israel from piston core studies: *Sedimentology*, v. 42, p. 575-592.
- Alsop, G. I., J. P. Brown, I. Davinson, and M. R. Gibling, 2000, The geometry of drag zones adjacent to salt diapirs: *Journal of the Geological Society (London)*, v. 157, p. 1019-1029.
- Al-Tarazi, E.A., 1999, Regional seismic hazard study for the eastern Mediterranean (Trans-Jordan, Levant and Antakia) and Sinai region: *Journal of African Earth Sciences*, v. 28, p. 743-750.
- Andersen, L. T., 2004, The Fanø Bugt Glaciotectonic Thrust Fault Complex, Southeastern Danish North Sea, Ph.D. Thesis, Faculty of Geology University of Aarhus.
- Andreassen, K., K. Hogstad, and K. A. Berteussen, 1999, Gas hydrate in the southern Barents Sea, indicated by shallow seismic anomaly: *First break*, v. 8, p. 235-245.
- Arieh, E., 1967, Seismicity of Israel and adjacent areas: *Geological Survey of Israel Bulletin*, v. 43, p. 1-4.
- Anketell, J. M., J. Cegla, and S. Dzulynski, 1970, On the deformational structures in systems with reversed density gradients: *Rocznik Polskiego Towarzystwa Geologicznego*, v. 40, 1, p. 3-30.
- Aksu, A. E., and R. N. Hiscott, 1989, Slides and debris flows on the high-latitude continental slopes of Baffin Bay: *Geology*, v. 17, p. 885-888.

B

- Bankwitz, P., E. Bankwitz, K. Bräuer, H. Kämpf, and M. Störr, 2003, Deformation structures in Plio- and Pleistocene sediments (NW Bohemia, Central Europe) in P. Van Rensbergen, R. R. van Hillis, A. J. Maltman, and C. K. Morley, eds., *Subsurface Sediment Mobilization: Geological Society (London) Special Publication*, v. 216, p. 73-93.
- Barley, B., 1999, Deepwater problems around the world: The Leading Edge, Tulsa, Oklahoma, v. 18, 4, p. 488-494.
- Barnes, P. M, and K. B. Lewis, 1991, Sheet slides and rotational failures on a convergent margin: the Kidnappers Slide, New Zealand: *Sedimentology*, v.38, p. 235-245.
- BG-Group Internal Report SA9029, 2000, Levant offshore processing report, Geco Sapphire.
- Bradley, D., and L. Hanson, 1998, Paleoslope analysis of slump folds in the Devonian Flysch of Maine: *The Journal of Geology*, v. 106, p. 305-318.
- Bjerrum, L., 1967, Progressive failure in slope of overconsolidated clay and clay shales: *Journal of Soil Mechanics and Foundations Engineering*, ASCE v. 93, p. 1-49.
- Ben-Avraham, Z., 1989, The structure and tectonic setting of the Levant continental margin-eastern Mediterranean: *Tectonophysics*, v. 8, p. 351-362.
- Brooke, C. M., T. J. Trimble, and T. A. Mackay, 1995, Mounded shallow gas sands from the Quaternary of the North Sea: analogues for the formation of sand mounds in deep water Tertiary sediments? in A. J. Hartley, and D. J. Prosser, eds., *Characterisation of deep-marine clastic systems: Geological Society (London) Special Publication*, v. 94, p. 95-101.
- Brown, A. R., 2003, Interpretation of three-dimensional seismic data: *AAPG Memoir*, 6th edition, v. 42, p. 541, Tulsa, OK.
- Bryn, P., S. R. Østmo, R. Lien, K. Berg, and T. I. Tjelta, 1998, Slope stability in the deep-water areas off Mid- Norway: *OTC Paper 8640*, Offshore Technology Conference, Houston, Texas, USA.
- Bryn, P., A. Solheim, K. Berg, R. Lien, C. F. Forsberg, H. Haflidason, D. Ottesen, and L. Rise, 2003, The Storegga Slide complex: repeated large scale sliding in response to climatic cyclicality, in J. Locat, and J. Mienert, eds., *Submarine Mass Movements and Their Consequences: Kluwer Academic Press*, The Netherlands, p. 215-222.
- Bøe, R., M. Hovland, A. Instanes, L. Rise, and S. Vassus, 2000, Submarine slide scars and mass movements in Karmsundet and Skudenesfjorden, southwestern Norway: morphology and evolution: *Marine Geology*, v. 167, 147-165.
- Booth, J.M., and D. W. O'Leary, 1991, A statistical overview of mass movement characteristics on the North American Atlantic outer continental margin: *Marine Geotechnology*, v. 10, 1-18.

- Booth, J. M., D. W. O'Leary, P. Popenoe, and W. W. Danforth, 1993, U.S. Atlantic continental slope landslides: Their distribution, general attributes, and implications, *in* W. C. Schwab, H. J. Lee and D. C. Twichell, eds., *Submarine Landslides: Selected Studies in the U. S. Exclusive Economic Zone: U.S. Geological Survey Bulletin*, 2002, p. 14-23.
- Brown, L.F., and W. L. Fisher, 1977, Seismic-stratigraphic interpretation of depositional systems: examples from Brazilian rift and pull-apart basins: *in* C. E. Payton, ed., *Seismic Stratigraphy-Applications to Hydrocarbon Exploration: AAPG Memoir*, v. 26, p. 213-248.
- Buchbinder, B., and E. Zilberman, 1997, Sequence stratigraphy of Miocene-Pliocene carbonate-siliciclastic shelf deposits in the eastern Mediterranean margin (Israel): effects of eustasy and tectonics: *Sedimentary Geology*, v. 112, p. 7-32.
- Bugge, T., 1983 Submarine slides on the Norwegian continental margin, with special emphasis on the Storegga area: *Sedimentary Geology*, v. 112, p. 7-32.
- Bugge, T., S. Befring, R. H. Balderson, T. Eidvin, J. Eystein, N. H. Kenyon, H. Holtedahl, and H.P. Sejrup, 1987, A giant three-stage submarine slide off Norway: *Geo-Marine Letters*, v. 7, p. 191-198.

C

- Canals, M., G. Lastras, R. Urgeles, J. L. Casamor, J. Mienert, A. Cattaneo, M. De Batist, H. Haflidason, Y. Imbo, J. S. Laberg, J. Locat, D. Long, O. Longva, D. G. Masson, N. Sultan, F. Trincardi, and P. Bryn, in press, Slope failure dynamics and impacts from seafloor and shallow sub-seafloor geophysical data: case studies from the COSTA project: *Marine Geology*.
- Carpenter, G., 1981, Coincident slump/clathrate complexes on the U.S. Atlantic continental slope: *Geo-Marine Letters*, v. 1, p. 29-32.
- Cartwright, J. A., 1994, Episodic basin-wide fluid expulsion from geopressured shale sequences: *Bulletin of the Geological Society of America*, v. 110, p. 1242-1257.
- Cartwright, J. A., S. A. Stewart, and J. Clark, 2001, Salt dissolution and salt-related deformation of the Forth Approaches Basin, UK North Sea: *Marine and Petroleum Geology*, v. 18, p. 757-778.
- Cole, D., S. A. Stewart, and J. Cartwright, 2000, Giant irregular pockmark craters in the Palaeogene of the Outer Moray Firth Basin, UK North Sea: *Marine and Petroleum Geology*, v. 17, p. 563-577.
- Crans, W, G. Mandl, and J. Haremboure, 1980, On the theory of growth faulting; a geomechanical delta model on gravity sliding: *Journal of Petroleum Geology*, v. 2, p. 265-307.
- Croot, D. G., 1987, Glacio-tectonic structures; a mesoscale model of thin-skinned thrust sheets?:

Journal of Structural Geology, v. 9, 7, p. 797-808.

D

Dahlen, F. A., 1990, Critical taper model of fold-and-thrust belts and accretionary wedges: *Annual Review of Earth and Planetary Sciences*, v. 18, p. 55-99.

Davies, R. J., B. R. Bell, J. Cartwright, and S. Shoulders, 2002, Three-dimensional seismic imaging of Paleogene dike-fed submarine volcanoes from the northeast Atlantic margin: *Geology*, v. 30, p. 223-226.

Davies, R. J., 2003, Kilometre-scale fluidization structures formed during early burial of a deepwater slope channel on the Niger Delta: *Geology*, v. 30, p. 223-226.

Davison, I., G. I. Alsop, P. Birch, C. Elders, N. Evans, H. Nicholson, P. Rorison, D. Wade, J. Woodward, and M. Young, 2000, Geometry of late-stage structural evolution of Central Graben salt diapirs, North Sea: *Marine and Petroleum Geology*, v. 17, p. 499-522.

Dingle, R. V., 1977, The anatomy of a large submarine slump on a sheared continental margin (SE Africa): *Journal of the Geological Society (London)*, v. 134, p. 293-310.

Dixon, R. J., K. Schofield, R. Anderton, A. D. Reynolds, R. W. S. Alexander, M. C. Williams, and K. G. Davies, 1995, Sandstone diapirism and clastic intrusion in the Tertiary submarine fans of the Bruce-Beryl Embayment, Quadrant 9, UKCS, in A. J. Hartley, and D. J. Prosser, eds., Characterisation of deep-marine clastic systems: *Geological Society (London) Special Publication*, v. 94, p. 77-94.

Draganits, E., B. Grasemann, and H. P. Schmid, 2003, Fluidization pipes and spring pits in a Gondwanan barrier-island environment: Groundwater phenomenon, palaeo-seismicity or a combination of both? in P. Van Rensbergen, R. R. van Hillis, A. J. Maltman, and C. K. Morley, eds., Subsurface Sediment Mobilization: *Geological Society (London) Special Publication*, v. 216, p. 109-121.

Druckman, Y., B. Buchbinder, G. M. Martinotti, R. Siman Tov, and P. Aharon, 1995, The buried Afiq Canyon (eastern Mediterranean, Israel): a case of a Tertiary submarine canyon exposed in Late Messinian times: *Marine Geology*, v. 123, p. 167-185.

Duperret, A., J. Bourgois, Y. Lagabrielle, and E. Suess, 1995, Slope instabilities at an active continental margin: large-scale polyphase submarine slide along the northern Peruvian margin, between 5°S and 6°S: *Marine Geology*, v. 122, p. 303-328.

Duranti, D., A. Hurst, C. Bell, S. Goves, and R. Hanson, 2002, Injected and remobilised sands from the Alba Field (Eocene, UKCS): core and wireline log characteristics: *Petroleum*, v. 8, p. 99-107.

E

- Edgers, L., and K. Karlsrud, 1982, Soil flows generated by submarine slide-Case studies and consequences, in C. Chryssostomidis and J. J. Connor, eds., Proceedings of the Third International Conference on the Behaviour of Offshore Structures: *Hemispher*, Bristol, p. 425-437.
- Edwards, B. D., H. J. Lee, and M. F. Field, 1993, Seismically induced mudflow in Santa Barbara Basin, California, in W. C. Schwab, H. J. Lee and D. C. Twichell, eds., Submarine Landslides: Selected Studies in the U. S. Exclusive Economic Zone: *U.S. Geological Survey Bulletin*, 2000, p. 167-175.
- Elliot, G., 1970, Roselle lineament of southeast Missouri: *Geological Society of America Bulletin*, v. 81, 3, p. 975-982.
- Embley, R. W., and R. Jacobi, 1977, Distribution and morphology of large submarine sediment slides and slumps on the Atlantic continental margins: *Marine Geotechnology*, v. 2, 205-208.
- Embley, R. W., 1980, The role of mass transport in the distribution and character of deep ocean sediments with special reference to the North Atlantic: *Marine Geology*, v. 38, 23-50.
- Evamy, B. D., J. Haremboure, P. Kamerling, W. A. Knaap, F. A. Molloy, and P. H. Rowlands, 1978, Hydrocarbon habitat of Tertiary Niger delta: *AAPG Bulletin*, v. 62, p. 1-39.
- Evans, D., E. L. King, N. H. Kenyon, N. H. Brett, and D. Wallis, 1996, Evidence for long-term instability in the Storegga Slide region off western Norway: *Marine Geology*, v. 130, p. 281-292.
- Eyal, Y., 1996, Stress field fluctuations along the Dead-Sea Rift since the Middle Miocene: *Tectonics*, v. 15, p. 157-170.

F

- Farrell, S. G., 1984, A dislocation model applied to slump structures, Ainsa Basin, South Central Pyrenees: *Journal Structural Geology*, v. 6, p. 727-736.
- Farrell, S. G., and S. Eaton, 1987, Slump strain in the Tertiary of Cyprus and the Spanish Pyrenees. Definition of palaeoslopes and models of soft-sediment deformation, in M. E. Jones, and R. M. F. Preston, eds., Deformation of Sediments and Sedimentary Rocks: *Geological Society of London Special Publication*, v. 29, p. 181-196.
- Faugères, J. C., A. V. Stow-Dorrik, P. Patrice, and V. Adriano, 1999, Seismic features diagnostic of contourite drifts: *Marine Geology*, v. 162, p. 1-38.
- Field, M. E., and B. D. Edwards, 1980, Slopes of the southern California borderland: A regime of

mass transport, in M. E. Field, Ed., Processes of the Quaternary Depositional Environments of the Pacific Coast, Pacific Coast Paleogeography Symposium: *Society of Economical Paleontology and Mineralogy*, p. 169-184.

Field, M. E., J. V. Gardner, A. E. Jennings, and B. D. Edwards, 1982, Earthquake-induced sediment failures on a 0.25° slope, Klamath River delta, California: *Geology*, v. 10, p. 542-546.

Field, M. E., and J. H. Barber, 1993, A submarine landslide associated with shallow seafloor gas hydrates off northern California, in W. C. Schwab, H. J. Lee and D. C. Twichell, eds., Submarine Landslides: Selected Studies in the U. S. Exclusive Economic Zone: *U.S. Geological Survey Bulletin*, 2002, p. 151-157.

Fitches, W. R., R. Cave, J. Craig, and A. J. Maltman, 1986, Early veins as evidence of detachment in the Lower Palaeozoic rocks of the Welsh Basin: *Journal of Structural Geology*, v. 8, p. 607-620.

Fleischer, L., 2000, Index of Oil and Gas wells, drilled in Israel, updated January 2000: *Report OG/8/2000*, MNI, Jerusalem.

Frey-Martinez, J., J. Cartwright, and B. Hall, 2005, 3D seismic interpretation of slump complexes: examples from the continental margin of Israel. *Basin Research*, v. 17, p. 83-108.

Frydman, S., G. Wiseman, and G. Almagor, 1982, Effects of earthquakes on slope stability, continental shelf of Israel: *GSI Current Research*, p. 66-71.

G

Garfunkel, Z., A. Arad, T. Bugge, and G. Almagor, 1979, The Palmahim Disturbance and its regional setting: *Geological Survey of Israel Bulletin*, v. 72.

Garfunkel, Z., 1981, Internal structure of the Dead Sea leaky transform (rift) and its relations to plate kinematics: *Tectonophysics*, v. 80, p. 81-108.

Garfunkel, Z., 1984, Large-scale submarine rotational slumps and growth faults in the eastern Mediterranean: *Marine Geology*, v. 55, p. 305-324.

Garfunkel, Z., 1998, Constrains on the origin and history of the Eastern Mediterranean basin. *Tectonophysics*, v. 298, p. 5-35.

Garfunkel, Z., and B. Derin, 1984, Permian-Early Mesozoic tectonism and continental margin formation of Israel and its implications for the history of the eastern Mediterranean in J. E. Dixon, and A. H. F. Robertson, eds., The geologic evolution of the eastern Mediterranean MA, p. 187-201.

Garfunkel, Z., and G. Almagor, 1985, Geology and structure of the continental margin off northern Israel and the adjacent part of the Levantine Basin: *Marine Geology*, v. 62, p. 105-131.

Garfunkel, Z., and G. Almagor, 1987, Active salt dome development in the Levant basin southeast Mediterranean in I. Lerche, and J. O'Brien, eds., Dynamical geology of salt related structures, *Academic Press*, p. 263-300.

Gee, M. J. R. A. B. Watts, D. G. Masson, and N. Mitchell, 2001, Landslides and evolution of El Hierro in the Canary Islands: *Marine Geology*, v. 177, p. 271-293.

Gee, M. J. R., R. L. Gawthorpe, and J. S. Friedmann, in press, Giant striations at the base of a submarine landslide: *Marine Geology*.

Germanovich, L. N., A. M. Puzrin, and W. Xu, in press, The mechanism of tsunamigenic landslides: *Géotechnique*.

Gill, W., and P. H. Kuenen, 1958, Sand volcanoes on slumps in the Carboniferous of county Clare, Ireland: *Quarterly Journal of the Geological Society of London*, v. 113, Part 4; 425, p. 441-460.

Graue, K., 2000, Mud volcanoes in deepwater Nigeria: *Marine and Petroleum Geology*, v. 17, p. 959-974.

Grantz, A., and D. A. Dinter, 1980, Constraints of geologic processes on western Beaufort Sea oil developments: *Oil Gas Journal*, v. 78, p. 304-319.

Guargena C. G., G. B. Smith, J. Wardell, T. H. Nilsen, and T. M. Hegre, 2002, Sand injections at Jotum Field, North Sea-their possible impact on recoverable reserves: *64th EAGE Conference and Exhibition*, Florence, Extended Abstracts, H018.

Gvirtzman, G., and B. Buchbinder, 1978, The Late Tertiary of the coastal plain and continental shelf of Israel and its bearing on the history of the eastern Mediterranean, in K. J. Hsü, W. B. F. Ryan: Initial Reports of the Deep Sea Drilling Project, v. 13(2): *U.S. Government Printing Office*, Washington, p. 1195-1222.

H

Haflidason, H., H. P. Sejrup, P. Bryn, and R. Lien, 2001, The Storegga Slide; chronology and flow mechanism: *XI European Union of Geoscientists meeting*, Strasbourg, France.

Haflidason, H., H. P. Sejrup, P. Bryn, R. Lien, D. Masson, C. Jacobs, V. Huehnerbach, and K. Berg, 2002, The architecture and slide mechanism of the Storegga Slide, Mid Norwegian margin: The Norwegian Petroleum Society, Annual Meeting in Trondheim, October 2002, NPF Abstracts and Proceedings Number 2, p. 80-81.

Haflidason, H., R. Lien, H. P. Sejrup, C. F. Forsberg, and P. Bryn, in press, The dating and morphometry of the Storegga Slide: *Marine and Petroleum Geology*.

Hampton, M. A., A. H. Bouma, P. R. Carlson, B. F. Molnia, E. C. Clukey, and D. A. Sangrey,

- 1978, Quantitative study of slope instability in the Gulf of Alaska: *Offshore Technology Conference*, 10th Annual, OTC.
- Hampton, M. A., H. J. Lee, and J. Locat, 1996, Submarine landslides: *Review of Geophysics*, v. 34, p. 33-59.
- Hasiotis, T., G. Papatheodorou, G. Bouckovalas, C. Corbau, and G. Ferentinos, 2002, Earthquake-induced coastal sediment instabilities in the western Gulf of Corinth, Greece: *Marine Geology*, v. 3100, p. 1-17.
- Hanken, N. M., R. G. Bromley, and J. Miller, 1996, Plio-Pleistocene sediments in coastal grabens, north-east Rhodes, Greece: *Geological Journal*, v. 31, p. 271-298.
- Hedberg, H. D., 1974, Relation of methane generation to undercompacted shales, shale diapirs, and mud volcanoes: *AAPG Bulletin*, v. 58, p. 661-673.
- Hiscott, R. N., and Aksu, A. E., 1994, Submarine debris flows and continental slope evolution in front Quaternary ice sheets, Baffin Bay, Canadian Arctic: *AAPG Bulletin*, v. 78, p. 445-460.
- Huguen, C., J. Mascle, E. Chaumillon, J. M. Woodside, J. Benkhelil, A. Kopf, and A. Volkonskaia, 2001, Deformational styles of the eastern Mediterranean Ridge and surroundings from combined swath mapping and seismic reflection profiling: *Tectonophysics*, v. 343, p. 21-47.
- Hühnerbach, V., and D. G. Masson, 2004, Landslides in the North Atlantic and its adjacent seas: an analysis of their morphology, setting and behaviour: *Marine Geology*.
- Hurst, A., J. Cartwright, M. Huuse, R. Jonk, A. Schwab, D. Duranti, and B. Cronin, 2003, Significance of large-scale sand injectites as long-term fluid conduits: evidence from seismic data: *Geofluids*, v. 3, p. 263-276.
- Hsü, K. J., L. Montadert, D. Bernoulli, M. B. Cita, A. Erikson, R. G. Garrison, R. B. Kidd, F. Meliers, C. Muller, and R. Wright, 1978, History of the Mediterranean salinity crisis: *Init. Report DSDP*, v. 42A, p. 153-1078.
- Huguen, C., J. Mascle, E. Chaumillon, J. M. Woodside, J. Benkhelil, A. Kopf, and A. Volkonskaia, 2001, Deformational styles of the eastern Mediterranean Ridge and surroundings from combined swath mapping and seismic reflection profiling: *Tectonophysics*, v. 343, p. 21-47.
- Huuse, M., and Lykke-Andersen, H., 2000, Large-scale glaciotectonic structures in the eastern Danish North Sea, in A. J. Maltman, B. Hubbard, and M. J. Hambrey, eds., *Deformation of Glacial Materials: Geological Society (London) Special Publications*, v. 176, p. 293-305.
- Huuse, M., D. Duranti, C. G. Guargena, P. Prat, K. Holm, N. Steinsland, B. T. Cronin, A. Hurst, and J. Cartwright, 2003, Sandstone intrusions detection and significance for exploration and production: *First Break*, v. 21, p. 33-42.
- Huuse, M., D. Duranti, N. Steinsland, C. G. Guargena, P. Prat, K. Holm, B. T. Cronin, J.

Cartwright, and A. Hurst, 2004, Seismic characteristics of large-scale sandstone intrusions in the Paleogene of the South Viking Graben, UK and Norwegian North Sea. *in* R. J. Davies, J.

Cartwright, S. A. Stewart, J. R. Underhill and M. Lappin, eds., 3D Seismic Technology: Application to the Exploration of Sedimentary Basins. *Geological Society (London) Memoir*, v. 29, 263-277.

Huvenne, V. A. I., F. Croker-Peter, and J. P. Henriot, 2002, A refreshing 3D view of an ancient sediment collapse and slope failure : *Terra Nova*, v. 14, 1, p. 33-40.

I

Imbo, Y., M. De Batist, M. Canals, M. J. Prieto, and J. Baraza, 2002, The Gebra Slide: a submarine slide on the Trinity Peninsula Margin, Antarctica: *Marine Geology*, v. 3259, p. 1-18.

Ingram, G. M., T. J. Chisholm, C. J. Grant, C. A. Hedlund, P. Stuart-Smith, and J. Teasdale, 2004, Deepwater North Borneo: hydrocarbon accumulation in active fold and thrust belt: *Marine and Petroleum Geology*, v. 21,7, p. 879-887.

J

Jackson, M. P. A., and C. J. Talbot, 1991, A glossary of salt tectonics: University of Texas at Austin, *Bureau of Economic Geology Geological Circular No. 91-4*, p. 44.

Jansen, E., S. Befring, T. Bugge, T. Eidvin, H. Holtedahl, and H. P. Sejrup, 1987, Large submarine slides on the Norwegian continental margin: Sediments, transport and timing: *Marine Geology*, v. 78, p. 77-107.

Jenssen, A. I., D. Bergslien, M. Rye-Larsen, and R. M. Lindhom, 1993, Origin of complex mound geometry of Paleocene submarine-fan reservoirs, Balder Field, Norway, *in* J. R. Parker, ed., *Petroleum geology of northwest Europe: Proceedings of the 4th Conference*, London, Geological Society, p. 135-143.

Jenyon, M. K., 1986, *Salt tectonics*: London, *Elsevier*, 191 p.

Jenyon, M. K., 1988, Overburden deformation related to the pre-piercement development of salt structures in the North Sea: *Journal of the Geological Society (London)*, v. 145, p. 445-454.

Jolly, J. H. R., and L. Lonergan, 2002, Mechanisms and control on the formation of sand intrusions: *Journal of the Geological Society (London)*, v. 159, p. 605-617.

K

Keefer, D. K., 1994, The importance of earthquake-induced landslides to long-term slope erosion and slope-failure hazards in seismically active region: *Geomorphology*, v. 10, p. 265-284.

- Kempler, D., Y. Mart, B. Herut, and F. W. McCoy, 1996, Diapiric features in the southeastern Mediterranean Sea: indication of extension in a zone of incipient continental collision: *Marine Geology*, v. 134, p. 237-248.
- Kenyon, N. H., 1987, Mass-wasting features on the continental slope of northwestern Europe: *Marine Geology*, v. 74, p. 57-77.
- King, E. L., H. P. Sejrup, H. Haflidason, A. Elverhøi, and I. Aaseth, 1996, Quaternary seismic stratigraphy of the North Sea Fan: glacially-fed gravity flow aprons, hemipelagic sediments, and large submarine slides: *Marine Geology*, v. 130, p. 293-315.
- Knebel, H., and B. Carson, 1979, Small-scale slump deposits, middle Atlantic Continental Slope, off eastern United States: *Marine Geology*, v. 29, p. 221-236.
- Knox, G. J., and E. M. Omatsola, 1989, Development of the Cenozoic Niger Delta in terms of the "Escalator Regression" model and impact on hydrocarbon distribution in W. J. M. Van der Linden, S. A. P. L. Cloetingh, J. P. K. Kaasschieter and J. A. M. Van der Gun, eds., *Proceedings KNGMG symposiums coastal lowstands, geology and geotechnology*, Kluwer Academic Publishers, Amsterdam, p. 181-202.
- Knutz, P., and J. A. Cartwright, 2004, 3D anatomy of late Neogene contourite drifts and associated mass flows in the Faroe-Shetland Basin, in R. J. Davies, J. A. Cartwright, S. A. Stewart, M. Lappin, and J. R. Underhill, eds., *3D Seismic Technology: Application to the Exploration of Sedimentary Basins: Geological Society (London) Memoirs*, v. 29, p. 63-71.
- L**
- Laberg, J. S., and T. O. Vorren, 2000, The Trænadjupet Slide, offshore Norway-morphology, evacuation and triggering mechanisms: *Marine Geology*, v. 171, p. 95-114.
- Lastras, G., M. Canals, R. Urgeles, J. E. Hughes-Clarke, and J. Acosta, 2004, Shallow slides and pockmarks in the Eivissa Channel, Western Mediterranean Sea: *Sedimentology*, v. 51, p. 837-850.
- Lee, H. J., W. C. Schwab, B. D. Edwards, and R. E. Kayen, 1991, Quantitative controls on submarine slope failure morphology: *Marine Geotechnology*, v. 10, p. 143-157.
- Lee, H. J., J. Locat, P. Dartnell, K. Israel, and F. Wong, 1999, Regional variability of slope stability: application to the Eel margin, California: *Marine Geology*, v. 154, p. 305-321.
- Lee, H. J., J. P. M. Syvitski, G. Parker, D. Orange, J. Locat, E. W. H. Hutton, and J. Imram, 2002, Distinguishing sediment waves from slope failure deposits: field examples, including the "Humboldt slide", and modelling results: *Marine Geology*, v. 192, p. 79-104.
- Lemke, R. W., 1967, Effects of the earthquake of March 27, 1964, at Seward, Alaska: *U.S. Geological Survey Professional Papers*, v. 542-E, p. 43.

- Lenat, J. V., P. Cochonat, P. Bachelery, P. Boivin, B. Cornaglia, C. Deniel, P. Labazuy E. Le-Drezen, P. W. Lipman, G. Ollier, B. Savove, P. Vincent, and M. Voisset, 1989, Large landslides on the submarine east flank of Piton de la Fournaise Volcano: new results from high-resolution sonar imaging and rock sampling: *Bulletin of New Mexico Bureau of Mines and Mineral Resources*, p. 162.
- Lewis, K. B., 1971, Slumping on a continental slope inclined at 1°-4°: *Sedimentology*, v. 16, p. 97-110.
- Lindberg, B., J. S. Laberg, and T. O. Vorren, in press, The Nyk Slide-morphology, progression, and age of a partly buried submarine slide offshore northern Norway: *Marine Geology*.
- Lipman, P. W., W. R. Normark, J. G. Moore, J. B. Wilson, and C. E. Gutmacher, 1998, The giant submarine Alike debris slide, Mauna Loa, Hawaii, in R. I. Tilling, Ed., How volcanoes work: *Journal of Geophysical Research*, v. 93, p. 4279-4299.
- Locat, J., and Lee, H., 2002, Submarine landslides: advances and challenges: *Canadian Geotechnical Journal*, v. 39, p. 193-212.
- Lonergan, L., and J. A. Cartwright, 1999, Polygonal faults and their influence on reservoir geometries, Alba Field, United Kingdom Central North Sea: *AAPG Bulletin*, v. 83, p. 410-432.
- Lonergan, L., N. Lee, H. D. Johnson, J. Cartwright, and R. J. H. Jolly, 2000, Remobilization and injection in deepwater depositional systems: implications for reservoir architecture and prediction in P. Weimer, R. M. Slatt, J. Coleman, N. C. Rosen, H. Nelson, A. H. Bouma, M. J. Styzen and D. T. Lawrence, eds., Deep-water reservoirs of the world, p. 515-532. *GCSSEPM Foundation, 20th Annual Conference*, Houston.
- Løseth, H., L. Wensaas, B. Arntsen, N. Hanken, C. Basire, and K. Graue, 2001, 1000 m long gas blow-out pipes. 63rd EAGE Conference & Exhibition, Amsterdam, Extended Abstracts, P524.
- Løseth, H., L. Wensaas, B. Arntsen, and M. Hovland, 2003, Gas and fluid injection triggering shallow mud mobilization in the Hordaland Group, North Sea in P. Van Rensbergen, R. R. van Hillis, A. J. Maltman, and C. K. Morley, eds., Subsurface Sediment Mobilization: *Geological Society (London) Special Publication*, v. 216, p. 139-157.

M

- Maltman, A., and A. Bolton, 2003, How sediments become mobilized, in P. Van Rensbergen, R. R. van Hillis, A. J. Maltman, and C. K. Morley, eds., Subsurface Sediment Mobilization: *Geological Society (London) Special Publication*, v. 216, p. 9-20.
- Mandl, G., and W. Crans, 1981, Gravitational gliding in deltas, in K. R. McClay, Ed., Thrust and Nappe Tectonics: *Geological Society (London) Special Publication*, v. 9, p. 41-54.

- Mandl, G., and R. M. Harkness, 1987, Hydrocarbon migration by hydraulic fracturing, in M. E. Jones, and R. M. F. Preston, eds., *Deformation of Sediments and Sedimentary Rocks: Geological Society (London) Special Publication*, v. 29, p. 395-417.
- Martinsen, O. J., 1989, Styles of soft-sediment deformation on a Namurian (Carboniferous) delta slope, western Irish Namurian Basin, Ireland in M. K. G. Whateley, and K. T. Pickering, eds., *Deltas: Sites and Traps for Fossil Fuels: Geological Society (London) Special Publication*, v. 210, p. 167-177.
- Martinsen, O. J., and B. Bakken, 1990, Extensional and compressional zones in slumps and slides in the Namurian of County Clare, Ireland: *Journal of the Geological Society (London)*, v. 147, p. 153-164.
- Masson, D. G., M. Canals, B. Alonso, R. Urgeles, and V. Huhnerbach, 1998, The Canary debris flow; source area morphology and failure mechanisms: *Sedimentology*, v. 45, 2, p. 411-432.
- Masson, D. G., A. B. Watts, M. J. R. Gee, R. Urgeles, N. C. Mitchell, T. P. Le-Bas, and M. Canals, 2002, Slope failures on the flanks of the western Canary Islands: *Earth Science Reviews*, v. 57, v. 1-2, p. 1-35.
- McAdoo, B. G., L. F. Pratson, and D. L. Orange, 2000, Submarine landslide geomorphology, U. S. continental slope: *Marine Geology*, v. 169, p. 103-136.
- Menard, H. W., 1956, Archipelagic aprons (Pacific Ocean): *AAPG Bulletin*, v. 40, 9, p. 2195-2210.
- Molyneux, S., J. Cartwright, and L. Lonergan, 2002, Conical sandstone injection structures imaged by 3D seismic in the central North Sea, UK: *First Break*, v. 20, p. 383-393.
- Moore, D. G., J. R. Curray, and F. J. Emmel, 1976, Large submarine slide (olistostrome) associated with Sunda Arc subduction zone, northeast Indian Ocean: *Marine Geology*, v. 21, p. 211-226.
- Moore, J. G., D. A. Clague, R. T. Holcomb, P. W. Lipman, W. R. Normark, and M. E. Torresan, 1989, Prodigious submarine landslides on the Hawaiian Ridge: *Journal of Geophysical Research*, v. 94 (B12), p. 17465-17484.
- Moore, J. G., W. R. Normark, and R. T. Holcomb, 1994a, Giant Hawaiian landslides: *Annual Review of Earth Planetary Sciences*, v. 22, p. 119-144.
- Moore, J. G., W. R. Normark, and R. T. Holcomb, 1994b, Giant Hawaiian underwater landslides: *Science*, v. 264, p. 46-47.
- Montadert, L., J. Letouzey, and A. Mauffret, 1978, Messinian Event: Seismic evidence: *Initial Reports DSDP*, v. 42, p. 1032-1050.
- Morgan, J. P., J. M. Coleman, and S. M. Cagliano, 1968, Mudlumps-diapiric structures in the

- Mississippi delta sediments, in Diapirism and diapirs: *AAPG Memoir*, v. 8, p. 145-161.
- Morgenstern, N. R., 1967, Submarine slumping and the initiation of turbidity currents: *Marine Geotechnique*, p. 189-210.
- Morley, C. K., P. Crevello, and Z. H. Ahmad, 1998, Shale tectonics and deformation associated with active diapirism: the Jerudong Anticline, Brunei Darussalam: *Journal of the Geological Society (London)*, v. 155, p. 475-490.
- Morley, C.K., 2003, Mobile shale related deformation in large deltas developed on passive and active margins in P. Van Rensbergen, R. R. van Hillis, A. J. Maltman, and C. K. Morley, eds., Subsurface Sediment Mobilization: *Geological Society (London) Special Publication*, v. 216, p. 335-357.
- Mulder, T., and H. P. Cochonat, 1996, Classification of offshore mass movements: *Journal of Sedimentary Research*, v. 66, p. 43-57.

N

- Nardin, T. R., F. J. Hein, D. S. Gorsline, and B. D. Edwards, 1979, A review of mass movement processes and acoustic characteristics, and contrasts in slope and base-of-slope system versus canyon-fan-basin floor systems in L. J. Doyle, and O. H. Pilkey, eds., *Geology of Continental Slopes: Society of Economic Palaeontologists and Mineralogists Special Publication*, v. 27, p. 61-73.
- Netoff, D., 2002, Seismogenically induced fluidization of Jurassic erg sands, south-central Utah: *Sedimentology*, v. 49, p. 65-80.
- Nichols, R. J., R. S. J. Sparks, and C. J. N. Wilson, 1994, Experimental studies of the fluidization of layered sediments and the formation of fluid escape structures: *Sedimentology*, v. 41, p. 233-253.
- Nichols, R. J., 1995, The liquefaction and remobilization of sandy sediments, in A. J. Hartley, and D. J. Prosser, eds., Characterisation of deep-marine clastic systems: *Geological Society (London) Special Publication*, v. 94, p. 63-76.
- Normark, W. R., and C. E. Gutmacher, 1988, Sur submarine slide, Monterey Fan, central California: *Sedimentology*, v. 35, p. 629-647.

O

- O'Leary, D. W., 1991, Structures and morphology of submarine slab slides: clues to origin and behaviour: *Marine Geotechnology*, v. 10, p. 53-69.
- O'Leary, D. W., 1993, Submarine mass movement, a formative process of passive continental

margins: the Munsen-Nygren landslide complex and the southeast New England landslide complex, in W. C. Schwab, H. J. Lee and D. C. Twichell, eds., Submarine Landslides: Selected Studies in the U. S. Exclusive Economic Zone: *U.S. Geological Survey Bulletin*, 2000, p. 167-175.

Ollier, G., M. A. Garcia-del-Cura, J. Soria, A. Melendez-Hevia, and A. R. Soria, 1998, Deep-sea volcanoclastic sedimentary systems; an example from La Fournaise Volcano, Reunion Island, Indian Ocean: 15th international sedimentological congress; sedimentology at the dawn of the third millennium, p. 586.

P

Pedersen, S. A. S., 1987, Comparative studies of gravity in tectonic Quaternary sediments and sedimentary rocks related to fold belts, in M. E. Jones, and R. M. F. Preston, eds., Deformation of sediments and sedimentary rocks: *Geological Society (London) Special Publication*, v. 29, p. 165-180.

Piper, D. J. W., P. Cochonat, and M.L. Morrison, 1999, The sequence of events around the epicenter of the 1929 Grand Banks earthquake : initiation of debris flows and turbidity current inferred from sidescan sonar : *Sedimentology*, v. 46, p. 79-97.

Price, N. J., and J. W. Cosgrove, 1990, Analysis of geological structures: *Cambridge University Press*, Cambridge.

Prior, D. B., and J. M. Coleman, 1978, Submarine landslides on the Mississippi River Delta-front slope: *Geoscience and Man*, v. 19, p. 41-53.

Prior, D. B., and J. M. Coleman, 1979, Submarine landslides- Geometry and nomenclature: *Geomorphology*, v. 23, p. 415-426.

Prior, D. B., and J. M. Coleman, 1982, Active slides and flows in underconsolidated marine sediments on the slopes of the Mississippi Delta, in S. Saxov, and J. Nieuwenhuis, eds., Workshop on Marine Slides and Other Mass Movements: *NATO Conference Series IV Plenum Press*, New York, p. 225-234.

Prior, D. B., B. D. Bornhold, and M. W. Johns, 1984, Depositional characteristics of a submarine debris flow: *Journal of Geology*, v. 92, p. 707-727.

Prior, D. B., and J. M. Coleman, 1984, Submarine slope instability, in D. Brundsen, and D. B. Prior, eds., Slope Instability: *Wiley*, Chichester, New York, p. 419-455.

Puzrin, A. M., L. N. Germanovich, and S. Kim, Catastrophic failure of submerged slopes in normally consolidated sediments: *Géotechnique*, v. 54, 10, p. 631-643.

Q

R

Rettger R. E., 1935, Experiments of soft-rock deformation: *AAPG Bulletin*, v. 19, p. 271-292.

Ryan, W. B. F., D. J. Stanley, J. B. Hersey, D. A. Fahlquist, and T. D. Allan, 1971, The tectonics and geology of the Mediterranean Sea in A. E. Maxwell, ed., *The Sea*, 4(2). Wiley, New York, N.Y., 387-492.

Robertson, A. H. F., J. E. Dixon, S. Brown, A. Collins, A. Morris, E. Pickett, I. Sharp, and T. Ustaömer, 1996, Alternative tectonic models for the Late Paleozoic-Early Tertiary development of Tethys in the Eastern Mediterranean in A. Moris, D. H. Tarling, eds., *Palaeomagnetism and Tectonics of the Mediterranean: Geological Society (London) Special Publication*, v. 105, p. 239-263.

Robertson, A. H. F., 1998, Mesozoic-Tertiary tectonic evolution of the easternmost Mediterranean area: integration of marine and land evidence in A. H. F. Robertson, K. C. Emeis, C. Richter, A. Camerlenghi, eds., *Proc. ODP Scientific Results*, v. 160, p. 723-782.

Schultz-Ela, D. D., 2003, Origin of drag folds bordering salt diapirs: *AAPG Bulletin*, v. 87, p. 757-780.

S

Sivan, D., G. Gvirtzman, and E. Sass, 1999, Quaternary stratigraphy and paleogeography of the Galilee coastal plain, Israel: *Quaternary Research*, v. 51, p. 280-294.

Smith, J. R., A. Malahoff, and A. N. Shor, 1999, Submarine geology of the Hilina slump and morpho-structural evolution of Kilauea volcano, Hawaii: *Journal of Volcanology and Geothermal Research*, v. 94, p. 59-88.

Stovba, S. M., and R. A. Stephenson, 2003, Style and timing of salt tectonics in the Dniepr-Donets Basin (Ukraine): implications for triggering and driving mechanisms of salt movement in sedimentary basins: *Marine and Petroleum Geology*, v. 19, p. 1169-1189.

Stow, D.A.A., 1986, Deep clastic seas, in H. G. Reading Ed., *Sedimentary Environment and Facies*, 2nd edn, p. 399-444: *Blackwell Scientific Publications*, Oxford.

Strachan, L., 2002, Slump-initiated and controlled syndepositional sandstone remobilisation: an example from the Namurian of County Clare, Ireland: *Sedimentology*, v. 49, p. 25-41.

Suppe, J., and D. A. Medwedeff, 1990, Geometry and kinematics of fault-propagation folding, in J. Peter, N. Thomas, S. Schmid, and D. Bernoulli, eds., *The Hans Laubscher volume*, v. 83, 3, p. 409-454.

Sultan, N., P. Cochonat, J. P. Foucher, and J. Mienert, 2004, Effects of gas hydrates melting on seafloor slope instability: *Marine Geology*, v. 213, p. 379-401.

T

Trincardi, F., and W. R. Normark, 1989, Sediment waves on the Tiber prodelta slope: interaction of deltaic sedimentation and currents along the shelf: *Geo-Marine Letters*, v. 8, p. 149-157.

Trincardi, F., and A. Argnani, 1990, Gela Submarine slide: a major basin-wide event in the Plio-Quaternary foredeep of Sicily: *Geo-Marine Letters*, v. 10, p. 13-21.

Tibor, G., and Z. Ben-Avraham, 1992, Late Tertiary seismic facies and structures of the Levant passive margin off central Israel: *Marine Geology*, v. 105, p. 253-273.

U

Urgeles, R., M. Canals, J. Baraza, B. Alonso, and D. Masson, 1997, The most recent megalandslides of the Canary Islands; El Golfo debris avalanche and Canary debris flow, West El Hierro Island: *Journal of Geophysical Research*, v. 102, 9, p. 20305-20323.

V

Van der Wateren, F. M., 1995, Structural geology and sedimentology of push moraines: *Mededelingen Rijks Geologische Dienst*, v. 54.

Van Rensbergen P., and C. K. Morley, 2003, Re-evaluation of mobile shale occurrences on seismic sections of the Champion and Baram deltas, offshore Brunei, in P. Van Rensbergen, R. R. van Hillis, A. J. Maltman, and C. K. Morley, eds., *Subsurface Sediment Mobilization: Geological Society (London) Special Publication*, v. 216, p. 395-409.

Varnes, D. J., 1978, Slope movement types and processes, in R. L. Shuster, and R. J. Krizek, eds., *Landslides-analysis and control*, Spec. Report 176, p. 12-33. *National Academy of Sciences*, Washington, 11-33.

Vidal, N., J. Alvarez-Marrón, and D. Klaeschen, 2000, Internal configuration of the Levantine Basin from seismic reflection data (eastern Mediterranean): *Earth and Planetary Science Letters*, v. 180, p. 77-89.

W

Watts, A. B., and D. G. Masson, 1995, A giant landslide on the north flank of Tenerife, Canary Islands: *Journal of Geophysical Research*, v. 100(B12), p. 24487-24498.

Weimer, P. and R. M. Slatt, 2004, Petroleum Systems of Deepwater Settings: *Society of*

Exploration Geophysicists and European Association of Geoscientists and Engineers.

Wever, H. E., 2000, Petroleum and source rock characterization based on C-7 star plot results: examples from Egypt: AAPG Bulletin, v. 84, p. 1041-1054.

Whelan, T. A., J. M. Coleman, and J. N. Suyayda, 1976, The geochemistry of recent Mississippi river delta sediments: gas concentration and sediment stability. Paper 94: *Offshore Technology Conference*, Texas, p. 71-84.

Wilson, C. F., D. Long, J. Bulat, and H. Hafidason, 2003, The morphology, setting and processes of the Afen Slide, COSTA. Continental Slope Stability Workshop, v. 4, p. 10-13.

Woodcock, N. H., 1979, Sizes of submarine slides and their significance: *Journal of Structural Geology*, v. 1, p. 137-142.

Y

Yassir, N., 2003, The role of shear stress in mobilizing deep-seated mud volcanoes: geological and geomechanical evidence from Trinidad and Taiwan in P. Van Rensbergen, R. R. van Hillis, A. J. Maltman, and C. K. Morley, eds., Subsurface Sediment Mobilization: *Geological Society (London) Special Publication*, v. 216, p. 461-474.

